RILEM Bookseries

Konstantin Kovler
Semion Zhutovsky
Sabrina Spatari
Ole M. Jensen *Editors*

Concrete Durability and Service Life Planning

Proceedings of ConcreteLife'20

Springer

Concrete Durability and Service Life Planning

RILEM BOOKSERIES

Volume 26

RILEM, The International Union of Laboratories and Experts in Construction Materials, Systems and Structures, founded in 1947, is a non-governmental scientific association whose goal is to contribute to progress in the construction sciences, techniques and industries, essentially by means of the communication it fosters between research and practice. RILEM's focus is on construction materials and their use in building and civil engineering structures, covering all phases of the building process from manufacture to use and recycling of materials. More information on RILEM and its previous publications can be found on www.RILEM.net.

Indexed in SCOPUS, Google Scholar and SpringerLink.

More information about this series at http://www.springer.com/series/8781

Konstantin Kovler · Semion Zhutovsky ·
Sabrina Spatari · Ole M. Jensen
Editors

Concrete Durability and Service Life Planning

Proceedings of ConcreteLife'20

Springer

Editors
Konstantin Kovler
Civil and Environmental Engineering
Technion – Israel Institute of Technology
Haifa, Israel

Semion Zhutovsky
Civil and Environmental Engineering
Technion – Israel Institute of Technology
Haifa, Israel

Sabrina Spatari
Civil and Environmental Engineering
Technion – Israel Institute of Technology
Haifa, Israel

Ole M. Jensen
Department of Civil Engineering
Technical University of Denmark
Kgs. Lyngby, Denmark

ISSN 2211-0844 ISSN 2211-0852 (electronic)
RILEM Bookseries
ISBN 978-3-030-43331-4 ISBN 978-3-030-43332-1 (eBook)
https://doi.org/10.1007/978-3-030-43332-1

© RILEM 2020
No part of this work may be reproduced, stored in a retrieval system, or transmitted in any form or by any means, electronic, mechanical, photocopying, microfilming, recording or otherwise, without written permission from the Publisher, with the exception of any material supplied specifically for the purpose of being entered and executed on a computer system, for exclusive use by the purchaser of the work. Permission for use must always be obtained from the owner of the copyright: RILEM.
The use of general descriptive names, registered names, trademarks, service marks, etc. in this publication does not imply, even in the absence of a specific statement, that such names are exempt from the relevant protective laws and regulations and therefore free for general use.
The publisher, the authors and the editors are safe to assume that the advice and information in this book are believed to be true and accurate at the date of publication. Neither the publisher nor the authors or the editors give a warranty, expressed or implied, with respect to the material contained herein or for any errors or omissions that may have been made. The publisher remains neutral with regard to jurisdictional claims in published maps and institutional affiliations.

This Springer imprint is published by the registered company Springer Nature Switzerland AG
The registered company address is: Gewerbestrasse 11, 6330 Cham, Switzerland

Preface

The 3rd International RILEM Workshop on Concrete Durability and Service Life Planning will be held in Technion, Haifa, Israel, on January 14–16, 2020. It was preceded by "ConcreteLife'06," which was co-sponsored by RILEM and Japan Concrete Institute (JCI) and took place in the Dead Sea, Israel, in March 2006, and "ConcreteLife'09," which was organized in Technion, Haifa, in conjunction with the 63rd Annual RILEM Week (September 2009).

The object of "ConcreteLife'20" is to discuss the future trends in research, development, and practical engineering applications related to durable concrete construction. The focus of the workshop will be the design and construction of concrete structures exposed to different environmental conditions and mechanical loading. Although reinforced concrete structures can be designed and built to be durable in harsh conditions, there are numerous occasions where this potential is not materialized.

The economic implications of the damage when such deterioration occurs are quite large. For example, the annual cost of repairs of concrete and reinforced concrete structures deteriorated due to chloride corrosion, only in the Middle East, Japan, North Europe, and North America, is estimated to be hundreds of billions of dollars. Therefore, the problem of durable concrete materials and life-cycle evaluation of concrete structures for use under severe environmental conditions and mechanical loading is crucial. The research cooperation in studying the processes of concrete deterioration in different conditions, and the development of advanced high-performance materials, with a focus on utilization of industrial by-products, coal fly ash and granulated slag, is expected to bring scientific and practical benefits for the society.

The workshop serves as a stage for the presentation of up-to-date research on concrete durability, which has resurfaced as a key issue in modern concrete technology.

The themes include concrete curing, cracking in concrete structures, corrosion of steel in concrete, thermal and hygral effects, concrete in cold climate and under high temperatures, recycling and other environmental aspects, alkali–silica reaction,

chloride and sulfate attack, marine structures, transport phenomena, durability design, microstructure of concrete, volume changes, and life-cycle assessment.

The workshop is expected to highlight the trend in the research community to provide a greater focus on issues of technological significance, based on fundamental scientific concepts, which are of need to the engineering community to solve problems related to concrete durability.

RILEM (www.rilem.net), International Union of Laboratories and Experts in Construction Materials, Systems and Structures, is a scientific sponsor of the workshop. This guarantees a high quality of presentations, a wide geography, good visibility in the media, and excellent resonance within the scientific and engineering community dealing with concrete, in both materials and structures fields.

The 3rd International RILEM Workshop on Concrete Durability and Service Life Planning is organized in conjunction with the EuroTech PhD Winter School "Concrete Life Cycle: from Cradle to Grave" (January 12–14, 2020). This Winter School is organized jointly by the three universities and members of the EuroTech alliance (http://eurotech-universities.eu/): Technion—Israel Institute of Technology, Technical University of Denmark (DTU), and Eindhoven University of Technology (TU/e).

We hope that the exposure of the young doctorate students to the lectures by leading international experts in the field and the open workshop discussion format will enrich the participants' knowledge—both those who are seriously considering to start academic career following their defense and those planning to become experts in the industry.

Konstantin Kovler

Organization

Local Organizing Committee

Konstantin Kovler (Chair)
Arnon Bentur
Avraham Dancygier
Amnon Katz
Yossi Sikuler
Sabrina Spatari
Semion Zhutovsky
Anat Avital (Conference Administrator)

Website: https://rilem2020.net.technion.ac.il

International Organization by

Konstantin Kovler	Technion—Israel Institute of Technology
Ole M. Jensen	Technical University of Denmark
Jiaping Liu	Southeast University, China

Sponsors

Tambour
www.tambourpaints.com/

Haifa Municipality
www.haifa.muni.il/

Nesher Israel Cement Enterprises
www.nesher.co.il/

Sponsored by

RILEM
International Union of Laboratories and Experts in Construction Materials, Systems and Structures

Organized by

National Building Research Institute

Faculty of Civil and Environmental Engineering,
Technion—Israel Institute of Technology

Contents

RILEM Publications

The following list is presenting the global offer of RILEM Publications, sorted by series. Each publication is available in printed version and/or in online version.

RILEM Proceedings (PRO)

PRO 1: Durability of High Performance Concrete (ISBN: 2-912143-03-9; e-ISBN: 2-351580-12-5; e-ISBN: 2351580125); *Ed. H. Sommer*

PRO 2: Chloride Penetration into Concrete (ISBN: 2-912143-00-04; e-ISBN: 2912143454); *Eds. L.-O. Nilsson and J.-P. Ollivier*

PRO 3: Evaluation and Strengthening of Existing Masonry Structures (ISBN: 2-912143-02-0; e-ISBN: 2351580141); *Eds. L. Binda and C. Modena*

PRO 4: Concrete: From Material to Structure (ISBN: 2-912143-04-7; e-ISBN: 2351580206); *Eds. J.-P. Bournazel and Y. Malier*

PRO 5: The Role of Admixtures in High Performance Concrete (ISBN: 2-912143-05-5; e-ISBN: 2351580214); *Eds. J. G. Cabrera and R. Rivera-Villarreal*

PRO 6: High Performance Fiber Reinforced Cement Composites - HPFRCC 3 (ISBN: 2-912143-06-3; e-ISBN: 2351580222); *Eds. H. W. Reinhardt and A. E. Naaman*

PRO 7: 1st International RILEM Symposium on Self-Compacting Concrete (ISBN: 2-912143-09-8; e-ISBN: 2912143721); *Eds. Å. Skarendahl and Ö. Petersson*

PRO 8: International RILEM Symposium on Timber Engineering (ISBN: 2-912143-10-1; e-ISBN: 2351580230); *Ed. L. Boström*

PRO 9: 2nd International RILEM Symposium on Adhesion between Polymers and Concrete ISAP '99 (ISBN: 2-912143-11-X; e-ISBN: 2351580249); *Eds. Y. Ohama and M. Puterman*

PRO 10: 3rd International RILEM Symposium on Durability of Building and Construction Sealants (ISBN: 2-912143-13-6; e-ISBN: 2351580257); *Eds. A. T. Wolf*

PRO 11: 4th International RILEM Conference on Reflective Cracking in Pavements (ISBN: 2-912143-14-4; e-ISBN: 2351580265); *Eds. A. O. Abd El Halim, D. A. Taylor and El H. H. Mohamed*

PRO 12: International RILEM Workshop on Historic Mortars: Characteristics and Tests (ISBN: 2-912143-15-2; e-ISBN: 2351580273); *Eds. P. Bartos, C. Groot and J. J. Hughes*

PRO 13: 2nd International RILEM Symposium on Hydration and Setting (ISBN: 2-912143-16-0; e-ISBN: 2351580281); *Ed. A. Nonat*

PRO 14: Integrated Life-Cycle Design of Materials and Structures - ILCDES 2000 (ISBN: 951-758-408-3; e-ISBN: 235158029X); (ISSN: 0356-9403); *Ed. S. Sarja*

PRO 15: Fifth RILEM Symposium on Fibre-Reinforced Concretes (FRC) - BEFIB'2000 (ISBN: 2-912143-18-7; e-ISBN: 291214373X); *Eds. P. Rossi and G. Chanvillard*

PRO 16: Life Prediction and Management of Concrete Structures (ISBN: 2-912143-19-5; e-ISBN: 2351580303); *Ed. D. Naus*

PRO 17: Shrinkage of Concrete – Shrinkage 2000 (ISBN: 2-912143-20-9; e-ISBN: 2351580311); *Eds. V. Baroghel-Bouny and P.-C. Aïtcin*

PRO 18: Measurement and Interpretation of the On-Site Corrosion Rate (ISBN: 2-912143-21-7; e-ISBN: 235158032X); *Eds. C. Andrade, C. Alonso, J. Fullea, J. Polimon and J. Rodriguez*

PRO 19: Testing and Modelling the Chloride Ingress into Concrete (ISBN: 2-912143-22-5; e-ISBN: 2351580338); *Eds. C. Andrade and J. Kropp*

PRO 20: 1st International RILEM Workshop on Microbial Impacts on Building Materials (CD 02) (e-ISBN 978-2-35158-013-4); *Ed. M. Ribas Silva*

PRO 21: International RILEM Symposium on Connections between Steel and Concrete (ISBN: 2-912143-25-X; e-ISBN: 2351580346); *Ed. R. Eligehausen*

PRO 22: International RILEM Symposium on Joints in Timber Structures (ISBN: 2-912143-28-4; e-ISBN: 2351580354); *Eds. S. Aicher and H.-W. Reinhardt*

PRO 23: International RILEM Conference on Early Age Cracking in Cementitious Systems (ISBN: 2-912143-29-2; e-ISBN: 2351580362); *Eds. K. Kovler and A. Bentur*

PRO 24: 2nd International RILEM Workshop on Frost Resistance of Concrete (ISBN: 2-912143-30-6; e-ISBN: 2351580370); *Eds. M. J. Setzer, R. Auberg and H.-J. Keck*

PRO 25: International RILEM Workshop on Frost Damage in Concrete (ISBN: 2-912143-31-4; e-ISBN: 2351580389); *Eds. D. J. Janssen, M. J. Setzer and M. B. Snyder*

PRO 26: International RILEM Workshop on On-Site Control and Evaluation of Masonry Structures (ISBN: 2-912143-34-9; e-ISBN: 2351580141); *Eds. L. Binda and R. C. de Vekey*

PRO 27: International RILEM Symposium on Building Joint Sealants (CD03; e-ISBN: 235158015X); *Ed. A. T. Wolf*

PRO 28: 6th International RILEM Symposium on Performance Testing and Evaluation of Bituminous Materials - PTEBM'03 (ISBN: 2-912143-35-7; e-ISBN: 978-2-912143-77-8); *Ed. M. N. Partl*

PRO 29: 2nd International RILEM Workshop on Life Prediction and Ageing Management of Concrete Structures (ISBN: 2-912143-36-5; e-ISBN: 2912143780); *Ed. D. J. Naus*

PRO 30: 4th International RILEM Workshop on High Performance Fiber Reinforced Cement Composites - HPFRCC 4 (ISBN: 2-912143-37-3; e-ISBN: 2912143799); *Eds. A. E. Naaman and H. W. Reinhardt*

PRO 31: International RILEM Workshop on Test and Design Methods for Steel Fibre Reinforced Concrete: Background and Experiences (ISBN: 2-912143-38-1; e-ISBN: 2351580168); *Eds. B. Schnütgen and L. Vandewalle*

PRO 32: International Conference on Advances in Concrete and Structures 2 vol. (ISBN (set): 2-912143-41-1; e-ISBN: 2351580176); *Eds. Ying-shu Yuan, Surendra P. Shah and Heng-lin Lü*

PRO 33: 3rd International Symposium on Self-Compacting Concrete (ISBN: 2-912143-42-X; e-ISBN: 2912143713); *Eds. Ó. Wallevik and I. Níelsson*

PRO 34: International RILEM Conference on Microbial Impact on Building Materials (ISBN: 2-912143-43-8; e-ISBN: 2351580184); *Ed. M. Ribas Silva*

PRO 35: International RILEM TC 186-ISA on Internal Sulfate Attack and Delayed Ettringite Formation (ISBN: 2-912143-44-6; e-ISBN: 2912143802); *Eds. K. Scrivener and J. Skalny*

PRO 36: International RILEM Symposium on Concrete Science and Engineering – A Tribute to Arnon Bentur (ISBN: 2-912143-46-2; e-ISBN: 2912143586); *Eds. K. Kovler, J. Marchand, S. Mindess and J. Weiss*

PRO 37: 5th International RILEM Conference on Cracking in Pavements – Mitigation, Risk Assessment and Prevention (ISBN: 2-912143-47-0; e-ISBN: 2912143764); *Eds. C. Petit, I. Al-Qadi and A. Millien*

PRO 38: 3rd International RILEM Workshop on Testing and Modelling the Chloride Ingress into Concrete (ISBN: 2-912143-48-9; e-ISBN: 2912143578); *Eds. C. Andrade and J. Kropp*

PRO 39: 6th International RILEM Symposium on Fibre-Reinforced Concretes - BEFIB 2004 (ISBN: 2-912143-51-9; e-ISBN: 2912143748); *Eds. M. Di Prisco, R. Felicetti and G. A. Plizzari*

PRO 40: International RILEM Conference on the Use of Recycled Materials in Buildings and Structures (ISBN: 2-912143-52-7; e-ISBN: 2912143756); *Eds. E. Vázquez, Ch. F. Hendriks and G. M. T. Janssen*

PRO 41: RILEM International Symposium on Environment-Conscious Materials and Systems for Sustainable Development (ISBN: 2-912143-55-1; e-ISBN: 2912143640); *Eds. N. Kashino and Y. Ohama*

PRO 42: SCC'2005 - China: 1st International Symposium on Design, Performance and Use of Self-Consolidating Concrete (ISBN: 2-912143-61-6; e-ISBN: 2912143624); *Eds. Zhiwu Yu, Caijun Shi, Kamal Henri Khayat and Youjun Xie*

PRO 43: International RILEM Workshop on Bonded Concrete Overlays (e-ISBN: 2-912143-83-7); *Eds. J. L. Granju and J. Silfwerbrand*

PRO 44: 2nd International RILEM Workshop on Microbial Impacts on Building Materials (CD11) (e-ISBN: 2-912143-84-5); *Ed. M. Ribas Silva*

PRO 45: 2nd International Symposium on Nanotechnology in Construction, Bilbao (ISBN: 2-912143-87-X; e-ISBN: 2912143888); *Eds. Peter J. M. Bartos, Yolanda de Miguel and Antonio Porro*

PRO 46: ConcreteLife'06 - International RILEM-JCI Seminar on Concrete Durability and Service Life Planning: Curing, Crack Control, Performance in Harsh Environments (ISBN: 2-912143-89-6; e-ISBN: 291214390X); *Ed. K. Kovler*

PRO 47: International RILEM Workshop on Performance Based Evaluation and Indicators for Concrete Durability (ISBN: 978-2-912143-95-2; e-ISBN: 9782912143969); *Eds. V. Baroghel-Bouny, C. Andrade, R. Torrent and K. Scrivener*

PRO 48: 1st International RILEM Symposium on Advances in Concrete through Science and Engineering (e-ISBN: 2-912143-92-6); *Eds. J. Weiss, K. Kovler, J. Marchand, and S. Mindess*

PRO 49: International RILEM Workshop on High Performance Fiber Reinforced Cementitious Composites in Structural Applications (ISBN: 2-912143-93-4; e-ISBN: 2912143942); *Eds. G. Fischer and V.C. Li*

PRO 50: 1st International RILEM Symposium on Textile Reinforced Concrete (ISBN: 2-912143-97-7; e-ISBN: 2351580087); *Eds. Josef Hegger, Wolfgang Brameshuber and Norbert Will*

PRO 51: 2nd International Symposium on Advances in Concrete through Science and Engineering (ISBN: 2-35158-003-6; e-ISBN: 2-35158-002-8); *Eds. J. Marchand, B. Bissonnette, R. Gagné, M. Jolin and F. Paradis*

PRO 52: Volume Changes of Hardening Concrete: Testing and Mitigation (ISBN: 2-35158-004-4; e-ISBN: 2-35158-005-2); *Eds. O. M. Jensen, P. Lura and K. Kovler*

PRO 53: High Performance Fiber Reinforced Cement Composites - HPFRCC5 (ISBN: 978-2-35158-046-2; e-ISBN: 978-2-35158-089-9); *Eds. H. W. Reinhardt and A. E. Naaman*

PRO 54: 5th International RILEM Symposium on Self-Compacting Concrete (ISBN: 978-2-35158-047-9; e-ISBN: 978-2-35158-088-2); *Eds. G. De Schutter and V. Boel*

PRO 55: International RILEM Symposium Photocatalysis, Environment and Construction Materials (ISBN: 978-2-35158-056-1; e-ISBN: 978-2-35158-057-8); *Eds. P. Baglioni and L. Cassar*

PRO 56: International RILEM Workshop on Integral Service Life Modelling of Concrete Structures (ISBN 978-2-35158-058-5; e-ISBN: 978-2-35158-090-5); *Eds. R. M. Ferreira, J. Gulikers and C. Andrade*

PRO 57: RILEM Workshop on Performance of cement-based materials in aggressive aqueous environments (e-ISBN: 978-2-35158-059-2); *Ed. N. De Belie*

PRO 58: International RILEM Symposium on Concrete Modelling - CONMOD'08 (ISBN: 978-2-35158-060-8; e-ISBN: 978-2-35158-076-9); *Eds. E. Schlangen and G. De Schutter*

PRO 59: International RILEM Conference on On Site Assessment of Concrete, Masonry and Timber Structures - SACoMaTiS 2008 (ISBN set: 978-2-35158-061-5; e-ISBN: 978-2-35158-075-2); *Eds. L. Binda, M. di Prisco and R. Felicetti*

PRO 60: Seventh RILEM International Symposium on Fibre Reinforced Concrete: Design and Applications - BEFIB 2008 (ISBN: 978-2-35158-064-6; e-ISBN: 978-2-35158-086-8); *Ed. R. Gettu*

PRO 61: 1st International Conference on Microstructure Related Durability of Cementitious Composites 2 vol., (ISBN: 978-2-35158-065-3; e-ISBN: 978-2-35158-084-4); *Eds. W. Sun, K. van Breugel, C. Miao, G. Ye and H. Chen*

PRO 62: NSF/ RILEM Workshop: In-situ Evaluation of Historic Wood and Masonry Structures (e-ISBN: 978-2-35158-068-4); *Eds. B. Kasal, R. Anthony and M. Drdácký*

PRO 63: Concrete in Aggressive Aqueous Environments: Performance, Testing and Modelling, 2 vol., (ISBN: 978-2-35158-071-4; e-ISBN: 978-2-35158-082-0); *Eds. M. G. Alexander and A. Bertron*

PRO 64: Long Term Performance of Cementitious Barriers and Reinforced Concrete in Nuclear Power Plants and Waste Management - NUCPERF 2009 (ISBN: 978-2-35158-072-1; e-ISBN: 978-2-35158-087-5); *Eds. V. L'Hostis, R. Gens, C. Gallé*

PRO 65: Design Performance and Use of Self-consolidating Concrete - SCC'2009 (ISBN: 978-2-35158-073-8; e-ISBN: 978-2-35158-093-6); *Eds. C. Shi, Z. Yu, K. H. Khayat and P. Yan*

PRO 66: 2nd International RILEM Workshop on Concrete Durability and Service Life Planning - ConcreteLife'09 (ISBN: 978-2-35158-074-5; ISBN: 978-2-35158-074-5); *Ed. K. Kovler*

PRO 67: Repairs Mortars for Historic Masonry (e-ISBN: 978-2-35158-083-7); *Ed. C. Groot*

PRO 68: Proceedings of the 3rd International RILEM Symposium on 'Rheology of Cement Suspensions such as Fresh Concrete (ISBN 978-2-35158-091-2; e-ISBN: 978-2-35158-092-9); *Eds. O. H. Wallevik, S. Kubens and S. Oesterheld*

PRO 69: 3rd International PhD Student Workshop on 'Modelling the Durability of Reinforced Concrete (ISBN: 978-2-35158-095-0); *Eds. R. M. Ferreira, J. Gulikers and C. Andrade*

PRO 70: 2rd International Conference on 'Service Life Design for Infrastructure' (ISBN set: 978-2-35158-096-7, e-ISBN: 978-2-35158-097-4); *Ed. K. van Breugel, G. Ye and Y. Yuan*

PRO 71: Advances in Civil Engineering Materials - The 50-year Teaching Anniversary of Prof. Sun Wei' (ISBN: 978-2-35158-098-1; e-ISBN: 978-2-35158-099-8); *Eds. C. Miao, G. Ye, and H. Chen*

PRO 72: First International Conference on 'Advances in Chemically-Activated Materials – CAM'2010' (2010), 264 pp, ISBN: 978-2-35158-101-8; e-ISBN: 978-2-35158-115-5, *Eds. Caijun Shi and Xiaodong Shen*

PRO 73: 2nd International Conference on 'Waste Engineering and Management - ICWEM 2010' (2010), 894 pp, ISBN: 978-2-35158-102-5; e-ISBN: 978-2-35158-103-2, *Eds. J. Zh. Xiao, Y. Zhang, M. S. Cheung and R. Chu*

PRO 74: International RILEM Conference on 'Use of Superabsorsorbent Polymers and Other New Additives in Concrete' (2010) 374 pp., ISBN: 978-2-35158-104-9; e-ISBN: 978-2-35158-105-6; *Eds. O.M. Jensen, M.T. Hasholt, and S. Laustsen*

PRO 75: International Conference on 'Material Science - 2nd ICTRC - Textile Reinforced Concrete - Theme 1' (2010) 436 pp., ISBN: 978-2-35158-106-3; e-ISBN: 978-2-35158-107-0; *Ed. W. Brameshuber*

PRO 76: International Conference on 'Material Science - HetMat - Modelling of Heterogeneous Materials - Theme 2' (2010) 255 pp., ISBN: 978-2-35158-108-7; e-ISBN: 978-2-35158-109-4; *Ed. W. Brameshuber*

PRO 77: International Conference on 'Material Science - AdIPoC - Additions Improving Properties of Concrete - Theme 3' (2010) 459 pp., ISBN: 978-2-35158-110-0; e-ISBN: 978-2-35158-111-7; *Ed. W. Brameshuber*

PRO 78: 2nd Historic Mortars Conference and RILEM TC 203-RHM Final Workshop – HMC2010 (2010) 1416 pp., e-ISBN: 978-2-35158-112-4; *Eds J. Válek, C. Groot, and J. J. Hughes*

PRO 79: International RILEM Conference on Advances in Construction Materials Through Science and Engineering (2011) 213 pp., ISBN: 978-2-35158-116-2, e-ISBN: 978-2-35158-117-9; *Eds Christopher Leung and K.T. Wan*

PRO 80: 2nd International RILEM Conference on Concrete Spalling due to Fire Exposure (2011) 453 pp., ISBN: 978-2-35158-118-6, e-ISBN: 978-2-35158-119-3; *Eds E.A.B. Koenders and F. Dehn*

PRO 81: 2nd International RILEM Conference on Strain Hardening Cementitious Composites (SHCC2-Rio) (2011) 451 pp., ISBN: 978-2-35158-120-9, e-ISBN: 978-2-35158-121-6; *Eds R.D. Toledo Filho, F.A. Silva, E.A.B. Koenders and E.M.R. Fairbairn*

PRO 82: 2nd International RILEM Conference on Progress of Recycling in the Built Environment (2011) 507 pp., e-ISBN: 978-2-35158-122-3; *Eds V.M. John, E. Vazquez, S.C. Angulo and C. Ulsen*

PRO 83: 2nd International Conference on Microstructural-related Durability of Cementitious Composites (2012) 250 pp., ISBN: 978-2-35158-129-2; e-ISBN: 978-2-35158-123-0; *Eds G. Ye, K. van Breugel, W. Sun and C. Miao*

PRO 84: CONSEC13 - Seventh International Conference on Concrete under Severe Conditions – Environment and Loading (2013) 1930 pp., ISBN: 978-2-35158-124-7; e-ISBN: 978-2-35158-134-6; *Eds Z.J. Li, W. Sun, C.W. Miao, K. Sakai, O.E. Gjorv & N. Banthia*

PRO 85: RILEM-JCI International Workshop on Crack Control of Mass Concrete and Related issues concerning Early-Age of Concrete Structures – ConCrack 3 – Control of Cracking in Concrete Structures 3 (2012) 237 pp., ISBN: 978-2-35158-125-4; e-ISBN: 978-2-35158-126-1; *Eds F. Toutlemonde and J.-M. Torrenti*

PRO 86: International Symposium on Life Cycle Assessment and Construction (2012) 414 pp., ISBN: 978-2-35158-127-8, e-ISBN: 978-2-35158-128-5; *Eds A. Ventura and C. de la Roche*

PRO 87: UHPFRC 2013 – RILEM-fib-AFGC International Symposium on Ultra-High Performance Fibre-Reinforced Concrete (2013), ISBN: 978-2-35158-130-8, e-ISBN: 978-2-35158-131-5; *Eds F. Toutlemonde*

PRO 88: 8th RILEM International Symposium on Fibre Reinforced Concrete (2012) 344 pp., ISBN: 978-2-35158-132-2, e-ISBN: 978-2-35158-133-9; *Eds Joaquim A.O. Barros*

PRO 89: RILEM International workshop on performance-based specification and control of concrete durability (2014) 678 pp, ISBN: 978-2-35158-135-3, e-ISBN: 978-2-35158-136-0; *Eds. D. Bjegović, H. Beushausen and M. Serdar*

PRO 90: 7th RILEM International Conference on Self-Compacting Concrete and of the 1st RILEM International Conference on Rheology and Processing of Construction Materials (2013) 396 pp, ISBN: 978-2-35158-137-7, e-ISBN: 978-2-35158-138-4; *Eds. Nicolas Roussel and Hela Bessaies-Bey*

PRO 91: CONMOD 2014 - RILEM International Symposium on Concrete Modelling (2014), ISBN: 978-2-35158-139-1; e-ISBN: 978-2-35158-140-7; *Eds. Kefei Li, Peiyu Yan and Rongwei Yang*

PRO 92: CAM 2014 - 2nd International Conference on advances in chemically-activated materials (2014) 392 pp., ISBN: 978-2-35158-141-4; e-ISBN: 978-2-35158-142-1; *Eds. Caijun Shi and Xiadong Shen*

PRO 93: SCC 2014 - 3rd International Symposium on Design, Performance and Use of Self-Consolidating Concrete (2014) 438 pp., ISBN: 978-2-35158-143-8; e-ISBN: 978-2-35158-144-5; *Eds. Caijun Shi, Zhihua Ou, Kamal H. Khayat*

PRO 94 (online version): HPFRCC-7 - 7th RILEM conference on High performance fiber reinforced cement composites (2015), e-ISBN: 978-2-35158-146-9; *Eds. H.W. Reinhardt, G.J. Parra-Montesinos, H. Garrecht*

PRO 95: International RILEM Conference on Application of superabsorbent polymers and other new admixtures in concrete construction (2014), ISBN: 978-2-35158-147-6; e-ISBN: 978-2-35158-148-3; *Eds. Viktor Mechtcherine, Christof Schroefl*

PRO 96 (online version): XIII DBMC: XIII International Conference on Durability of Building Materials and Components (2015), e-ISBN: 978-2-35158-149-0; *Eds. M. Quattrone, V.M. John*

PRO 97: SHCC3 – 3rd International RILEM Conference on Strain Hardening Cementitious Composites (2014), ISBN: 978-2-35158-150-6; e-ISBN: 978-2-35158-151-3; *Eds. E. Schlangen, M.G. Sierra Beltran, M. Lukovic, G. Ye*

PRO 98: FERRO-11 – 11th International Symposium on Ferrocement and 3rd ICTRC - International Conference on Textile Reinforced Concrete (2015), ISBN: 978-2-35158-152-0; e-ISBN: 978-2-35158-153-7; *Ed. W. Brameshuber*

PRO 99 (online version): ICBBM 2015 - 1st International Conference on Bio-Based Building Materials (2015), e-ISBN: 978-2-35158-154-4; *Eds. S. Amziane, M. Sonebi*

PRO 100: SCC16 - RILEM Self-Consolidating Concrete Conference (2016), ISBN: 978-2-35158-156-8; e-ISBN: 978-2-35158-157-5; *Ed. Kamal H. Kayat*

PRO 101 (online version): III Progress of Recycling in the Built Environment (2015), e-ISBN: 978-2-35158-158-2; *Eds I. Martins, C. Ulsen and S. C. Angulo*

PRO 102 (online version): RILEM Conference on Microorganisms-Cementitious Materials Interactions (2016), e-ISBN: 978-2-35158-160-5; *Eds. Alexandra Bertron, Henk Jonkers, Virginie Wiktor*

PRO 103 (online version): ACESC'16 - Advances in Civil Engineering and Sustainable Construction (2016), e-ISBN: 978-2-35158-161-2; *Eds. T.Ch. Madhavi, G. Prabhakar, Santhosh Ram and P.M. Rameshwaran*

PRO 104 (online version): SSCS'2015 - Numerical Modeling - Strategies for Sustainable Concrete Structures (2015), e-ISBN: 978-2-35158-162-9

PRO 105: 1st International Conference on UHPC Materials and Structures (2016), ISBN: 978-2-35158-164-3, e-ISBN: 978-2-35158-165-0

PRO 106: AFGC-ACI-fib-RILEM International Conference on Ultra-High-Performance Fibre-Reinforced Concrete – UHPFRC 2017 (2017), ISBN: 978-2-35158-166-7, e-ISBN: 978-2-35158-167-4; *Eds. François Toutlemonde & Jacques Resplendino*

PRO 107 (online version): XIV DBMC – 14th International Conference on Durability of Building Materials and Components (2017), e-ISBN: 978-2-35158-159-9; *Eds. Geert De Schutter, Nele De Belie, Arnold Janssens, Nathan Van Den Bossche*

PRO 108: MSSCE 2016 - Innovation of Teaching in Materials and Structures (2016), ISBN: 978-2-35158-178-0, e-ISBN: 978-2-35158-179-7; *Ed. Per Goltermann*

PRO 109 (2 volumes): MSSCE 2016 - Service Life of Cement-Based Materials and Structures (2016), ISBN Vol. 1: 978-2-35158-170-4, Vol. 2: 978-2-35158-171-4, Set Vol. 1&2: 978-2-35158-172-8, e-ISBN : 978-2-35158-173-5; *Eds. Miguel Azenha, Ivan Gabrijel, Dirk Schlicke, Terje Kanstad and Ole Mejlhede Jensen*

PRO 110: MSSCE 2016 - Historical Masonry (2016), ISBN: 978-2-35158-178-0, e-ISBN: 978-2-35158-179-7; *Eds. Inge Rörig-Dalgaard and Ioannis Ioannou*

PRO 111: MSSCE 2016 - Electrochemistry in Civil Engineering (2016), ISBN: 978-2-35158-176-6, e-ISBN: 978-2-35158-177-3; *Ed. Lisbeth M. Ottosen*

PRO 112: MSSCE 2016 - Moisture in Materials and Structures (2016), ISBN: 978-2-35158-178-0, e-ISBN: 978-2-35158-179-7; *Eds. Kurt Kielsgaard Hansen, Carsten Rode and Lars-Olof Nilsson*

PRO 113: MSSCE 2016 - Concrete with Supplementary Cementitious Materials (2016), ISBN: 978-2-35158-178-0, e-ISBN: 978-2-35158-179-7; *Eds. Ole Mejlhede Jensen, Konstantin Kovler and Nele De Belie*

PRO 114: MSSCE 2016 - Frost Action in Concrete (2016), ISBN: 978-2-35158-182-7, e-ISBN: 978-2-35158-183-4; *Eds. Marianne Tange Hasholt, Katja Fridh and R. Doug Hooton*

PRO 115: MSSCE 2016 - Fresh Concrete (2016), ISBN: 978-2-35158-184-1, e-ISBN: 978-2-35158-185-8; *Eds. Lars N. Thrane, Claus Pade, Oldrich Svec and Nicolas Roussel*

PRO 116: BEFIB 2016 – 9th RILEM International Symposium on Fiber Reinforced Concrete (2016), ISBN: 978-2-35158-187-2, e-ISBN: 978-2-35158-186-5; *Eds. N. Banthia, M. di Prisco and S. Soleimani-Dashtaki*

PRO 117: 3rd International RILEM Conference on Microstructure Related Durability of Cementitious Composites (2016), ISBN: 978-2-35158-188-9, e-ISBN: 978-2-35158-189-6; *Eds. Changwen Miao, Wei Sun, Jiaping Liu, Huisu Chen, Guang Ye and Klaas van Breugel*

PRO 118 (4 volumes): International Conference on Advances in Construction Materials and Systems (2017), ISBN Set: 978-2-35158-190-2, Vol. 1: 978-2-35158-193-3, Vol. 2: 978-2-35158-194-0, Vol. 3: ISBN:978-2-35158-195-7, Vol. 4: ISBN:978-2-35158-196-4, e-ISBN: 978-2-35158-191-9; *Eds. Manu Santhanam, Ravindra Gettu, Radhakrishna G. Pillai and Sunitha K. Nayar*

PRO 119 (online version): ICBBM 2017 - Second International RILEM Conference on Bio-based Building Materials, (2017), e-ISBN: 978-2-35158-192-6; *Eds. Sofiane Amziane, Mohammed Sonebi*

PRO 120 (2 volumes): EAC-02 - 2nd International RILEM/COST Conference on Early Age Cracking and Serviceability in Cement-based Materials and Structures, (2017), Vol. 1: 978-2-35158-199-5, Vol. 2: 978-2-35158-200-8, Set: 978-2-35158-197-1, e-ISBN: 978-2-35158-198-8; *Eds. Stéphanie Staquet and Dimitrios Aggelis*

PRO 121 (2 volumes): SynerCrete18: Interdisciplinary Approaches for Cement-based Materials and Structural Concrete: Synergizing Expertise and Bridging Scales of Space and Time, (2018), Set: 978-2-35158-202-2, Vol.1: 978-2-35158-211-4, Vol.2: 978-2-35158-212-1, e-ISBN: 978-2-35158-203-9; *Eds. Miguel Azenha, Dirk Schlicke, Farid Benboudjema, Agnieszka Knoppik*

PRO 122: SCC'2018 China - Fourth International Symposium on Design, Performance and Use of Self-Consolidating Concrete, (2018), ISBN: 978-2-35158-204-6, e-ISBN: 978-2-35158-205-3; *Eds. C. Shi, Z. Zhang, K. H. Khayat*

PRO 123: Final Conference of RILEM TC 253-MCI: Microorganisms-Cementitious Materials Interactions (2018), Set: 978-2-35158-207-7, Vol.1: 978-2-35158-209-1, Vol.2: 978-2-35158-210-7, e-ISBN: 978-2-35158-206-0; *Ed. Alexandra Bertron*

PRO 124 (online version): Fourth International Conference Progress of Recycling in the Built Environment (2018), e-ISBN: 978-2-35158-208-4; *Eds. Isabel M. Martins, Carina Ulsen, Yury Villagran*

PRO 125 (online version): SLD4 - 4th International Conference on Service Life Design for Infrastructures (2018), e-ISBN: 978-2-35158-213-8; *Eds. Guang Ye, Yong Yuan, Claudia Romero Rodriguez, Hongzhi Zhang, Branko Savija*

PRO 126: Workshop on Concrete Modelling and Material Behaviour in honor of Professor Klaas van Breugel (2018), ISBN: 978-2-35158-214-5, e-ISBN: 978-2-35158-215-2; *Ed. Guang Ye*

PRO 127 (online version): CONMOD2018 - Symposium on Concrete Modelling (2018), e-ISBN: 978-2-35158-216-9; *Eds. Erik Schlangen, Geert de Schutter, Branko Savija, Hongzhi Zhang, Claudia Romero Rodriguez*

PRO 128: SMSS2019 - International Conference on Sustainable Materials, Systems and Structures (2019), ISBN: 978-2-35158-217-6, e-ISBN: 978-2-35158-218-3

PRO 129: 2nd International Conference on UHPC Materials and Structures (UHPC2018-China), ISBN: 978-2-35158-219-0, e-ISBN: 978-2-35158-220-6;

PRO 130: 5th Historic Mortars Conference (2019), ISBN: 978-2-35158-221-3, e-ISBN: 978-2-35158-222-0; *Eds. José Ignacio Álvarez, José María Fernández, Íñigo Navarro, Adrián Durán, Rafael Sirera*

PRO 131 (online version): 3rd International Conference on Bio-Based Building Materials (ICBBM2019), e-ISBN: 978-2-35158-229-9; *Eds. Mohammed Sonebi, Sofiane Amziane, Jonathan Page*

PRO 132: IRWRMC'18 - International RILEM Workshop on Rheological Measurements of Cement-based Materials (2018), ISBN: 978-2-35158-230-5, e-ISBN: 978-2-35158-231-2; *Eds. Chafika Djelal, Yannick Vanhove*

PRO 133 (online version): CO2STO2019 - International Workshop CO2 Storage in Concrete (2019), e-ISBN: 978-2-35158-232-9; *Eds. Assia Djerbi, Othman Omikrine-Metalssi, Teddy Fen-Chong*

RILEM Reports (REP)

Report 19: Considerations for Use in Managing the Aging of Nuclear Power Plant Concrete Structures (ISBN: 2-912143-07-1); *Ed. D. J. Naus*

Report 20: Engineering and Transport Properties of the Interfacial Transition Zone in Cementitious Composites (ISBN: 2-912143-08-X); *Eds. M. G. Alexander, G. Arliguie, G. Ballivy, A. Bentur and J. Marchand*

Report 21: Durability of Building Sealants (ISBN: 2-912143-12-8); *Ed. A. T. Wolf*

Report 22: Sustainable Raw Materials - Construction and Demolition Waste (ISBN: 2-912143-17-9); *Eds. C. F. Hendriks and H. S. Pietersen*

Report 23: Self-Compacting Concrete state-of-the-art report (ISBN: 2-912143-23-3); *Eds. Å. Skarendahl and Ö. Petersson*

Report 24: Workability and Rheology of Fresh Concrete: Compendium of Tests (ISBN: 2-912143-32-2); *Eds. P. J. M. Bartos, M. Sonebi and A. K. Tamimi*

Report 25: Early Age Cracking in Cementitious Systems (ISBN: 2-912143-33-0); *Ed. A. Bentur*

Report 26: Towards Sustainable Roofing (Joint Committee CIB/RILEM) (CD 07) (e-ISBN 978-2-912143-65-5); *Eds. Thomas W. Hutchinson and Keith Roberts*

Report 27: Condition Assessment of Roofs (Joint Committee CIB/RILEM) (CD 08) (e-ISBN 978-2-912143-66-2); *Ed. CIB W 83/RILEM TC166-RMS*

Report 28: Final report of RILEM TC 167-COM 'Characterisation of Old Mortars with Respect to Their Repair (ISBN: 978-2-912143-56-3); *Eds. C. Groot, G. Ashall and J. Hughes*

Report 29: Pavement Performance Prediction and Evaluation (PPPE): Interlaboratory Tests (e-ISBN: 2-912143-68-3); *Eds. M. Partl and H. Piber*

Report 30: Final Report of RILEM TC 198-URM 'Use of Recycled Materials' (ISBN: 2-912143-82-9; e-ISBN: 2-912143-69-1); *Eds. Ch. F. Hendriks, G. M. T. Janssen and E. Vázquez*

Report 31: Final Report of RILEM TC 185-ATC 'Advanced testing of cement-based materials during setting and hardening' (ISBN: 2-912143-81-0; e-ISBN: 2-912143-70-5); *Eds. H. W. Reinhardt and C. U. Grosse*

Report 32: Probabilistic Assessment of Existing Structures. A JCSS publication (ISBN 2-912143-24-1); *Ed. D. Diamantidis*

Report 33: State-of-the-Art Report of RILEM Technical Committee TC 184-IFE 'Industrial Floors' (ISBN 2-35158-006-0); *Ed. P. Seidler*

Report 34: Report of RILEM Technical Committee TC 147-FMB 'Fracture mechanics applications to anchorage and bond' Tension of Reinforced Concrete Prisms – Round Robin Analysis and Tests on Bond (e-ISBN 2-912143-91-8); *Eds. L. Elfgren and K. Noghabai*

Report 35: Final Report of RILEM Technical Committee TC 188-CSC 'Casting of Self Compacting Concrete' (ISBN 2-35158-001-X; e-ISBN: 2-912143-98-5); *Eds. Å. Skarendahl and P. Billberg*

Report 36: State-of-the-Art Report of RILEM Technical Committee TC 201-TRC 'Textile Reinforced Concrete' (ISBN 2-912143-99-3); *Ed. W. Brameshuber*

Report 37: State-of-the-Art Report of RILEM Technical Committee TC 192-ECM 'Environment-conscious construction materials and systems' (ISBN: 978-2-35158-053-0); *Eds. N. Kashino, D. Van Gemert and K. Imamoto*

Report 38: State-of-the-Art Report of RILEM Technical Committee TC 205-DSC 'Durability of Self-Compacting Concrete' (ISBN: 978-2-35158-048-6); *Eds. G. De Schutter and K. Audenaert*

Report 39: Final Report of RILEM Technical Committee TC 187-SOC 'Experimental determination of the stress-crack opening curve for concrete in tension' (ISBN 978-2-35158-049-3); *Ed. J. Planas*

Report 40: State-of-the-Art Report of RILEM Technical Committee TC 189-NEC 'Non-Destructive Evaluation of the Penetrability and Thickness of the Concrete Cover' (ISBN 978-2-35158-054-7); *Eds. R. Torrent and L. Fernández Luco*

Report 41: State-of-the-Art Report of RILEM Technical Committee TC 196-ICC 'Internal Curing of Concrete' (ISBN 978-2-35158-009-7); *Eds. K. Kovler and O. M. Jensen*

Report 42: 'Acoustic Emission and Related Non-destructive Evaluation Techniques for Crack Detection and Damage Evaluation in Concrete' - Final Report of RILEM Technical Committee 212-ACD (e-ISBN: 978-2-35158-100-1); *Ed. M. Ohtsu*

Report 45: Repair Mortars for Historic Masonry - State-of-the-Art Report of RILEM Technical Committee TC 203-RHM (e-ISBN: 978-2-35158-163-6); *Eds. Paul Maurenbrecher and Caspar Groot*

Report 46: *S*urface delamination of concrete industrial floors and other durability related aspects guide - Report of RILEM Technical Committee TC 268-SIF (e-ISBN: 978-2-35158-201-5); *Ed. Valerie Pollet*

Concrete Materials

You can use an eraser on the drafting table or a sledgehammer on the construction site.– Frank Lloyd Wright

Turning Marginal Aggregates into Useful Concrete Components

A. Bentur(✉) and P. Larianovsky

National Building Research Institute, Faculty of Civil and Environmental Engineering, Technion - Israel Institute of Technology, Haifa, Israel
bentur@technion.ac.il

Keywords: Marginal aggregates · Clays · Micro-fines · Rheological properties · Strength · Shrinkage

1 Introduction

There is increasing pressure to use marginal aggregates for the production of cementitious systems which is motivated by environmental considerations and the depletion of high-quality resources.

Within this context, special attention is given to replacement of fine natural aggregate (sand) in view of the depletion and limitations in quarrying natural material. A major source for replacement is crushed aggregate, known as industrial graded sand, as well as sand which is obtained from various sites where excavations are taking place. The full efficient utilization of such sources of sand is often limited by regulations regarding the presence of large quantities of material smaller than 75 or 63 microns, which are often considered as deleterious dust, as well as contamination of clays. The usual practice is to wash away these materials, and they are being piled up as wastes, leading to an environmental burden on top of the washing process itself which is wasteful in nature. There is interest in allowing incorporation of higher levels of such micro-fines in the concrete, with special focus on the standard methylene blue test for detection of clays, the effects of clays on rheology and on the general properties of cementitious systems, as well as the use of admixtures to mitigate the negative influences of clays and micro-fines, e.g. [1–8].

The advancement in concrete technologies, especially high strength and self compacting concretes, are to a large extent based on efficient use of fillers, having size smaller than 75 microns, in combination with water reducing admixtures which disperse the fillers and turn them into useful component, both at the fresh and hardened state, improving workability and strength and reducing permeability. Normal strength concrete is produced presently with water reducing admixtures and thus there is room to consider this state of affairs to mobilize micro-fines in aggregates which exceed the current standard limitations as fillers, by incorporation of adequate admixtures. This implies a revision in the approach to aggregates, by considering their composition as well as the admixture technologies to be used in the concrete, to optimize the whole pipe-line, ranging from the aggregates to the concrete. The feasibility of this holistic approach was the object of the present study which evaluated crushed fine aggregates

© RILEM 2020
K. Kovler et al. (Eds.): ConcreteLife 2020, RILEM Bookseries 26, pp. 3–7, 2020.
https://doi.org/10.1007/978-3-030-43332-1_1

obtained from local quarries in Israel, in which the micro-fines content was high, as well as presence of swelling clays, all beyond the standard limits.

2 Overview of Research and Testing Program

The study included two parts, the first one dealing with characterization of micro-fines obtained from various sources and studying their mineralogy, particle size and the rheological behavior in mortars prepared with "engineered sand", which was made up of high quality siliceous sand in which replacements of up to 30% by the various micro-fines were implemented.

The second part included study of the rheological properties of concretes made with these micro-fines and adjustment of their fresh properties to obtain adequate workability (similar to reference concrete) by adjustment of admixtures: lignosulfonate, polycarboxylate and clay mitigating admixture (CMA).

The current paper presents part of the results, only those which are relevant to engineering practices and considerations for modifications in the standards.

3 Microfines Characterization

The micro-fines contained a range of montmorillonite clays, up to about 10% by weight, which corresponds to methylene blue values (MBV) higher than 7. Based on calibration curves of methylene blue vs. montmorillonite and kaolinite clays contents, the equivalent montmorillonite content could be calculated from the MBV, and reasonable agreement between that value and the one obtained by XRD were found. The effect of the micro-fines content and their MBV on the yield value was determined in rheological tests (1:3 mortars at a constant w/c ratio of 0.70). The curves can be classified into 3 types, based on the nature of the relation between the yield value and the micro-fines content of the engineered sand. In type I (Low MBV, less than 3), the curve increases monotonously, up to the highest micro-fines content studied, 30%. In type II (Medium MBV, between 4 and 6), the curve increases monotonously, at a rate higher than type I, and at about 25% micro-fines content it shows a turning point of a sharp increase. In type III (High MBV, bigger than 7), there is a steeper monotonous increase and the sharp turning point takes place at a lower micro-fine content of about 15%.

The differences between the three categories can be observed alternatively, in more "friendly" engineering terms, by determining the increase in the mortars water demand for 20% micro-fines content engineered sand, as a function of the MBV, Fig. 1.

For type I, the increase in water demand is about 8%, and it remains constant up to about MBV of 3, in type II it increases gradually to about 13%, and at type III the increase is very sharp.

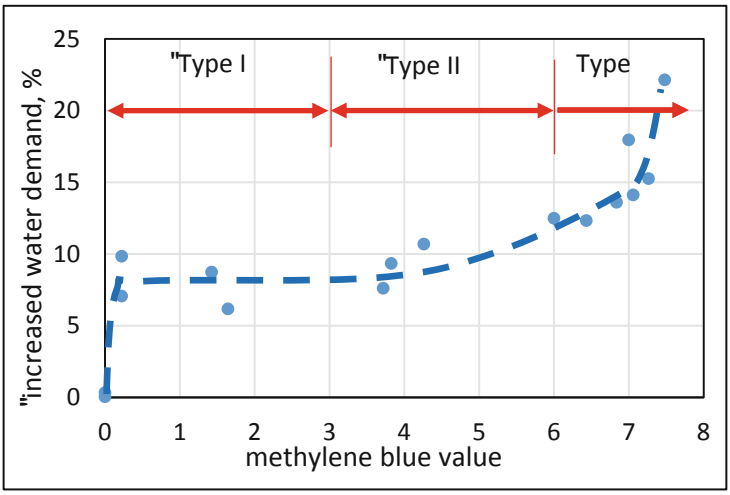

Fig. 1. The increase in water demand of mortars prepared with engineered sands containing 20% different types of micro-fines, as a function of their MBV

4 Concretes

The three categories identified in Fig. 1 were reflected also in the means which need to be taken with regards to reducing the water content to the level of the reference concrete. In the case of Type I and II, water reducing admixtures were sufficient (lignosulfonate or polycarboxylate), while in type III there was a need to use a combination of polycarboxylate and CMA.

The study of concretes resolved that in the mix design the more relevant inputs should be the total content of micro-fines in the concrete rather than the micro-fines content in a specific aggregate, as shown in Fig. 2. This figure presents the type and content of admixture required to obtain workability (slump or yield value) similar to the reference concrete, as a function of the content of the micro-fines and their nature (low, medium and high MBV).

It can be seen that for the low and medium MBV either lignosulfonate or polycarboxylate was sufficient. There seems to be a threshold level of micro-fines, in the range between 100 and 150 kg/m^3, where transition from lignosulfonate to polycarboxylate is required; contents of lignosulfonate bigger than about 1% by weight of cement induced retardation, and that is where the transition threshold was placed. Above the threshold, the content of polycarboxylate required increased with the micro-fines content, and the range of admixture contents in the figure reflects the differences between the types I and II micro-fines (low and medium MBV). The type III micro-fines (high MBV) required combination of polycarboxylate and CMA. The CMA required was found to be about 1/3 of the content of equivalent montmorillonite, as calculated from the MBV.

The tests of mature concretes with micro-fines and optimal admixture indicated that filler effects could be mobilized, as indicated by microstructural observations and

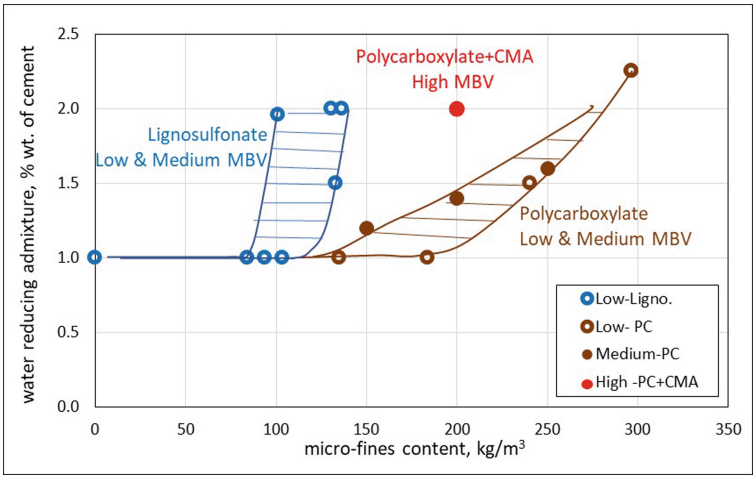

Fig. 2. The content and type of admixture required to achieve workability similar to reference concrete as a function of the content of micro-fines and their nature as determined by the MBV

strength determination. In concretes with micro-fines content bigger than 100 kg/m^3 the strength gradually increased above the reference concrete having the same w/c ration. The strength gain at 28 days is about 30%, while at one day the strength gain was even higher. The higher strength at early age could be related with the effects of the carbonate and dolomitic micro-fines on acceleration of hydration reactions.

Shrinkage tests demonstrated that at the optimum admixture contents the shrinkage was practically independent of the micro-fine content.

5 Conclusions

- In order to mobilize effectively the use of marginal aggregates with high micro-fines content there is a need for a holistic approach, considering the whole pipeline of the aggregates and concretes, which should be based on concrete performance rather than aggregate composition.
- Micro-fines can be categorized into three types, depending on their MBV, low (<3), medium (4–6) and high (>7), showing differences in increased water demand at each category.
- The strategy for neutralizing the effect of micro-fines on increased water demand in concrete can be quantified in terms of combination of their content in concrete and their MBV.
- The effect of low and medium MBV aggregates on the water requirement can be neutralized by lignosulfonates when their content in the concrete is below a threshold value of about 150 kg/m^3, and polycarboxylates are required at higher content; for high MBV aggregate, combination of polycarboxylate and CMA is required.

- At the optimum admixture content and type, beneficial effect of strength increase is obtained, due to mobilization of a filler effect of the micro-fines. This strength increase can be considered in terms of economic effect, to counteract the added cost of the required admixtures.

References

1. Katz, A., Baum, H.: Effect of high levels of fines content on concrete properties. ACI Mater. J. **103**, 474–482 (2006)
2. Quiroga, P.N., Ahn, N., Fowler, D.W.: Concrete mixtures with high microfines. ACI Mater. J. **103**, 258–264 (2006)
3. Nehdi, M.I.: Clay in cement based materials: critical review of state of the art. Constr. Build. Mater. **51**, 372–382 (2014)
4. Yukselen, Y., Kaya, A.: Suitability of the methylene blue tests for surface area, cation exchange capacity and swell potential of clayey soils. Eng. Geol. **102**, 38–45 (2008)
5. Fernandes, V.A., Purnell, P., Still, G.T., Thomas, T.H.: The effect of clay content in sands used for cementitious materials in developing countries. Cem. Con. Res. **37**, 751–758 (2007)
6. Tregger, N.A., Pakula, M.E., Shah, S.P.: Influence of clays on the rheology of cement pastes. Cem. Concr. Res. **40**, 384–391 (2010)
7. Norvell, J.K., Stewart, J.G., Juenger, M.C.G., Fowler, D.W.: Influence of clay-sized particles on concrete performance. ASCE J. Mat. Civ. Eng. **19**, 1053–1059 (2007)
8. Jeknavorian, A.A., Jardine, L., Ou, C.C., Koyata, H., Folliard, K.: Interaction of superplasticizers with clay-bearing aggregates. In: Malhotra, V.M. (ed.) Proceedings of the 7th CANMET/ACI International Conference on Superplasticzers and Other Chemical Admixtures in Concrete, Special Publication (SP-217). American Concrete Institute (2003)

Variation in Phase Quantification of White Portland Cement by XRD

J. A. Canul-Polanco(✉) and O. M. Jensen

Technical University of Denmark, Lyngby, Denmark
janpo@byg.dtu.dk

Keywords: White Portland cement · X-ray diffraction · Rietveld refinement

1 Introduction

X-ray diffraction has been used for at least a century in the cement industry to identify the crystalline phases of Portland cement [1]. More recently, the quantification of phases by X-ray diffraction (QRXD) together with other microstructural techniques have been successfully applied to Portland cement [2].

To improve the QXRD analysis, different pretreatments procedures have been considered, such as grinding to a particle size below 5 μm and chemical selective dissolution [3]. For example, an aqueous solution of KOH and sucrose is used to produce a residue rich in alite and belite, whereas salicylic acid and methanol results in a residue containing aluminate, ferrite, sulfate, and other minor phases. However, those methods can be time-consuming, and in the cement industry, it is preferred to use fast but still reliable methods.

In this project, QXRD was used for phase quantification of white Portland cement (WPC) without any selective chemical dissolution or physical grinding before the measurements. This paper also describes the challenges presented during the measuring and refinement to quantify the crystalline phases of the WPC. All samples were analyzed through the software High Score Plus (HSP) and the external method for quantification of the amorphous phase.

2 Experimental Details

The samples were measured under the following conditions (Table 1):

© RILEM 2020
K. Kovler et al. (Eds.): ConcreteLife 2020, RILEM Bookseries 26, pp. 8–12, 2020.
https://doi.org/10.1007/978-3-030-43332-1_2

Table 1. Conditions of the XRD measurements.

Data collection properties and settings		
Model	Type	PANalytical, X'Pert3 powder
X-ray source	X-ray radiation	CuK$\alpha_{1,2}$ (λ = 1.5406 Å), line focus
	Generator operation	45 kV, 40 mA
Diffractometer optics	Incident divergence slit	0.5° fixed
	Incident anti-scatter slit	1° fixed
	Incident beam mask	10 mm
	Incident Soller slits	0.04 rad
	Receiving anti-scatter slit	1° fixed
	Receiving Soller slits	0.04 rad
	Scanning mode	Continuous
	Detector type	X'celerator
	Detector length	2.122° 2θ linear position-sensitive X-ray det.
	Spinning speed	4 rpm
	Sample	Back loaded in powder
Scan parameters	Angular range	5–70° 2θ
	Step size	0.02° 2θ
	Time per step	30 s
	Total measurement	30 min

For the XRD pattern deconvolution, the Rietveld refinement method was used with the HSP software. The refinement was done under the following considerations:

- The background was refined using a flat background, a polynomial function with 4–5 coefficients, the 1/x term, and the correction for specimen displacement was applied.
- The zone between 5 and 7° 2θ was left out of the analysis.
- The scale factor, unit cell, and profile (w Cagliotti parameter) were refined for each crystalline phase. The variation for the unit cell was constrained to one percent, and the w parameter had a limit between 0.0001 to 0.2.
- Preferred orientation correction factors were applied for some phases constraining the factor between 0.7 and 1 with March-Dollase correction. In the particular case of gypsum, two different approaches were performed, the spherical harmonics with an order of 8, and the March-Dollase correction with a factor constrained between 0.4 and 1.
- The external standard used was α-Al_2O_3 corundum, with a known crystallinity of 99.5%. The same conditions of measurement and refinement were applied. In addition to this, the refinement included an asymmetry function "split width and shape".

3 Results

Figure 1 (left) shows an XRD measurement of WPC under the conditions given in Table 1. The main crystalline phases found were: Alite M3 (A-M3), Alite M1 (A-M1), β-Belite (β-B), γ-Belite (γ-B), tricalcium aluminate cubic (C3A), basanite (BA), gypsum (G), portlandite and calcite (the last two not indicated in Fig. 1). However, the gypsum peak in plane 020 (position °2θ: 11.68) shows a high degree of preferred orientation (PO). Therefore, the measurement was performed in a total of four times on the same WPC: two different samples were measured at two different instruments (with repacking between measurements). The gypsum peak (020) remained with a similar high intensity. Figure 1 (right) shows a measurement performed with different conditions, but the gypsum peak (020) remained the same, and other phases showed less intensity.

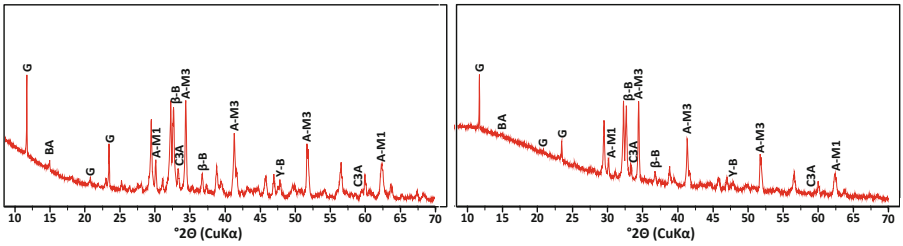

Fig. 1. Crystalline phases found in the WPC. Left: XRD measurement, as described in Table 1. Right: XRD measurement under an incident anti-scatter slit of 2°, receiving anti-scatter slit of 2°, and a higher spinning speed of 16 rpm. Both measurements are done on instrument 1.

Among the different approaches to minimize PO [4, 5], it was chosen to mix the cement with an amorphous filler material. In this case, silica fume (SF) was used. Therefore, a mixture of anhydrous WPC with 5% SF was measured (Fig. 2 left and right). Also, these measurements were done like for the WPC samples above; two different samples were measured at two different instruments and different instrument settings. It is seen that the addition of a second powder offset the gypsum peak (position °2θ: 11.68).

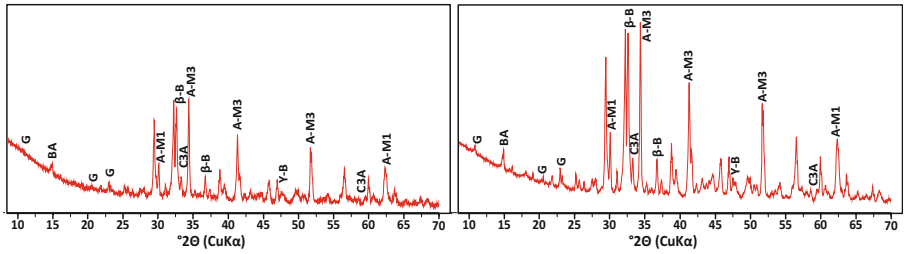

Fig. 2. XRD measurements of WPC with 5% SF with two different diffractometers (Left: Instrument 1 and Right: Instrument 2). Left: XRD measurement conditions, as given in Table 1. Right: XRD measurement conditions such as incident anti-scatter slit of 2°, receiving anti-scatter slit of 7.5 mm, and spinning speed of 4 rpm. Instrument 2 was a PANalytical, Empyrean model.

The Rietveld refinement was applied to all measurements, as described in the section of experimental details. One of the challenges during refinement was to identify the PO of phases besides gypsum: calcite (104), alite (606), and portlandite (002). Another important parameter during the refinement was the background. The phase content could change as a function of the choice of background [6]. In HSP, a manual or automatic background can be chosen. All refinements were performed on automatic with a bending factor of 0 and granularity of 6.

The phase quantification of the cement is shown in Table 2. Results were normalized to 100%, excluding amorphous content (in particular SF). Some significant differences can be observed. There are three possible reasons for these variations: instrument type, measurement configuration, or the SF addition. The dry mixture of a crystalline material with the amorphous filler material gives rise to scattering in the diffraction pattern, increasing the background (not seen in Fig. 2 due to scaling), plus contamination [5]. Even if it is not noticeable in Fig. 2, the statistical improvement (R_{wp} and GOF) in the WPC-SF and WPC-SF-2 results is partly a consequence of increasing the background by adding SF (see Table 2).

Table 2. Phases quantification results of samples with and without SF addition. R_{wp}: weighted R profile, GOF: goodness of fit. NC: No correction for preferred orientation during refinement, Total $CaSO_4$: refers to the sum of the percentage contents of gypsum and basanite.

Phases	Instrument 1			Instrument 2		
	XRD Rietveld WPC^{NC} (wt%)	XRD Rietveld WPC (wt%)	XRD Rietveld WPC-SF (wt%)	XRD Rietveld $WPC\text{-}2^{NC}$ (wt%)	XRD Rietveld WPC-2 (wt%)	XRD Rietveld WPC-SF-2 (wt%)
Alite M3	39,0	43,6	43,5	41,3	42,1	43,0
Alite M1	26,7	21,9	24,1	25,3	24,1	25,0
B-belite	22,3	22,3	22,2	22,2	23,2	23,4
γ-belite	1,9	2,5	2,1	1,9	1,8	1,8
C_3A	2,8	3,2	1,7	2,7	3,0	1,8
Portlandite	1,0	1,1	0,4	1,7	1,4	1,0
Calcite	0,8	0,5	0,6	0,6	0,8	1,1
Gypsum	3,6	2,3	1,3	3,1	2,4	0,0
Basanite	1,9	2,6	4,0	1,3	1,2	2,9
Total alite	**65,7**	**65,5**	**67,6**	**66,6**	**66,2**	**68,0**
Total belite	**24,2**	**24,8**	**24,3**	**24,1**	**25**	**25,2**
Total $CaSO_4$	**5,5**	**4,9**	**5,3**	**4,4**	**3,6**	**2,9**
R_{wp}	*11,2*	*6,8*	*6,5*	*7,8*	*6,5*	*6,1*
GOF	*4,6*	2,9	*2,7*	*5,5*	*4,6*	*4,3*

The Rietveld refinement was performed with and without the PO models (March Dollase and Spherical Harmonics). The use of PO models resulted in a better refinement considering only R_{wp} and GOF factors (Table 2). However, the use of these

models might reduce the accuracy of the quantification of other phases without any PO. The two alite polymorphs M3 and M1 are difficult to quantify individually by XRD due to their close similarities in XRD spectra. However, their quantified sum seems to be fairly constant independently of the analysis, method, and instrumentation. Since the reactivity and other properties of the alite polymorphs are almost identical, the uncertainty of their individual quantification has no practical relevance.

The followed methodology in this project can lead to 2% or less variation in phases content. It is shown in Table 2 how the SF addition increases the variation of quantification of minor phases for the same WPC refined with the same software and method. On the other hand, using a different instrument and configuration leads to a variation of no more than 1.5%.

The preferred orientation of phases should be analyzed carefully. For this particular applied method, the total $CaSO_4$ content did not vary more than 1% between the refinements with and without SF. However, it was mentioned that for a specific phase determination, other methods might be applied to have more precise results.

4 Conclusions

The following conclusions can be drawn for the specific WPC evaluated in this study:

1. The high intensity of gypsum in the plane 020 due to preferred orientation was confirmed by using a dry mix of 5% silica fume and 95% white Portland cement.
2. The SF addition method can significantly reduce the intensity and PO of some phases.
3. Statistically, the use of PO models improves refinement.
4. The refinement method used in this project gives an approximately 2% variation (max.) in the quantification of samples measured in different instruments and measurement configurations.

References

1. Brownmiller, L.T., Bogue, R.H.: The X-Ray method applied to a study of the constitution of Portland cement. Bur. Stan. J. Res. **5**, 813–830 (1930)
2. Stutzman, P.E., Feng, P., Bullard, J.W.: Phase analysis of Portland cement by combined quantitative X-ray powder diffraction and scanning electron microscopy. J. Res. Nat. Inst. Stan. Technol. **121**, 47–107 (2016)
3. Scrivener, K., Snellings, R., Lothenbach, B.: A Practical Guide to Microstructural Analysis of Cementitious Materials. Taylor & Francis Group, Abingdon (2016)
4. Christidis, G.E.: Advances in the characterization of industrial minerals. The mineralogical society of Great Britain & Ireland, 9, London, UK (2011)
5. Bish, D.L., Post, J.E., et al.: Modern powder diffraction. The mineralogical society of America, 20, Washington, D.C. (2018)
6. Kocaba, V.: Development and evaluation of methods to follow microstructural development or cementitious systems including slags. École polytechnique fédérale de Lausanne, Ph.D. thesis, Switzerland (2009)

Comparison of Clinkers Produced Using Different Layers of Oil Shale

A. Goncharov(✉) and S. Zhutovsky

Technion - Israel Institute of Technology, Haifa, Israel
gantonina@campus.technion.ac.il

Keywords: Oil shale · Clinker · Cement production · Clinker raw meal

1 Introduction

Oil shale is one of the largest energy resources today. Oil shales are horizontally layered rocks that have rich organic content called kerogen and mineral part is usually composed of clay, quartz, and carbonates such as calcite and dolomite [1]. Oil shale can be used either to extract liquid hydrocarbons or to burn directly to produce electric energy. Due to their different origins, oil shales have different calorific values because of the variation in the content and composition of kerogen. The composition of the mineral matrix in oil shales also varies. Oil shales can be classified into three categories based on mineral composition: carbonate-rich shale, siliceous shale and cannel shale [2]. Silica-rich oil shale ashes are likely to develop pozzolanic properties whereas carbonate-rich materials can also develop hydraulic properties. Oil shale has been used for cement production in Estonia, Germany, Russia, China, and the USA.

The inorganic part of oil shale can be an attractive source of raw materials for the cement industry. Oil shale can replace the typical raw materials in clinker, such as clay, without significantly changing the mineral composition of clinker, which is especially valuable for the Israeli cement industry. Israel has proven reserves of oil shale that are currently not developed in sufficient volume [3]. Earlier, the experimental power plant, which produced electric energy by burning oil shale, operated by the PAMA Company that began operation in 1989 and has since been closed, because the grade of the Rotem oil shale was not uniform (the calorific value ranged from 2.7 to 5 MJ/kg). In addition, Israeli oil shale has a high ash content, which also negatively affects its use as a fuel in power plants. Also, the calcium oxide contained in the ashes is active and reacts with carbon dioxide to form calcite. Calcite, in turn, reacts with sulfur dioxide and forms anhydrite, which deposits hard plaque on the surface of equipment reducing the efficiency of thermal power plants [4]. In combination with low organic content, the use of oil shale for the production of electricity becomes ineffective from an economic and practical point of view.

Previous research demonstrated that oil shales ashes from Israeli power plant Pama contain clinker minerals, anhydrite, calcite, free lime, quartz, and potentially could be used as a binder [5]. Based on this preliminary conclusion, oil shale can be used as a substitute material for clinker production for Portland cement is feasible. Portland cement is made primarily from finely ground clinker, which itself is composed of

© RILEM 2020
K. Kovler et al. (Eds.): ConcreteLife 2020, RILEM Bookseries 26, pp. 13–17, 2020.
https://doi.org/10.1007/978-3-030-43332-1_3

calcium silicate and aluminate minerals formed when limestone and clay are burnt at high temperatures. Limestone serves as a source of calcium, and clay serves as a source of silica, alumina, and iron. These minerals are generally mined in open quarries. Israel has sufficient resources of limestone, but the clay is already in short supply. Oil shale can be used as fuel and raw material in clinker kilns, as cement clinker manufacture requires energy and minerals. The usage of oil shale can significantly reduce fuel consumption in a rotary kiln, which can be beneficial for the environmental situation due to the reduction of CO_2 emissions to the atmosphere.

The primary aim of this study is to research the potential of Israeli oil shale utilization as a raw clinker material for production clinker for Portland Cement. In this research, the oil shales from Northern Negev, Israel were used. The oil shales of 2 types were studied: upper layer (poor in organic part), the lower layer (rich in organic part) according to the occurrence in oil shale deposition. Many technological aspects, as well as properties of the produced cement, depending on the properties of local oil shale. For this reason, the objective of the current research is the study the physical properties, chemical and mineral composition of raw Israeli oil shale as a potential material for cement production. Another part of the study is the calculation of the clinker raw meal composition for upper and lower oil shale layers, determination of the energy released during the burning process and the mineral composition of the produced clinker.

2 Results

The oil shales from Ghareb Formation mined from quarry Mishor Rotem, Northern Negev, Israel were investigated. Mineral and chemical composition of oil shale were determined using x-ray diffraction (XRD) and inductively-coupled plasma (ICP) spectroscopy, respectively. The results are presented in Table 1. It can be concluded from

Table 1. Mineral and chemical composition of upper and lower raw oil shale layers, % wt.

	Upper layer	Lower layer
Calcite	62.2	59.8
Quartz low	2	2.2
Apatite	0.6	1.8
Anhydrite	0.4	0.4
Gypsum	8.4	15.7
Potassium Phosphate	0.6	1.5
Pyrite	0.9	2.2
Amorphous	24.8	16.3

	Upper layer	Lower layer
CaO	35.6	37.5
SiO_2	10.5	9
Al_2O_3	4.4	3.3
Fe_2O_3	2	1.9
MgO	0.5	0.6
TiO_2	0.19	0.14
K_2O	0.32	0.38
Na_2O	0.19	0.15
P_2O_5	1.02	2.61
Mn_2O_3	0.01	0
SO_3	3.7	4.6
LOI	38.3	40.4

Table 1 that Israeli oil shale belongs to the carbonate-rich oil shales. Silica content in oil shale was low. Therefore its ashes will not be pozzolanically active. However, chemical composition shows, in addition to calcium oxide, the presence of three other main oxides required for clinker: silica, alumina and iron oxide.

The presence of phosphorus can have a significant impact on the clinker quality and production process. Therefore, the use of oil shale as a raw material for clinker can be limited by the concentration of phosphates in it. Calorific values as determined by DSC were 1.97 MJ/kg and 3.616 MJ/kg for upper and lower oil shale layers, respectively.

The target chemical composition of the clinker and chemical composition of each layer of oil shale after burning are presented in Table 2. Based on target mineral composition and clinker moduli (LSF– lime saturation factor, SR–silica ratio, AR–alumina ratio), the maximum oil shale content in the raw meal was calculated as 35 and 39% for upper and lower layer, respectively.

The results of the thermal analysis of raw meals are presented in Fig. 1. It can be seen that dehydration takes place in the range between 30 and 150 °C. In a temperature range from 200 to 600 °C, the major mass loss is due to the decomposition of organic components of oil shale. In a temperature range from 650 to 900 °C, there is the highest mass loss, which is mainly due to the decomposition of calcium carbonate. Above 1100 °C the formation of clinker minerals takes place. With regards to the energy contribution of oil shales to clinker production, it can supply energy from the burning of the organic

Table 2. Target clinker composition and moduli for lower and upper layers

	Upper layer	Lower Layer	OPC Clinker
CaO, %	57.7	62.9	[63 - 67]
SiO_2, %	17.0	15.1	[21 - 24]
Al_2O_3, %	7.1	5.5	[4 - 8]
Fe_2O_3, %	3.2	3.2	[2 - 4]
Energy, MJ/kg	1.97	3.62	[1.68-3.74]

	Upper layer	Lower layer	OPC Clinker
Content	35%	39%	
LSF	0.93	0.95	[0.92-0.98]
SR	2.34	2.37	[2-3]
AR	1.53	1.86	[1-4]
C_3S	56.5	59.8	[50-70]
C_2S	18.5	15.2	[15-30]
C_3A	8.5	10.1	[5-10]
C_4AF	10.9	9.5	[5-15]

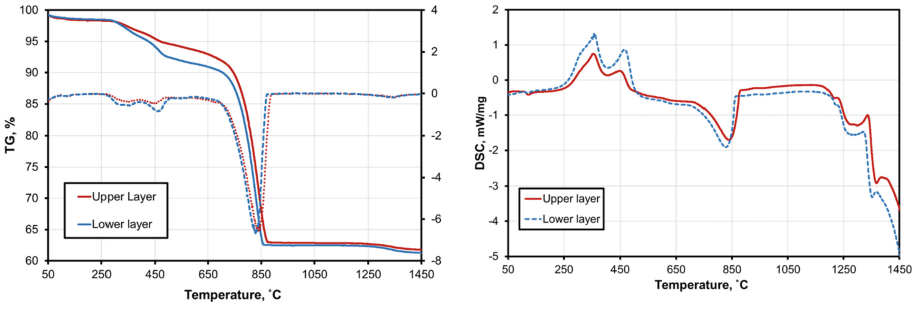

Fig. 1. TGA and DTG (left) and DSC (right) of raw meals in a dry air atmosphere.

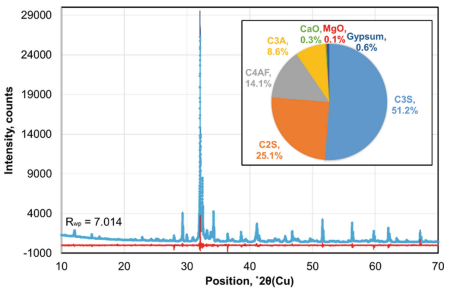

Fig. 2. XRD and phase composition of clinker with oil shale 35% (Upper layer)

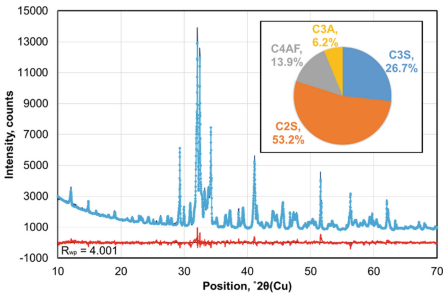

Fig. 3. XRD and phase composition of clinker with oil shale 39% (Lower layer).

fraction at the stages of preheating and calcination. Oil shale can provide 0.7 MJ/kg and 1.4 MJ/kg of clinker for upper and lower layers, respectively.

The clinker raw materials and burned oil shale were weighted and mixed with water to form nodules that were dried in an oven. Clinker nodules were burned at 1450 °C and cooled at the rate of 20 °C/min. to produce clinker. XRD diffractogram of the clinker with oil shale from the upper layer and lower layers are presented in Figs. 2 and 3. These diffractograms show that the clinker rich in alite was obtained from the upper layer and clinker rich in belite was obtained from the lower one. This can be explained by the high concentration of phosphorus oxide in the lower layer of oil shale. For solving this problem magnesium oxide was added as a dopping for stabilizing alite. As shown in Fig. 4, alite clinker was obtained with the addition of 1% magnesia.

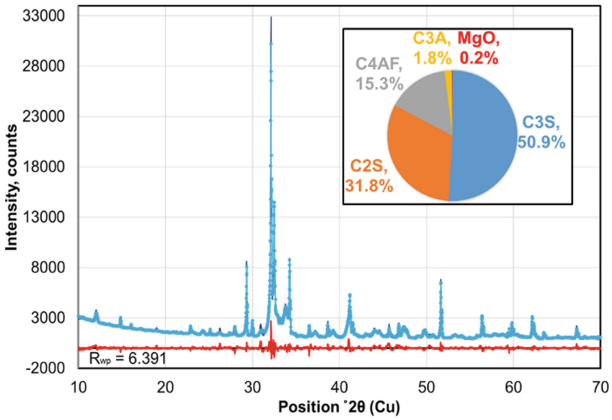

Fig. 4. XRD of clinker oil shale from the lower layer with the addition of 1% MgO.

3 Conclusions

In this study, Israeli oil shale was investigated as a potential raw material for cement production. It was demonstrated that oil shale can replace about 30–40% of raw materials for clinker production. The oil shales can be used unburned partially replacing fuel consumed for clinker preheating and calcination. The lower layer proved the higher potential for clinker production because of lower phosphate content. However, it was demonstrated the problem with phosphates in the upper layer oil shale can be overcome by the use of magnesium dopping.

Acknowledgments. This study was supported by the Ministry of National Infrastructures, Energy and Water Resources, Israel.

References

1. Torres, M., Castiglioni, J., Yermán, L., Suescun, L., Conti, B., Demarco, M.M., Gristo, P., Portugau, P., Cuña, A.: Assessment of Uruguayan Oil Shales: physicochemical, thermal and morphological characterization. Fuel **234**, 347–357 (2018)
2. Kumar, R., Bansal, V., Badhe, R.M., Madhira, I.S.S., Sugumaran, V., Ahmed, S., Christopher, J., Patel, M.B., Basu, B.: Characterization of Indian origin oil shale using advanced analytical techniques. Fuel **113**, 610–616 (2013)
3. Minster, D.T.: Oil Shale Occurrences in Israel. Samuel Neaman Institute, Haifa (2013)
4. Yoffe, O., Wohlfarth, A., Nathan, Y., Cohen, S., Minster, T.: Oil shale fueled FBC power plant-Ash deposits and fouling problems. Fuel **86**, 2714–2727 (2007)
5. Freidin, C., Motzafi-Haller, W.: Cementless building units based on oil shale and coal fly ash binder. Constr. Build. Mater. **13**, 363–369 (1999)

The Effect of Grinding Process on Recycled Cement Paste Fines

D. Kulisch(✉)

National Building Research Institute,
Faculty of Civil and Environmental Engineering,
Technion - Israel Institute of Technology, Haifa, Israel
dkulisch@campus.technion.ac.il

Keywords: Grinding time · Grinding aids · Cement paste fines · Cement paste recycling

1 Introduction

In many countries, major portions of construction and demolition waste (C&DW) consists of concrete waste [1]. The uses of recycled aggregate from concrete waste include both base/sub-base infrastructure and structural applications. Each application requires a different quality and therefore, a different treatment. When concrete waste is crushed, a certain amount of paste/mortar from the original cement mortar remains attached to the aggregate particles, which forms a weak, porous and cracky layer [2]. The use of recycled aggregate in new concrete requires a beneficiation process, which separates the natural aggregate from the attached cement paste/mortar. The clean natural aggregate is used as recycled aggregate, while the attached cement paste/mortar is of no use. As a result, the majority of concrete recycling studies focus on the recycled aggregate only, clean from the attached cement paste/mortar. This work focuses on the old cement paste/mortar itself.

In this work, recycled cement paste fines are produced by different grinding processes. The processes include different grinding techniques; different grinding times and the use of grinding aids (GA) at different concentrations. Grinding aids have been extensively used in the comminution process of cementitious materials due to the reduction in energy consumption, carbon dioxide emissions and costs [3, 4].

2 Materials

Cement: The cement used in this study is Portland cement CEM I 52.5 N produced by Nesher Israel Cement Enterprises Ltd. The chemical and physical properties of the cement are presented in Table 1 (data obtained from Nesher).

© RILEM 2020
K. Kovler et al. (Eds.): ConcreteLife 2020, RILEM Bookseries 26, pp. 18–22, 2020.
https://doi.org/10.1007/978-3-030-43332-1_4

Table 1. Chemical and physical analysis of cement CEM I 52.5 N

Parameter	Value	Parameter	Value
CaO (%)*[1]	62.16	P_2O_5 (%)*[1]	0.4
SiO_2 (%)*[1]	19.02	Mn_2O_3 (%)*[1]	0.05
Al_2O_3 (%)*[1]	5.42	SO_3 (%)*[2]	2.48
Fe_2O_3 (%)*[1]	3.82	IR (%)*[2]	0.76
MgO (%)*[1]	1.31	FL (%)*[4]	2.8
TiO_2 (%)*[1]	0.53	LOI_{950} (%)*[3]	2.52
K_2O (%)*[1]	0.37	Specific surface area (cm^2/g)*[2]	4679
Na_2O (%)*[1]	0.22	Specific density (g/cm^3)*[2]	3.125

*[1]According to inductively coupled plasma (ICP);
*[2]According to EN 196: Methods of testing cement
*[3]According to thermogravimetric analysis (TGA);
*[4]According to ethylene glycol titration method

Chemical Admixture: The chemical admixture used in this study is HTC 698 (Glenium SKY 698), a high range water reducing superplasticizer admixture based on polycarboxylic ether (PCE), with specific gravity of 1.079 and active/solid content of 30% (by mass).

Grinding Aids (GA): The type of grinding aids used in this study is triethanolamine (TEA), a liquid additive of molecular formula of $N(CH_2CH_2OH)_3$, based on amino alcohols, with specific gravity of 1.12 and molecular weight of 149.19 g/mol.

3 Methods

Parent Cement Paste Production

The parent material is produced using cement, water and superplasticizer admixture (SP), with a water/cement ratio of 0.30. Preliminary tests are performed and the workability of the cement paste is adjusted by the addition of SP, achieving a 0.4% of the active/solid content (by mass) in relation to the mass of cement. Cement paste specimens are produced in 50 mm cubes molds. Curing is started one day after casting, when the specimens are removed from the molds and placed in water at (20 ± 1) °C for 7 days. After curing, the specimens are dried in oven at 105 °C until reaching constant mass and after, they are transferred to a low humidity room.

Cement Paste Fines Production

At 28 days from casting, the specimens are tested for compressive strength according to ASTM C109/C109M-2016a [5], followed by crushing in a jaw crusher and several grinding processes, including different grinding techniques (planetary ball mill and vibratory ball mill); different grinding times (15, 30 and 60 min) and the use of grinding aids (GA) at different concentrations (0.05, 0.1, 0.2%).

A planetary ball mill (Planetary Mono Mill Pulverisette 6 classic line) was used, with a zirconia grinding bowl of 80 ml and zirconia grinding balls of 10-mm diameter.

TEA at different concentrations (0.05, 0.1, 0.2%) and grinding times (15, 30 and 60 min.) were used. A vibratory ball mill was used, with a material/cylpebs ratio of 1/20 (stainless steel cylpebs used).

The measurements of Particle Size Distribution (PSD) were performed using Malvern Mastersizer 3000 with isopropyl alcohol as dispersion liquid.

4 Results

Compressive strength at 28 days results in an average of 53.6 MPa with a standard deviation of 6.2 (25 cubes were prepared and tested). It should be noticed that the compressive strength refers to a 7-days strength due to the sample preparation process, where samples were are dried in oven at 105 °C and transferred to a low humidity room at the age of 7 days, stopping the further development of hydration. PSD results are presented in Fig. 1 and the parameters extracted from the test are summarized in Table 2.

In order to perform a better analysis and understanding, the curves from Fig. 1 are separated as follows in Figs. 2 and 3.

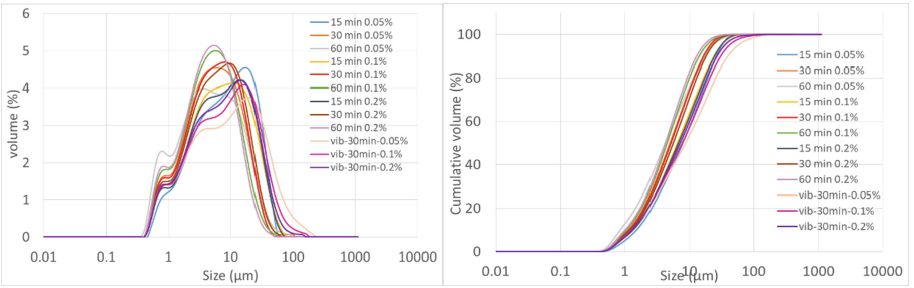

Fig. 1. PSD of cement paste fines. Left: volume curves, Right: cumulative volume curves.

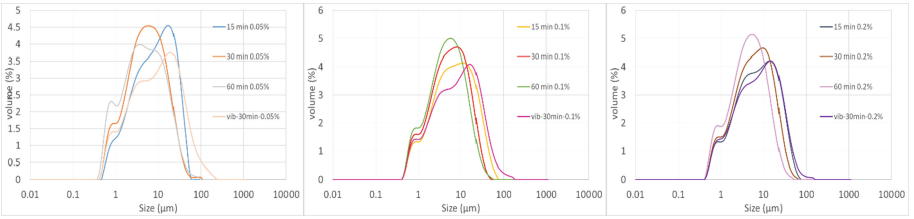

Fig. 2. Volume curves of cement paste fines. Left: different grinding times for 0.05% TEA; Middle: different grinding times for 0.1% TEA; Right: different grinding times for 0.2% TEA.

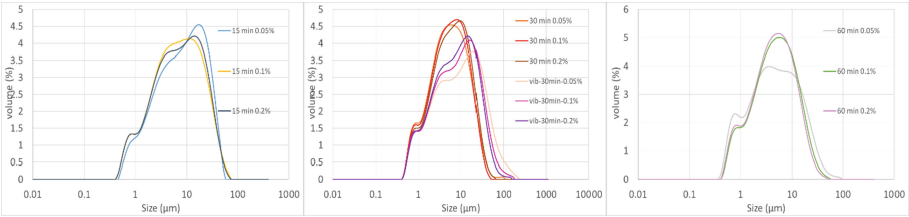

Fig. 3. Volume curves of cement paste fines. Left: different TEA concentrations for 15 min grinding; Middle: different TEA concentrations for 30 min grinding; Right: different TEA concentrations for 60 min grinding.

Table 2. Parameters from PSD

Grinding technique	Grinding time and GA	D10 (µm)	D50 (µm)	D90 (µm)	Specific surface area (m^2/kg)
Planetary	15 min, 0.05%	1.71	8.90	29.70	1382
	30 min, 0.05%	1.29	5.60	19.50	1860
	60 min, 0.05%	0.95	4.54	18.90	2344
	15 min, 0.1%	1.51	7.31	28.00	1574
	30 min, 0.1%	1.34	6.06	19.40	1788
	60 min, 0.1%	1.19	5.01	15.70	2010
	15 min, 0.2%	1.48	7.33	27.20	1595
	30 min, 0.2%	1.37	6.12	20.20	1758
	60 min, 0.2%	1.13	4.72	14.20	2116
Vibratory	30 min, 0.05%	1.39	9.01	42.00	1557
	30 min, 0.1%	1.41	8.27	33.60	1583
	30 min, 0.2%	1.44	7.82	30.00	1586

5 Conclusions

From the results, there is a clear tendency in the planetary mill samples, in which at the same concentration of GA, the shorter grinding (15 min) generates coarser particles and the longest grinding (60 min) generates finer particles, for all GA concentrations (Fig. 2). These results are confirmed by the parameters shown in Table 2. At the same grinding time, the tendency is not so clear. For 15 min grinding, samples with 0.1% and 0.2% TEA presented very similar results, while the 0.05% TEA presented coarser particles (Fig. 3, left). For 60 min grinding, the same tendency is found in particles larger than approximately 5 µm. However, below this size, samples with 0.1% and 0.2% TEA presented very similar results, while the 0.05% TEA presented finer particles (Fig. 3, right). For 30 min grinding, all the TEA concentrations presented similar results (Fig. 3, middle).

In the vibratory mill, the tendency is clear. A higher concentration of TEA generates finer particles and a lower concentration of TEA generates coarser particles (Fig. 3, middle). These results are confirmed by the parameters shown in Table 2.

It is interesting to notice that the same grinding time and the same TEA concentration using both methods (vibratory and planetary mills) presented different results, which proves that not only time and grinding aids affect the grinding efficiency but also the grinding technique and equipment. When comparing both techniques at the same TEA concentration, we can see that for all TEA concentrations, the vibratory mill (30 min) generates results similar to the planetary mill (between 15 and 30 min) for the finest portion of the sample (below 2-4 μm), and similar to the 15 min grinding (even coarser) for the portion above this size (Fig. 2).

Regarding solely PSD, the planetary milling seems to be a more suited technique for grinding cement paste into recycled cement paste fines.

References

1. Akhtar, A., Sarmah, A.K.: Construction and demolition waste generation and properties of recycled aggregate concrete: a global perspective. J. Clean. Prod. **186**, 262–281 (2018)
2. Tam, V.W.Y., Tam, C.M., Le, K.N.: Removal of cement mortar remains from recycled aggregate using pre-soaking approaches. Resour. Conserv. Recycl. **50**(1), 82–101 (2007)
3. Toprak, N.A., Altun, O., Aydogan, N., Benzer, H.: The influences and selection of grinding chemicals in cement grinding circuits. Constr. Build. Mater. **68**, 199–205 (2014)
4. Sun, Z., Liu, Y.: A grindability model for grinding aids and their impact on cement properties. Adv. Cem. Res. **28**(7), 475–484 (2016)
5. ASTM C109/C109M-2016: Standard Test Method for Compressive Strength of Hydraulic Cement Mortars (Using 2-in. or [50-mm] Cube Specimens) (2016)

Effect of Soaking Time in a Solvent on Hydration Stoppage of Cement

A. Mezhov(✉), D. Kulisch, A. Goncharov, and S. Zhutovsky

National Building Research Institute,
Faculty of Civil and Environmental Engineering,
Technion – Israel Institute of Technology, Haifa, Israel
alexander.m@technion.ac.il

Keywords: Hydration stoppage · Soaking time · MIP · X-ray diffraction

1 Introduction

In order to study the composition and microstructure of any hardening cementitious material, the ongoing hydration must be stopped [1]. At early hydration stages, the hydration stoppage is needed to suppress the further progress of hydration [2], allowing the analysis of several properties and characterization of the same sample at the same hydration age and therefore, at the same degree of hydration [3, 4]. After stopping hydration, the samples can receive additional treatments (crushing, cutting, drying, putting under vacuum) with no further progress of hydration [3]. At longer hydration times (longer than 1 month), since the progress of hydration is very slow, the hydration stoppage is performed to fulfill a requirement of several materials characterization techniques, such as thermogravimetric analysis, infrared and Raman spectroscopy, mercury intrusion porosimetry, scanning electron microscopy [1, 2], nitrogen sorption/desorption and transmission electron microscopy [3]. Even for techniques that do not specifically require hydration stoppage, such as X-ray diffraction and nuclear magnetic resonance, the process is usually done since it enables sample storage, helps to minimize carbonation due to the low relative humidity after stoppage and allows the characterization at the same degree of hydration [2].

The main goal of the hydration stoppage is the removal of water inside the pores without altering the hydration products and preserving the microstructure [2]. Commonly used hydration stoppage methods include direct drying techniques: oven drying, vacuum drying and freeze-drying [2, 4] and solvent exchange methods: free water is replaced by an organic solvent miscible with water (first step) and the solvent is removed by evaporation (second step). Commonly used solvents are isopropanol, ethanol, methanol and acetone [4]. In case of a solvent exchange method, the main critical factor influencing on the hydration stopping efficiency is solvent soaking time, which is expressed through (Eq. 1):

$$t_E = \frac{a^2}{D} \tag{1}$$

where t_E is equilibrium time, a is the characteristic dimension and D is the diffusivity.

© RILEM 2020
K. Kovler et al. (Eds.): ConcreteLife 2020, RILEM Bookseries 26, pp. 23–27, 2020.
https://doi.org/10.1007/978-3-030-43332-1_5

The process is modeled as diffusion from a sphere into a surrounding bath. If the volume of a bath is much greater than that of the sample, then the composition of the bath can be assumed to be constant (e.g., pure isopropyl alcohol) [3]. Using the diffusion equation for a sphere and a typical value of diffusivity for alcohol in cement paste ($D = 10^{-11}$ m^2/s), the time to replace the water with 99.9% isopropyl alcohol in a granule of cement paste with a radius of 1 mm would be roughly 18 h [3]. In [5], using the same diffusion coefficient and the same thickness the time for ion diffusion starting to have effects on ion concentration throughout the specimen is calculated as less than 1 h. The value of 15 min suggested in [4] for the same particle size.

Since there is no consensus regarding the required time for the complete stopping of hydration further research is needed. The current paper aims to investigate the influence of the soaking time in a solvent on the mineral composition and pore structure of the hydrated cement paste.

2 Materials and Methods

2.1 Materials

CEM I 52.5N supplied by Nesher Cement, Israel is used for this study. Its mineral and chemical composition are presented in Table 1.

Table 1. Mineral and chemical composition of cement.

Mineral composition	wt.-%
Alite	61.02
Belite	12.95
C_3A cubic	5.86
C_4AF	12.42
Bassanite	1.87
Anhydrite	0.28
Portlandite	1.83
Calcite	2.25
Arcanite	0.97
Aphthitalite	0.55

Chemical composition	wt.-%
CaO	62.16
SiO_2	19.02
Al_2O_3	5.42
Fe_2O_3	3.82
MgO	1.31
TiO_2	0.53
K_2O	0.37
Na_2O	0.22
P_2O_5	0.4
Mn_2O_3	0.05
SO_3	2.48
IR	0.76
FL	2.8
LOI total	2.93

2.2 Preparation of Samples

Cement was mixed with water in a pan mixer and then cast in molds 2.5 × 2.5 × 2.5 cm. The water to cement ratio was 0.40. After 24 h hydration in sealed molds, samples were immersed in water for the additional 6 days. Then the cubes were crushed manually by a

mortar and pestle and sieved. Particles that passed a sieve 4.75 mm and retained on a sieve 2.36 mm were immersed with isopropyl alcohol (IPA) for ¼, ½, 1 and 24 h. Immediately after removing the samples from the solvent they were placed in a vacuum oven at 40 °C for 3 h.

2.3 X-Ray Diffraction (XRD)

The X-ray diffraction analysis was performed using a Malvern PANAlytical EMPYREAN X-ray diffractometer with the following configuration: an X-ray source was CuKα1,2 (λ = 1.5408 Å) with X-Ray generator operated at a voltage of 45 kV and a current of 40 mA; a Goniometer radius was 240 mm; the incident beam optics included 10 mm mask, 0.04 rad Soller slit along with ¼° divergence and 1° anti-scatter fixed slits; the diffracted beam optics consisted of 8 mm anti-scatter fixed slit and 0.04 rad Soller slit. The detector was PIXcel 3D detector used in 1D continuous scan mode. The scan was performed using Brag-Brentano geometry, between 10 and 70 °2θ for unhydrated cement and between 5 and 70 °2θ for hydrated cement paste. After stopping hydration, configuration was changed because of different scanning angles. Also time step, step size and total time were different between cement and cement paste. Timestep of 80.32 s along with a step size of 0.013 °2θ were used resulting in a total measurement time of 25.22 min. For cement paste, one program for all samples was applied because the same intensity and range of scanning angles were used. The quantitative analysis was performed by means of Rietveld refinement using HighScore Plus software. The analysis of the amorphous phase was performed using the external standard method. Fully crystalline alumina (α-Al_2O_3) was used as a standard.

2.4 Mercury Intrusion Porosimetry (MIP)

Total pore volume and pore size distribution of hardened pastes were determined using Mercury Intrusion Porosimeter Quantachrome PoreMaster-60 with a pressure up to 60000 psi (400 MPa). The following parameters were taken in calculations: Hg surface tension – 0.485 N/m, Hg contact angle - (I) 140°. Mercury volume was normalized by the sample volume. MIP dilatometer was full of the sample as much as possible for a constant sample mass, increasing the number of pieces of the sample increases its surface-to-volume ratio, which reduces boundary effects.

3 Results

Results of X-ray diffraction and MIP are presented in Fig. 1(a, b). It can be seen that the duration of a solvent replacement has a significant influence on the phase development (Fig. 1(a)). When the sample is immersed in a solvent for less than 30 min the reduced amount of ettringite is observed, further soaking leads to the stabilization of ettringite. After 15 min of soaking the total amount of belite is the highest and further keeping in a solvent induces its reduction. This process is accompanied by a slight

increase in portlandite content. However, after 60 min of presence in a solvent belite remains stable, while portlandite is slightly decreased, which in turn is related to an increment of calcite amount. The increasing of calcite is related to the carbonation of portlandite which is consistent with results published earlier [3]. The only phase remaining stable regardless of the soaking time is alite. It worth noting that phase development is observed only at short (15 min) or prolonged (24 h) soaking time, i.e. apart this period most of the phases are stable and stopping of hydration might be considered sufficient. An unusual increase of ettringite and decrease of belite amounts might be connected to a specific interaction with isopropyl alcohol and/or time of soaking. In case of ettringite its reduction after short soaking time seems to be induced by a partial loss of ettringite water. Concerning the reduction of belite content, there is no certain explanation except interaction with a solvent which has to be investigated in detail.

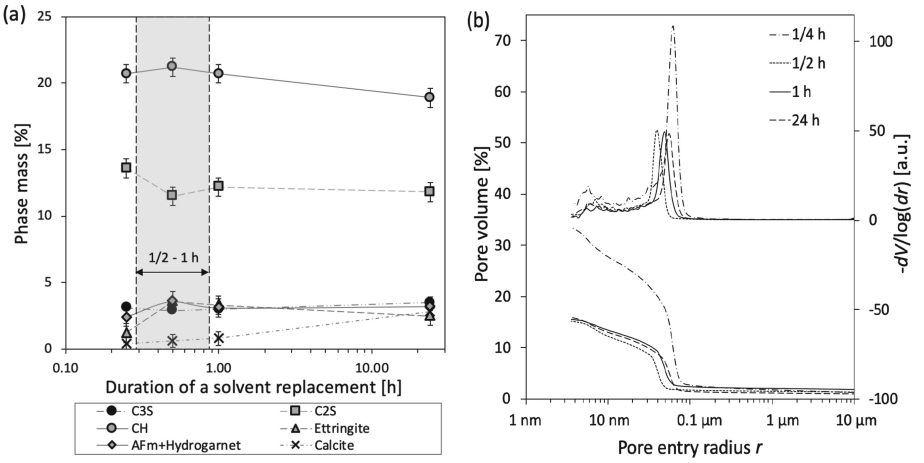

Fig. 1. Influence of duration of a solvent replacement on: (a) mineral composition; (b) pore size distribution of hardened cement paste.

4 Conclusions

In this study hydration of a hardened cement paste was stopped by a solvent replacement method. Samples were immersed in isopropyl alcohol for ¼, ½, 1 and 24 h. By means of XRD and MIP analyses, the mineral composition of samples and its pore structure was investigated as a function of soaking time in the solvent. After 15 min of soaking, the reduced amount of ettringite and increased amount of belite were detected, whereas total pore volume was abnormally high. The increasing of soaking time to 1 h led to the stabilization of phases. Yet, pore entry radius continuously increased with soaking time after ½ h. Further increase of solvent replacement time up to 24 h resulted in notable carbonation of cement paste and an increase of a pore entry radius.

The optimum time of a solvent replacement might be considered as a period when the main mineral phases and total percolated pore volume preserved unchanged. Based on the obtained result this time interval is between ½ and 1 h.

References

1. Collier, N.C., Sharp, J.H., Milestone, N.B., Hill, J., Godfrey, I.H.: The influence of water removal techniques on the composition and microstructure of hardened cement pastes. Cem. Concr. Res. **38**, 737–744 (2008)
2. Scrivener, K., Snellings, R., Lothenbach, B.: A Practical Guide to Microstructural Analysis of Cementitious Materials. Taylor & Francis Group, Boca Raton (2016)
3. Zhang, J., Scherer, G.W.: Comparison of methods for arresting hydration of cement. Cem. Concr. Res. **41**, 1024–1036 (2011)
4. Snellings, R., Chwast, J., Cizer, Ö., De Belie, N., Dhandapani, Y., Durdzinski, P., Elsen, J., Haufe, J., Hooton, D., Patapy, C., Santhanam, M., Scrivener, K., Snoeck, D., Steger, L., Tongbo, S., Vollpracht, A., Lothenbach, B., Winnefeld, F.: Report of TC 238 SCM: hydration stoppage methods for phase assemblage studies of blended cements - results of a round robin test. Mater. Struct. **51**, 1–12 (2018)
5. Zhang, Z., Scherer, G.W., Bauer, A.: Morphology of cementitious material during early hydration. Cem. Concr. Res. **107**, 85–100 (2018)

Nanoscale Observations of Tricalcium Aluminate Dissolution in Water by Digital Holographic Microscopy

Shaoxiong Ye[1], Pan Feng[1,2(✉)], and Jiaping Liu[1,2]

[1] Jiangsu Key Laboratory of Construction Materials, School of Materials Science and Engineering, Southeast University, Nanjing, China
pan.feng@seu.edu.cn
[2] State Key Laboratory of High Performance Civil Engineering Materials, Nanjing, China

Keywords: Tricalcium aluminate dissolution · In situ · DHM

1 Introduction

Mineral dissolution is a key process in geochemical reactions and environmentally relevant processes [1]. In recent years, the dissolution behaviors of cement clinkers have been obtaining increasing attention [2–6]. Portland cement is a low-cost material with multi-minerals, including alite, belite, tricalcium aluminate (C_3A), gypsum, etc. The hydration of cement, which is a complex reaction that combines mineral dissolution and product precipitation, is the origin of strength and determines other properties of cement paste. According to Julliand et al. [2], dissolution plays an important role in alite hydration, and the change of alite dissolution mechanism is responsible for the onset of the induction period. Similarly, Nicoleau et al. [5] proposed that the dissolution of C_3S is the rate-controlling step in the early hydration based on the change of saturation index of C_3S.

Besides alite, C_3A is also a key component of Portland cement. Though its content is much lower than alite, it has an important effect on the early properties of cement paste, especially for the workability [7]. Because C_3A has much higher reactivity than alite, it reacts much faster with water than C_3S, which makes it an even bigger challenge to measure its dissolution rate in water. To slow down the dissolution rate of C_3A, Brand and Bullard [8] lowered the water activity by incorporating ethanol in water and measured the dissolution rate in solutions with a high content of ethanol. However, the presence of ethanol is likely to change the dissolution mechanism of C_3A due to its adsorption to the C_3A surface [9, 10]. Thus how the dissolution rate of C_3A in the mixture solutions is related to that in water still remains unresolved.

For the purpose of measuring the net dissolution rate of C_3A in water, this paper provides a new technique, the Digital Holographic Microscopy (DHM), to monitor the surface height change of polished C_3A samples on nano-scale. Because of the unique capability of fast image collection of DHM, the real-time observation of fast dissolution is realized.

© RILEM 2020
K. Kovler et al. (Eds.): ConcreteLife 2020, RILEM Bookseries 26, pp. 28–32, 2020.
https://doi.org/10.1007/978-3-030-43332-1_6

2 Results

2.1 Flow Rate Effects

A flow-through liquid cell, like the cell used in [6], was built to provide water to flowing across the surface of tricalcium aluminate with specific flow rates. Figure 1 shows the dependence on the flow rate of the overall dissolution rate in the first few seconds. It can be seen that with the increase of flow rate, the measured dissolution rates firstly reach a maximum value at a flow rate of 34 ml min^{-1}, and then drops a little when the flow rate continuously increasing. It indicates that when the flow rate is lower than 34 ml min^{-1}, ionic diffusion may play a more important role than the surface reaction in controlling dissolution, and when the flow rate is higher, the flow becomes turbulent, resulting in the actual flow rate lower than the target value. Therefore, 34 ml min^{-1} is adopted as the flow rate for the following study.

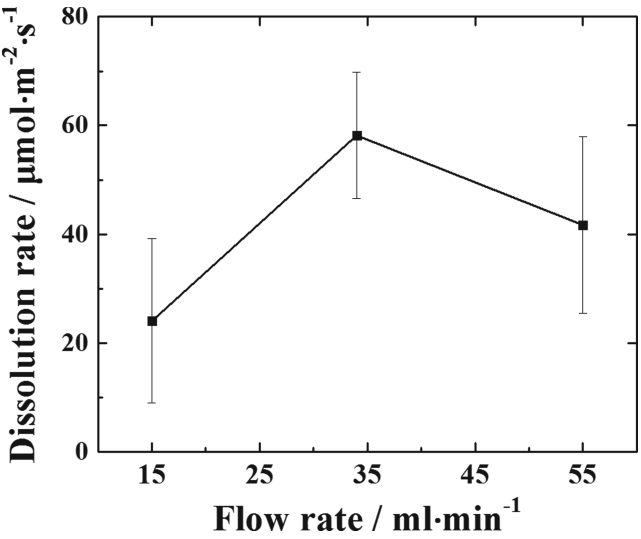

Fig. 1. Overall dissolution rate as a function of water flow rate. Error bars are one standard deviation of the average overall dissolution rate for at least three samples at each flow rate.

2.2 Surface Morphology After Initial Dissolution

The surface morphology of C_3A after the contact with water for about 2 s can be seen in Fig. 2(a), in which the right bottom of Fig. 2(a) is the reference surface, and it remains smooth during the measurement, though a small amount of hydration products appear in some local areas. This is due to the incomplete coverage of inert platinum in the reference surface, especially at the regions with deep scratches. Different from the reference surface, the surface not covered with a chemically-inert layer becomes very

rough and a layer of hydration product with crumpled foil shape can be clearly seen, as shown in Fig. 2(b). The thickness of this hydrates layer is measured from the side view of the specimen based on the brightness contrast with the bulk material, as shown in Fig. 2(c). The thickness is about 300 nm.

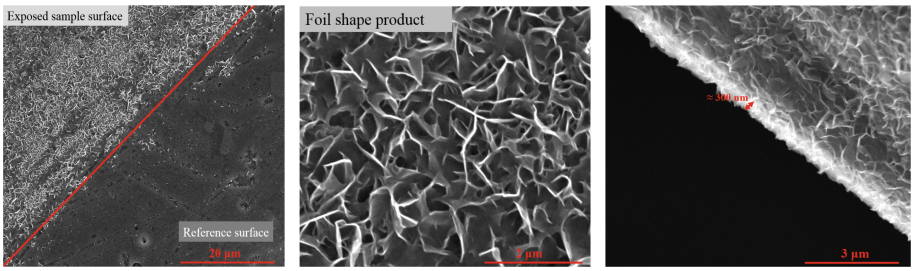

Fig. 2. Surface morphology after initial dissolution (a) The front view of C_3A surface after dissolution. (b) Morphology of hydration product layer. (c) The side view of C_3A surface after dissolution.

2.3 Analysis of C_3A Dissolution Kinetics

By tracing the average relative surface height change to the reference surface, it is clearly seen in Fig. 3 that the surface height changing can be roughly divided into three periods, including the initial fast height reducing, followed by the slow height increasing and the moderate height reducing. It suggests that after the rapid dissolution lasting for about half of a second in the first stage, the surface starts to be gradually covered by the hydration product in the second stage, in agreement with the results shown in Fig. 2(a)–(c). Though covered by a layer of product, the dissolution continues because the product has foil shape and not able to stop dissolution completely. Nevertheless, combined with the decreasing effect of dissolution and increasing effect of hydration on surface height change, the average relative surface height decreases at a relatively constant rate which is much slower than the initial dissolution. The overall dissolution behavior is similar to the heat flow during C_3A powder hydration in water [11]. For C_3S and cement, it also can be found in the literature that the heat flow behaves similarly [12, 13]. Although it is not completely the same with protective layer hypothesis which assumes that a layer formed on the surface can control the hydration reaction for a much longer-term, often dozens or hundreds of minutes [14–16], according to the DHM measurements, this surface layer is able to decrease the dissolution rate dramatically within the time frame of a quarter of a second.

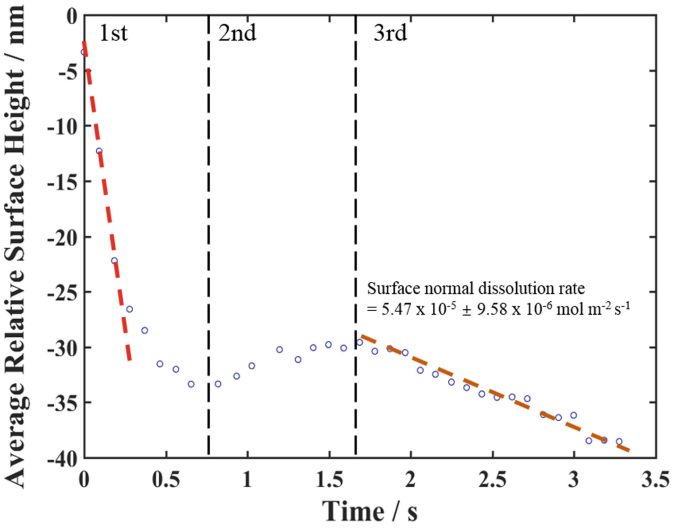

Fig. 3. The average surface height change during dissolution.

2.4 Probable Initial Dissolution Behavior (A Timescale of a Few Seconds)

As mentioned above, precipitation happens even within the first second of contact with water. Therefore, any dissolution measurement longer than one second is actually a result of the combination of both dissolution and precipitation. By analyzing the data in Fig. 3, it can be seen that the average pure dissolution rate of C_3A (in the first quarter of a second) is about 15 to 20 times larger than the rates obtained after two seconds. So according to the surface height change, $\Delta h/\Delta t$, is about 73.6–97.6 nm s^{-1}. Given the uncertainty of the measurement results shown in Fig. 1, $\Delta h/\Delta t$ can reach a maximum value at about 140 nm s^{-1}. If we assume that the pure dissolution rate of C_3A and the pure precipitation rate of hydration product remain constant during the first few seconds, so combined Fig. 3 and the value calculated above, the absolute value of precipitation rate should be just slightly lower than that of dissolution rate. Within 2 s of contact with water, the product layer thickness is estimated to be able to reach 200–300 nm. This is close to the value measured under SEM (Fig. 2(c)), which is actually slightly higher. This small difference can be attributed to the higher reactivity of the edge region of the sample measured under SEM than the flat regions measured by DHM [17].

3 Conclusions

In-situ nanoscale measurement on C_3A dissolution was for the first time performed by DHM in flowing deionized water. At a flow rate of 34 ml min^{-1}, C_3A can dissolve at an average rate of 0.5–1.5 mmol m^{-2} s^{-1} within the first a quarter of a second after

contact with water. After that, a crumple foil-like hydration product starts to form, which dramatically reduces the dissolution rate of C_3A.

Funding. The authors would like to acknowledge the financial support by National Natural Science Foundation of China (No. 1706222, No. 51890904, No. 51708108), and State Key Laboratory of High Performance Civil Engineering Materials Open Fund (No. 2018CEM001).

References

1. Lüttge, A.: Crystal dissolution kinetics and Gibbs free energy. J. Electron Spectrosc. Relat. Phenom. **150**, 248–259 (2006)
2. Juilland, P., Gallucci, E., Flatt, R., Scrivener, K.: Dissolution theory applied to the induction period in alite hydration. Cem. Concr. Res. **40**, 831–844 (2010)
3. Juilland, P., Gallucci, E.: Morpho-topological investigation of the mechanisms and kinetic regimes of alite dissolution. Cem. Concr. Res. **76**, 180–191 (2015)
4. Nicoleau, L., Nonat, A., Perrey, D.: The di-and tricalcium silicate dissolutions. Cem. Concr. Res. **47**, 14–30 (2013)
5. Nicoleau, L., Nonat, A.: A new view on the kinetics of tricalcium silicate hydration. Cem. Concr. Res. **86**, 1–11 (2016)
6. Feng, P., Brand, A.S., Chen, L., Bullard, J.W.: In situ nanoscale observations of gypsum dissolution by digital holographic microscopy. Chem. Geol. **460**, 25–36 (2017)
7. Yaylor, H.F.W.: Cement Chemistry, 2nd edn. Thomas Telford, London (1997)
8. Brand, A.S., Bullard, J.W.: Dissolution kinetics of cubic tricalcium aluminate measured by digital holographic microscopy. Langmuir **33**, 9645–9656 (2017)
9. Sand, K.K., Stipp, S.L.S., Hassenkam, T., et al.: Ethanol adsorption on the $\{10\bar{1}4\}$ calcite surface: preliminary observations with atomic force microscopy. Mineral. Mag. **72**, 353–357 (2008)
10. Sand, K.K., Yang, M., Makovicky, E., et al.: Binding of ethanol on calcite: the role of the OH bond and its relevance to biomineralization. Langmuir **26**, 15239–15247 (2010)
11. Alonso, M.M., Puertas, F.: Adsorption of PCE and PNS superplasticisers on cubic and orthorhombic C_3A. Effect of sulfate. Constr. Build. Mater. **78**, 324–332 (2015)
12. Ouzia, A., Scrivener, K.: The needle model: a new model for the main hydration peak of alite. Cem. Concr. Res. **115**, 339–360 (2019)
13. Jansen, D., Goetz-Neunhoeffer, F., Lothenbach, B., Naubauer, J.: The early hydration of Ordinary Portland Cement (OPC): an approach comparing measured heat flow with calculated heat flow from QXRD. Cem. Concr. Res. **42**, 134–138 (2012)
14. Jennings, H.M., Pratt, P.L.: An experimental argument for the existence of a protective membrane surrounding Portland cement during the induction period. Cem. Concr. Res. **9**, 501–506 (1979)
15. Birchall, J.D., Howard, A.J., Bailey, J.E.: On the hydration of Portland cement. Proc. Roy. Soc. Lond. A Math. Phys. Sci. **360**, 445–453 (1978)
16. Fischer, C., Luttge, A.: Beyond the conventional understanding of water–rock reactivity. Earth Planet. Sci. Lett. **457**, 100–105 (2017)
17. Arvidson, R.S., Ertan, I.E., Amonette, J.E., Luttge, A.: Variation in calcite dissolution rates: a fundamental problem? Geochim. Cosmochim. Acta **67**, 1623–1634 (2003)

Fine Recycled Concrete Aggregates Particle Morphological Parameters and Packing Properties

L. G. Pedersen(✉) and L. M. Ottosen

Department of Civil Engineering, Technical University of Denmark, Kgs. Lyngby, Denmark

Keywords: Fine recycled concrete aggregates · Packing properties · Workability · Rheology

1 Introduction

In the European Union, concrete accounts for 25% of the construction and demolition waste generated each year. At the same time, in many places around Europe the availability of natural rounded aggregates for the production of concrete is becoming a crucial question. These two trends suggest that crushed particles, such as crushed stone aggregates and recycled concrete aggregates (RCA), can be a necessity for concrete production to accommodate resource scarcity. When recycling concrete as aggregates, an important part to investigate is to use the fraction of fine recycled concrete aggregates (FRCA) as it constitutes 40–60% of the crushed concrete.

The proportioning of aggregates for the use in concrete is influenced by morphology characteristics of particles, such as shape, angularity and surface texture, which has a significant effect on the workability, rheology and mechanical properties of cementitious suspensions, among others [1] reviews the effect of packing characteristics of aggregates on the rheo-physical properties. This study investigates the morphology of crushed particles, FRCA, with nonspherical shapes.

2 Materials and Methods

Four sands were studied (Fig. 1), the first sand is a naturally rounded sea dredge 0–4mm sand (S1), whereas the other three sands S2, S3 and S4 are produced by crushed concrete (0–4mm). The FRCAs were obtained from three different construction sites in the area around Copenhagen and the concrete was crushed with gyratory crusher (cone crusher).

The investigation of the FRCA includes:

- Evaluation of particle shape
- Grain size distribution
- Packing

© RILEM 2020
K. Kovler et al. (Eds.): ConcreteLife 2020, RILEM Bookseries 26, pp. 33–36, 2020.
https://doi.org/10.1007/978-3-030-43332-1_7

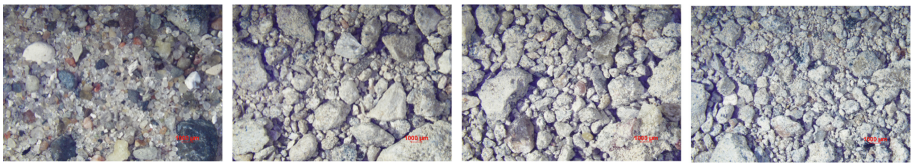

Fig. 1. The four sands studied in this paper, from left S1–S4.

3 Results

The sands particle shape, shown in Fig. 2, is quantified by the roundness, R (the average radius of curvature of the surface features) [2], the sphericity, S (reflecting the similarity between the length and height of a particle) [3], and regularity, ρ, described

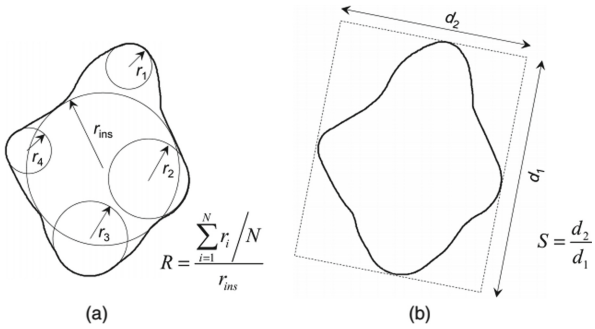

Fig. 2. Definitions of (a) roundness, R, (b) sphericity, S, (adapted from [4]).

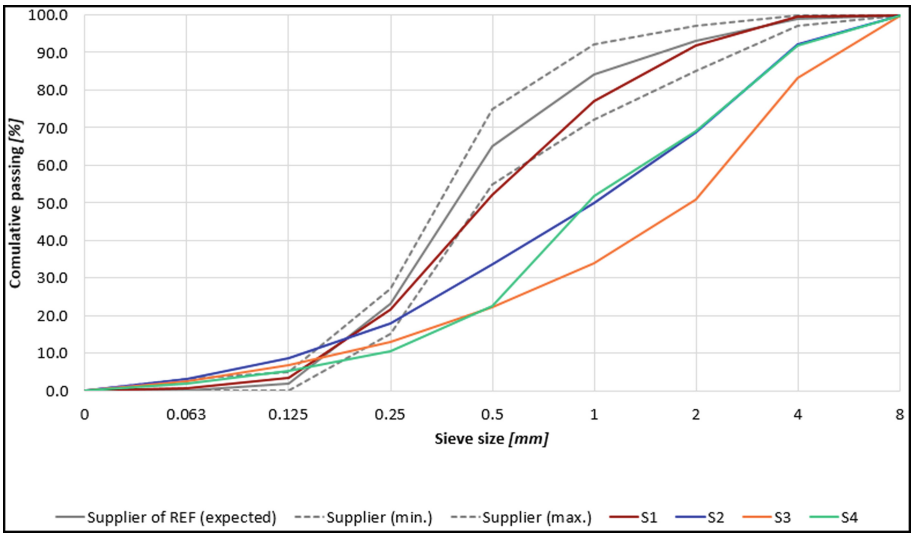

Fig. 3. Particle size distribution of the sands.

as $\rho = \frac{R+S}{2}$. The particle shape was determined as the average values of a visual assessment from microscope images.

The particle size distributions were determined according to DS/EN 933-1 and are shown in Fig. 3 for the four sands. Two specific packing fractions were measured for the four sands to characterize their properties further. The packing fractions were determined according to [5], the random loose packing fraction (RLP fraction), which

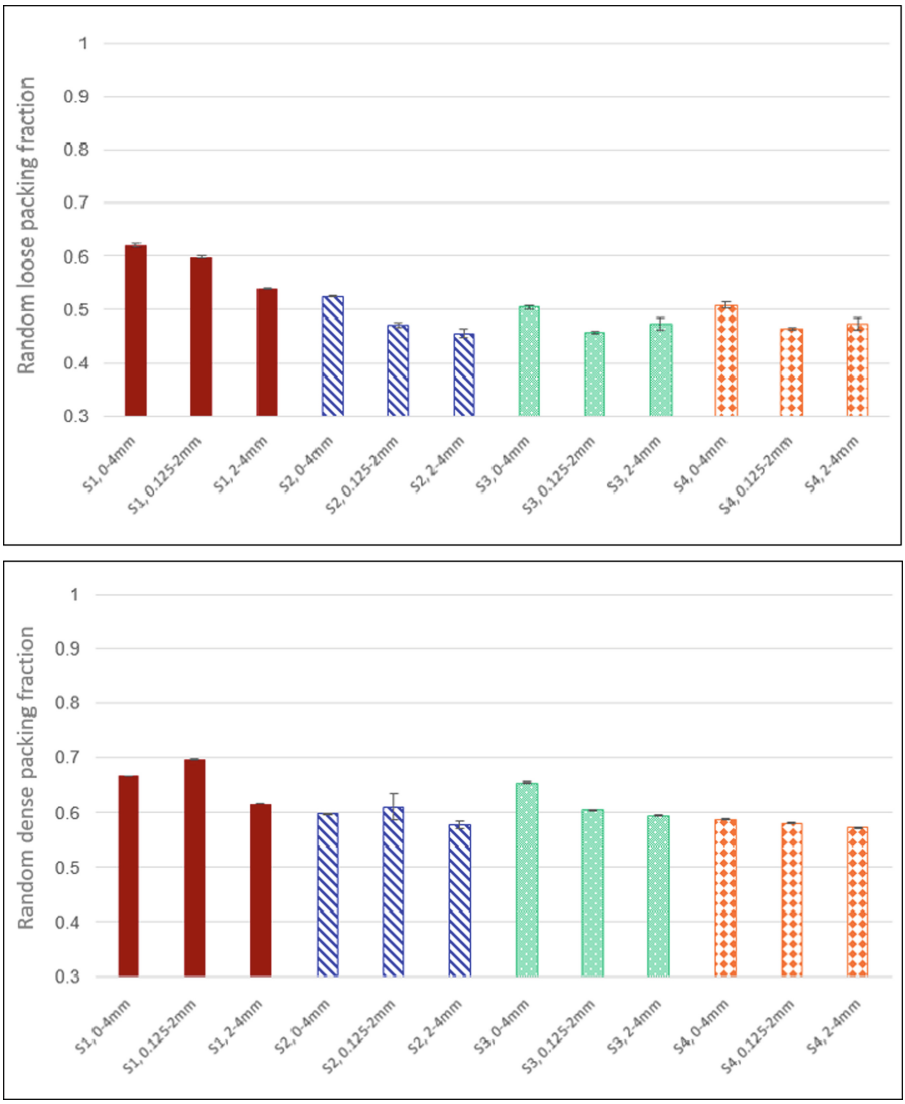

Fig. 4. Random loose packing fraction (top) and random dense packing fraction (bottom) for the sands and various fractions.

theoretical is defined as the loosest packing fraction by pouring grains, and the random dense packing fraction, this value is empirically defined and depends on the specific amount of energy brought to the system. All FRCA tested here have lower packing fractions than the reference sea dredged sand.

4 Conclusions

In this study, the particle morphology and packing properties were investigated for various FRCAs, and the FRCAs are more angular than the sea dredge sand where weathering has beside rounding the particles removed most of the weak minerals. The packing properties showed the sphericity of the particles as the dominant morphological parameter regarding packing. The study also showed that the packing properties similar to the morphology parameters depends on the type of sand and not on the sand fraction.

Acknowledgements. Norrecco and Dansk Beton are greatly acknowledged for collaboration and financial support.

References

1. Mehdipour, I., Khayat, K.H.: Understanding the role of particle packing characteristics in rheophysical properties of cementitious suspensions: a literature review. Constr. Build. Mater. **161**, 340–353 (2018)
2. Wadell, H.: Volume, shape, and roundness of rock particles. J. Geol. **40**(5), 443–451 (1932)
3. Powers, M.C.: A new roundness scale for sedimentary particles. J. Sediment. Petrol. **23**(2), 1117–1119 (1953)
4. Hryciw, R.D., Zheng, J., Shetler, K.: Particle roundness and sphericity from image assemblies by chart estimates and computer methods. J. Geotech. Geoenviron. Eng. **142**(9), 04016038 (2016)
5. DGF: Laboratoriehåndbogen – DGF Bulletin 15. Dansk Geoteknisk Forening, Lyngby, Denmark (2001)

Effect of Seawater on the Hydration of Tricalcium Silicate

Yanjie Sun and Chi Sun Poon(✉)

Department of Civil and Environmental Engineering, The Hong Kong Polytechnic University, Hong Kong, People's Republic of China
chi-sun.poon@polyu.edu.hk

Abstract. Coastal cities like Hong Kong rely heavily on their coastal and marine infrastructure for social-economic development. A major challenge for marine infrastructure is steel corrosion, which is the main cause for infrastructure deterioration. Also, fresh water is a scarce resource for some remote islands, and to meet the water requirement for concrete preparation in these regions, seawater is increasingly being considered as an alternative which would inevitable aggravate the deterioration problem due to steel corrosion. Up to now, a number of studies have focused on the effects of seawater on the workability, mechanical strength and durability (in particular corrosion of steel reinforcement) of cement pastes and reinforced concrete. However, the understanding on the influence of seawater on the composition and microstructure of cement hydration products is limited. This paper presents a preliminary study on the effects of individual salt components of seawater on the hydration process of C_3S. The microstructure changes of the hydration products were also studied. The mechanism of the acceleration effect is analyzed. Na^+ and Mg^{2+} can affect the dissolution of C_3S and the participation of the hydration products. For the later age, Mg^{2+} can substitute part of Ca^{2+} and change the composition of the final reaction products.

1 Introduction

Cement and concrete are most-used construction materials in the world, and about 4.1 billion tonnes of cement was produced worldwide in the year 2017. IEA's report shows that cement consumption is expected to continually increase in foreseeable future. Freshwater is still the key constituent for concrete mixing, and it is estimated that about 250–300 L mixing water is needed for the preparation of 1 m^3 concrete, which means a large quantity of freshwater is required. However, in some places of the world, the shortage of freshwater has always been an important issue, such as in the Middle East, North Africa and some remote islands. About 71% of the earth's surface is covered by water, but about 96.5% is seawater. So, it is of great interest to assess whether seawater can be used to substitute freshwater as an alternative mixing water for concrete.

In the past, the application of seawater in construction is prohibited due to its deleterious effect on the properties of steel bars embedded in concrete as the abundant chloride ions (Cl^-) contribute to the corrosion of steel bars. However, with the development of fiber reinforced polymer (FRP) concrete, the adoption of seawater as a

© RILEM 2020
K. Kovler et al. (Eds.): ConcreteLife 2020, RILEM Bookseries 26, pp. 37–41, 2020.
https://doi.org/10.1007/978-3-030-43332-1_8

mixing water seems to be possible, since the Cl^- content at seawater level has limited effect on FRP composites. Many past studies focused on the effects of seawater on the workability, mechanical strength and durability (in particular corrosion of steel reinforcement) of cement pastes and reinforced concrete. However, the understanding on the influence of seawater on the composition and microstructure of cement hydration products is limited.

2 Materials and Methods

The elemental and crystalline phase compositions of C_3S used in this study are shown in Table 1. The prepared simulated seawater was based on the specifications of ASTM D1141-98. Also, NaCl (NC), $MgCl_2$ (MC), and Na_2SO_4 (NS) solutions with a concentration of 0.48 M, 0.055 M and 0.029 M respectively were prepared.

Table 1. Oxide and crystalline phase compositions of raw material

Composition	wt. %
MgO	0.0866
Al_2O_3	0.912
SiO_2	26.4
P_2O_5	0.114
SO_3	0.0234
K_2O	0.0473
CaO	72.4
Fe_2O_3	0.0224
SrO	0.0142
ZrO_2	0.0238
Alite-M	8.2
Alite-T	81.1
B-C_2S	10.7

C_3S was mixed evenly with different types of single salt solutions of the simulated seawater at W/C ratio of 10. Samples are sealed in plastic bottles and cured at 20 °C for 6 h, 12 h, 1 d, 3 d, 7 d, 14 d, and 28 d. At the desired curing age, the solid phase was separated from the solutions by 0.45 μm filter papers. The solid phase was immersed in 50 mL isopropanol and the solution phase was acidified after pH measurement for ICP tests. Isothermal calorimetry test was conducted to determine the heat evolution patterns of the different mixees. Powder samples were inter-ground with 20 wt% internal standards (α-Al_2O_3) for characterization by X-ray diffraction (XRD).

The calorimetry test results (Fig. 1) show that the hydration process of C_3S was accelerated by the addition of NC, NS and MC solutions when compared with the reference samples prepared with deionized water (DI). The addition of single salt shortened the induction period and led to a higher rate of hydration in the acceleration period. NS induced the most significant acceleration effect followed by NC and MC.

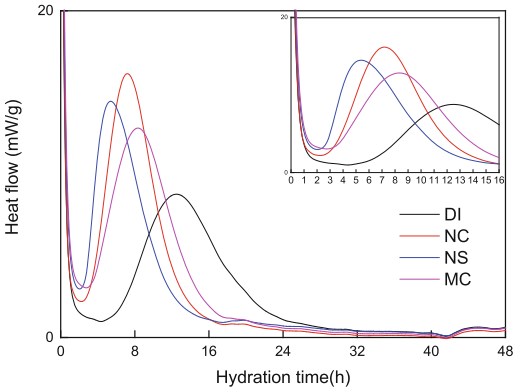

Fig. 1. Calorimetry tests results

The variation of different ions in solution are shown in Figs. 2 and 3. Initially, the concentration of Ca^{2+} in NC and NS solutions increased and were higher than that of the reference group. Then the concentration decreased to a stable level similar to the reference group. The concentration of Ca^{2+} increased in the MC sample continually before 1 d, and the final concentration was higher than that of the reference group. Na^{+} concentrations in NC and NS solutions showed the reverse trend. These results are consistent with the calorimetry test results in which Na^{+} and Mg^{2+} tended to react with the silicate ions released by the congruent dissolution of C_3S, lowering the concentration of silicate ions and accelerating the dissolution of C_3S. That caused the increase of Ca^{2+} and the decrease of Na^{+} and Mg^{2+} concentrations. When the concentration of Ca^{2+} reached a limiting value, C-S-H and CH began to nucleate and grow, and the concentration of Ca^{2+} decreased. Since C-S-H is more insoluble than sodium silicate, Na^{+} was replaced by Ca^{2+} and the concentration of Na^{+} increased. Mg^{2+} was precipitated with the silicate ions initially, and there was no big difference at the later age.

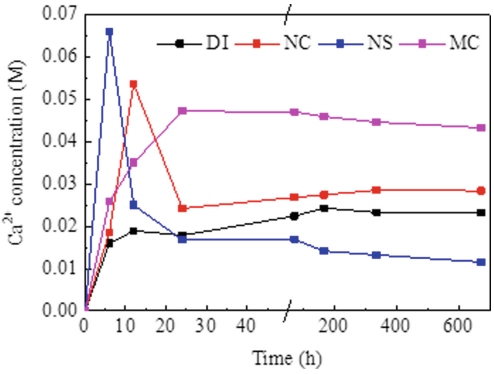

Fig. 2. Concentration of Ca^{2+} in solution

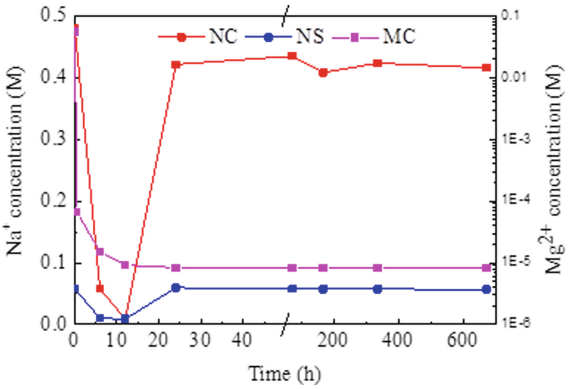

Fig. 3. Concentrations of Na^+ and Mg^{2+} in solution

The evolution of the crystalline phases of C_3S hydration in different single salt solutions was studied over a period of one month. The phases were primarily identified and analyzed by X-ray diffraction and quantified by the Rietveld method (Fig. 4). The XRD results of the 28 d samples show besides the conventional portlandite that there was no new crystalline phase produced except for the MC group, where part of Mg^{2+} precipitated with OH^- to form brucite. In general, the hydration rate of C_3S was enhanced with the addition of the single salt solutions compared with the reference group within one day, and this was no big difference at 28 d. At 28 d, over 95 wt% C_3S was consumed. Within 1 d, NC and MC had more significant effects on the hydration rate than that of NS. After the first 6 h, over 70 wt% of C_3S was hydrated for the NC group, and that for NS and MC and the reference groups were 47 wt%, 49 wt% and 29 wt% respectively. This was consistent with the calorimetry test results.

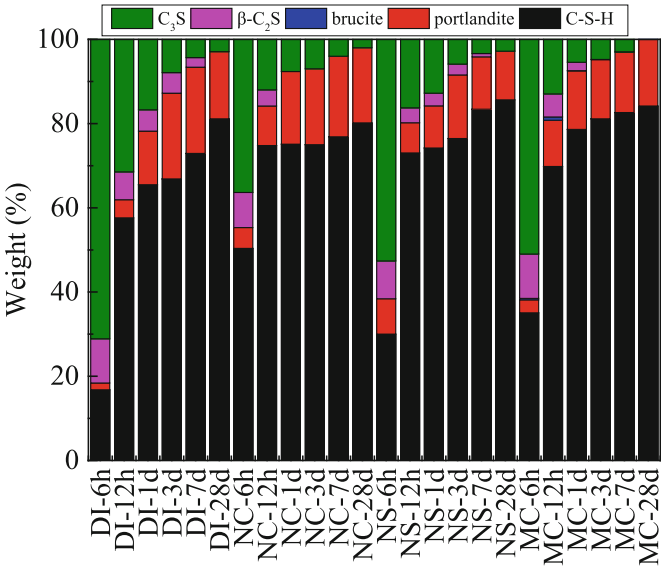

Fig. 4. Phase compositions determined by XRD-Rietveld method

3 Conclusion

C_3S was hydrated in four single salts solutions (DI, NC, NS, MC) of the simulated seawater to reveal the hydration mechanisms. Based on the results of this study, the following conclusions can be drawn: the incorporation of the single salts of the simulated seawater accelerates the hydration of C_3S. The induction period is shortened and more C_3S is dissolved in solution in a short time period due to the presence of Na^+ and Mg^{2+}, which tend to combine with silicate ions released from the C_3S. That can contribute to the enhancement of the dissolution of C_3S, and more Ca^{2+} would be produced in a short time period and the oversaturation of $Ca(OH)_2$ and C-S-H is reached at an early age.

Acknowledgement. The authors wish to thank the financial supports of the Research Grants Council Theme Based Research Scheme and the Hong Kong Polytechnic University.

Portland Cement Production from Fine Fractions of Concrete Waste

S. Zhutovsky and A. Shishkin(✉)

National Building Research Institute, Faculty of Civil and Environmental Engineering, Technion – Israel Institute of Technology, Haifa, Israel
andreis@cv.technion.ac.il

Keywords: Recycling · Concrete waste utilization · Portland cement · Clinker

1 Introduction

The recycling of concrete can reduce the environmental impact of Portland cement production and concrete construction, and decrease the damping and landfilling of demolition waste. Currently, concrete recycling is widely used for aggregate extraction [1], though concrete fines which are a mix of aggregate and the hydrated cement paste are not a part of the recycling process [1]. Research efforts have been directed to the production of new Portland cement from recycled fines, but most research attempts run into problems [2, 3].

The common way to use recycled concrete fines for new cement production is to add them in small proportions, according to chemical and mineralogical limitations, to the traditional raw meal of clinker rotary kiln. But the clinker of acceptable quality has not been obtained. Alite was not synthesized in satisfactory content. In many cases, the only belite was formed and there was an excess of silica [2, 3]. The compressive strength of cement was low and decreased with the increase of concrete fines content in the raw meal [2, 4]. The best results were achieved for mixtures correctly adjusted with the main clinker modulus. The produced Portland clinker had the composition similar to an ordinary Portland cement clinker [3].

The mineral transformations in a burned raw meal containing 22.8% of recycled concrete wastes were studied using X-ray diffraction (XRD). The results indicate that concrete waste fines can be completely recycled to obtain a new Portland cement.

2 Materials and Methods

Normal strength concrete (30 MPa) was prepared with dolomite coarse aggregate and natural sea quartz sand. The concrete was crushed with a jaw crusher and sieved. The fraction below 2.36 was used in the current research. Their mineral composition of the concrete fines as measured by XRD is shown in Table 1. The chemical composition was measured using Inductively coupled plasma (ICP) mass spectrometry test. Table 2 represents oxide mass percent of concrete fines.

© RILEM 2020
K. Kovler et al. (Eds.): ConcreteLife 2020, RILEM Bookseries 26, pp. 42–46, 2020.
https://doi.org/10.1007/978-3-030-43332-1_9

It can be seen in Tables 1 and 2 that fine material contained some contamination of magnesium oxide, whose origin is in the coarse dolomite aggregate, which may pose some problems for clinker burning. For clinker manufacturing, the concrete waste fines were mixed with limestone, bauxite and iron scale. Target Portland clinker composition was calculated according to the main four oxides content to satisfy the general requirements of basic Portland clinker moduli: Lime Saturation Factor (LSF) = 0.92–0.98, Silica ratio (SR) = 2–3, and Alumina ratio (AR) = 1–4. The clinker composition was optimized for maximum concrete fines content in the raw meal according to the limits of the clinker moduli. It was found that concrete waste fines contain sufficient silica and no addition of silica is needed to the raw meal. The optimal calculated raw meal composition and final content in clinker after the loss on ignition (LOI) are shown in Table 3.

Table 1. The mineral composition of concrete fines, % wt.

	Quartz	Dolomite	Calcite	Portlandite	Other minerals	Amorphous
% wt	35.3	19.6	8.8	3.5	8.5	23.9

Table 2. The oxide components % wt of recycled concrete waste fines by ICP.

	CaO	SiO_2	Al_2O_3	Fe_2O_3	MgO	SO_3	P_2O_5	Na_2O	K_2O	TiO_2	MnO_2
% wt	17.77	61.32	2.28	1.05	1.93	0.86	0.16	0.29	0.33	0.15	0.02

Table 3. The raw material mix design and their content in final clinker for recycled concrete fines, % wt

	Burned clinker				Raw meal			
Ingredient	Concrete waste fines	Lime stone	Bauxite	Iron scale	Concrete waste fines	Lime stone	Bauxite	Iron scale
% wt	29.3	63.4	4.9	2.4	22.8	71.8	3.8	1.6

The burning of the raw meal for clinker production was applied using round nodules of approximately 15 mm in size. The burning took place in the high-temperature bottom-loading laboratory. Phase transformations were tested at steps of 100 °C between 800 and 1100 °C, and at steps of 50 °C between 1100 and 1450 °C. After burning, samples were removed from the furnace at the maximum temperature and air quenched. Burned materials were ground and tested using a Malvern PANAlytical EMPYREAN X-ray diffractometer with a Goniometer radius of 240 mm. An X-ray source was CuKα1, 2 (λ = 1.5408 Å) with X-Ray generator operated at a voltage of 45 kV and a current of 40 mA. The following optical XRD configuration was used: the incident beam optics included 10 mm mask, 0.04 rad Soller slit along with ¼° divergence and 1° anti-scatter fixed slits; the diffracted beam optics consisted of 8 mm anti-scatter fixed slit and 0.04 rad Soller slit. The detector was PIXcel 3D detector used in 1D continuous scan mode. The scan was performed using

Brag-Brentano θ-θ geometry, between 10 and 70 °2θ. Timestep of 80.32 s with a step size of 0.013 °2θ was used resulting in a total measurement time of 25.22 s. The quantitative analysis was performed by means of Rietveld refinement using HighScore Plus software.

3 Results

The phase transformations of a raw meal containing 22.8% of concrete waste fines at burning at temperatures between 800 and 1450 °C are shown in Figs. 1 and 2. Figure 1 demonstrates the content of alite and belite, while Fig. 2. Shows the changes in alumina and iron-containing phases. It can be seen in Fig. 1 that belite gradually forms starting at 1000 °C and alite forms starting from 1300 °C. It can be seen in Fig. 2 that Ferrite (brownmillerite) is present at 800 °C in a small amount and its content gradually increased with temperature. Mayenite has the maximum content of almost 10% at 900 °C gradually decreases with the increase of temperature of burning, while tricalcium aluminate start to form appears only at 1150 °C.

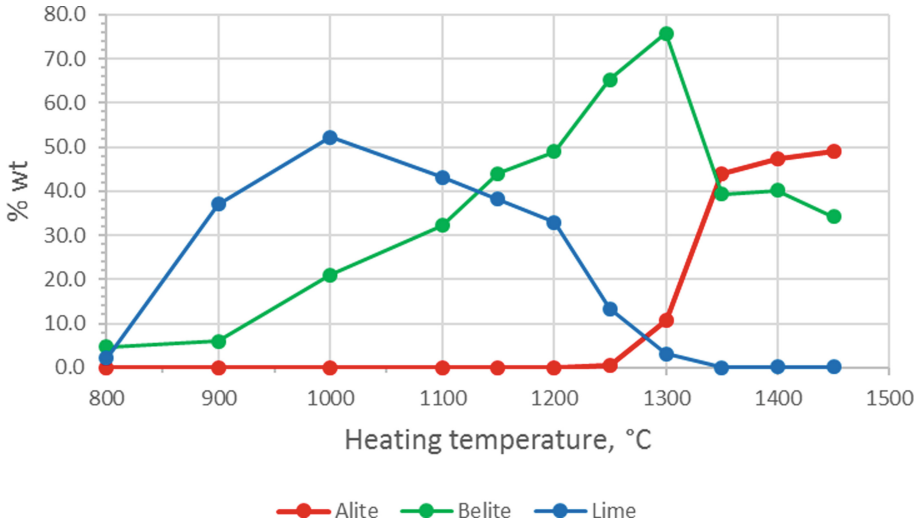

Fig. 1. Alite belite and lime mass percent with the heating temperature of raw meal.

Figure 3 shows the XRD scan and quantification of the final Portland clinker manufactured using recycled concrete waste fines obtained at 1450 °C. It can be seen that clinker with high alite content of 67% and belite content of 19% was obtained that corresponds to a good quality Portland cement. The XRD results show the low amount of Periclase in spite of the relatively high content of magnesia in raw meal. This can be explained by the absorption of MgO by alite.

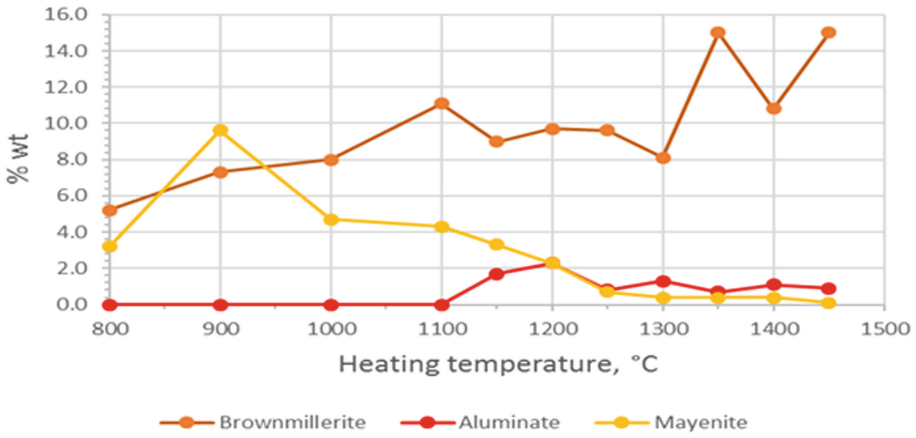

Fig. 2. Alumina and iron-containing minerals mass percent with the heating temperature of raw meal.

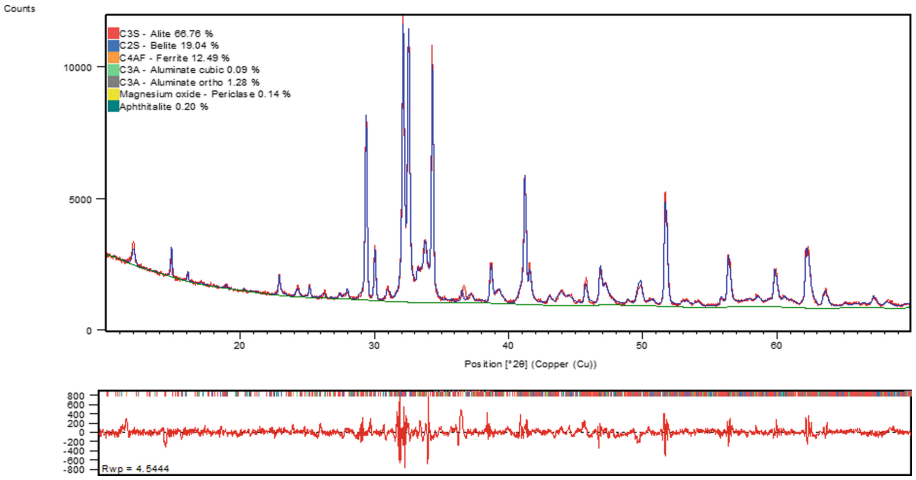

Fig. 3. XRD quantification of Portland clinker, manufactured using 22.8% of recycled concrete waste fines

4 Conclusions

The phase transformations of a raw meal containing concrete waste fines during heating between 800 and 1450 °C and formation of main clinker constituents were studied using XRD. The results of the research demonstrated that a Portland cement clinker can be produced using recycled concrete fines. The mass percent concrete waste fines with dolomite and quartz sand aggregates in raw meal were limited to 22.8% by the content of silica in the concrete waste fines.

References

1. Pacheco-Torgal, F., Tam, V.W.Y., Labrincha, J.A., Ding, Y., de Brito, J.: Handbook of recycled concrete and demolition waste. Woodhead Publishing Limited, Cambridge (2013). Francis Do
2. Schoon, J., De Buysser, K., Van Driessche, I., De Belie, N.: Fines extracted from recycled concrete as alternative raw material for Portland cement clinker production. Cem. Concr. Compos. **58**, 70–80 (2015). https://doi.org/10.1016/j.cemconcomp.2015.01.003
3. Diliberto, C., Lecomte, A., Mechling, J.-M., Izoret, L., Smith, A.: Valorisation of recycled concrete sands in cement raw meal for cement production. Mater. Struct. **50**, 127 (2017)
4. Kwon, E., Ahn, J., Cho, B., Park, D.: A study on development of recycled cement made from waste cementitious powder. Constr. Build. Mater. **83**, 174–180 (2015)

Life Cycle Assessment of Lightweight Aggregates from Coal Ashes: A Cradle-to-Gate Analysis

K. J. O'Hare[1], G. Pizzulli[2], M. Torelli[1], M. Balapour[1], Y. Farnam[1], Y. Grace Hsuan[1], P. Billen[3], and S. Spatari[1,4(✉)]

[1] Civil, Architectural and Environmental Engineering, Drexel University, 3141 Chestnut Street, Philadelphia, PA 19104, USA
[2] Mechanical Engineering, University of Bologna, Bologna, Italy
[3] Italy University of Antwerp, Biogem, Salesianenlaan 90, 2660 Hoboken, Belgium
[4] Faculty of Civil and Environmental Engineering, Technion – Israel Institute of Technology, Haifa, Israel
ssabrina@technion.ac.il

Keywords: Lightweight aggregates · Coal ashes · Life cycle assessment · Cost analysis

1 Introduction

Power plant coal combustion residues (CCR) that consist of bottom ash and off-spec fly ash may be beneficially converted to value-added construction materials thereby reducing disposal costs and landfilled waste. Coal ashes have been investigated as sources of raw material for lightweight aggregates owing to their mineral properties, using well-known processes for agglomeration of fine particles (e.g., via sintering or autoclaving processes). Recent literature by Billen et al. [1]. Proposed converting coal bottom ash to spherical porous reactive aggregates (SPoRA) using a sintering process and fluxing agents that allow lowering the operating temperature of the rotary furnace used to produce the lightweight aggregates (LWAs). The authors used constitutive modeling to optimize the operating temperature needed to produce slag where viscosity was maximized in order to retain a spherical shape during melt formation. At the same time the authors tested converting CCR materials experimentally at different NaOH additions and modeled the thermodynamic conditions for producing slag with optimal spherical properties.

In addition, Balapour et al. [2] recently tested the same SPoRA materials as possible candidates for internal curing of concrete owing to the porous structure of the manufactured aggregate. The authors prepared samples of LWAs made from low- and high-calcium waste coal bottom ash and evaluated the total porosity using x-ray computed tomography (XCT), which was measured to fall within the range between 39.6% to 57.8%. This showed that theoretically, the LWAs possessed a great capacity for storing water in their pore structure. The sphericity of LWAs, which is an influential factor on the workability if used in concrete, was measured ranging from 1 (meaning

© RILEM 2020
K. Kovler et al. (Eds.): ConcreteLife 2020, RILEM Bookseries 26, pp. 47–51, 2020.
https://doi.org/10.1007/978-3-030-43332-1_10

perfect sphere) to 0.75. Generally, the sphericity reduced when increasing the fluxing agent for preparation of the LWAs. Low-calcium LWAs passed the perfect spherical shape beyond 10% incorporation of NaOH, while high-calcium LWAs passed this point beyond 5.85% incorporation of NaOH [2].

Our objective in this paper is to understand the life cycle environmental impacts and costs of SPoRA LWAs for select environmental metrics, namely, the 100-year global warming potential (GWP), ozone depletion potential (ODP), eutrophication potential (EP) and acidification potential (AP). We use life cycle impact assessment (LCIA) characterization factors from the CML 2015 database developed at Leiden University. We examine the use of NaOH as a fluxing agent and discuss the possibility of using waste glass (soda lime glass or fluorescent lamp glass) as alternative fluxing agents as investigated by Torelli [3].

We evaluate the conversion of CCR to LWA using a sintering process that uses NaOH as fluxing agent, which lowers the temperature needed to form slag, and based on the properties of CCR collected from two power plants located in the U.S. Experiments together with thermodynamic and viscosity models described in Billen et al. [1] identified optimal additions of fluxing agent to attain desired characteristics in the final lightweight aggregate. Thermodynamic calculations were used to approximate the change in enthalpy and thermal input requirements for the sintering process based on the heat capacity of ash constituents using Eqs. 1 and 2, where t is temperature in K/1000 and A through E are constants for each material at a certain temperature and phase. A cradle-to-gate life cycle inventory (LCI) model (Fig. 1) that treats the ash as a waste material, and therefore accounts for transportation steps to haul the ash to a LWA processing facility that is assumed to be close to concrete end-use markets (e.g., within a 150 km radius of a city) was built using GaBi 6.0 LCA software [4]. Table 1 summarizes the properties of the ash samples modeled and Table 2 summarizes the reference flows (material and energy inputs) needed to process 1 metric tonne of ash.

$$Q = mC_p\Delta T \tag{1}$$

$$C_p\left[\frac{J}{mol} * K\right] = A + Bt + Ct^2 + Dt^3 + \frac{E}{t^2} \tag{2}$$

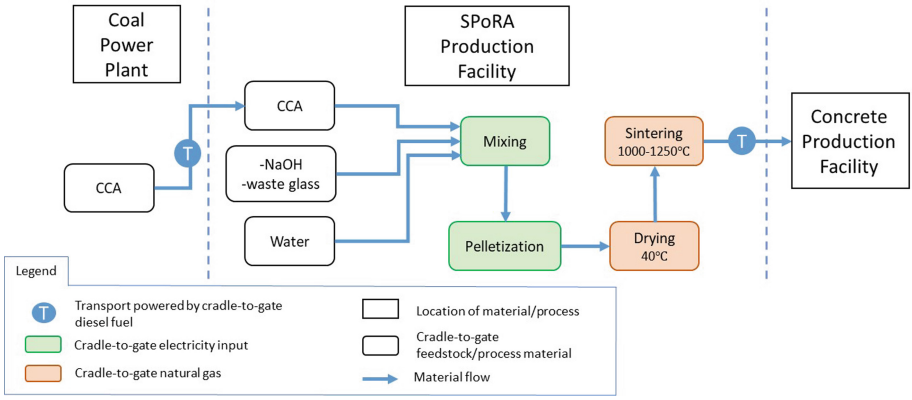

Fig. 1. Process flow diagram for industrial-scale SPoRA production using coal combustion ash (CCA) and either NaOH or waste glass as fluxing agents. Water would be added to the case with NaOH but may not be necessary for waste glass, which may enter "wet" to the manufacturing facility. The system boundary shows processes expected to use electrical or thermal (natural gas) energy inputs into the system.

Table 1. Chemical composition by weight percent from Billen et al. [1].

Chemical composition (% wt)	WP	NV
SiO_2	43.1	63.2
Al_2O_3	17.1	20.1
Fe_2O_3	7.29	6.66
SO_3	0.64	0.39
CaO	22.5	3.51
Na_2O	1.19	1.43
MgO	4.10	0.97
K_2O	0.41	1.13
P_2O_5	0.91	0.09
TiO_2	1.25	1.03

Table 2. Inputs of energy, utilities, and chemicals needed to transport raw materials and process them to LWA (SPoRA).

Energy input	WP	NV
Diesel	119.42 kg	90.51 kg
Electric	.18 MJ	.18 MJ
NaOH	16 kg	20 kg
Water	384 kg	380 kg
Thermal energy	1934 MJ	1937 MJ

2 Results

Life cycle assessment results were carried for two ash samples for four life cycle impact assessment (LCIA) metrics (Table 3). Results in Table 3 assume 4% and 5% NaOH addition to the WP and NV samples presented, respectively, based on experimental observations found to achieve spherical properties in the LWA. The NV ash sample, which is lower in Ca concentration, was found to have slightly better environmental performance (lower LCIA metrics) compared to WP, and additionally, according to research by Balapour et al. [2], it also possessed better sphericity, which aids the workability of concrete, and small uniform pore structure, which is desired for internal curing of concrete. While NV ash needed slightly more thermal energy input for the drying and sintering steps owing to its composition, the increment did not have an impact on the environmental indicators studied. Rather, a lower upstream transportation distance to move the ash feed from the coal plant to the assumed location of the SPoRA facility resulted in lower input of diesel. Napolano et al. [5] evaluated select LCIA metrics for recycled and natural clay-based lightweight aggregates using high temperature processing conditions (1200–1380 °C) and reports a GWP between 39 and 339 kg CO_2e/metric ton LWA, which are lower than our results (Table 3) owing to co-product credits, different operating conditions, including thermal processing only without use of a fluxing agent. As a reference, cradle-to-gate crushed stone aggregate, which is minimally processes, has a GWP of approximately 12 kg CO_2e/metric ton, but this does not include the transportation steps that would be required to ship lightweight natural aggregates to concrete mixing sites.

Table 3. Cradle-to-gate LCIA metrics for two ash samples converted to LWA using NaOH as fluxing agent. Basis of analysis is 1 metric ton ash treated.

Indicator	WP ash (4% NaOH)	NV ash (5% NaOH)
GWP (kg CO_2-eq)	896	625.5
AP (kg SO_2-eq)	1.2	0.926
EP (kg Phosphate-eq)	0.291	0.228
ODP (kg R11-eq)	$5.24E^{-9}$	$4.57E^{-9}$

3 Conclusions

Findings from this research suggest that CCR can be a beneficial raw material for producing SPoRA. Additional benefits of using waste material beneficially should be further explored by investigating the possible benefits of avoiding the treatment or impoundment of CCR generated from the many coal power plants around the U.S. Furthermore, exploring substitution of waste glass for NaOH can further reduce environmental burden owing to use of waste material.

References

1. Billen, P., et al.: Melt ceramics from coal ash: Constitutive product design using thermal and flow properties. Resour. Conserv. Recycl. **132**, 168–177 (2018)
2. Balapour, M., et al.: Potential use of lightweight aggregate (LWA) produced from bottom coal ash for internal curing of concrete systems. Cement Concr. Compos. **105**, 103428 (2020)
3. Torelli, M.: A thermodynamic modeling approach for environmentally optimized prospective design of spherical porous reactive aggregates. In: Environmental Engineering, Drexel University, Philadelphia, p. 58 (2018)
4. Spatari, S., et al.: Using GaBi 3 to perform life cycle assessment and life cycle engineering. Int. J. Life Cycle Assess. **6**(2), 81–84 (2001)
5. Napolano, L., et al.: Environmental life cycle assessment of lightweight concrete to support recycled materials selection for sustainable design. Constr. Build. Mater. **119**, 370–384 (2016)

Evolution of the Mass Balance of Water in the Hardening Process of Cement Compositions

D. Stackelberg(✉) and B. Wilge

Concretec Ltd., Yavne, Israel
davids@concretec.biz

Keywords: Cement compositions · Hardening · Structured water · Mass balance

1 Introduction

Hardening and strengthening of cementitious materials is the result of simultaneous growth and interaction (in the thermodynamic sense) of chemical and structural transformations [1]. The source material, a visco-plastic mixture, gradually transforms into artificial stone with dominating elastic properties.

A characteristic feature of the hardening of cement systems is the interaction between their liquid and solid phases. The liquid phase – the pore-filling solution, is a structural component, which *binds together* solid-phase elements of different dimensions and configurations. The structured liquid phase is a dispersed matrix-like medium that has a direct contribution to the strength balance of the material.

In addition, the liquid phase possesses a highly important property: it is always in a state of thermodynamic equilibrium with the solid phase onto which it is adsorbed (or by which it is absorbed). For this reason, structured physical water (mixing water minus chemically-bound water) is the most informative component of hardening cement-concrete compositions: any change in its condition adequately reflects the dependencies of structure development, and therefore – of strengthening during all stages of hardening.

It must be noted that physical water is not of homogeneous structure and properties. Thus, according to the "gel-space" concept of Powers [2], the overall mass of water in cement paste, m, is composed of chemically-bound m_{ch}, evaporable m_{evp} and non-evaporable water. In turn, evaporable water is composed of capillary water m_L and gel water m_g; in other words:

$$m = m_{ch} + m_{evp} + m_{non-evp} = m_{ch} + m_L + m_g + m_{non-evp} \quad (1)$$

The hardening process of cement compositions is characterized by continuous quantitative and qualitative changes in the mass balance of structured water (1). Variations in the components of the balance of the liquid phase, which is in equilibrium with solid surfaces, occur as the solid skeleton of the hardening material forms. In

© RILEM 2020
K. Kovler et al. (Eds.): ConcreteLife 2020, RILEM Bookseries 26, pp. 52–55, 2020.
https://doi.org/10.1007/978-3-030-43332-1_11

practice, these variations are realized as transformations of one type of water into another, for example, $m_L \rightarrow m_{ch}$.

The aforesaid suggests that the process of structural formation and hardening of cementitious materials can be studied experimentally and described analytically by studying the dependencies of formation and transformation of the moisture composition. These changes occur as a result of redistribution of the structured water in the volume of the forming capillary-porous structure.

2 Results and Discussion

The analysis of mass balance evolution during the hardening process of cement materials was carries out based on the experimental results of work [3]. Halperin *et al.* used an NMR method to study the hardening of white cement paste with water to cement ratio W/C = 0.43 over 1500 h. Based on the measurement of spin-spin relaxation of hydrogen atoms, the authors determined the variations in the quantity of evaporable water, the specific surface of hydration products and the mean radius of pores in the hardening process.

Based on these results, and using the formulas of Powers [2], we calculated the variations in moisture mass balance components m_{ch}, m_L, m_g and $m_{non-evp}$ (1) in the process of cement paste hardening. The results of the calculations are presented as a kinetic diagram in Fig. 1.

The diagram shows that the chemical bonding of water ($m_{ch} \rightarrow$ max), the formation of thin adsorption films of liquid on hard surfaces ($m_{non-evp} \rightarrow$ max) and the formation of cement gel ($m_g \rightarrow$ max) occur owing to a decrease in the mass of capillary water ($m_L \rightarrow$ min) as a combination of the following transformations:

- $m_L \rightarrow m_{ch}$ – transformation of bulk capillary water into a solid-phase state during processes of chemical bonding,
- $m_L \rightarrow m_{non-evp}$ – transformation of bulk capillary water into a strongly-bound state of thin adsorbed layers,
- $m_L \rightarrow m_g$ – transformation of bulk capillary water into a strongly-bound state of gel water.

By differentiating Eq. (1) in time, we can determine the rate of transformation of each component in the balance. Comparison of the rates allows us to evaluate the correspondence between the progress and the history of the processes. For example, we can evaluate the correspondence between the gel formation process and the nature and intensity of chemical bonding. In light of this, we have the possibility of exerting directed regulation of the transitions between the balance components using chemical additions and other methods.

The diagram allows us to isolate and consider various aspects of the hardening and strengthening of cement compositions. In particular, a joint analysis of the variation of the capillary and gel components allows us to evaluate the nature and intensity of formation of the porosity of the hardening material, which, in accordance with the "gel-space" concept [2], opens a new pathway to the evaluation of the strength.

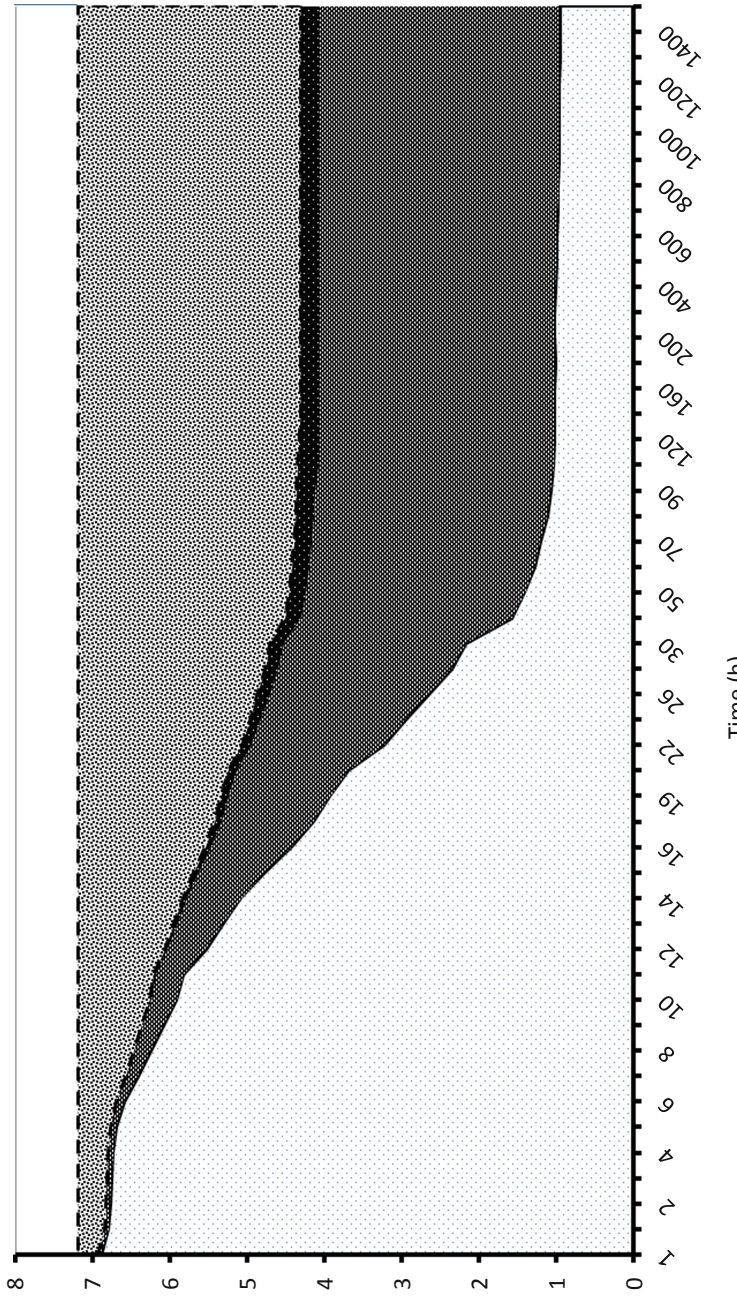

Fig. 1. Kinetic diagram of water mass balance evolution during cement paste hardening

Additionally, the diagram offers indirect, but practically full information on the development of the electricity-conducting properties of the material during hardening. Since the gel and non-evaporable components of the structured water conduct electricity to a very limited extent, or not at all, the transfer of electric charges occurs only in capillary water. Therefore, the variation in m_L in Fig. 1 uniquely determines the decrease in electric conductivity (or the increase in electric resistivity) in the hardening process.

3 Conclusions

The joint analysis of the mass component development kinetics of structured water and the interaction of these components opens new possibilities for the analysis of structure formation and hardening of cement-concrete compositions. In particular, this allows one to study the formation of porosity and hardening, the development of electric conductivity properties etc.

References

1. Shtakelberg, D.I., Sytchov, M.M.: Self-Organization in Dispersive Systems. Zinatne Publishing House, Riga (1990). (in Russian)
2. Powers, T.C.: The non-evaporable water content of hardened Portland cement paste – its significance for concrete research and its methods of determination. ASTM Bull. **158**, 68–76 (1949)
3. Halperin, W.P., Jehng, J.-Y., Song, Y.-Q.: Application of spin-spin relaxation analysis of surface area and pore size distributions in a hydrating cement paste. Magn. Reson. Imaging **12**(2), 169–173 (1994)

Concrete Composites

Every 10 years, an area the size of Britain disappears under a jungle of concrete.– Sir David Attenborough

The Effect of Compatibility and Dimensionality of Carbon Nanofillers on Cement Composites

A. Alatawna[1(✉)], M. Birenboim[1], R. Nadiv[1], M. Buzaglo[1], S. Peretz-Damari[1], A. Peled[2], O. Regev[1,3], and R. Sripada[1]

[1] Department of Chemical Engineering, Ben-Gurion University, Beer-Sheva, Israel
amra@post.bgu.ac.il
[2] Department of Structural Engineering, Ben-Gurion University, Beer-Sheva, Israel
[3] Ilse Katz Institute for Nanoscale Science and Technology, Ben-Gurion University, Beer-Sheva, Israel

Keywords: Nanofillers · Reinforced cement · Agglomeration · Graphene oxide · Flexural strength

1 Introduction

Cement is by far the most important and widespread building material in the industrialized world, with 4.2 billion tons of cement being produced in 2017. Cement production is, nonetheless, ecologically harmful, as a result of the CO_2 produced both by clinker and cement kilns. One possible solution lies in reducing the amount of clinker in the cement composites. This demand could be met by enhancing the mechanical properties of cement-based composites, for example, by loading them with nanofillers (NFs) that improve the resistance to crack propagation in the cement-based composites.

When using NFs to improve the properties of cement matrixes, the optimal reinforcing effect is achieved when the NFs are individually dispersed in the host matrix. Poor dispersion resulting in agglomeration of the nanofiller leads, in turn, to the formation of stress concentration, from which a crack can start developing. Most carbon-based nanofillers, such as carbon nanotubes (CNTs) and graphene nanoplatelets (GNPs), are *hydrophobic*, which poses a challenge for dispersing them in the *hydrophilic* cement matrix. This problem is usually addressed by sonicating an aqueous medium containing the carbon-based nanofiller in the presence of a surfactant prior to its mixing with the cement powder. However, the nanofiller will dramatically increase the viscosity of the cementitious composite, thereby reducing its workability. This problem is commonly dealt by the addition of a superplasticizer (SP).

In the present work, we investigated four NF systems namely: CNTs, GNPs, and their hydrophilic versions graphene oxide (GO) and functionalized CNTs (f-CNT). This systematically study would isolate the effects of the NF *dimensionality* [namely, 1D (CNT or f-CNT) vs 2D (GNP or GO)] and *compatibility* (oxidized, non-oxidized) on the mechanical properties of the cement nanocomposites. In addition, we optimized

© RILEM 2020
K. Kovler et al. (Eds.): ConcreteLife 2020, RILEM Bookseries 26, pp. 59–62, 2020.
https://doi.org/10.1007/978-3-030-43332-1_12

the NF loading for maximal enhancement in the mechanical strength for each type of NF. The mechanical properties enhance with the increased NF loading up to a certain limit called optimal NF concentration (ONC) and beyond this, the properties deteriorate gradually.

2 Results and Discussion

2.1 Mechanical Properties

The influence of incorporating NFs at various concentrations on the compressive and flexural strengths of the nanocomposites is shown in Fig. 1. Both compressive and flexural strengths increased up to the ONC and then deteriorate with further increase in the NF concentration. This behavior is typical of NFs in cementitious matrixes. The decrease in the compressive and flexural strengths beyond the ONC is due to agglomeration of the nanoparticles, leading to the formation of weak points in the hardened matrix. Under loading, these weak points can become focal points of failure [1].

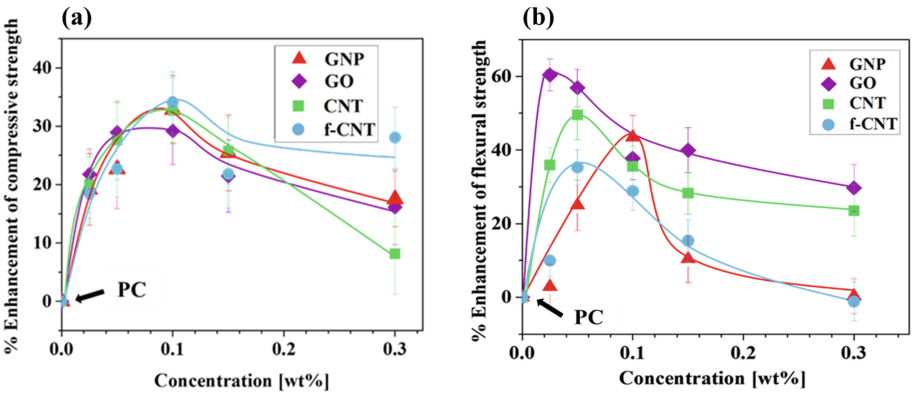

Fig. 1. Enhancement of (a) compressive strength and (b) flexural strength of hardened composites as a function of NF concentration relative to plain cement paste. The lines are drawn as a guide for the eye. [SP] = 0.2 wt% for all examined systems. The systems were examined at age for 14 days. The compressive strength (cubes: 15 × 15 × 15 mm^2) of the PC was 44 MPa and flexural strength (prisms: 8 × 8 × 60 mm^2) 7 MPa.

The enhancement in compressive strength of the composites relative to the plain cement paste without NFs (PC) is presented in Fig. 1a. An enhancement of ~30% in the compressive strength was obtained for all the NFs, and for most of them at an ONC loading of 0.1 wt% (Fig. 1a), which was independent of the NF type. GO showed the same compressive strength enhancement at a lower loading of 0.05 wt%. While all NFs showed similar enhancement of the compressive strength measurements, a wide spectrum of ONC values characterized the enhancement in flexural strength measurements

(Fig. 1b). For the flexural strength, GO demonstrated the best reinforcement, with 62% enhancement at a very low ONC value of 0.025 wt% (Fig. 1b), while the CNT- and GNP-based composites showed enhancements of 49% (ONC = 0.05 wt%) and 44% (ONC = 0.1 wt%), respectively. The f-CNT showed an enhancement of as little as 35% at an ONC value of 0.05 wt%.

The effect of the NF compatibility (hydrophobic-hydrophilic) with the hydrophilic cement matrix was examined while keeping the dimensionality (1D or 2D) constant. The compatibility of the oxidized NFs, f-CNT and GO, with the aqueous cement matrix was superior to that of the non-oxidized nanocarbons, CNT and GNP. For the 1D nanofillers, it was expected that the functionalization of CNT would substantially enhance the interaction of the NF with the cement matrix, leading to better mechanical performance. Nevertheless, f-CNT conferred only a relatively low enhancement of 35% in the flexural strength as compared to the 49% enhancement conferred by CNT (Fig. 1b). A possible reason for this finding could be the introduction of defects into f-CNT during the functionalization procedure. The induced defects also made the f-CNT more prone to breakage under mechanical agitation (ultrasonication and mixing) [2]. For the 2D NFs, GO gave far better enhancement (62%) and at a lower ONC (0.025 wt %) than GNP. GO showed better compatibility with the cement matrix due to the presence of oxygen functional groups in higher amount (40.1 vs. 3.6%).

Evaluating the effect of NFs dimensionality at a given degree of oxidation gave the following findings. For the hydrophobic nanofillers CNT and GNP, the 1D CNT exhibited better flexural reinforcement compared to the 2D GNP, due to the cylindrical shape and the higher aspect ratio of the particles, which contribute to bridging nano-cracks [3]. For the hydrophilic NFs GO and f-CNT, the 2D GO exhibited higher flexural enhancement compared to the 1D f-CNT (62% vs 35%). It was expected that functional groups in the f-CNT would make it more compatible with the cement matrix, thereby providing greater enhancement in mechanical properties, but f-CNT was found, in fact, to be less effective. Again, a possible explanation is that the functional groups of f-CNT weaken the nanotubes, which become prone to shortening upon sonication

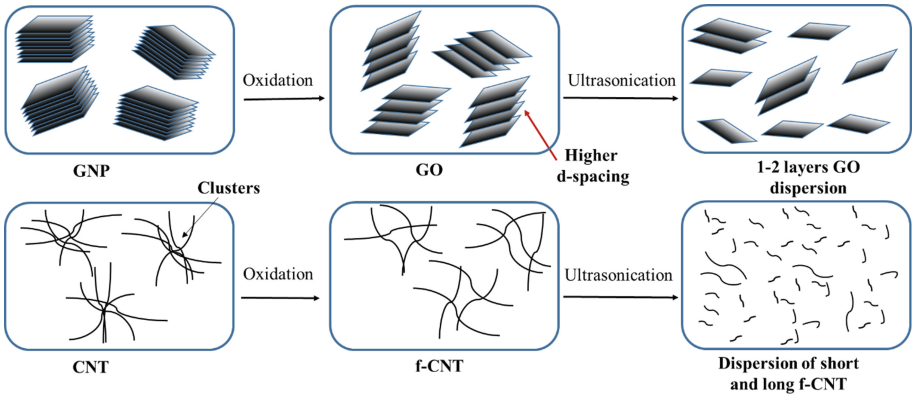

Fig. 2. Schematic representation of stages of functionalization and dispersion of GNP (top) and CNT (bottom).

and mixing. The suggested effect of functionalization in GO and f-CNT is depicted schematically in Fig. 2. For GO, the oxygen functional groups contribute to reducing the number of layers in the material (leading to a high aspect ratio and therefore more efficient reinforcement). In contrast, for f-CNT, the functionalization becomes counterproductive, as the nanotubes tend to break due to the introduced defects; the shorter f-CNTs so formed are less effective in enhancing the mechanical properties of the composites.

3 Summary and Conclusions

- The effect of the nanofillers on the mechanical properties of the hardened composites was evident in both the compressive strength and the flexural strength. All the nanofillers conferred the same enhancement in compressive strength at the same ONC, with the exception of GO, which gave the same enhancement at half the loading.
- In contrast, the flexural strength of the cement-based composites was strongly influenced by both the dimensionality and compatibility of the nanofillers. GO – giving 62% enhancement of the flexural strength – was found to be the best reinforcing agent among the four nanofiller materials due to its compatibility with the cementitious paste and its high aspect ratio.
- GO was followed by the 1D CNT, with 49% enhancement, and then by GNP, with 44% enhancement. f-CNT was found to be less effective than CNT, as the functionalization weakened the nanotubes, causing them to break during mechanical agitation.

In summary, –graphene oxide (2D-GO) provided the highest efficiency combined with the lowest ONC, making it an ideal filler for cementitious systems. GO is, however, much more expensive, making Graphene nanoplatelets (2D-GNP) the most cost-effective alternative, as it provides 75% of the GO enhancement.

References

1. Coleman, J.N., Khan, U., Gun'ko, Y.K.: Mechanical reinforcement of polymers using carbon nanotubes. Adv. Mater. **18**, 689–706 (2006). https://doi.org/10.1002/adma.200501851
2. Inam, F., Vo, T., Jones, J.P., Lee, X.: Effect of carbon nanotube lengths on the mechanical properties of epoxy resin: an experimental study. J. Compos. Mater. **47**, 2321–2330 (2013). https://doi.org/10.1177/0021998312457198
3. Manzur, T., Yazdani, N., Emon, M.A.B.: Potential of carbon nanotube reinforced cement composites as concrete repair material. J. Nanomater. **2016**, 1–10 (2016). https://doi.org/10.1155/2016/1421959

The Chemical Durability of Cement Pastes and Geopolymers Substituted with Dolomite-Based Quarry-Dust

E. Cohen[1], A. Peled[2], and G. Bar-Nes[3(✉)]

[1] Energy Engineering Unit,
Ben-Gurion University of the Negev, Be'er-Sheva, Israel
[2] Structural Engineering Department, Ben-Gurion University of the Negev,
Be'er-Sheva, Israel
[3] Chemistry Department, Nuclear Research Centre Negev (NRCN),
Be'er-Sheva, Israel
gabi.barnes@gmail.com

Keywords: Dolomite · Geopolymer · Cement · Sulfuric acid resistance · Thermal-expansion

1 Introduction

In recent years, growing environmental concerns have led the cement industry to make modifications in cement production, manifested by the use of supplementary cementitious materials (SCMs) as raw materials within the cement mixture. In the present study the use of dolomite-based quarry-dust (QD) to generate a low-energy, environmentally-friendly structural material was explored. QD was added either as an additive to conventional Portland Cement (PC) or to geopolymeric binders, formed by the alkali activation of local class F fly ash (FA). A significant increase in compressive strength, due to QD addition, was found for both CEM- and FA- based mixtures [1]. The chemical durability of the cementitious systems and FA-based geopolymeric mixtures for which the binder (cement/FA) was replaced with 40% wt. QD was evaluated using two different tests: (a) Expansion tests to assess the durability of these dolomite-based, Mg-rich mixtures - as brucite ($Mg(OH)_2$) may be formed according to Eq. (1) (known as the 'alkali-carbonate reaction') and hence induce volume increase and expansion.

$$MgCO_3 + 2\ NaOH \rightarrow Mg(OH)_2 + Na_2CO_3 \quad (1)$$

Expansion tests were performed according to ASTM C490 test method. Bar samples were cast in 25×25×285 mm stainless steel molds. Cement bar samples were kept in a moist cabin for 24 h from casting. Later, submerged in 80 °C tap water container for an additional 24 h and finally tap water was replaced by 1 molar NaOH solution pre-heated to 80 °C. Geopolymeric test samples were kept in an oven at 40 °C for 48 h from casting. Later, bars were submerged in 1 molar NaOH solution pre-heated to 80 °C. Both samples remained in the heated alkali solution for more than

© RILEM 2020
K. Kovler et al. (Eds.): ConcreteLife 2020, RILEM Bookseries 26, pp. 63–66, 2020.
https://doi.org/10.1007/978-3-030-43332-1_13

14 days. Length measurement was carried out with a dedicated length comparator apparatus, every 2–4 days.

This testing procedure is an adaptation of the ASTM C1260 method which permits detection, within 16 days, of the potential for deleterious alkali-silica reaction of aggregate in mortar bars. In our study this test is used to assess the alkali-carbonate reaction; (b) susceptibility of the QD containing products to acidic conditions was measured as the weight loss of the samples immersed in 5% wt sulfuric acid solution during a period of 100 days.

2 Results

Expansion-test results for both the cementitious systems and FA-based geopolymeric mixtures replaced with 40%wt QD, denoted respectively CEM40 and FA40, have been performed [1] and are presented in Fig. 1. Table 1 presents the mix compositions of all samples. The test results revealed that all the mixtures expanded below the standard limit value of 0.1% [2], classifying the dolomite-based QD used here as a non-alkali-reactive aggregate.

Table 1. Mix composition of samples

Samples	Cement [%wt]	Quarry dust [%wt]	Water [%wt]	Samples	Fly ash [%wt]	Quarry dust [%wt]	Activator [%wt]
CEM	100	0	50	*FA*	100	0	50
*CEM*40	60	40	30	*FA*40	60	40	30

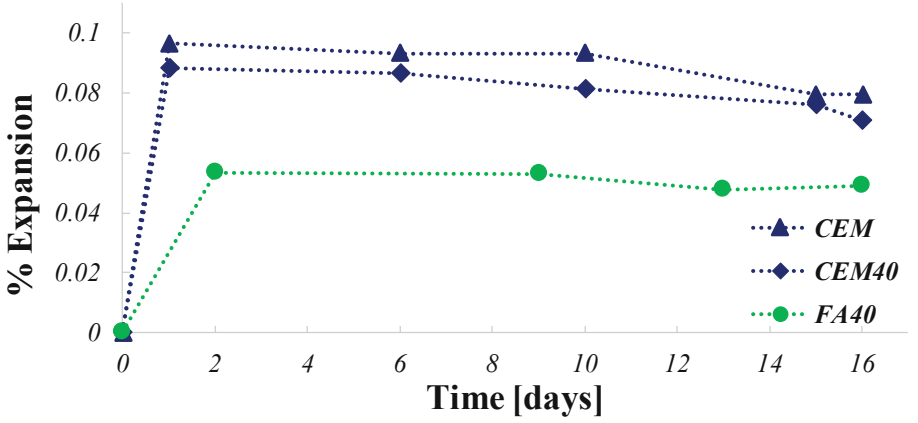

Fig. 1. Expansion results of CEM mixtures, with and without QD, and FA mixtures with QD. (the dashed lines are only visual aids). Experimental data obtained from [1].

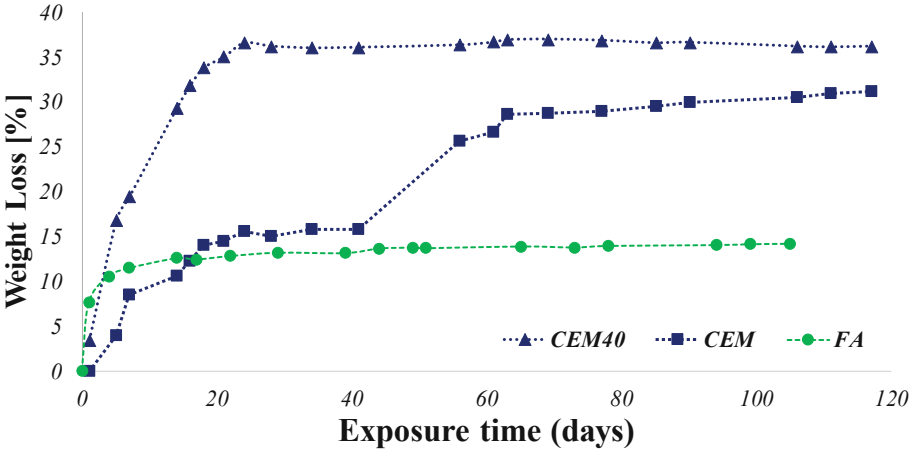

Fig. 2. Weight loss in 5% sulfuric-acid solution of FA and CEM mixtures, as well as the weight loss of a CEM-based mixture with QD additive (CEM40). (The dotted lines are visual aids). Experimental data obtained from [1].

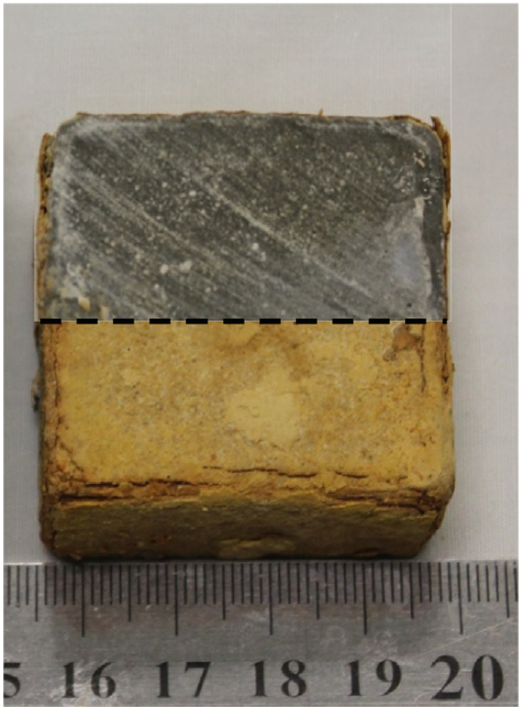

Fig. 3. Image of the CEM0 sample after immersion in a 5% sulfuric acid solution. Bottom image presents the outer sample surface (in direct contact with the acid solution) and top image taken from the middle of the cube (no direct contact with the acid solution)

The weight loss in the CEM, CEM40 and FA mixtures during the acidic immersion process is described in Fig. 2. The highest weight loss was measured for the CEM40 sample (36%). A slightly lower weight loss of 30% was obtained for the CEM0 sample, which shows a change in the trend after approximately 40 days of immersion, i.e., a step-like function. This change probably occurred when the delamination of the gypsum layer developed on the sample surface area (Fig. 3). The weight loss in QD-free FA (FA0) was significantly more moderate, leading to a total weight loss of only 13%. However, in the FA40 mixture, the sample disintegrated so rapidly that it could not be accurately measured (not presented).

3 Conclusions

The chemical durability of QD bearing matrices was explored in the present study. One of the main concerns of using Mg-rich additives such as QD is the formation of magnesium hydroxide phase, brucite, which relates to volume increase and cracks in the hardened mix. Expansion measurements proved that QD has no effect on thermal expansion and all samples measured complied with the standard limit average expansion percent of 0.1%.

Static immersion tests in sulfuric acid solution emphasized the differences between FA based geopolymers and hydraulic calcium silicate-based cements such as PC. The FA based materials were found to be more durable to the acidic solution, with an overall weight loss of 14% compared to more than 30% weight loss in CEM sample. However, for the QD bearing samples this trend has reversed, as the formation of calcium sulfate (gypsum) on CEM sample surface produced a sealing effect which delayed the dissolution of QD, which is highly susceptible to acid [3]. The high permeability of the FA matrix facilitated the dissolution of QD in the acidic media and it dissolved rapidly. Therefore the vulnerability of these QD containing products to acidic conditions must be further studied and carefully considered.

References

1. Cohen, E., Peled, A., Bar-Nes, G.: Dolomite-based quarry-dust as a substitute for fly-ash geopolymers and cement pastes. J. Clean. Prod. **235**, 910–919 (2019)
2. Hooton, R.D., Rogers, C.A.: Development of the NBRI rapid mortar bar test leading to its use in North America. Constr. Build. Mater. **7**(3), 145 (1993)
3. Franzoni, E., Sassoni, E.: Correlation between microstructural characteristics and weight loss of natural stones exposed to simulated acid rain. Sci. Total Environ. **412–413**, 278–285 (2011)

Chloride-Enhanced Delayed Ettringite Formation (CLDEF): An Obscure Process

S. O. Ekolu(✉)

Department of Civil Engineering Science, University of Johannesburg, Auckland Park, South Africa
sekolu@uj.ac.za

Keywords: Chloride ingress · Delayed ettringite formation · Monosulphates · Friedel's salt

1 Introduction

From the historical perspective Delayed Ettringite Gormation (DEF) is known to occur usually in cementitious systems made at high cement contents with rapid hardening Portland cements (RHPC) such as Type III cements. Elevated curing temperatures exceeding 70 °C are necessary for DEF to occur. However, there have been controversies, leading to speculations that DEF could occur outside these generally recognized conditions [1–9]. For example, large pours of concretes under hot weather concreting could increase concrete temperature levels to DEF critical temperatures. Johansen and Thaulow [10] found that a concrete beam of 1 m × 1 m cross-section developed a peak temperature of 84 °C at ambient temperatures of 35 °C, without heat treatment. Hobbs [11] also suggested that large sections of field concretes made with high cement contents of about 500 kg/m^3, could attain maximum temperatures in the range of 85 °C. So in hot or tropical climates, concreting conditions similar to those found under heat curing, could arise as a combined effect of the following factors:- use of RHPC/Type III cement, mix designs of high cement contents such as 500 kg/m^3, large concrete pours or casting of large sections, and ambient temperatures exceeding 30 °C. In laboratory studies, however, there are no reports of DEF occurrence in the absence of heat curing.

2 The Controversies of Chloride-Sulphate Interactions in Concrete

Chlorides commonly migrate or are incorporated into concrete, leading to two categories comprising:

- *Admixed* chlorides, that are added or incorporated during mixing of concrete, and may be considered as 'internal chlorides' or
- *Ingressed* chlorides, which migrate into hardened concrete from external sources and may be regarded as 'external chlorides'.

© RILEM 2020
K. Kovler et al. (Eds.): ConcreteLife 2020, RILEM Bookseries 26, pp. 67–73, 2020.
https://doi.org/10.1007/978-3-030-43332-1_14

In the early ages of concrete technology development during the first half of the 20th century, chloride-based chemical admixtures were extensively used as accelerators, to promote hydration of concrete especially for casting under cold weather conditions. Various researches were devoted to understanding of the effects of admixed chlorides on cement hydration [12–14]. The understanding that emerged showed that the admixed chlorides compete with internal sulphate ions to react with C_3A in a Cl-C_3A interaction, to form Friedel's salt as the end reaction product. The interactions involving ingressed chlorides are quite different from those of admixed or internal chlorides, since most of the C_3A will have reacted by the time external chlorides migrate into concrete. Accordingly, the unstable product that chlorides may find available in the hardened concrete system is monosulphate (AFm), which sets up the Cl-AFm interaction. The different interaction processes for admixed or ingressed chlorides, eventually determine their effects on volume stability of the material system.

The Cl-AFm interactions of ingressed chlorides in concrete, has resulted in controversies regarding their effects on sulphate attack, for which each of the following observations have been reported in the literatures:

- No effect [15]
- Suppressive [16–18]
- Increase [19–21]

A close look at the experimental set-ups of the various researches lead to two important deductions that:

(i) *The effect of ingressed chlorides is a function of chloride concentration*. There is agreement on the experimental observations showing that high chloride concentrations suppress sulphate attack, as reported in the literatures [16–21]. Further evidence is also available from field investigations done at the Arabian Gulf, which showed sulphate attack to have been majorly suppressed owing to exposure of the concrete structures to high chloride concentrations in the environments [22].

(ii) *Only heat-treated systems appear to exhibit the DEF expansion enhancing effect of ingressed chlorides*. To the best knowledge of the author, no chloride – induced expansions have been reported in moist-cured cementitious systems. The author's researches [20, 21, 23] have consistently found chlorides to enhance DEF expansions in heat-treated cementitious systems. It is also possible that non – expansive systems of low SO_3 can become DEF expansive as a consequence of exposure to chlorides. The second important consideration is that only low chloride concentrations produce the chloride-enhanced DEF expansion (CLDEF). The researches done so far indicate 0.5 M chloride concentration to give the most severe CLDEF expansion.

3 Review and Discussion

3.1 Incidental Observations

In this section, the DEF experiments that were conducted in Canada and in South Africa under completely different investigations, are reviewed. The early evidence of CLIDEF was first reported in [20, 21]. In the study, concrete cylinders 100 dia 200 mm height were made at 0.45 water/cement ratio (w/c) with 7% entrained air, then heat-cured at 95 °C in accordance with the 18-h conventional steam curing cycle [21]. The Type 30 Portland cement used in the study was known to be DEF expansive, as shown in Fig. 1 [21]. Its high $SO_3 > 4.0\%$ met the requirement for sulphate expansive cements [24, 25].

Following heat curing, the cylinder samples were exposed outdoors for 28 days. In preparation for the bulk diffusion test ASTM C1556 [26], cores of size 100 dia 50 mm thick were cut from the concrete cylinders then ponded in 2.8 M NaCl solution for 90 days. Prior to profile grinding of the cores for chloride analysis, the cores were

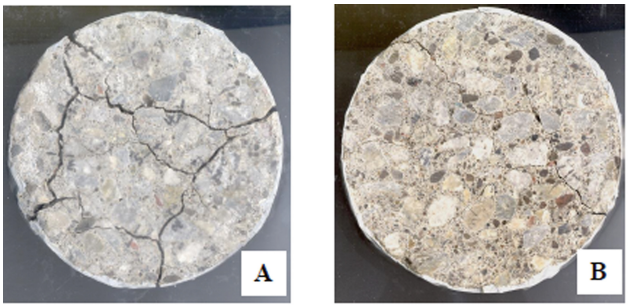

(a) Cracked cores after 22 months of storage in a freezer

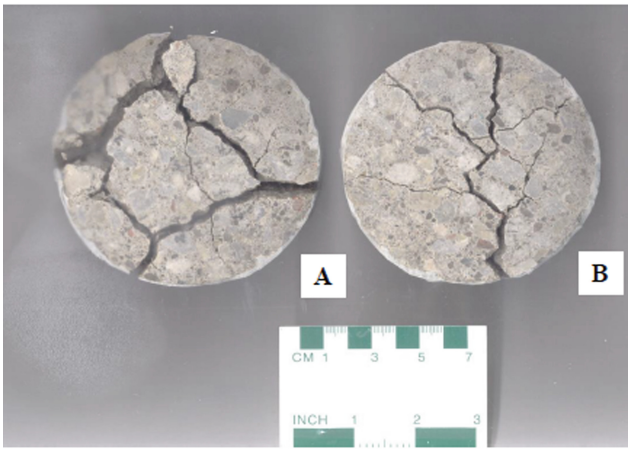

(b) Severely cracked cores after 26 months of storage in a freezer

Fig. 1. DEF expansion of Type 30 Portland cement [20]

removed from the chloride solution then dry - stored in a freezer at −18 °C. It was during the frozen storage that strangely interesting observations appeared. It was found that after the dry-storage of the cores in the freezer for 9 months, cracks developed in some cores. These observed cracks were monitored and found to continue growing rapidly with age while under storage in the freezer.

Figure 1 shows photographs of crack growth in the Cores A and B. It can be seen that Core A showed rapid crack growth attaining average sizes 0.1, 0.32, 7.3 mm at 9, 22, and 26 months respectively. Similarly, Core B rapidly developed cracks from about 0.0 mm at 9 months to 0.07 mm and 3.0 mm at 22 and 26 months, respectively. Once the onset of cracking occurred, crack development progressed rapidly, increasing by 43% and by 17.6% for the Cores A and B respectively, over a duration of 17 months.

3.2 Experimental Investigations

In order to further investigate the incidental observations discussed in the foregoing section, two experiments were conducted at different times. One study was done in Canada [21] while the other was carried out in South Africa [22]. The experiment conducted in Canada was a detailed study done using 25 × 25 × 285 mm bars made at 1:2.25:0.47 cement to sand to water, and using 75 × 75 × 285 mm concrete prisms made at 0.45 w/c. Both sets of samples were steam-cured at 95 °C then stored in water (for the control), 0.5 M or 2.8 M NaCl as reported in [21].

While the earlier study [21] was done in Canada, the later study [23] was conducted in South Africa using CEM I 42.5R supplied by Afrisam (pty) Ltd. The cement contained clinker SO_3 of 2.0% which is very low and non-expansive. In the experiment, the sulphate content of the cement was increased to a total of 5.0% SO_3, by adding Na_2SO_3 of technical grade supplied by Merck (pty) Ltd. The CEM I 42.5R cement was used to prepare mortar prisms of 25 × 25 × 285 mm at 1.0:2.25:0.5 cement to sand to water. The mortars were heat-cured at 95 °C then stored in water (0 M), 0.5 M, 1.0 M, 1.5 M, 2.0 M NaCl solutions. Both of the studies conducted in Canada and in South Africa, confirmed that indeed ingressed chlorides of low concentrations 0.25 M to 1.5 M enhance DEF, as seen in Fig. 2a,b [21, 23]. The mechanism by which chlorides enhance DEF expansion was proposed in [21]. This process was attributed to instability of monosulphate upon exposure to low chloride concentrations leading to CLDEF. At high chloride concentrations, the instability of both monosulphate and ettringite occurred, leading to suppression of DEF expansion. The proposed mechanism was also found to be consistent with kinetic theory that was employed for mathematical modelling of the chloride-DEF interation [27].

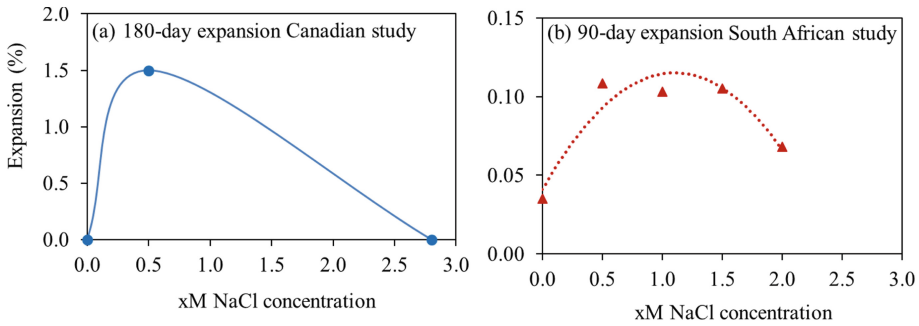

Fig. 2. Mortar expansions showing the pessimum effect of ingressed chlorides on DEF at (a) 180 days [21] (b) 90 – days [23]

4 Conclusions

This paper has provided additional insights on a less known mechanism by which externally applied chlorides can enhance delayed ettringite formation, to form a process that may be referred to as *chloride – enhanced delayed ettringite formation* (CLDEF), which was first reported in [21]. The present study has affirmed the following findings:

- Externally applied chlorides indeed exhibit pessimum effect on DEF expansion
- Low concentrations of about 0.25 to 1.5 M NaCl give the most severe enhancement of DEF
- Only expansive cements with SO_3 exceeding 4.0% can develop CLDEF
- Low expansive cementitious systems can develop expansive behaviour exceeding 0.10% threshold due to CLDEF

References

1. Heinz, D., Ludwig, U.: Mechanism of subsequent ettringite formation in mortars and concretes after heat treatment. In: Proceedings of the 8th International Congress on the Chemistry of Cement, Rio de Janeiro, Brasil, vol. V, Theme 4, pp. 189–194, 22–27 September 1986
2. Heinz, D., Ludwig, U.: Mechanism of secondary ettringite formation in mortars and concretes subjected to heat treatment. In: Scanlon, J.M. (ed.) Concrete Durability, Katharine and Bryant Mather International Conference, SP-100, vol. 2, pp. 2059–2071. American Concrete Institute, Detroit (1987)
3. Heinz, D., Kalde, M., Ludwig, U., Ruediger, I.: Present state of investigation on damaging late ettringite formation(DLEF) in mortars and concretes. In: Erlin, B. (ed.) Ettringite-The Sometimes Host of Destruction, SP-177. ACI Spring Convention, Seattle (1999)
4. Ekolu, S.O.: Heat curing practice in concrete precasting technology - problems and filture directions. J. Concr. Soc. South. Afr. **114**, 5–10 (2006)
5. Ekolu, S.O., Thomas, M.D.A., Hooton, R.D.: Dual effectiveness of lithium salt in controlling both delayedettringite fonnation and ASR in concretes. Cem. Concr. Res. **37**(6), 942–947 (2007)

6. Ekolu, S.O., Thomas, M.D.A., Hooton, R.D.: Implications of pre-formed microcracking in relation to theories ofDEF mechanism. Cem. Concr. Res. **37**, 161–165 (2007)
7. Ekolu, S., Rakgosi, G., Hooton, D.: Long-term mitigating effect of lithium nitrate on delayed ettringite fonnatiou andASR in concrete - microscopic analysis. Mater. Charact. **133**, 165–175 (2017)
8. ASTM C684-99: Standard test method for making, accelerated curing, and testing concrete compression testspecimens. ASTM International, West Conshohocken (1999). www.astm.org
9. BS 1881-112: Testing Concrete Part 112: Methods of accelerated curing of test cubes. British Standards Institution(BSI), London, UK (1983)
10. Johansen, V., Thaulow, N.: Heat curing and late formation of ettringite. In: Erlin, B. (ed.) Program on Ettringite-The Sometimes Host of Destruction, ACI SP-177, 1999, pp. 47–64. ACI, Seattle, April 1997
11. Hobbs, D.W.: Expansion and cracking in concrete attributed to delayed ettriugite formation. In: Erlin, B. (ed.) Program on Ettringite-The Sometimes Host of Destruction, AC1 SP-177, 1999, pp. 159–181. ACI Spring Convention,Seattle,April 1997
12. Skalny, J., Odler, I.: The effect of chlorides upon the hydration of Portland cement and upon some clinkerminerals. Mag. Concr. Res. **19**(61), 203–210 (1967)
13. Rosenberg, A.M.: Study of the mechanism through which calcium chloride accelerates the set of Portland cement. J.Am. Concr. Inst. Proc. **61**, 1261–1269 (1964)
14. Neville, A.M.: Properties of Concrete. 4th edn. Wiley, New York (1996). (also 3rd edition 1981)
15. Midgley, H.G., Illston, J.M.: The penetration of chlorides into hardened cement pastes. Cem. Concr.Res. **14**(4), 546–558 (1983)
16. Zuquan, J., Wei, S., Yunsheng, Z., Jinyang, J., Jianzhong, L.: Interaction between sulfate and chloride solution attackof concretes with and without fly ash. Cem. Concr. Res. **37**, 1223–1232 (2007)
17. Lee, S.T., Park, D.W., Ann, K.Y.: Mitigating effect of chloride ions on sulfate attack of cement mortars with or withoutsilica fume. Can. J. Civ. Eng. **35**, 1210–1220 (2008)
18. Sotiriadis, K., Nikolopoulou, E., Tsivilis, S., Pavlou, A., Chaniotakis, E., Swamy, R.N.: The effect of chlorides onthe thaumasite form of sulfate attack of limestone cement concrete containing mineral admixtures at low temperature.Constr. Build. Mater. **43**, 156–164 (2013)
19. Marks, V.J., Dubberke, W.G.: A different perspective for investigation of Portland cement concrete deterioration.Transp. Res. Rec. **1525**, 91–96 (1996)
20. Ekolu, S.O.: Role of heat curing in concrete durability: effects of lithium salts and chloride ingress on delayed ettringiteformation, Ph.D. thesis, Civil Engineering Department, University of Taroma, Canada (2004). 217p.
21. Ekolu, S.O., Thomas, M.D.A., Hooton, R.D.: Pessimum effect of externally applied chlorides on expansion due toDEF - proposed mechanism. Cem. Concr. Res. **36**, 688–696 (2006)
22. Matta, Z.G.: Deterioration of concrete structures in the Arabian Gulf. Concr. Int. 33–36 (1993)
23. Ekolu, S.O.: Influence of synthetic zeolite on delayed ettringite formation - preliminary investigation. In: 2nd InternationalWorkshop on Durability and Sustainability of Concrete Structures (DSCS), Moscow, Russia, 6–7 June 2018, SP 326-42, pp. 42.1–42.8 (2018)
24. Crammond, N.J.: Examination of mortars containing varying percentages of coarsely crystalline gypsum as aggregate.Cem. Concr. Res. **14**, 225–230 (1984)
25. Xu, A., Shayan, A., Baburamani, P.: Test methods for sulphate resistance of concrete and mechanism of sulphateattack: a state-of-the-art review. ARRB Transport Research Ltd., Review Report 5 (1998). 44 p.

26. ASTM C1556-11a(2016): Standard test method for determining the apparent chloride diffiJsion coefficient ofcementitious mixtures by bulk diffusion. ASTMIntematianal, West Conshohocken, PA (2016). www.astm.org
27. Mulongo, L., Ekolu, S.O.: Mathematical modelling of the pessimum action of chlorides on the extent of delayedettringite formation, Part 1: formulation. Key Eng. Mater. 400–402, 203–208 (2008)

Geopolymer Damage Due to Leaching When Exposed to Water

M. Guerrieri[1(✉)], J. Sanjayan[2], and A. Z. Mohd Ali[3]

[1] Victoria University, Werribee, Australia
maurice.guerrieri@vu.edu.au
[2] Swinburne University of Technology, Melbourne, Australia
[3] Tun Hussein Onn Malaysia, Parit Raja, Johor, Malaysia

Abstract. An investigation on the effect of water immersion on the compressive strength of geopolymer pastes was investigated. Specimen's exposure to water showed a detrimental effect on the compressive strength of the geopolymer pastes (up to 25% strength loss). It was shown that the leaching of the sodium silicate when geopolymers were immersed in water decreases the compressive strength.

Keywords: Compressive strength · Concrete · Drying · Geopolymer · Leaching

1 Introduction

Since the invention of geopolymers, there has been advances in the literature exploring the properties of geopolymer materials on a laboratory scale [1] which has provided confidence that geopolymers can offer similar if not superior performance to Ordinary Portland Cement (OPC). Whilst the durability of geopolymers exposed to various aggressive environments have shown excellent resistance to chemical attack by chlorine (including sea water), various acids, alkali and sulphate, [1–5], others have reported that the durability of geopolymers is hindered when exposed to magnesium sulphate and sulfuric acid solutions [6].

Another durability concern is the effect of water on geopolymers, especially in relation to efflorescence and leaching. Whilst the effects of the reactivity of raw materials, alkali metal type and reaction conditions on the intensity of efflorescence and leaching of geopolymers has been reported [7–12], the literature is either scant or silent in respect to the effect on mechanical strength of geopolymer exposed to water. The effect of leaching and efflorescence on the compressive strength of geopolymer when specimens were under dry, in water contact and submerged in water for a period of up to 28 days has been studied [12]. Results indicated submerged specimens experienced strength loss postulated to be due to leaching which contributes to the restriction of the geopolymer to develop strength due to late geopolymerization whilst water contact specimens experienced strength loss due to efflorescence. This suggests that geopolymers placed in humid conditions should be given attention due to the phenomenon's in play which can effect strength loss [12]. This is partially important given

© RILEM 2020
K. Kovler et al. (Eds.): ConcreteLife 2020, RILEM Bookseries 26, pp. 74–78, 2020.
https://doi.org/10.1007/978-3-030-43332-1_15

that geopolymers are being considered as a possible medium for the encapsulation of radioactive and hazardous waste [13, 14] and other applications that have direct contact with water, for example, sewer pipes, bridge pillars and water waste treatment facilities. Zhang et al. [12] sighted previous works Skvara et al. [15] who reported that geopolymer mortars immersed in water exhibited lower compressive strengths than those exposed to ambient conditions. It was postulated that the leaching of sodium through diffusion of the alkali cations was attributed to this strength reduction.

Resistance to water is an important durability parameter for geopolymers that needs investigation. The results presented in this study aimed to investigate and explain the effect of water exposure to cured geopolymers and their effect on compressive strength. It should be noted that the water exposure damage reported here is only applicable to the particular mixtures used. Further work of the authors is underway to obtain geopolymer mixtures which are resistant to water exposure.

2 Experimental Program

The aluminosilicate source for the geopolymer used in this study was fly ash sourced from Pozzolanic Gladstone in Queensland, Australia. Chemical composition for this fly ash has been studied by Kong and Sanjayan [16]. Alkaline activator used was a combination of sodium silicate, Na_2SiO_3 and sodium hydroxide, NaOH (molarity of 8.0M). Sodium silicate used in this experiment has a ratio of SiO_2/Na_2O of 2. Sodium hydroxide of 8.0M solution comprises 26.2% of NaOH solids and 73.8% of water [17].

All specimens had dimensions of 38 mm × 73 mm (diameter × height) and were cast in PVC moulds. The ratios of Na_2SiO_3/NaOH were 2.5, 1.75 and 1.0. Alkaline solution to fly ash ratio was kept constant at 0.4. Further specimens with 0.57 alkaline solution to fly ash ratio and 2.5 Na_2SiO_3/NaOH ratio were made to investigate the effect of saturation and dry conditions of high strength geopolymer. Ten specimens were made for each mix design, five each for the dry and saturated tests.

3 Results and Discussion

The compressive strength results are based on five specimens from each mix apart from the Na_2SiO_3/NaOH = 1.0, Alkaline solution/fly ash = 0.4 mix which only had four specimens for the saturated state condition. In dry condition, specimens with 0.4 alkaline solution to fly ash ratio produced average compressive strength of 92.76 MPa, 89.62 MPa and 74.54 MPa for 2.5, 1.75 and 1.0 Na_2SiO_3/NaOH ratios respectively which is dependent upon the amount of Na_2O per total geopolymer mix (fly ash + alkaline solution).

Higher strength losses were recorded in higher Na_2SiO_3/NaOH ratios. These results demonstrated the trend that higher strength can be achieved by using a higher Na_2SiO_3/NaOH ratio. In saturated condition, the strengths of the specimens were less than the dry condition. The saturated strengths were 68.96 MPa, 76.46 MPa and 64.40 MPa for 2.5, 1.75 and 1.0 Na_2SiO_3/NaOH ratios respectively. These are 25.66%, 14.69 and

13.60% less than the dry strengths. Figure 1 and Table 1 shows the compressive strength of geopolymers in dry and saturated conditions and their water absorption characteristics are shown in Table 2.

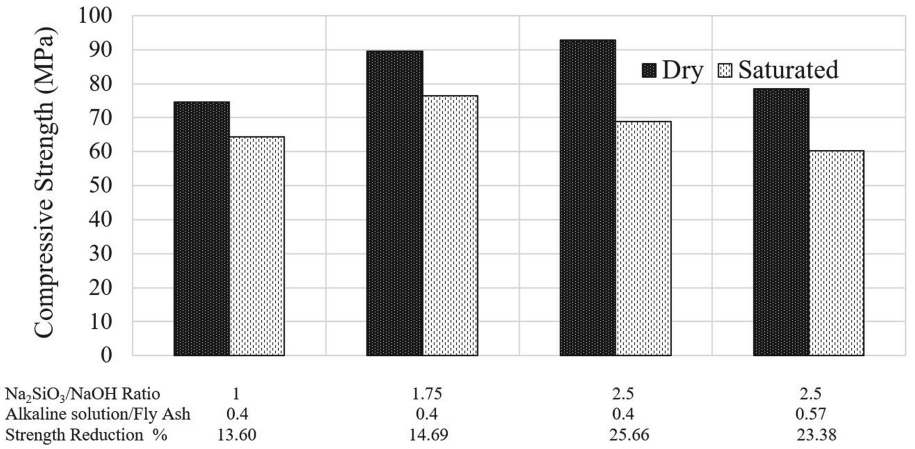

Fig. 1. Compressive strengths of dry and saturated geopolymer pastes

Table 1. Compressive strengths of geopolymer pastes under dry and saturated conditions

Alkaline solution/FA	Na_2SiO_3/NaOH	Compressive strengths (MPa)				
		Average dry	STDEV	Average saturated	STDEV	% Loss
0.4	1	74.54	2.31	64.40	4.22	13.60
0.4	1.75	89.62	3.91	76.46	1.50	14.69
0.4	2.5	92.76	2.67	68.96	4.74	25.66
0.57	2.5	78.53	4.31	60.17	5.98	23.38

Table 2. Average saturated weights and absorption percentages of geopolymer pastes under dry and saturated conditions

Alkaline solution/FA	Na_2SiO_3/NaOH	Average weights (g)					
		Average dry	STDEV	Average saturated	STDEV	Absorbed (%)	STDEV
0.4	1	155.80	0.16	161.58	0.15	3.73	0.05
0.4	1.75	155.40	0.51	162.06	0.48	4.28	0.15
0.4	2.5	155.04	2.80	161.78	2.89	4.34	0.26
0.57	2.5	151.76	0.59	158.98	0.38	4.74	0.18

Similar strength reductions of geopolymers due to water immersion reported in literature are shown in Fig. 2. The strength reduction of the results presented in this investigation are purely from the effect of leaching.

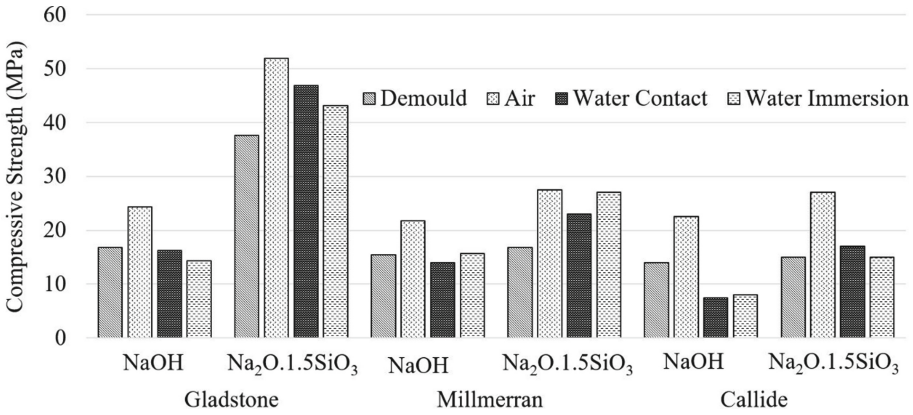

Fig. 2. Compressive strengths of demolded geopolymer pastes followed by air curing, water contact and water immersion conditions. Modified from [12]

4 Conclusions

1. There is compressive strength reduction ranging from 13.60% to 25.66% for geopolymer immersed to water. Geopolymer specimens with 2.5 ratio of Na_2SiO_3/NaOH and 0.4 alkaline solution to fly ash ratio provides the highest average compressive strength of 92.76 MPa and the highest average strength reduction of 25.66%.
2. Geopolymer specimens with 1.0 ratio of Na_2SiO_3/NaOH and 0.4 alkaline solution to fly ash ratio provides the lowest average compressive strength of 74.54 MPa and the lowest average strength reduction of 13.60%.
3. Initial geopolymer strength is not the influencing factor in the strength reduction. This was proven by same strength but different Na_2SiO_3/NaOH specimens. The trend of increasing Na_2SiO_3/NaOH with increasing strength reductions remained for the same strength specimens.
4. The strength reduction is caused by sodium silicate leaching out from specimens when immersed in water which caused strength damage. This conclusion was reached by eliminating strength as the cause of this and by measuring leached chemicals in the immersing water.
5. Strength reduction due to leaching during curing is an important consideration when developing geopolymer mixes. Some mixes seem more vulnerable to leaching than others and better understanding of this phenomenon will lead to better design of geopolymer mixes.

References

1. Duxson, P., et al.: The role of inorganic polymer technology in the development of 'green concrete'. Cem. Concr. Res. **37**(12), 1590–1597 (2007)
2. Palomo, A., et al.: Chemical stability of cementitious materials based on metakaolin. Cem. Concr. Res. **29**(7), 997–1004 (1999)
3. Allahverdi, A., Škvára, F.: Nitric acid attack on hardened paste of geopolymeric cements—part 1. Ceram.-Silik. **45**(3), 81–88 (2001)
4. Allahverdi, A., Skvara, F.: Sulfuric acid attack on hardened paste of geopolymer cements Part 1. Mechanism of corrosion at relatively high concentration. Ceram.-Silik. **49**(4), 225–229 (2005)
5. Bakharev, T.: Durability of geopolymer materials in sodium and magnesium sulfate solutions. Cem. Concr. Res. **35**(6), 1233–1246 (2005)
6. Lavanya, G., Jegan, J.: Durability study on high calcium fly ash based geopolymer concrete. Adv. Mater. Sci. Eng. **2015**, 7 (2015)
7. Škvára, F., et al.: Aluminosilicate polymers–influence of elevated temperatures, efflorescence. Ceram.-Silik. **53**(4), 276–282 (2009)
8. Szklorzová, H., Bílek, V.: Influence of alkali ions in the activator on the performance of alkali-activated mortars. In: Proceedings of the 3rd International Symposium on Non-Traditional Cement and Concrete (2008)
9. Temuujin, J., van Riessen, A.: Effect of fly ash preliminary calcination on the properties of geopolymer. J. Hazard. Mater. **164**(2–3), 634–639 (2009)
10. Zhang, Z.H., et al.: Fly ash-based geopolymers: the relationship between composition, pore structure and efflorescence. Cem. Concr. Res. **64**, 30–41 (2014)
11. Zhang, Z.: Efflorescence a critical challenge for geopolymer applications? In: Concrete Institute of Australia's Biennial National Conference (Concrete 2013), Understanding Concrete, 16–18 October 2013, Gold Coast, Australia (2013)
12. Zhang, Z.H., Yang, T., Wang, H.: The effect of efflorescence on the mechanical properties of fly ash-based geopolymer binders. In: 23rd Australasian Conference on the Mechanics of Structures and Materials (ACMSM23), Byron Bay, NSW (2014)
13. Ly, L., et al.: Leaching of geopolymers in deionised water. Adv. Technol. Mater. Mater. Process. J. **8**(2), 236 (2006)
14. Davidovits, J.: Geopolymers: man-made rock geosynthesis and the resulting development of very early high strength cement. J. Mater. Educ. **16**, 91–139 (1994)
15. Skvara, F., et al.: A weak alkali bond in (N, K)-A-S-H gels: evidence from leaching and modeling. Ceram.-Silik. **56**(4), 374–382 (2012)
16. Kong, D.L.Y., Sanjayan, J.G.: Effect of elevated temperatures on geopolymer paste, mortar and concrete. Cem. Concr. Res. **40**(2), 334–339 (2010)
17. Rangan, B.V.: Fly ash-based geopolymer concrete. Indian Concr. J. **80**(2), 35 (2006)

Air Void Analysis of Hardened Concrete Without Colour Enhancement

Gui Li(✉), M. T. Hasholt, and O. M. Jensen

Department of Civil Engineering,
Technical University of Denmark, Lyngby, Denmark
guili@byg.dtu.dk

Keywords: Air void analysis · Hardened concrete · Optical microscopy · Shape From Focus (SFF) · Focused image

1 Introduction

Air void structure plays a key role in the durability of concrete structures in cold regions. This is because water in the microstructure can escape into the air voids which, thereby, effectively reduce the stresses during cyclic freezing and thawing. This protects the concrete structures from developing frost damage [1, 2]. Therefore, to assure the frost resistance of conventional concrete, it is necessary to quantify its air void structure.

The most widely used methods for measuring the air void parameters in hardened concrete are the microscopy-based methods described in ASTM C457/457M-16 [3]. The linear-traverse method determines the air void parameters by analysing the data that include the number of air voids traversed by a set of regularly spaced lines and the distances traversed through paste and air voids along these lines. The modified point-count method counts the number of air voids traversed through the lines as well, but instead of summing the traverse distances, a grid of points is used to record the frequency of locations in paste and air voids. Both methods can be conducted manually, but this is time-consuming, tedious and expensive. In addition, the results can be influenced by operator judgment. To address these drawbacks, the contrast-enhanced methodscan be used to identify the air voids by image analysis. Then colour enhancement needs to be done before the microscopy analysis. This also needs significant efforts for sample preparation. Furthermore, the quality of surface treatment can influence the accuracy of test results [4].

In the 1990s, Nayar [5] developed a shape from focus method to analyse the texture of different objects that have a rough surface. An optical microscope is used to get a sequence of images with different focus planes. Then the focused image and 3D texture of the object surface can be reconstructed and the depth map can be computed. In the present study, the shape from focus method is used to obtain the focused image and the depth information of the concrete surface. This enables automatic identification of the air void structure in hardened concrete, without pre-treatment like colour enhancement.

© RILEM 2020
K. Kovler et al. (Eds.): ConcreteLife 2020, RILEM Bookseries 26, pp. 79–83, 2020.
https://doi.org/10.1007/978-3-030-43332-1_16

2 The Principle of a New Test Method: Shape from Focus (SFF)

Before introducing the principle of the shape from focus method (SFF), the image formation process should be kept in mind. As shown in Fig. 1, when the light rays radiated by a point pass through the lens, they are refracted and converged at a single point. For a thin lens, the relationship between the focal length of the lens f, the distance from the point to the lens plane o, and the distance from the image plane to the lens plane i, follow the Gaussian lens law [5]:

$$\frac{1}{o} + \frac{1}{i} = \frac{1}{f} \tag{1}$$

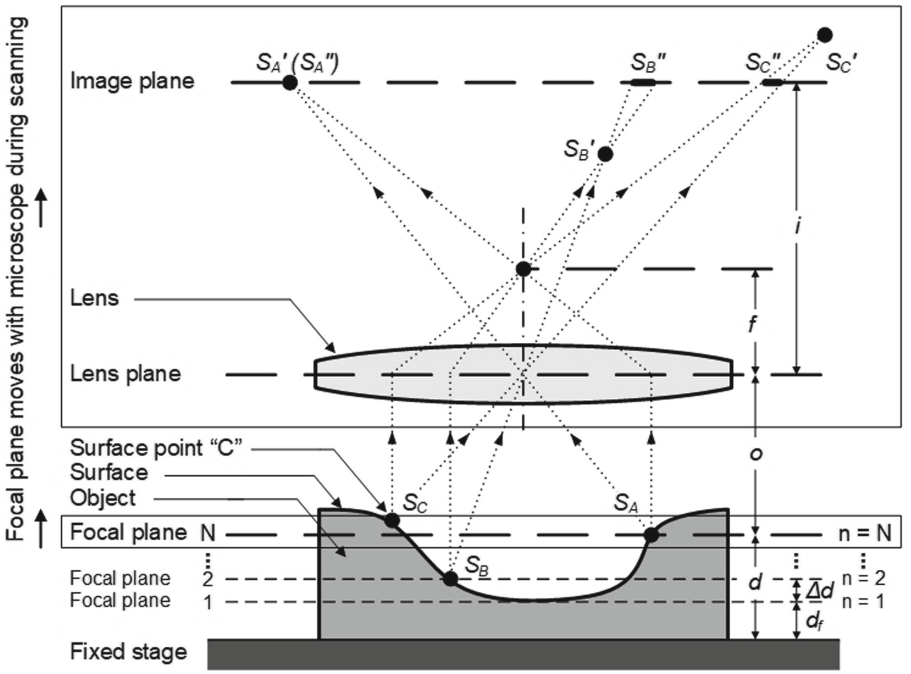

Fig. 1. Principle of the image formation and the shape from focus method. (Note: The microscope can be moved from top to bottom as well.)

Therefore, for an optical microscope system, when the configuration of the lens plane and the image plane is fixed, the only focal plane is defined, see Fig. 1. It means that only the surface points that lie on the focal plane (like S_A) will be perfectly focused on the image plane. Other points located outside the focal plane (like S_B and S_C) will form defocused or blurred areas on the image plane (S_B'' and S_C'').

Based on this, when an object with a rough surface is placed on a fixed stage, moving the focal plane away from the stage by moving the microscope allows getting the focused image of each point located in different positions, as presented in Fig. 1. For each point on the object surface, it is possible to determine its degree of focus in different image frames by using a focus measure operator and then record the displacement of the microscope at the position of maximum focus. After that, the height of the point with respect to the stage d can be calculated by Eq. (2):

$$d = d_f + (n-1)\Delta d \tag{2}$$

Where d_f is the distance between the initial position of the focal plane $(n = 1)$ and the fixed stage, which can be measured directly, n is the number of steps, and Δd is the displacement of the microscope at each step. This procedure allows determining of the height of all points with respect to the stage independently to get the focused image and the depth map of the entiresurface. And it can also be used to calculate the distance between all points and other planes such as the lens plane.

3 Materials and Methods

3.1 Sample Preparation

A concrete sample was prepared using Portland cement CEM I 52.5 N, sea sand, and crushed granite (4–16 mm). Instead of traditional air entraining agents, suspension polymerized superabsorbent polymers (SAP) was used to create the air void structure in the hardened concrete. The total w/c was 0.52, and the SAP dosage was 0.4% relative to the mass of cement. The SAP absorption capacity was 17 g/g. The percentage by volume of sand and coarse aggregate was approx. 23% and 35%, respectively. The sample was cast in a cylindrical mould (Ø 150 mm × 300 mm) and demoulded after 24 h. Then the sample was cured in a polythene bag at 20 ± 1 °C 14 days after mixing, a 20 ± 1 mm thick specimen was cut from the cylinder perpendicular to the end surfaces. Finally, the surface of the specimen was ground with successively finer silicon carbide abrasive papers (grit sizes corresponding to 75, 35, 17.5 and 12.5 μm).

3.2 Image Acquisition and Preliminary Analysis

A Nikon SMZ25 stereo microscope equipped with NIS-Elements software was used. The specimen was placed on the fixed microscope stage and adjusted, so the test surface was horizontal. The magnification was 70× (obtained by an objective lens with the magnification of 2× and azoom of 35×). After setting the displacement of the microscope (Δd = 10 μm) and the number of steps (n = 51), the program digitized and stored images at each position.

The NIS-Elements software was used to obtain the preliminary results, see Fig. 2. The software module is based on the so-called extended depth of focus method (EDF), instead of the shape from focus method. The principle of EDF is different from that of SFF, but both methodscan be used to obtain the focused image and the depth

information of the object surface [6]. As shown in Fig. 2 left, it is impossible, without colour enhancement, to distinguish air voids from aggregates by using traditional threshold segmentation methods directly. However, due to the difference of depth between air voids and the rest of the test surface, air voids can be identified from the depth map presented in Fig. 2 centre via a threshold segmentation method, see Fig. 2 right. Thus, preliminary results illustrate that it is generally possible to distinguish air voids from aggregates based on the depth information. However, some air voids are not detected, and this is the topic for further investigations.

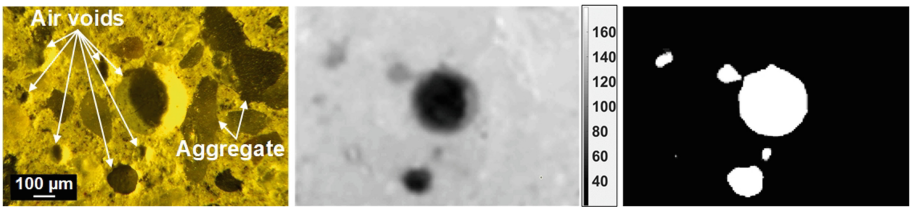

Fig. 2. Images obtained by the NIS-Elements software in the microscope system. Left: focused image; centre: depth map; right: binary image.

3.3 Upcoming Work

In the near future, the SSF method will be used to process and analyse microscopeimages. After image acquisition, a modified Laplacian focus measure operator is used to determine the degree of focus of each pixel [5]. Based on this, the image frame with the maximum sharpness measure at each pixel is determined. After that, the focused image and depth map of the concrete surface can be obtained to enable analysis of the air void structure of hardened concrete.

To test the accuracy and robustness of the SFF method, a comparison between the results obtained by the SFF method and that of the modified point-count method will be performed. A study will also be conducted on influencing factors including the brightness and resolution of images, the number and magnitude of the displacement steps, the smoothness of the specimen surface, etc.

Acknowledgement. The authors would like to thank China Scholarship Council and Technical University of Denmark for funding this research project. Shengying Zhao, guest PhD student at Technical University of Denmark, provided the polished specimen, and this is also acknowledged.

References

1. Powers, T.C.: The air requirement of frost resistant concrete. Proc. Highw. Res. Board **29**, 184–221 (1949)
2. Pigeon, M., Pleau, R.: Durability of Concrete in Cold Climates. CRC Press, Boca Raton (1995). Spon

3. ASTM C457/C457M-16: Standard Test Method for Microscopical Determination of Parameters of the Air-Void System in Hardened Concrete. ASTM International, West Conshohocken, PA (2016)
4. Pleau, R., Michel, P., Jean, L.L.: Some findings on the usefulness of image analysis for determining the characteristics of the air-void system on hardened concrete. Cem. Concr. Compos. **23**(2–3), 237–246 (2001)
5. Nayar, S.K.: Shape from focus system. In: IEEE Computer Society Conference on Computer Vision and Pattern Recognition (1992)
6. Zalevsky, Z.: Extended depth of focus imaging: a review. SPIE Rev. **1**(1), 018001 (2010)

Autogenous Shrinkage Revisited

O. M. Jensen(✉)

Department of Civil Engineering, Technical University of Denmark,
Lyngby, Denmark
omj@byg.dtu.dk

Keywords: Autogenous · Shrinkage · Deformation · RH-change · Cracking

1 Introduction

In the 1990s it became generally accepted in the scientific community that autogenous shrinkage is a major reason for cracking observed during hardening of high-performance concrete [1, 2]. Within this decade suitable measurement techniques to identify autogenous deformation were developed, a large amount of scientific studies on the phenomenon were done all over the World, and various methods to mitigate its adverse effects were tested [3]. Today, about 25 years later, clearly the general knowledge on autogenous shrinkage and its mitigation strategies are extensive, but practice is slow to adopt it. To some extent cracking is in practice considered part of the nature of concrete. In this presentation an overview is given regarding mitigation of autogenous shrinkage in the cementitious binder. Certainly cracking, including that generated by autogenous shrinkage, can be, and should be minimized.

2 Experimental Details

Experiments were done with a high-performance cementitious mixture consisting of: White Portland cement (Blaine surface: 419 m^2/kg, Bogue composition by mass%: C_3S: 66.1, C_2S: 21.2, C_3A: 4.3, C_4AF: 1.1, $CaSO_4$: 3.4, free CaO: 2.0, Na_2O eq.: 0.020), dry silica fume (BET surface 20 m^2/g, composition by mass%: SiO_2: 89.9, LOI: 2.9, Na_2O eq.: 1.7), and a dry sodium naphthalene sulphonate superplasticizer. Water/cement-ratio is 0.30, the silica fume/cement ratio is 20%, and superplasticizer/(cement + silica fume) is 0.010. For mortars quartz sand 0–2.5 mm with a water absorption of 0.1% was used. By volume the mortars contain 60% aggregate.

The methods for measuring development of autogenous properties and cracking sensitivity are described in [2].

© RILEM 2020
K. Kovler et al. (Eds.): ConcreteLife 2020, RILEM Bookseries 26, pp. 84–88, 2020.
https://doi.org/10.1007/978-3-030-43332-1_17

3 Results

Measurement results of autogenous RH-change, autogenous deformation and stress build-up during restrained hardening are shown in Figs. 1, 2 and 3.

As seen the autogenous RH drops to approximately 80% RH after two weeks. It is expected that the RH will not develop much further from this level, even during years of sealed hardening. The observed, slight variation in curvature from 1 to 3 days is related to the silica fume [2]. The RH is a direct measure of the thermodynamic free-energy (G [J/mol)]) state of the water, which at 30 °C becomes:

$$G = G^{\Theta} + RT\ln(a) = G^{\Theta} + RT\ln\left(\frac{p_s}{p^{\Theta}} \cdot RH\right) = G^{\Theta} + RT\ln(0.042 \cdot RH)$$

R: Gas constant [J/mol/K]
T: Temperature [K]
a: activity [-]
Θ: standard state
s: saturated

As such, the reduction in RH has the consequence that the free energy of the water is lowered and it becomes less reactive. Though this may not be the cause of the generally observed limiting autogenous RH of about 75–80%, it does significantly

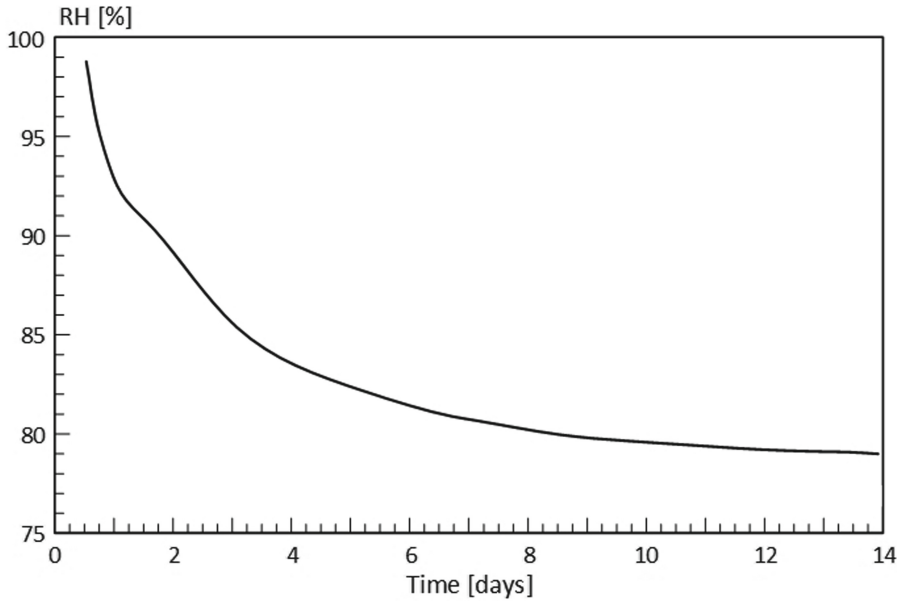

Fig. 1. Autogenous RH-change of cement paste with w/c = 0.30 and 20% silica fume addition. Temperature 30 °C.

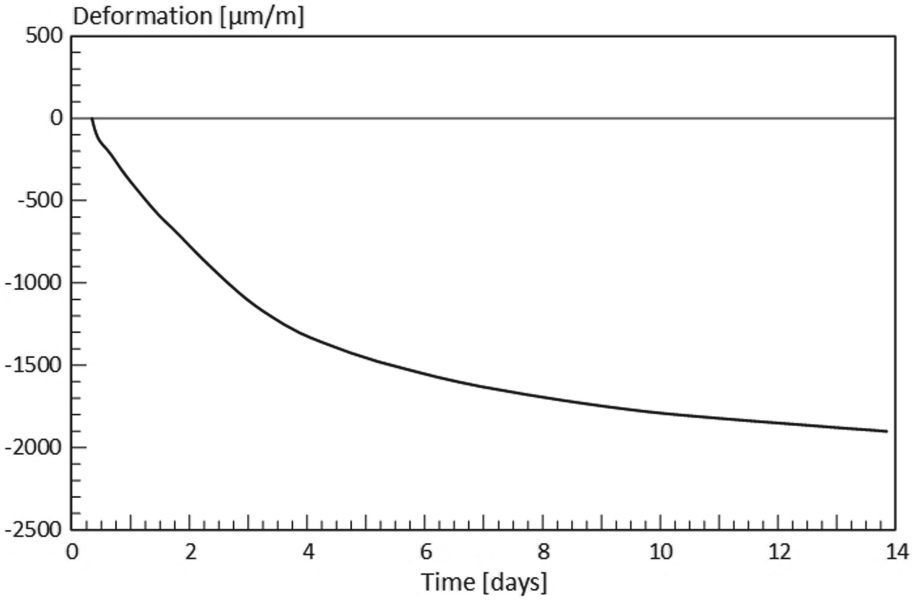

Fig. 2. Autogenous deformation after setting of cement paste with w/c = 0.30 and 20% silica fume addition. Temperature 30 °C.

influence hydration kinetics [2]. Experiments have indicated two phenomena to be involved in the autogenous RH-lowering: (1) Dissolution of salts in the pore water, and (2) formation of menisci. Salts dissolved in the pore water may account for a couple of % RH-lowering, i.e. most of the RH-lowering observed in Fig. 1 will be caused by menisci formation.

The menisci will also generate tensile stresses in the pore water (σ_{cap} [Pa]) which are related to the RH through the Kelvin and Laplace equation:

$$\sigma_{cap} = -\frac{RT}{V_m}\ln(RH) = -140\ \text{MPa} \cdot \ln(RH)(\text{at } 30\,^{\circ}\text{C})$$

V_m: molar volume of water [m^3/mol]

An RH-lowering from e.g. 100 to 80%, completely due to menisci formation, will according to this equation be related to an increase in the pore water tensile stress to approximately 30 MPa. Such tensile stresses in the pore water will lead to compressive stresses in the solid skeleton and shrinkage of the cementitious material. Calculative conversion of the pore water tensile stresses into outer shrinkage is not simple as it is influenced by many factors, of which several are ill-known: Porosity, degree of

saturation of the pores, elastic properties of the solid components, the structure of the composite material, creep, and in the early ages where autogenous RH-change and deformation are particularly active, the microstructure is developing in parallel with the autogenous RH-change and deformation. Furthermore, there are deformation mechanisms active which are not related to menisci stresses, such as shrinkage due to dissolution of restraining components in the solid material or expansion caused by the growth pressure of precipitating components.

Experimentally, in contrast with autogenous RH-change, autogenous deformation is not an absolute measurement, and this causes an additional problem: A "zero-point" for the deformation has to be defined. This is a difficult task as there is no well-defined state for this. The only meaningful option is to measure deformation from the time where the cementitious material transforms from a liquid to a solid, i.e. formally at the point of setting (final set). Obviously significant uncertainty is related to this since this liquid-solid transformation to some extent is smooth rather than instantaneous. A further and very considerable contribution to the complexity of simulation and interpretation of autogenous deformation measurements is that the deformation rate (in the form of shrinkage) reaches very high values before and up till around setting. No matter if the "time zero" is chosen from a physical setting measurement or if it is rather done by interpretation of autogenous deformation measurements the uncertainty related to it may cause a major shift on the deformation values. Luckily it has less consequence on calculated stress build-up during restrained deformation since the creep ability of the material is very high at this early point.

As seen in Fig. 2 the measured autogenous deformation occurs as shrinkage throughout which develops in a smooth and monotonous way. After two weeks almost 2000 μm/m of shrinkage has been generated. This is much more than the expected tensile strain capacity [2]. Apart from this, no particular, characteristic features are observed in Fig. 2.

Figure 3 illustrates the build-up of tensile stresses during sealed, restrained hardening. After an initial, fast stress build-up, it slows down, but before it stabilizes, the mortar cracks, and the stresses are relieved.

The curves shown in Figs. 1, 2, and 3 can be considerably changed by modification of the hardening temperature or in the composition of the paste or mortar. As shown in the literature it is possible by routine and by simple means to almost completely stop the autogenous RH-change, turn the autogenous shrinkage completely into expansion (or minimize it), and to avoid the stress build-up and cracking during restrained hardening [2]. Though it may not be possible to usefully predict autogenous shrinkage and stress build-up, or even reliably model the internal relations between the autogenous properties, sufficient knowledge does exist to safely control these phenomena.

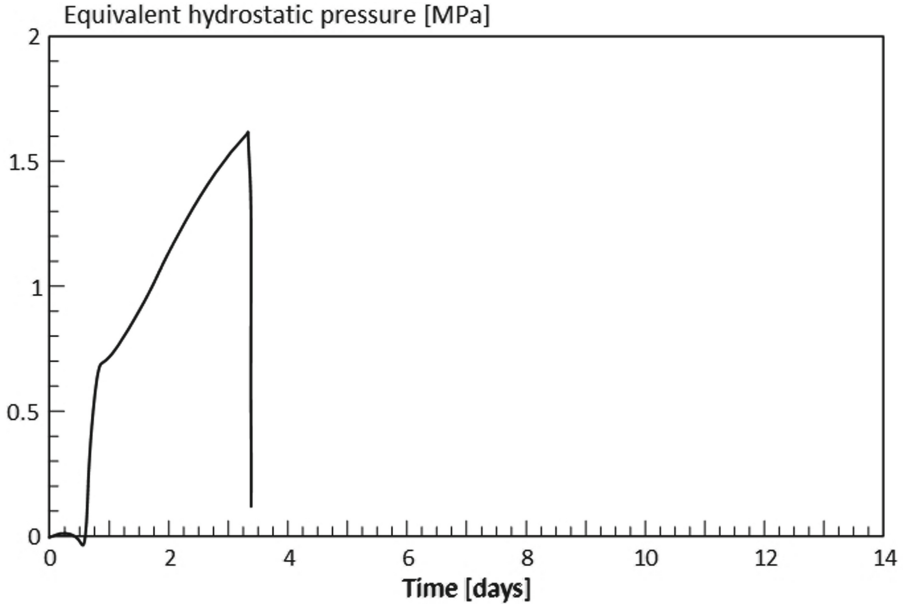

Fig. 3. Equivalent hydrotstatic pressure developed during restrained, sealed hardening in an annular shrinkage gauge, ASG, by mortar with w/c = 0.30, 20% silica fume addition, and 60% aggregate by volume. Temperature 20 °C.

4 Summarizing Comments

Since high-performance concrete was introduced into the market more than 30 years ago a lot of knowledge related to its autogenous material properties have been gained. Today we are able to reliably measure and control these properties on a scientific basis, and we do have a basic chemical and physical understanding of the underlying mechanisms involved. However, we still lack sufficient knowledge to reliably predict these phenomena by modeling. This remains a task to be accomplished by future efforts.

References

1. Aïtcin, P.-C.: High-Performance Concrete. E & FN Spon, London (1998)
2. Jensen, O.M.: Autogenous phenomena in cement-based materials. DSc thesis, Aalborg University, Aalborg, Denmark (2005)
3. Bentz, D.P., Jensen, O.M.: Mitigation strategies for autogenous shrinkage cracking. Cement Concr. Compos. **26**, 677–685 (2004)

A Simple Method for Determining the Diffusion Coefficient of Radon in Concrete Samples Using Charcoal

A. Tsapalov, T. Maslov(✉), and K. Kovler

National Building Research Institute,
Faculty of Civil and Environmental Engineering,
Technion – Israel Institute of Technology, Haifa, Israel
tatiana-m@campus.technion.ac.il

Keywords: Radon · Exhalation · Diffusion coefficient · Concrete · Activated charcoal

1 Introduction

Radon is one of the most dangerous carcinogens that causes cancer. For this reason, in many countries of the world, the indoor radon is limited. For example, in Israel, the reference level of the radon concentration is 200 Bq/m^3 for homes and 500 Bq/m^3 for working places.

The main source of indoor radon is soil, so building materials and structures in the underground part of the building, such as concrete in foundation slab, should prevent the transport of soil radon into the building. However, due to aging and deterioration of concrete in time, its permeability to radon increases. An important characteristic of material permeability is radon diffusion coefficient, which is often used to evaluate quality of radon barrier materials. In addition, radon diffusion coefficient can be used to indicate concrete performance in terms of its durability, similarly to diffusion coefficients of chloride ion, air, oxygen, carbon dioxide and water, which cause detrimental effects in concrete. The advantage of testing diffusion of radon is that it does not interact chemically with concrete constituents, because is a noble gas.

Over the past few decades, many different methods and approaches have been published to determine the diffusion coefficient of radon in building materials. Two international ISO standards are among them, they differ fundamentally in the test modes: one of them [1] is based on the non-stationary mode, and another [2] – on the stationary one. The main advantage of the non-stationary method is the short duration of the test, not exceeding 24 h, but this method uses a powerful radon source and non-standard measuring equipment, as well as a complex mathematical apparatus [3]. The duration of tests in the stationary mode is significantly longer (from 2 to 4 weeks). At the same time, a radon source of low activity and standard radon devices can be used [2]. The experimental setup in the stationary measurement methods usually includes two sealed chambers, one of them contains a radon source. The test sample is located between these two chambers.

© RILEM 2020
K. Kovler et al. (Eds.): ConcreteLife 2020, RILEM Bookseries 26, pp. 89–93, 2020.
https://doi.org/10.1007/978-3-030-43332-1_18

The main novelty of our approach is the use of only one chamber containing a radon source. In addition, we propose to use very simple equipment based on radon adsorption in activated charcoal for measuring its activity, as well as a standard plastic tube for the manufacture of the chamber and concrete samples.

2 Theory of the Method

The measurement scheme of the proposed method is shown in Fig. 1a, and its principle is as follows. The test cylindrical sample with a sealed lateral surface and unsealed ends is hermetically mounted in a cylindrical chamber, the lower end of which is hermetically sealed. The source of radon is located inside the chamber.

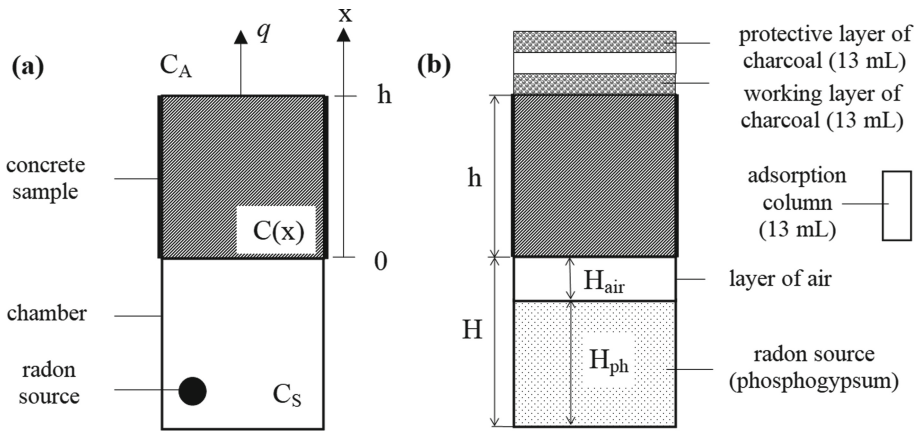

Fig. 1. Measurement scheme (a) and experimental setup (b)

After installing the sample, the concentration of radon in the chamber increases due to the source. However, in the stationary mode, the concentration of radon in the chamber, as well as the distribution of the radon concentrations along the height of the sample, is stabilized over time due to the equality of the rates of radon release from the source and its runoff, which is due to the natural decay and diffusion of radon through the sample into ambient air. The stationary radon diffusion in a homogeneous sample is described by the well-known equation:

$$D \cdot \frac{d^2C(x)}{dx^2} - \lambda \cdot C(x) = 0 \tag{1}$$

The boundary conditions on the lower and upper surfaces of the sample are as follows:

$$C(x = 0) = C_s \tag{2}$$

$$C(x = h) = C_A = 0 \tag{3}$$

where D is the radon diffusion coefficient (m^2/s), $C(x)$ is the distribution of radon concentration in the sample (Bq/m^3), C_s and C_A are the radon concentrations in the chamber and the ambient air, respectively (Bq/m^3), λ is radon decay constant ($2.09 \cdot 10^{-6}$ 1/s), h is the height of the sample (m).

The solution of the boundary task (1)–(3) has the form:

$$C(x) = C_s \cdot sh\left[(h - x) \cdot \sqrt{\lambda/D}\right] / sh\left(h \cdot \sqrt{\lambda/D}\right) \tag{4}$$

According to Fick's first law, the radon exhalation rate from the upper surface of the sample q ($Bq/m^2/s$) is described by equation:

$$q = -D \cdot \frac{dC(x)}{dx}|_{x=h}, \tag{5}$$

and the balance of radon in the chamber is described by the following equation:

$$Q - \lambda \cdot C_s \cdot V + S \cdot D \cdot \frac{dC(x)}{dx}|_{x=0} = 0, \tag{6}$$

where Q is the rate of radon release from the source, Bq/s, S is the sample (chamber) area, m^2, V is the free air volume in the chamber, m^3.

Then, considering (4)–(6),

$$q = Q \cdot \sqrt{\lambda \cdot D} / \left[\lambda \cdot V \cdot sh\left(h \cdot \sqrt{\lambda/D}\right) + S \cdot \sqrt{\lambda \cdot D} \cdot ch\left(h \cdot \sqrt{\lambda/D}\right)\right] \tag{7}$$

Thus, according to (7), the value of the radon diffusion coefficient can be obtained by measurements of the values of two parameters only: q and Q.

3 Equipment and Materials

Dry phosphogypsum [4] with the density about 1,000 kg/m^3 is used as a radon source. For the manufacture of the chamber and the casting of concrete samples, it is advisable to use a standard plastic tube with an external (internal) diameter of 75.0 (71.2) mm, then $S = 4.0 \cdot 10^{-3}$ m^2.

If 1.0 kg of phosphogypsum is used, then chamber height (Hph) should be at least 0.25 m, taking into account S and the density of phosphogypsum. It is advisable to increase the height of the chamber (H) to 0.34 m, so that there is a layer of air ($Hair = 0.09$ m) in order to reduce the uncertainty in estimating the value of V, which also depends on the porosity of the powder (phosphogypsum). If the porosity (p) of phosphogypsum is assumed to be 0.2, then $V \approx S \cdot (Hph \cdot p + Hair) \approx 0.0006$ m^3.

The proposed method for measuring the parameters q and Q, according to Fig. 1b is based on the ability of activated charcoal to adsorb radon. In order to measure q an activated charcoal layer (working layer) is located on the upper surface of the sample, which adsorbs radon released from the sample for a certain time (no more than 20 h). The protective layer of charcoal prevents the adsorption of radon in the working layer from the surrounding space, which provides $C_A = 0$, according to the boundary condition (3).

Using this method, the value of q is determined by the formula (8) considering the decay of radon in the charcoal layer during the exposure period:

$$\begin{aligned} q &= \lambda \cdot A \cdot exp\left(\lambda \cdot t_{keep}\right)/S/[1 - \exp(\lambda \cdot t)], \text{ or} \\ q &= A \cdot exp\left(\lambda \cdot t_{keep}\right)/(S \cdot t) \text{if } t < 5 \text{ h}, \end{aligned} \tag{8}$$

where A is the activity of radon in the working layer of charcoal, Bq, t is the exposure period, s, t_{keep} is the time interval between the end of the exposure and the start of measurements, s.

The activity of radon adsorbed in charcoal is measured on a very simple, but at the same time, highly sensitive detector [5]. This detector allows to measure the parameter A at a level of 1.0 Bq (0.5 Bq) with a statistical uncertainty of about 15% (25%).

The value of Q is determined in the same way as q, but without a concrete sample, according to the Fig. 1b, and $Q = q \cdot S$.

4 Results and Simulation

Based on multiple measurements with an exposure period of 3 to 6 h, the value of Q was determined to be $(2.2 \pm 0.2) \cdot 10^{-4}$ Bq/s, which is consistent with the data from [4] (the difference is not more than 20%).

An important task is the selection of the optimal height (h) of the concrete sample. The determining criteria are two basic conditions: (i) the ability to more accurately find the difference between the values of D; for example, in the new (with lower D-value) and artificially aged (D is higher) concrete samples, and (ii) the value of q must be at least 15 mBq/(m^{2}s), so that $A > 1.0$ Bq for the exposure period no more than 5 h (see above). To solve this task, modeling was carried out (Fig. 2) based on the obtained solution (7), taking into account the initial data and criteria presented before.

The expected range of D in new and aged concrete is about from $2 \cdot 10^{-8}$ (D_{min}) to $2 \cdot 10^{-7}$ (D_{max}) m^2/s. Then, considering the condition (ii), the height of sample should not exceed 0.10 m, according to Fig. 2. In other words, considering the condition (i), the sample height of 0.10 m is more preferable than 0.05 m, since a larger value of h provides greater sensitivity of the method ($k_{10} > k_5$) when comparing the diffusion rate of radon in the new and aged samples.

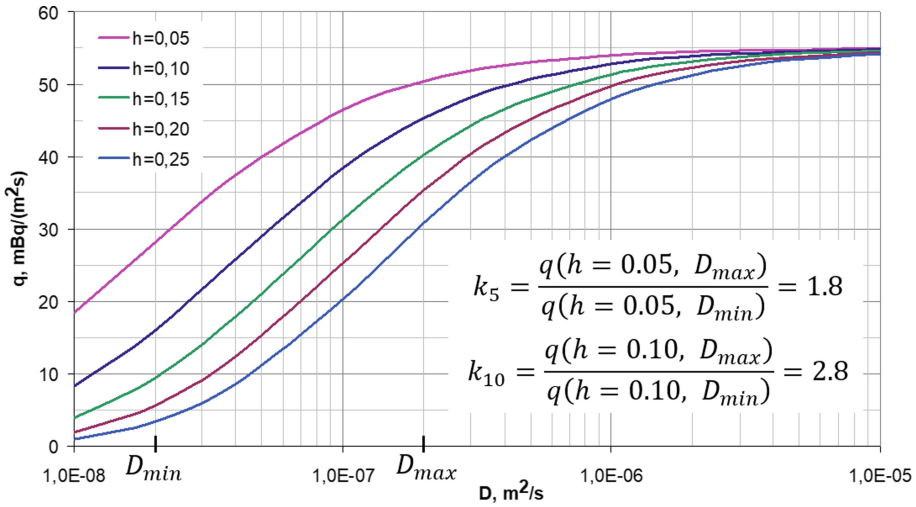

Fig. 2. Dependence of the radon exhalation rate from the upper surface of the sample on the radon diffusion coefficient and height of the sample (results of simulation)

5 Conclusions

A simple method for determining the radon diffusion coefficient in concrete based on the radon adsorption in activated charcoal is proposed. The geometry of the experimental setup is scientifically justified considering the characteristics of the existing radon source and the proposed method for measuring the activity of radon adsorbed in activated charcoal.

References

1. ISO/TS 11665-12:2018 Measurement of radioactivity in the environment—Air: radon 222—Part 12: Determination of the diffusion coefficient in waterproof materials: membrane one-side activity concentration measurement method
2. ISO/TS 11665-13:2017 Measurement of radioactivity in the environment—Air: radon 222—Part 13: Determination of the diffusion coefficient in waterproof materials: membrane two-side activity concentration test method
3. Tsapalov, A., Gulabyants, L., Livshits, M., Kovler, K.: New method and installation for rapid determination of radon diffusion coefficient in various materials. J. Environ. Radioact. **130**, 7–14 (2014)
4. Tsapalov, A., Kovler, K.: Control of radon emanation at determination of activity concentration index for building materials. Constr. Build. Mater. **160**, 810–817 (2018)
5. Tsapalov, A., Kovler, K., Shpak, M., Shafir, E., Golumbic, Y., Peri, A., Ben-Zvi, D., Baram-Tsabari, A., Maslov, T., Schrire, O.: A radon survey in Israel involving school children by means of the "RadonTest" online system. In: NORM IX Symposium Proceedings, Denver, USA (2019)

Dry Forced Packing of Blends for Ultra High Performance Concrete: Effect on Physical-Mechanical Properties of the Composition and Concrete Made from It

A. Ozersky[1(✉)], A. Khomyakov[1], and K. Peterson[2]

[1] Inkas Group, Toronto, ON, Canada
alex.ozersky@inkas.ca
[2] Department of Civil and Mineral Engineering, University of Toronto, Toronto, ON, Canada

Abstract. This study discusses a method for forced packing of dry multi-component mixtures, and studies the effect of such forced packing on physic-ochemical properties of the composition, microstructure, homogeneity, and mechanical properties of UHPC produced using standard blended mixtures, and dry forced packed mixtures.

Keywords: High performance concrete · Silica fume · Microstructure · Physical properties

1 Introduction

The close packing of raw materials is generally recognized as the first of the basic principles for design of Ultra High Performance Concrete (UHPC). There are numerous mathematical models for optimizing granular packing [1]. In these models particle packing density is primarily based on "ideal" powders, meaning that individual particles are loose and not interconnected into agglomerations. According to this concept, upon mixing silica fume with larger inorganic binders, the ultrafine microsilica particles are uniformly arranged in the voids between coarser cement particles, together creating a densely packed matrix. However, in actual practice, silica fume particles have a tendency to aggregate. The smaller the particle size, the more aggregation. Particle aggregation prevents uniform distribution of the silica fume particles, and the density, as well as other properties of the concrete matrix are jeopardized in various ways, including but not limited to higher porosity and permeability, and lower strength and durability. Many solutions have been identified to overcome the problem of silica fume particle aggregation, including introduction of silica fume after chemical pre-treatment [2], or as a colloidal suspension often in combination with sonication or combinations thereof [3]. Breaking down silica fume with cement in the process of cement milling has been proven successful and has become standard practice; however cement milling is generally performed in a factory utilizing a process of clinker milling which produces large batches for commercial use. One disadvantage of incorporating silica fume into

© RILEM 2020
K. Kovler et al. (Eds.): ConcreteLife 2020, RILEM Bookseries 26, pp. 94–98, 2020.
https://doi.org/10.1007/978-3-030-43332-1_19

the process of cement manufacturing is a lack of production flexibility. Specifically, it is impractical to produce relatively small and diverse batches of blended hydraulic cement according to requirements of dissimilar customers. Another drawback is that a limited amount of silica fume can be added into cement in the process of its manufacturing. Silica fume is normally added at a range between 3 and 10% by weight, and almost certainly under the maximum 15% defined by many national standards, and particularly by National Standard of Canada CAN/CSA-A3000-13. This quantity of silica fume is generally below its optimum amount (up to 25% in many UHPC compositions and higher in some) required for making blended cement compositions with maximum packing density. Besides, the milling cannot be used for optimum packing of multi-component mixtures, containing materials in addition to silica fume, for example other supplementary cementitious material like fly ash, slag, etc., or non-cementitious fillers like quartz powder, sand, etc. Another reason milling cannot be used for optimum packing of multi-component cementitious mixtures is that it is considered impossible to calculate the optimum ratio of the components based on their original sizes because of comminution of different components to varying and unpredictable degrees in the process of milling.

Initially, all of the dry materials (Table 1) were combined in an Eirich R09T 200 L intensive mixer (abbreviated IM) with a counter-current rotating pan and high speed rotor tool with a fixed pan scraper blade for a period of 1 min at rotor speed of 380 rpm.

Table 1. Mix design

Material	kg/m^3	kg/m^{3a}
Portland cement, Holcim Mississauga GU, spg 3.11	1030	946
Silica fume, Norchem densified SF, spg 2.20	258	236
Fine aggregate, Sand Fairmount Santrol LS-80, spg 2.64	640	588
Superplasticizer, BASF MasterGlenium 3400, spg 1.10	46.5	43.4
Water, City of Toronto, spg 1.00	238	296

[a]*Adjustment for mixture made in drum mixer due to water addition during mixing.*

The dry-blended materials were discharged and stored in sealed pails for subsequent UHPC production in the IM, plaster/mortar (PM), drum (DR), and ordinary flat pan (FP) mixers. A portion of the dry-blended materials was further subjected to forced packing using a mortar and pestle based high intimacy mixer (Fig. 1a). The dry force packed material exhibited an even distribution of silica fume particles coating the cement grains (Fig. 1b). To facilitate handling of the activated dry force packed material, pelletization (Figs. 1c, d) and briquetting (Figs. 1e, f) are additional options, that can also accomodate the introduction of fibres.

To produce UHPC, liquid admixtures were combined with the mix water, and added to the dry blended ingredients with the various mixers operated and mixed for a period of three minutes, followed by a two-minute resting period, followed by another

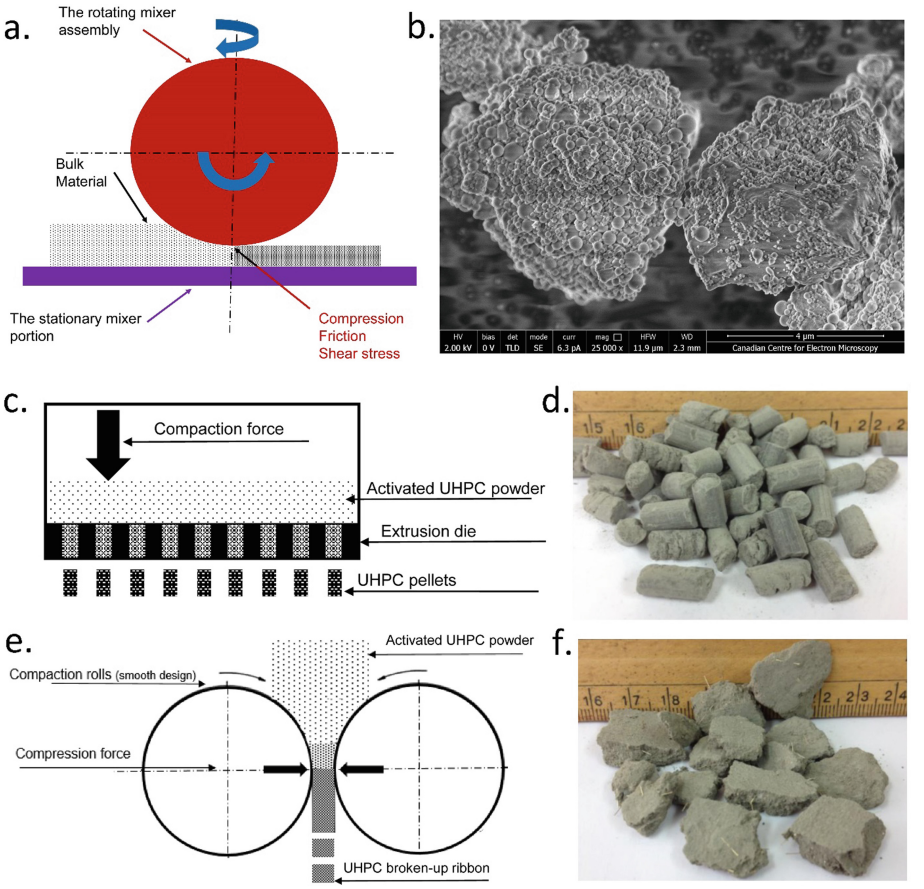

Fig. 1. Dry force packing functional principle (a), scanning electron microscope image of silica fume coated cement grain after dry force packing (b), pelletization by extrusion (c) and produced pellets (d), roller compaction (e) and produced ribbon with steel fibre addition (f).

two minutes of mixing. The same process was repeated with the dry force packed material, but only with the ordinary flat pan mixer. The mixture produced in the drum mixer was initially unworkable, so additional water was added during the final two minutes of mixing. UHPC was cast in 100 mm dia. × 200 mm cylinders, and moist cured prior to strength testing and preparation in thin section for microstructural image analysis of silica fume agglomeration content, size, and frequency.

2 Results

The UHPC produced with the dry force packed material exhibited superior strength, and no silica fume agglomerations were observed (Table 2). Figure 2 shows example transmitted plane polarized light micrographs from the thin sections.

Table 2. Compressive strength and silica fume agglomeration statistics.

		Agglomeration statistics				Compressive strength	
	Mixer ID	Vol. %	Avg. intercept (μm)	Specific surface (mm^{-1})	Frequency (aggl./cm)	7 d	28 d
Dry blended materials	IM	3.2	167	19.6	1.6	79.9 ± 0.8	93.1 ± 2.2
	PL	5.3	99	49.8	4.0	66.9 ± 1.4	93.1 ± 1.1
	DR	7.8	115	42.7	8.3	59.1 ± 1.1	92.7 ± 1.2
	FP	3.2	101	49.8	4.0	65.4 ± 1.2	98.0 ± 0.8
Dry force packed materials	FP	No agglomerations observed				129.5	152.5

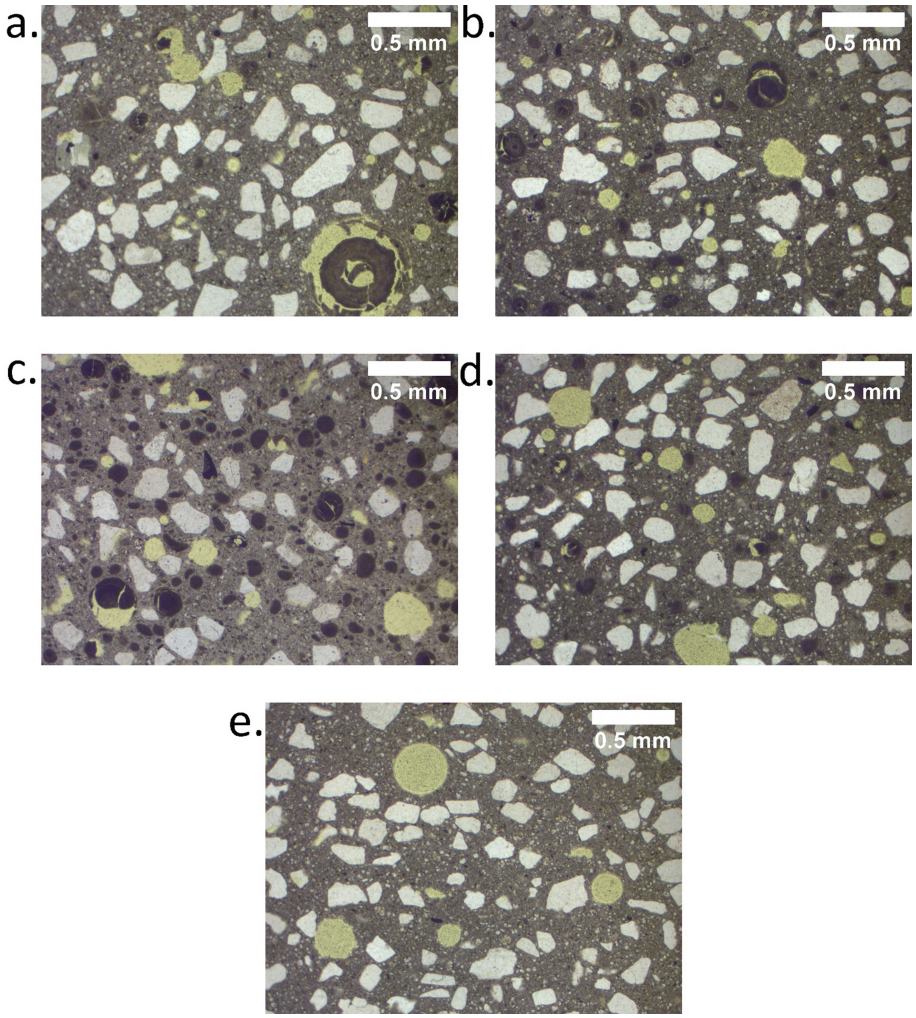

Fig. 2. Silica fume agglomerations in dry blended material IM (a), PM (b), DR (c) and FP (d) mixtures, and absence of agglomerations in dry force packed material FP mixture (e).

3 Conclusions

SEM analysis of the dry force packed mixture showed coating of the larger cement particles by smaller silica fume particles, providing thereby the maximum packing density. The forced packing resulted in physicochemical activation that provided the possibility for pelletization and briquetting. Petrographic microscope analysis demonstrated that dry blended material mixtures resulted in silica fume agglomerations, and only the mixture produced with dry forced packed materials achieved full dispersal of the silica fume. Compressive strength of the UHPC produced with the dry force packed material was the highest of all other UHPCs, which may be attributed to highest uniformity of the cementitious matrix.

References

1. Yu, R., Spiesz, P., Brouwers, H.J.H.: Mix design and properties assessment of Ultra-High Performance Fibre Reinforced Concrete (UHPFRC). Cem. Concr. Res. **56**, 29–39 (2014)
2. Tsardaka, E.-C., Stefanidou, M.: Application of an alternative way for silica fume dispersion in cement pastes without ultrasonication. Cem. Concr. Res. **115**, 59–69 (2019)
3. Elkady, H., Serag, M.I., Elfeky, M.S.: Effect of nano silica de-agglomeration, and methods of adding superplasticizer on the compressive strength, and workability of nano silica concrete. Civil Environ. Res. **3**(2), 21–34 (2013)

High-Performance Concrete Using Dolomite By-Products

G. Sahmenko(✉), A. Korjakins, and D. Bajare

Institute of Materials and Structures, Riga Technical University, Riga, Latvia
genadijs.sahmenko@rtu.lv

Keywords: High-performance concrete · Dolomite by-product · Self-compacting concrete

1 Introduction

Dolomite is the widespread sedimentary rock that finds a wide application in building industry and road engineering. During the treatment of dolomite rocks, a huge amount of fine fractions (0…8 mm) are produced and classified as by-products due to the limited range of applications. For example, nowadays more than 400 000–450 000 t dolomite by-products are deposited in a single quarry and the annual increase of this material is 50 000 t.

There have been efforts to incorporate dolomite residues as an aggregate and micro filler component in concrete mixes [1]. There is research that reports how carbonate micro filler accelerates the rate of hydration [2]. It was proved that the positive effect of the dolomite quarry by-product takes place for self-compacting concrete (SCC). It determines the necessary paste content and provides the consistency of SCC mixes [3]. Also, dolomite by-product has been tested as filler in the lightweight concrete made of expanded clay aggregates and the incorporation of dolomite by-products improved the workability and casting of concrete [4].

The goal of this research is to elaborate effective, high-strength and durable high-performance concrete compositions with maximum content of dolomite quarry by-products.

2 Materials and Methods

Experimental samples of dolomite by-product aggregate were taken from the accumulated stack in deposit quarry Birzi, one of the biggest dolomite aggregate producers in Latvia. Obtained by-products are a multi-fraction mix (range of sizes up to 8 mm) which contains a large amount of fine particles (up to 20%). It must be noted, that dolomite deposit Birzi is characterized by high strength (more than 80 MPa), freeze-thaw resistance and low water absorption (2%). Dolomite by-products are loose aggregate mix with bulk density 1500–1800 kg/m^3 and particle density 2640 kg/m^3. Grading analysis of dolomite by-product was done in accordance with standard EN

© RILEM 2020
K. Kovler et al. (Eds.): ConcreteLife 2020, RILEM Bookseries 26, pp. 99–103, 2020.
https://doi.org/10.1007/978-3-030-43332-1_20

911-1, using the method of wet sieving due to the high content of dust particles. Granulometric composition of dolomite by-product is presented in a wide range of particle sizes up to 8 mm. The content of micro filler (particles smaller than 0.063 mm) is about 26%. Almost half part of the material (47%) is sand fractions (0.1–4.0 mm) and 30% is the content of crushed stone (>4 mm) Samples taken from different places demonstrate quite good stability, grading deviations do not exceed 5%.

Normal type CEM I 42.5 N Portland cement (supplied by Schwenk Latvia) and also CEM I 52,5 R white Portland cement were used as binding material for sample preparation. The specific surface of CEM I 42.5 N was 3845 cm^2/g, compressive strength 28.4 MPa at the age of 2 days and 55.5 MPa at the age of 28 days.

Additional aggregates were used to produce concrete mix compositions: natural washed sand 0/4 mm and gravel fractions 2/8 mm. Additionally, highly reactive pozzolana - silica fume was used for producing high strength concrete compositions. Produced mix compositions are summarized in Table 1. Mix design is based on optimal grading (Fuller's) curve of an aggregate mix and control the volume of paste and mortar phases (Fig. 1).

Table 1. Mix composition of concrete with dolomite by-products

Compound	Mix 1: Normal concrete (NC)		Mix 2: High performance SCC		Mix 3: Architectural concrete	
	kg/m^3	Proportion	kg/m^3	Proportion	kg/m^3	Proportion
CEM I 42.5 N (Schwenk LV)	330		350			
CEM I 52.5 R (Aalborg)					530	
Gravel 2/11 mm	367	20%	532	29%		
Sand 0/4 mm	367	20%	532	29%		
Dolomite by-product	1100	60%	734	40%	1600	100%
Silica fume (SF)			30	2%		
Effective amount of water	220		180		220	
Superplasticizer	2.3		3.5		5.3	
Effective W/C ratio	0.67		0.51		0.42	
W/(C + k*SF) (k = 2 for SF – EN 206, section 5.2.5.2.)	–		0.44		–	

The first elaborated mix corresponds to economical normal strength concrete (water-cement ratio 0.73) and dolomite by-product replaces 60% of aggregate. The second mix corresponds to high-performance self-compacting concrete (water-cement ratio 0.56) and dolomite by-product replacing 40% of aggregate. Silica fume was used in this case for improving the properties of fresh and hardened concrete. The third composition corresponds to high-performance cement composite based on pure dolomite by-product and may be used for architectural exposed surfaces (mix 3).

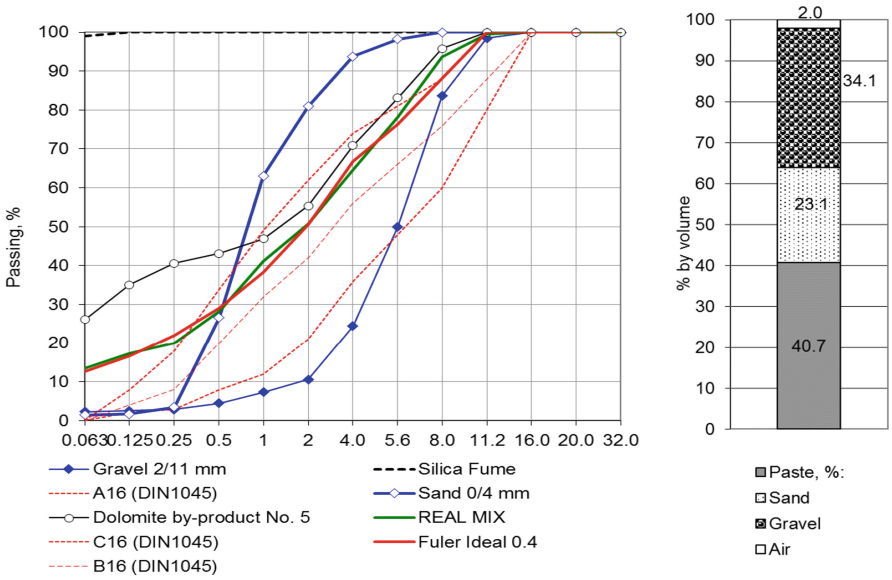

Fig. 1. Aggregate mix design and phases volume content for SCC (on the right)

Samples 10 × 10 × 10 cm were produced, cured in humid conditions at 20 ± 1 °C and tested in the ages of 7, 28 and 56 days. Compressive strength was determined in accordance with standard EN 12390-3; water permeability – EN 12390-8 by measuring the depth of water penetration under pressure. Frost resistance test was performed by freezing and thawing of partially immersed samples in 3% NaCl solution (cycling regime −20 °C/+ 20 °C in accordance with the CDF method). Water permeability under pressure was determined using EN 12390-8.

3 Results

The properties of fresh and hardened concrete are summarized in Table 2.

The first elaborated concrete (mix 1) is economical normal concrete mix composition with replacing 60% traditional aggregate, this concrete could have broad commercial use of C20/25 class concrete with high workability and satisfactory water resistance and frost resistance. It had S3 workability class (cone slump 150 mm) and cone flow 450 mm.

The second one is high-performance and self-compacting concrete [5] with replacing 40% traditional aggregate by dolomite by-product. It is characterized by a cone flow of 590 mm and corresponding class SF1. Compressive strength for SCC composition has increased up to 72.1 MPa at the age of 28 days and 82,1 MPa in 56 days, which is twice more compared to normal concrete. Sufficient paste content (40.7% in accordance with Fig. 1) and corresponding flowability are achieved by

incorporation of superplasticizer, silica fume, an increased amount of cement and fine fractions as a component of dolomite by-product [6].

The third mix is high-performance architectural composite with 100% aggregate replacing with dolomite by-product. A combination of white cement and dolomite filler makes possible to achieve light yellow color like natural dolomite rock with an architectural extra-fine surface (Fig. 2).

Table 2. Properties of hardened concrete samples

Concrete property	Normal concrete (NC)	High-performance self-compacting concrete (HP SCC)	High-performance architectural composite
Workability			
Cone slump, mm	150	–	175
Cone flow, mm	450	590 (SF1)	–
Strength			
28 day compressive strength, MPa	33.3	72.1	82.0
56-day compressive strength, MPa	38.6	82.1	
28-day tensile splitting strength, MPa	3.2	4.6	6.5
Durability			
Water penetration, mm	23	15	13
Frost resistance surface scaling after 28 cycles, g/m^2	350	150–250	<150

This mix is characterized by a high flowability class (at the same time, such mix has high viscosity due to the angular shape of the particles of dolomite aggregate).

The durability such as water penetration and frost resistance indicate that the water penetration of normal concrete was 23 mm and could be reduced to 13–15 mm for HP SCC while freeze-thaw resistance was similar for both mixture compositions. Surface scaling after 28 freeze-thaw cycles was in the range 150 to 350 g/m^2, and deals with the destroying of separate weak dolomite particles (Fig. 3).

Fig. 2. High performance architectural composite based on dolomite – white cement composition

Fig. 3. HP SCC (mix 2) sample after 28 freeze-thaw cycles

4 Conclusions

The study proved the possibility to utilize by-products of dolomite quarries both for conventional concrete and for high-performance self-compacting concrete which is characterized by a high degree of workability and resistance against freezing and thawing cycle.

The high content of fine particles makes possible to use it as a micro-filler component, which acts as a stabilizing agent and densifying filler. The main reason for limited flow-ability is the angular shape of dolomite aggregate particles, it may be compensated by the use of appropriate plasticizers and silica fume admixtures.

Replacing traditional aggregates and micro-fillers with dolomite by-product makes possible to obtain durable high-performance concrete with decrease environmental impact [7] and promotes rational use of local natural resources.

Acknowledgments. Financial support: European Regional Development Fund project Nr.1.1.1.1/16/A/007 "A New Concept for Sustainable and Nearly Zero-Energy Buildings".

References

1. Fraser, J., McBride, R.A.: The utility of aggregate processing fines in the rehabilitation of dolomite quarries. Land Degrad. Dev. **11**(1), 1–17 (2000)
2. Guemmadi, Z., Resheidat, M., Chabil, H., Toumi, B.: Modeling the influence of limestone filler on concrete: a novel approach for strength and cost. Jordan J. Civ. Eng. **3**(2), 158–171 (2009)
3. Rudžionis, Ž., Ivanauskas, E., Senkus, M.: The analysis of secondary raw materials usage in self-compacting concrete production. Mater. Sci. **11**(3), 272–277 (2005)
4. Korjakins, A., Shakhmenko, G., Bajare, D., Bumanis, G.: Application a dolomite waste as filler in expanded clay lightweight concrete. In: 10th International Conference on Modern Building Materials, Structures and Techniques, pp. 156–161 (2010)
5. Collepardi, M., Troli, R., Maringoni, S.: Self-compacting high performance concretes. In: Twelfth International Conference on Recent Advances in Concrete Technology and Sustainability Issues, pp. 27–33 (2012)
6. Utsi, S.: Performance based concrete mix-design aggregate and micro mortar optimization applied on self-compacting concrete containing fly ash (2008)
7. EU: Energy and climate framework 2030. European Council 23/24 October 2014 – Conclusions, EUCO 169/14 (2014)

Green Cementitious Systems Based on Off-spec Fly Ash

M. Kozhukhova[1,2], R. Wittenberg[1,2], and K. Sobolev[2(✉)]

[1] Ramboll, Milwaukee, WI, USA
[2] University of Wisconsin-Milwaukee, Milwaukee, WI, USA
sobolev@uwm.edu

Keywords: Sulfate attack · Spray dry absorber ash · Harvested fly ash · Concrete durability

1 Introduction

The amount of coal combustion by-products (CCPs) generated by power utilities is significant and anticipated to grow [1]. However, more than 30% of all generated CCPs in the USA are considered "off-spec" because they do not meet the ASTM C618 specification and are not utilized [2]. For example, CCPs with high carbon content and spray dryer absorber ash (SDA) containing high concentrations of gypsum compounds represent two primary off-spec CCP materials that need to be addressed. The development of innovative binders based on off-spec fly ash represents an opportunity for efficient and sustainable use of by-products.

To address the challenge with broader use of SDA, a ternary cementitious system consisting of portland cement combined with two types of off-spec ash is proposed. This cementitious system is based on SDA with high amounts of calcium sulfate/sulfite (CS) phases combined with harvested ash used as a pozzolanic component. Earlier studies confirmed that combining Class F fly ash with by-products containing calcium sulfates favorably affects durability performance [4]. Such composites demonstrated a very low degree of deterioration after long term exposure in a seawater environment. A feasibility study of the use of CCP with CS in road construction using Roller-Compacted Concrete (RCC) demonstrated improved workability and strength performance [5–7].

2 Experimental Study

The reported experimental study included an investigation of the effects of two off-spec CCPs, which were freshly collected SDA and harvested ash (HA) from landfills provided by the local power utility. These were used at up to 50% and 18%, respectively. Silica fume (SF) supplied from Elkem Microsilica was used at 7% as a model pozzolan material. Portland cement (PC) Type I/II supplied by LafargeHolcim, as well as chemical admixtures were used for the preparation of cementitious systems.

© RILEM 2020
K. Kovler et al. (Eds.): ConcreteLife 2020, RILEM Bookseries 26, pp. 104–108, 2020.
https://doi.org/10.1007/978-3-030-43332-1_21

The oxide composition revealed that the SO_3 amount in SDA is 12.6%, which is almost double of that accepted by ASTM C618 for coal ash recommended for use in commercial concrete applications. The percentage of unburned carbon represented as LOI content was 10.4%, which is considerably higher than the 6% limit recommended by the ASTM C618. The SDA consists of spherical particles of fly ash of smaller size and tabular and prismatic particles of calcium sulfates and sulfites represented by minerals of bassanite ($CaSO_4 \cdot 0.6H_2O$), anhydrate ($CaSO_4$) and hannebachite ($CaSO_3 \cdot 0.5H_2O$) (Fig. 1).

Five different mix designs (M1–M5) were prepared with the following proportions of PC, SDA, HA and SF: M1, 100% PC used as a reference; M2, 60:40 PC:SDA mix; M2, 50:50 PC:SDA mix; M4, 50:43:7 PC:SDA:SF mix; M5, 50:32:18 PC:SDA:SF mix (Table 1).

For the compressive strength investigation, 50-mm cube mortar samples were cast, cured in accordance with ASTM C 109 and ASTM C305 and then tested at the age of 3, 7, and 28 days. The W/C of 0.35 and S/C of 1 were kept constant for all mixes. For the sulfate resistance study, prismatic mortar samples with a size of $25 \times 25 \times 285$ mm were used. The prisms were cast and cured using the same standard procedure. The length change of investigated mortars due to expansion was measured and calculated according to ASTM C157 and ASTM C1012. The length change measurements to determine a sulfate expansion was performed for the test samples at the age of 7, 28, 90, and also 200 days.

Table 1. Mix design proportions

Mix ID	Cementitious components (%)				Amount of SO_3, %
	PC	SDA	HA	SF	
M1	50	–	–	–	2.7
M2	60	40	–	–	7.6
M3	50	50	–	–	3.8
M4	50	43	–	7	6.7
M5	50	32	18	–	6.6

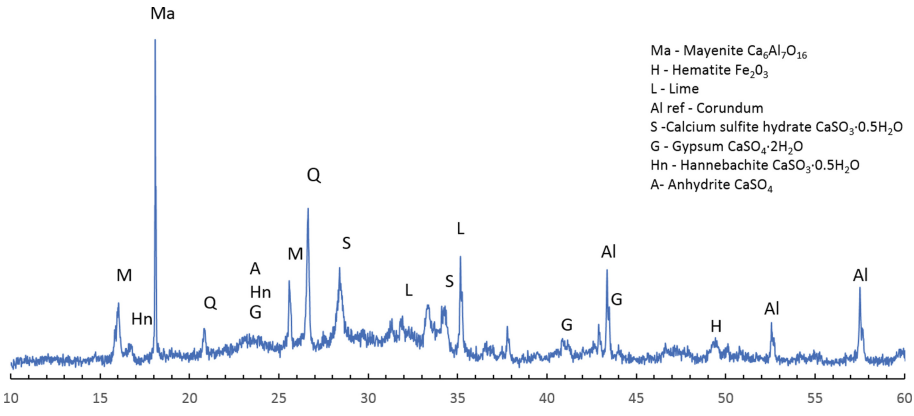

Fig. 1. The XRD for SDA material used in the study

3 Results and Discussion

The effect of partially replacing up to 50% of PC with a combination of SDA and HA (or SF) on compressive strength of mortar cubes demonstrated a positive trend of strength development for all tested compositions (Fig. 2). Although the compressive strength for reference samples M1 developed steadily with time, all SDA containing samples (M2–M5) with the replacement of up to 50% of PC had about 12% strength reduction at all ages.

Mortars M4 and M5 with a pozzolanic component demonstrated considerably lower strength at 7 days, but at 90 days M5 gained strength of 83.5 MPa. Similarly, M4 mix with SF reached a 90-day strength of 106 MPa overperforming all tested mortars. Here, the pozzolanic reaction between the amorphous SiO_2 in HA and SF and portlandite can be responsible for the strength enhancement at later ages.

The evaluation of expansion data demonstrated a positive trend for all experimental mortars (Fig. 3). The samples M4 and M5 with pozzolanic component compensating for SDA had a minimal total expansion of 0.020% and 0.028%, respectively vs. expansion of reference composition M1 of 0.043% over the tested period. The M2 with 40% of SDA, demonstrated 0.040% expansion, which is very close to that of the reference M1. On the contrary, the highest expansion of 0.054% was observed for the M3 mortar prisms with 50% SDA. By the age of 200 days, all mortars satisfied the requirements for severe sulfate environment, except for the sample M3, which, after 150 days of the exposure, passed the minimal acceptance limit for moderate sulfate exposure.

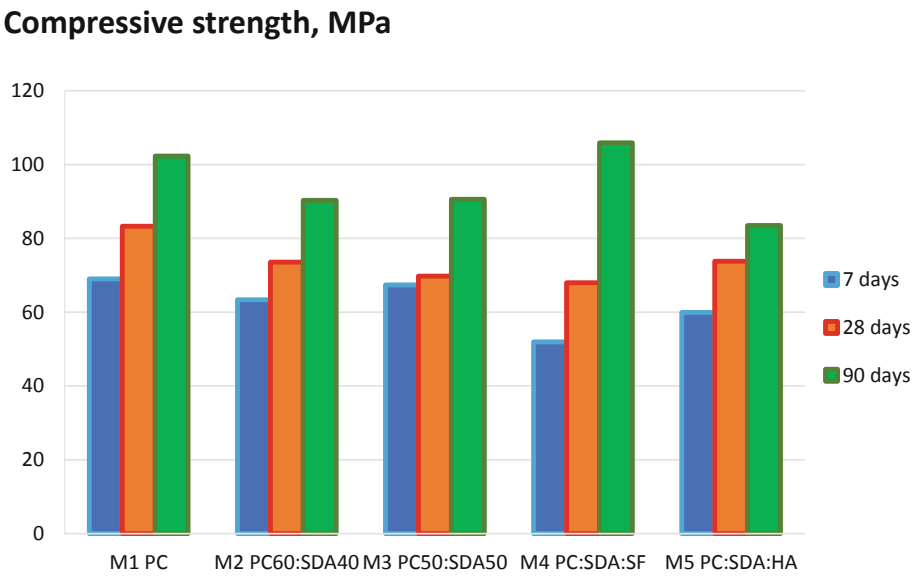

Fig. 2. The compressive strength of mortars

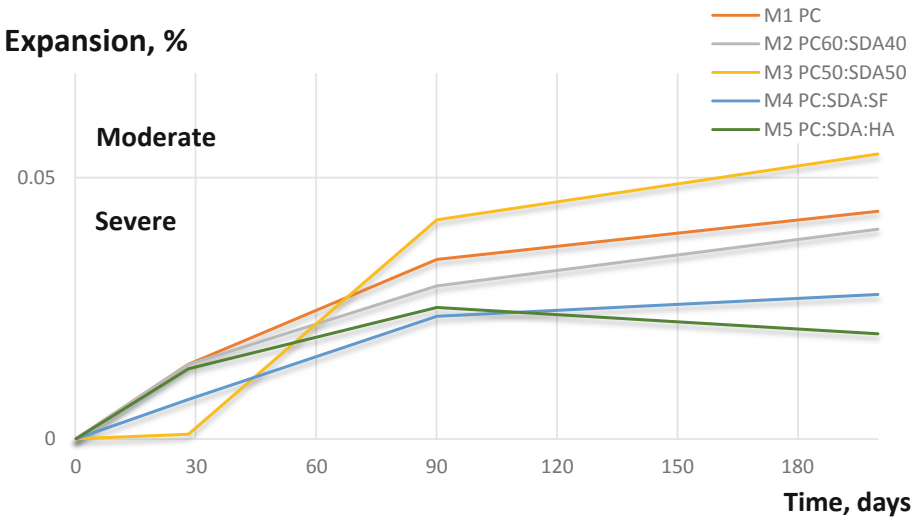

Fig. 3. Sulfate resistance of investigated compositions

4 Conclusions

The experimental results demonstrated a potential for application of two off-spec CCP, such as spray dry absorber fly ash and harvested ash in cement compositions at up to 50% replacement rates. Ternary blends with equivalent strength and long-term durability performance characteristics as required for conventional applications were developed. Strength and sulfate resistance results support the concept that combining SDA material with a pozzolanic component may help to offset the unfavorable effects of high concentrations of CS. Besides, harvested unprocessed pozzolanic fly ash from landfills and impoundments can be used in proposed systems. Bench-scale test results provide strong support for the application of ternary binder systems using conventional construction techniques that could streamline large scale applications in areas such as transportation, building materials, and environmental applications.

The critical objectives for these binder systems are to reduce the need for landfilling of off-spec CCP materials and turning waste into a commercially viable product. The opportunity for significant replacement of portland cement in concrete applications offers real benefits for the reductions in carbon emissions and efficient industrial waste utilization, which makes this approach green and sustainable. The replacement of portland cement could also have a significant economic benefit because of the high cost of portland cement that would be supplemented by lower-cost CCP materials.

Further bench and pilot-scale studies are underway to assess the long-term durability concerning sulfate resistance, freeze-thaw resistance, and field trials in pavement applications.

References

1. American Coal Ash Association: Production of coal combustion products in the U.S. (2015)
2. EPRI: A review of literature related to the use of spray dryer absorber material-production, characterization, utilization applications, barriers, and recommendations, TR1014915 (2007)
3. Shekhovtsova, J., Zhernovsky, I., Kovtun, M., Kozhukhova, N., Zhernovskaya, I., Kearsley, E.P.: Estimation of fly ash reactivity for use in alkali-activated cements - a step towards sustainable building material and waste utilization. J. Cleaner Prod. **178**, 22–33 (2018)
4. Magallanes-Rivera, R.X., Escalante-García, J.I.: Anhydrite/hemihydrate-blast furnace slag cementitious composites: strength development and reactivity. Constr. Build. Mater. **65**, 20–28 (2014)
5. Jansen, T., Wittenberg, R., Sobolev, K.: Multi-layer design approach for the utilization of high-volumes of off-spec coal combustion products in transportation infrastructure. In: EPRI Ponded Ash Workshop: Harvesting and Beneficiation of Coal Combustion Products (2019)
6. Wittenberg, R., Kozhukhova, M., Jansen, T.: Multi-layer pavement design approach for effective utilization of off-spec coal combustion products. In: WOCA-2019 (2019)
7. Jansen, T., Wittenberg, R., Kozhukhova, M., Sobolev, K.: Demonstration project: roller compacted concrete pavement with high volumes of off-spec coal ash. In: WOCA-2019 (2019)

Developing and Analyzing Mix Design for 3D Printable Concrete

A. Gopani[1(✉)], P. Shah[2], and R. Shah[3]

[1] CEPT University, Ahmedabad, India
aagam.gopani.btl4@cept.ac.in
[2] Artemis Cast Stone, Ahmedabad, India
[3] Crebo, Ahmedabad, India

Keywords: 3D printing · Admixtures · Buildability · Compressive strength · Flowability

1 Introduction

In the age of industrialization, resources available in nature are declining. There has been an alarming rate of increase of greenhouse gas emissions in recent years due to high consumption of materials. In order to close the gap between demand and supply, and to abate this problem, the purpose of innovation through digitalization promises to revolutionize the construction industry with the implementation of freeform architecture, reduced material waste, decrease in construction costs, decrease in pollution, and increased worker safety [2, 3].

In this article, a glimpse of an idea is given for developing an optimum mix design for printable concrete that can be pumped through a 3D printer using the concepts of additive manufacturing.

2 Printing Systems

The work involves various trial and error methods, by measuring the fresh and hardened properties of concrete comprising various raw materials such as cement, lime, sand, fly ash, silica fume and premix mortar, in addition to using admixtures by understanding their properties. Properties of fresh mortar such as buildability, flowability [1], extrudability [5] have been explained through standard specifications tests for material mix like setting test, flow test as well as hardened concrete tests like compressive strength test is included.

© RILEM 2020
K. Kovler et al. (Eds.): ConcreteLife 2020, RILEM Bookseries 26, pp. 109–113, 2020.
https://doi.org/10.1007/978-3-030-43332-1_22

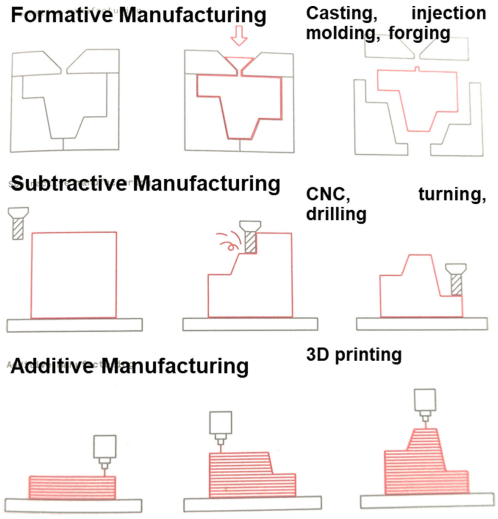

Fig. 1. Different types of manufacturing systems [2]

Several materials like plastics, chemicals, stainless steel may be manufactured through four types of manufacturing systems: (1) Subtractive, (2) Casting, (3) Forming and (4) Additive manufacturing (AM) (Fig. 1).

In AM, the material is added layer upon layer, opposite to conventional manufacturing method of subtract material. AM may be a new paradigm in design and fabrication because of the amazing feature of creating complex and customized products using various kinds of materials [4].

The AM process uses a computer-aided-design (CAD) system model as a blueprint and it will use this as a base to produce complex 3D designs in a layer-by-layer method.

3 Types of Additive Manufacturing and Mix Design Approach

Additive manufacturing systems and mix design approach are presented in Figs. 2, 3 and 4.

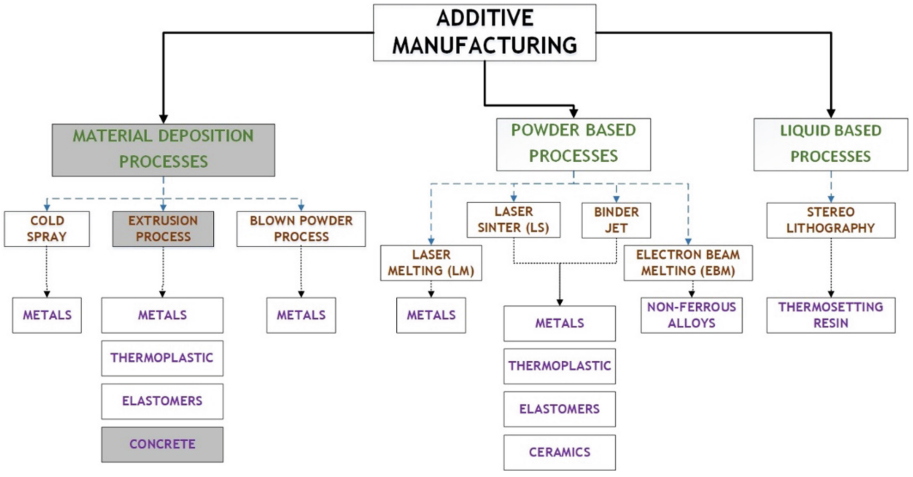

Fig. 2. Different types of additive manufacturing systems (Reference: http://3dprintingpress.blogspot.com/2014/08/additive-manufacturing-material.html)

4 Mix Design Approach

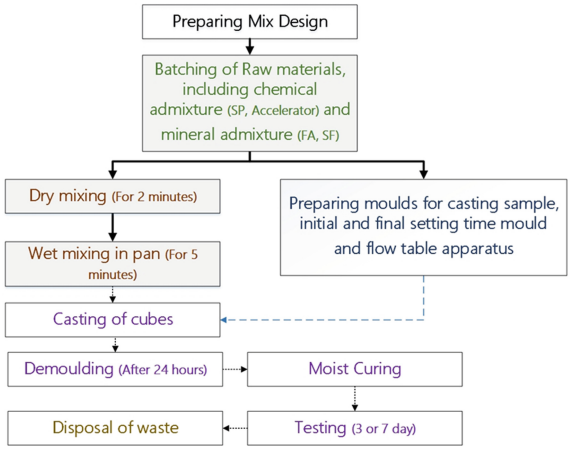

Fig. 3. Flowchart of laboratory work process

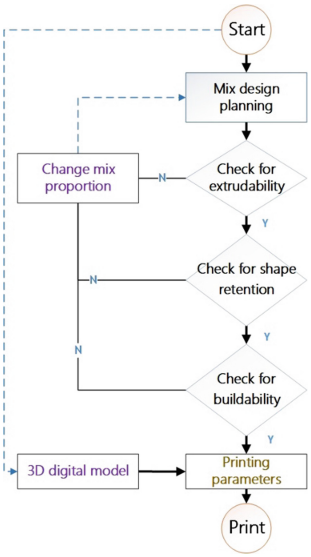

Fig. 4. Flowchart of experimental process

5 Selection for Optimum Mix Design

After the entire process of material exploration and understanding the different printing systems, it is required to understand the material behaviour amongst each other as well as the effect on physical properties of concrete.

For this, the following points are understood and ultimately, an optimum mix design selection needs to be carried out:

- Effect of fly ash on workability and compressive strength of 3D printable concrete
- Effect of micro-concrete on workability of 3D printable concrete
- Effect of glass fibers reinforcement on mix of 3D printable concrete
- Effect of sand replacement on mix of 3D printable concrete
- Effect of SP on mix of 3D printable concrete
- Effect of accelerator on buildability property of 3D printable concrete

6 Results

Table 1 shows the results of 4 mix designs, which have been considered ideal for 3D printing.

Table 1. Ideal mix design for 3D printable concrete

Trail no.	21	51	57	58
Cube no.	14, 15, 16	11, 21, 13, 114	12, 91, 30, 131	13, 21, 33, 134
Water/binder	w/c = 0.4	w/p = 0.257	w/p = 0.163	w/p = 0.15
Observations	Decent Workability and homogeneous mix is obtained	Mix is workable after addition of extra water. Good flow is obtained with layers being able to stay at the position when extruded. Total height achieved is 8.5 cm. Total **30% replacement** by weight of micro-concrete premix mortar **with sand** and **3.33%** by weight **with silica fume** is done	Mix is ideal as it is workable. Buildability of 5 layers is achieved. Total height achieved is 13 cm. Total **5% replacement** by weight of micro-concrete premix mortar **with sand** is done. Also, as material becomes brittle, dosage of SP and accelerator is decreased and qty of micro-concrete powder is increased which helps in achieving flowability	Mix is ideal and desirable flow is obtained. Buildability of 5 layers is achieved. Total **20% replacement** by weight of micro-concrete premix mortar **with sand** is done
Layer buildup	2 layers	4 layers	5 layers	5 layers
Average flow (mm)	–	143.04	135.78	135.11
Initial setting time	–	46 min	48 min	40 min
Final setting time	–	1 h 38 min	1 h 47 min	1 h 11 min
Avg. compressive strength (N/sq.mm)	26.88 @ 3 day	27.2 @ 7 day	25.74 @ 7 day	32.48 @ 7 day
w/c = water/cement, w/p = water/premix mortar				

7 Conclusions

Mix-51 is considered as an optimum mix, which shall be used for 3D printing system, with minor modifications if required. This mix contains 2000 g micro concrete premix powder (66.66%), 900 g fine aggregate (30%), 100 g silica fume (3.33%), 510 g water, 8 g accelerator, 10 g super plasticizer, 15 g glass fibre reinforcement. This mix has a water to premix mortar powder ratio of 0.258 [1]. The mix gives compressive strength

value of 27 N/mm^2, which is close to desired strength (30 N/mm^2), along with quicker final setting time (106 min).

Apart from this, as there is 30% replacement of sand by weight of micro concrete premix mortar and 3% replacement of silica fume by weight of micro concrete premix mortar (Total = 33.33%), average cost of material goes down as more amount of % replacement with sand will make the material quite cheaper.

As the material shows higher value of flow compared to mix-57 and 58 without losing its buildability property, the mix will not be harsh when extruded through nozzle. Also, as mix-58 matches with the desired properties as per hypothesis, this mix can also be used in 3DCP process.

8 Future Scope

The following points can be taken into consideration for further research work on same topic:

- Similar properties can be established to control the economy of production by using inexpensive materials such as recycled aggregate, industrial wastes like quarry dust.
- Other mineral admixtures such as rice husk, ground granulated blast furnace slag (GGBS), metakaolin, etc. can be inculcated in developing mix design.
- Use of different types of reinforcement system.
- Use of rapid hardening cement can be done, to achieve quick setting of the material.
- For developing mix design for high performance concrete.
- Use of large size aggregates (20 mm standard mesh size pass and 10 mm standard mesh size retain) can be used, if higher compressive strength is desired.
- Starting to do production of pieces from small scale and then gradually increase scale to residing units.

References

1. Marchment, T., Sanjayan, J., Xia, M.: Method of enhancing interlayer bond strength in construction scale 3D printing with mortar by effective bond area amplification. Mater. Des. **169**, 107684 (2019). https://doi.org/10.1016/j.matdes.2019.107684
2. Nematollahi, B., Xia, M., Sanjayan, J.G.: Current progress of 3D concrete printing technologies. In: Proceedings of the 34th ISARC, Taipei, Taiwan (2017). https://doi.org/10.22260/ISARC2017/0035
3. Paul, S.C., Tay, Y.W.D., Panda, B., Tan, M.J.: Fresh and hardened properties of 3D printable cementitious materials for building and construction. Arch. Civil Mech. Eng. **18**(1), 311–319 (2018). https://doi.org/10.1016/j.acme.2017.02.008
4. Wangler, T., Lloret, E., Reiter, L., Hack, N., Gramazio, F., Kohler, M., Bernhard, M., Dillenburger, B., Buchli, J., Roussel, N., Flatt, R.: Digital concrete: opportunities and challenges. RILEM Tech. Lett. **1**, 67 (2016). https://doi.org/10.21809/rilemtechlett.2016.16
5. Buswell, R.A., De Silva, W.R.L., Jones, S.Z., Dirrenberger, J.: 3D printing using concrete extrusion: A roadmap for research. Cem. Concr. Res. **112**, 37–49 (2018). https://doi.org/10.1016/j.cemconres.2018.05.006

Concrete Structures

We shape our buildings, thereafter they shape us.– Winston Churchill

Corrosion and Abrasion Resistance of Underwater Repair Concrete Under Hydrostatic Pressure

P. Brzozowski(✉)

West Pomeranian University of Technology, Szczecin, Poland
piotr.brzozowski@zut.edu.pl

Abstract. Concrete is widely used in the marine environment to create structures near, in, or under the water. Operating in the environment of the water influence, concrete is the subject to a variety of chemical and physical effects.

Keywords: Underwater concrete · Chloride corrosion · Abrasion resistance

1 Introduction

Concrete is widely used in the marine environment to create structures near, in, or under the water. Operating in the environment of the water influence, concrete is the subject to a variety of chemical and physical effects. Most common processes responsible for deterioration of a concrete in the marine environment are:

- chemical aggression,
- corrosion of reinforcement as a result of chlorides actions,
- frost destruction,
- salt erosion (so-called salt weathering),
- abrasive erosion as a result of the water flow and the impact of debris transported by sea water.

The aim of the study was to assess the possibility of using methods designed for natural stone testing for concrete corrosion and abrasion resistance examination.

2 Experimental

Types of the effects and their impact intensity on the particular structure depends on its location relative to the water surface. Generally there are three main zones: atmospheric, tidal and submerged [1, 2].

The underwater concrete was designed in such a way that it met the requirements given in [3] and DIN 1045-2. Portland cement CEM I 42.5N-HSR/NA according to EN 197-1, and the natural aggregate: gravel up to 16 mm and washed river sand up to 2 mm were used. The amounts of anti washout admixture (AWA) containing polysaccharides and high-range water reducing agent were calculated in the way to

© RILEM 2020
K. Kovler et al. (Eds.): ConcreteLife 2020, RILEM Bookseries 26, pp. 117–120, 2020.
https://doi.org/10.1007/978-3-030-43332-1_23

obtain acceptable wash-out losses and the flowability of self compacting concrete for 60 min after mixture preparation. Water/binder ratio was 0.4.

A special experimental stand has been used for testing underwater repair concrete under variable hydrostatic pressure [4]. Test elements with a volume of about 20 dm^3 were cured for 7 days under the hydrostatic pressure from 0 to 0.5 MPa and later were kept under the water in laboratory conditions. After 28 days of maturing, specimens were cut out from the test elements for further testing. The part of the test element from which specimen was taken was recorded as top or bottom. After preparation of the specimens the following tests were carried out:

- determination of resistance to ageing by salt mist (EN 14147),
- determination of air void characteristics in hardened concrete (EN 480-11),
- determination of the abrasion resistance - Boehme disc wet method (EN 14157),
- determination of the compressive strength of concrete (EN 12390-3).

Saturated specimens were used during the abrasion test. Water dripping onto the rotating disc contributed to hydro-abrasive wear of the concrete. The wear system consists of two solids, fluid and small particles.

3 Results

After 60 cycles in the salt chamber, the specimens showed no visual signs of surface damage. No scratches or peels were observed on their surfaces. Figure 1 shows the change in the mass of the specimens. Just after the test the weight gain of the specimens was observed, which was caused by accumulation of the salt. Even after desalination not whole salt introduced and absorbed by the specimens during the tests in the salt chamber was washed out, because all samples showed a slight increase in weight. This was confirmed by SEM images of concrete samples taken from the cubes.

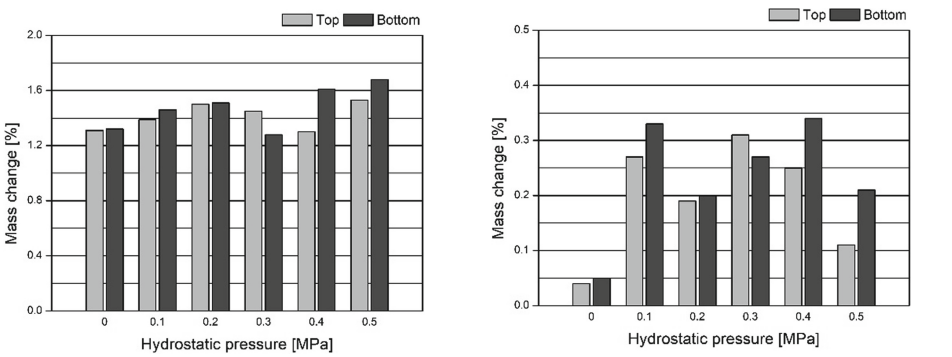

Fig. 1. Change in mass of the specimens after 60 cycles in salt chamber (left) and after desalination (right)

The results of determination of air void characteristics in hardened concrete are presented in the Fig. 2. The substantial impact of the hydrostatic pressure on the total air content of the tested specimens was observed. There was the decrease of air content of concretes exposed to the hydrostatic pressure. What is more, for pressures from 0.2 to 0.5 MPa there was higher percentage share of micropores in total porosity. In each case the specimens cut from the top parts of the elements had significantly lower total air content than those from the bottom sections.

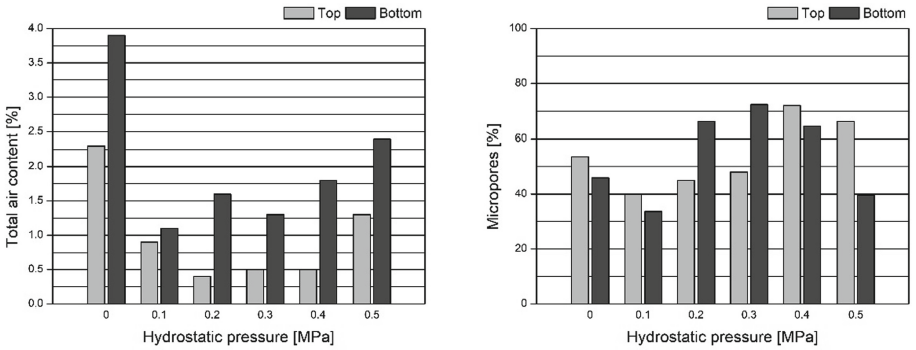

Fig. 2. Total air content (left) and percentage share of micropores in total porosity (right)

In the case of abrasion tests performed using Boehme disc an increase in volume loss of specimens exposed to the hydrostatic pressure was observed (Fig. 3). For most pressures, there was no significant change in compressive strength of tested concrete. In case of the pressure of 0.1 MPa there was a noticeable decrease of compressive strength of the concrete compared to the base value (0 MPa). On the other hand, the highest value was achieved for the pressure of 0,5 MPa.

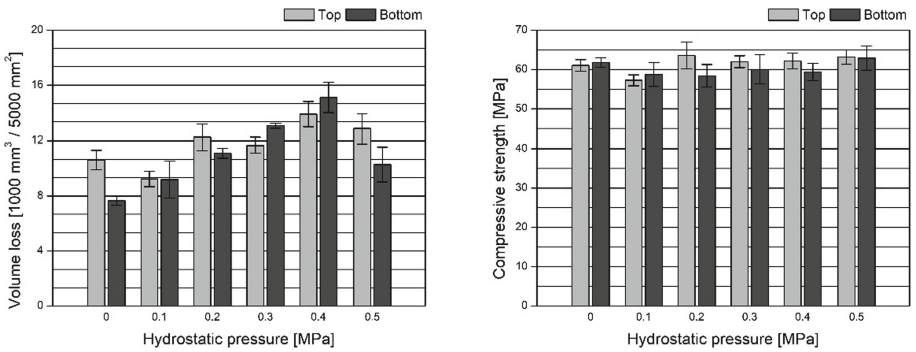

Fig. 3. Boehme disc wet method abrasion volume loss (left) and compressive strength of the concrete (right)

In most cases the specimens from the top part of test elements had higher compressive strength than those from the bottom, but the differences can be considered insignificant. However, in the same time they showed higher volume loss during the abrasion test (Fig. 3).

4 Conclusions

It is possible to use natural stone testing methods in concrete corrosion and abrasion resistance examination. Positive effect of hydrostatic pressure on the concrete resistance to ageing by salt mist was observed. This phenomenon was the effect of the change in air void characteristics of hardened concrete. As described in [5], micropores contribute to extending the life of materials by slowing down the effects of chloride corrosion taking place in their structure, while the open pores and external structure damages accelerate chloride corrosion.

Accumulation of salt inside the tested specimens during the action of the salt mist was observed. Even after desalination process some of the salt was left inside the concrete. This phenomenon can be associated with a different structure of the cement matrix than the stone. EN 14147 test method is therefore not very effective when assessing the concrete.

No clear relationship between abrasion resistance and compressive strength of the concrete was observed. The effect of the increased volume loss of the concrete exposed to the hydrostatic pressure can occur due to the decreased concrete porosity which results in more material being exposed to wear.

References

1. Alexander, M.G.: Marine Concrete Structures Design, Durability and Performance. Woodhead Publishing, Sawston, Cambridge (2016)
2. Mehta, P.K.: Concrete in the Marine Environment. Elsevier Science Publishers, Crown House, Essex (1991)
3. Yao, S.X., Gerwick Jr., B.C.: Underwater concrete part 2: proper mixture proportioning. Concr. Int. **2**, 77–82 (2004)
4. Horszczaruk, E., Brzozowski, P.: Bond strength of underwater repair concretes under hydrostatic pressure. Constr. Build. Mater. **72**, 167–173 (2014)
5. Gupta, S.: Sodium Chloride Crystallization in Dryling Poros Media: Influence of Inhibitor. Eindhoven University of Technology (2013)

Life Cycle Assessment on the Use of Ultra High Performance Fibre Reinforced Concretes with Enhanced Durability for Structures in Extremely Aggressive Environments: Case Study Analyses

M. C. Caruso[1(✉)], C. Pascale[1], E. Camacho[2], S. Scalari[3], F. Animato[3], M. C. Alonso[4], M. Gimenez[4], and L. Ferrara[5]

[1] Sviluppo Tecnologie e Ricerca per l'Edilizia Sismicamente Sicura ed Ecosostenibile S.c.ar.l. (STRESS), Naples, Italy
mariachiara.caruso@stress-scarl.it
[2] Research and Development Concretes SL (RDC), Valencia, Spain
[3] Enel Green Power (EGP), Rome, Italy
[4] Instituto Eduardo Torroja - Consejo Superior de Investigaciones Científicas (CSIC), Madrid, Spain
[5] Politecnico di Milano, Milan, Italy

Keywords: Ultra-High Durability Concrete · Comparative Life-Cycle Assessment · Structural durability · Aggressive environment · Concrete infrastructures

1 Introduction

Last decades have been characterized by growing attention on sustainable development. The European Commission interest in this topic is evident considering the global agreements and the related massive investments that have been, and still are, carried out to guarantee a sustainable approach to global growth. A contribution to pursue this challenging goal is provided by the EU-funded ReSHEALience Project (GA n° 760824). ReSHEALience Project aims at developing Ultra High Performance Fibre Reinforced Concretes with enhanced durability (Ultra High Durability Concrete – UHDC) that will be characterized by at least 30% longer service life as compared to traditional concretes. The increase of durability will be analyzed also from a sustainability point of view taking into account all the environmental, economic and social impacts, associated to the longer life-cycle of the structures.

In this paper, comparative environmental analyses of traditional and innovative solutions for infrastructures exposed to extremely aggressive environments are presented.

© RILEM 2020
K. Kovler et al. (Eds.): ConcreteLife 2020, RILEM Bookseries 26, pp. 121–125, 2020.
https://doi.org/10.1007/978-3-030-43332-1_24

2 Project Overview

In detail, the first analyzed case study deals with off-shore aquaculture rafts exposed to marine environments (XS); whilst the second case study concerns basins for collection of cooling tower water in geothermal power plants, exposed to chemical attack (XA). The analyzed off-shore aquaculture rafts are located in Spain and used for farming mussels or other mollusks, supporting 70 tons of harvest. Traditionally these rafts are made of wooden primary and secondary beams, connected with steel nails. Wooden beams can last up to 15 years and are subjected to continuous maintenance, such as paint protection or beams replacement. Moreover, bolt (re)screwing and inspections are often needed. The aquaculture raft solution studied is based on the design launched in 2015 by the company RDC, made with Ultra-High Performance Concrete (UHPC). Here, the study is done using proposing Ultra High Durability Concrete (UHDC). The mix design for 1 m^3 of this material includes 800 kg of cement, 1062 kg of siliceous sand, 175 kg of silica fume, 30 kg of superplasticizer, 160 kg of steel fibers as reinforcement and 0.8% of cement weight of crystalline self-healing stimulating admixture (Penetron ADMIX®); w/c ratio is equal to 0,2. UHDC beams do not need maintenance during all their life, which has been assumed at least equal to 50 years. The analyzed cooling tower water basin is located in Chiusdino, Italy, close to a geothermal plant, owned by Enel Green Power (EGP). Traditional solutions are made of conventional concrete, with Ordinary Portland Cement (OPC). Due to chemical attack, traditional basins, whose walls can be as thick as 400 mm, can last up to 20 years; moreover, they need maintenance about every 5 years, mainly due to concrete and waterproof coatings degradation. Two alternative solutions for innovative water basins are herein considered, as a preliminary design, having different geometry: INN1, with 300 mm walls; INN2 with 200 mm walls and buttresses. Innovative water basins are made of Ultra High Durability Concrete (UHDC): the mix design of 1 m^3 of INN1 concrete includes: 600 kg of Portland Cement, 982 kg of sand, 33 l of superplasticizer, 500 kg of slag, 120 kg of steel fibers as the sole reinforcement, and 0.8% of cement weight of crystalline self-healing stimulator Penetron ADMIX®, and a w/c ratio equal to 0,33; the mix design of 1 m^3 of INN2 concrete is similar to INN1, but also includes 0.25% of cement weight of alumina nanofibers for enhanced durability (10% dispersion of NAFEN®). Innovative water basins can last 50 years; moreover, they require less maintenance activities.

For both case studies, a reference unit, the so-called “Functional Unit (FU)”, is set, together with the life-cycle phases of traditional and innovative structures to be compared, in order to assure the functional equivalence between the analyzed solutions. Environmental impacts of the alternative solutions of the analyzed case studies are compared according to Life-Cycle Assessment (LCA) standards (ISO 14040:2006 [1] and 14044:2006 [2]) and performed with the European EPD 2013 (Environmental Product Declaration) method [3] for Life Cycle Impact Assessment (LCIA). Results are reported in percentage terms in order to show the comparison between the impacts of alternative solutions.

3 Life Cycle Assessment Study and Results

According to LCA standards, the FU and the System Boundary of infrastructures to be compared are defined. System Boundary is set according to the EN 15804 [4], as reported in Fig. 1.

Life cycle stage	PRODUCTION			CONSTRUCTION		USE							END OF LIFE				BENEFITS
Modules	A1	A2	A3	A4	A5	B1	B2	B3	B4	B5	B6	B7	C1	C2	C3	C4	D
	Raw material supply	Transport	Manufacturing	Transport	Construction	Use	Maintenance	Repair	Replace	Refurbishment	Operation energy use	Operational water use	Demolition	Transport	Waste processing	Disposal	Reuse/ Recovery/ recycling potential

Fig. 1. Life Cycle stages for construction products – EN 15804 [4]

Then, the data collection of all inputs and outputs related to each stage of the infrastructures life cycle is performed in order to realize the Inventory that is necessary for LCIA. This has been performing using the SimaPro 9.0 [5] software. Comparative environmental results are then provided in terms of the following environmental categories: Acidification; Eutrophication; Global warming; Photochemical oxidation; Ozone layer depletion; Abiotic depletion; Abiotic depletion, fossil fuels.

In the following, the comparative LCA study and related results are provided for the off-shore aquaculture rafts and the cooling tower water basins.

Off-shore Aquaculture Raft

A comparison between a traditional and an innovative off-shore aquaculture raft is here performed. The FU is "the whole mussel raft, used for the production of 70t of mussels in marine environment". The System Boundary includes the following phases according to EN 15804:

- production (modules A1-A2-A3), transport from the manufacturing to the building site (A4) and raft installation (A5);
- maintenance operation considering a lifetime of 50 years (B2). It should be noticed that the lifetime of a wooden raft is 15 years, while the lifetime of a UHDC raft has been set to 50 years. In order to compare both solutions, a lifetime of 50 years is considered; this means that for the wooden raft, maintenance operations until 50 years have been considered;
- deconstruction of the raft (C1), transport of the raft to the landfill site or the recycling plant (module C2), waste processing of steel components (C3) as well as reuse of the wooden components of raft (Module D).

Moreover, two maintenance options are considered for the traditional raft: Option 1, in which the substitution of primary and secondary beams and relative connections is made with manual operations (every year approximately 4 t of wood are substituted);

Option 2, in which protective paint is applied (paint is applied each year during the first 3 years, later it is not painted until year 6, when it is painted again every year until the end of its lifetime).

Figure 2a shows that the highest environmental impacts are caused by the traditional raft when paint protection is choosen as a maintenance option. For 4 out of 7 impact categories (Acidification, Global Warming, Ozone Layer Depletion and Abiotic Depletion, fossil), the traditional raft, in case logs replacement is choosen as maintenance, provides the lowest impacts; for 3 out of 7 impact categories (Eutrophication, Photochemical Oxidation and Abiotic Depletion), the innovative raft provides the lowest impacts. Considering Option 2 maintenance, environmental impact reduction of innovative solution varies from 28% in case of Ozone Layer Depletion to 87% in case of Acidification.

Cooling Tower Water Basin

A comparison between a traditional and two innovative concrete cooling tower water basins is here performed. The FU is "whole water collection basin of the cooling tower, designed for containing the same amount of water flow". The System Boundary includes the following phases according to EN 15804:

- production (modules A1-A2-A3), and construction of the (A4-A5) considering that the elements may be precast on site (the only kind of transport considered is transport of raw material to construction site);
- repair of basin components, considering a lifetime of 50 years (B3);
- demolition of the basins (C1), transport of the materials to the landfill site or the recycling plant (module C2), concrete waste processing (C3), disposal of basin components (C4) as well as recycling of the basin concrete (D).

Figure 2b shows that the highest environmental impacts are caused by the traditional water basin. Environmental impacts of INN1 and INN2 are very similar, leading to an environmental reduction varying from 11% in case of Eutrophication, to 71% in case of Abiotic Depletion.

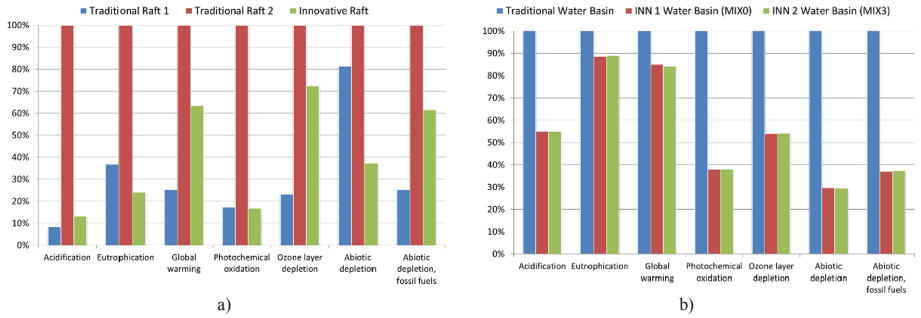

Fig. 2. (a) Comparative LCA of the Off-shore aquaculture raft; (b) Comparative LCA of the Cooling tower water basin

4 Conclusions

The paper focuses on the assessment of environmental impacts related to the life cycle of infrastructures exposed to extremely aggressive environments. The LCA study performed between traditional and innovative solutions (the latter realized with Ultra High Durability Concrete materials conceived and tested in the framework of the H2020 ReSHEALience project) highlights the better performances of the latter in environmental terms. In particular, when comparing traditional and innovative concrete solutions (Cooling tower water basins), the innovative UHDC ones always show a whole better environmental performance; whilst the comparison of wooden solutions with UHDC ones (Off-shore aquaculture rafts) highlights the good performance of the innovative concrete mainly due to its increased durability and thus longer lifetime. Future developments will include the addition of economic and social performances for sustainability assessment.

Acknowledgement. The activity described in this paper has been performed in the framework of the project "Rethinking coastal defence and Green-energy Service infrastructures through enHancEd-durAbiLity high-performance cement-based materials-ReSHEALience", funded by the European Union Horizon 2020 research and innovation programme under GA No 760824. The authors also acknowledge Enrico Gastaldo and Valentina Violante from PENETRON Italy, and Alexey Tretjakov and Denis Lizunov from ANF Development for helping in collecting data on PENETRON ADMIX® and NAFEN® alumina nanofibers, respectively.

References

1. International Standards Organisation: ISO 14040:2006, Environmental management – Life cycle assessment - Principles and framework, Brussels: CEN (European Committee for Standardisation) (2006)
2. International Standards Organisation: ISO 14044:2006, Environmental management – Life cycle assessment - Requirements and guidelines, Brussels: CEN (European Committee for Standardisation) (2006)
3. EPD International: General Programme Instructions of the International EPD® System. Version 2.01, dated 2013-09-18 (2013)
4. EN 15804:2012+A1:2013: Sustainability of construction works - Environmental product declarations - Core rules for the product category of construction products
5. PRé - Goedkoop, M., Oele, M., Leijting, J., Ponsioen, T., Meijer, E.: Introduction to LCA with SimaPro. v.5.2, January 2016

Macro-Synthetic Fiber Reinforced Concrete – Experience with Port Pavements Application

V. Chernov(✉)

Ashdod Port Company Ltd., Ashdod, Israel
vladimirc@ashdodport.co.il

Keywords: Port pavements · Macro fiber · Fiber reinforced concrete

1 Introduction

Ashdod Port successfully tries a use of Macro-Synthetic Fiber Reinforced Concrete (MSFRC) pavements since 2007. The pavements in ports are subjected to rather rough (sometimes brutal) handling, due to unavoidable impacts.

Concrete pavements are very popular at cargo terminals. Some manuals and standards recommend a use of steel fiber reinforced concrete pavements, especially at container stacking yards [1, 2].

It is known that fiber reinforcement does not prevent concrete cracking, as fibers get involved at a post-peak stage. That makes fibers exposed to an environment, which is chlorides-rich in marine conditions. That is the reason why for the experiments in the port synthetic macro fibers, mostly polypropylene ones, which correspond to the most modern recommendations for concrete pavements, were chosen [3]. The following text presents some results of these experiments with different types of fibers, fiber dosage, concrete mixes, types of concrete floor' joints, etc.

2 First Experience

In 2007 the trial area of about 2,500 m^2 was cast on Quay #5 (Bulk cargo quay), for which a pavement thickness of 33 cm was chosen as for non-reinforced concrete. According to our previous experience [4], the "Enduro 600" fiber has been chosen with a fiber dosage of 5 kg/m^3 ($\sim$0.5% of the volume). The concrete specification's requirements were as follows:

- The cement content in concrete should not exceed 280 kg/m^3 (of CEM II type) to limit a hydration heat
- The aggregate should be type A by Israeli Standard 3, such as dolomite one
- The concrete should be suitable for pumping
- The flexural strength of concrete should be at least 4 MPa.

© RILEM 2020
K. Kovler et al. (Eds.): ConcreteLife 2020, RILEM Bookseries 26, pp. 126–131, 2020.
https://doi.org/10.1007/978-3-030-43332-1_25

The fibers were added to concrete mixer on site.

The first casts were controlled by the concrete plant's technologist. A helicopter troweling was applied.

Two weeks after completion of the work it was found that the crane operators preferred to execute bulk operations without steel "bath", which should prevent the pavement from an impact caused by a free fall of a grab. Such impact resulted in appearance of local damages up to 15 mm deep. However, no concrete cracks were observed.

The most considerable problem of this pavement was low friction at the area in rain periods due to the bulk material spread together with water on the pavement – it made the driving dangerous there. So, the scrubbing of the surface had to be executed. In the specifications of all next projects a rough helicopter troweling together with rough brushing were required.

Another problem was durability of the floor joints, when the pavement's rough cleaning from bulk products was executed by a bulldozer to collect the maximum amount of spilled material. As a result of such cleaning, a lot of elastomeric material of joints' fill was damaged and sometimes detached. Hereinafter, a height of the sonomeric fill was increased and an angle cutting of joint areas was added.

3 Next Projects

As the trial was in general successful, the new projects with the total area of about 36,000 m^2 have been executed. The concrete mix was changed to the standard grade B-40 (equal to European C30 concrete), with the reduced fiber dosage of 4.5 kg/m^3 only.

Different examples of fibers were tested to ensure the equality of MSFRC behavior. The following fibers were studied:

- "Enduro 600" (#1 in Fig. 1)
- "Ferro" by Forta (#2 on Fig. 1)
- "Mayco" by BASF (#3 on Fig. 1)
- "Durus S200" by Adfil (#4 on Fig. 1)
- "Durus 50" by Adfil (#5 on Fig. 1)

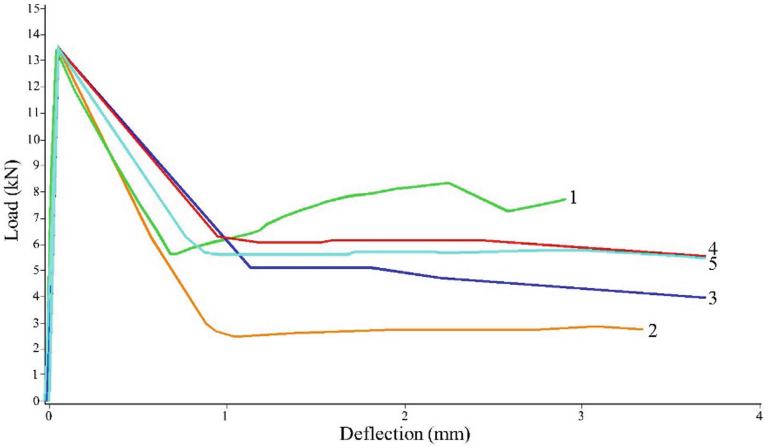

Fig. 1. Flexural toughness test results by ASTM C 1018 (for comparison purposes)

Actually, only fibers 1 and 2 were used in described projects, as no difference in the pavement's behavior was found.

During the first projects, the fibers were added to concrete mix on site by manufacturer's recommendation to prevent fibers balling. In the following projects, the mix was delivered from a concrete plant already with fibers. In these cases, no difference in the mix behavior was found.

The pavements were tested for different types of bulk and general cargo and found suitable even for the steel scrap handling – the most harsh (for pavements) cargo type (Fig. 2). The maximal pavement damage observed for this cargo type is shown in Fig. 3.

4 Joints

The structural joints span was predetermined by the cast technology – along the quay, with the strips of 5 m wide width. Two days after casting, the saw cut joints were executed perpendicularly to the quay line direction. The details of the two types of joints are presented in Figs. 4 and 5.

It is possible to say that most of the joints fulfilled their function, but sometimes the pavement cracked, even next to the joint – see Fig. 6.

Fig. 2. Steel scrub handling on the concrete pavement in Ashdod port

Fig. 3. The depth of maximal pavement's damage after steel scrubs handling

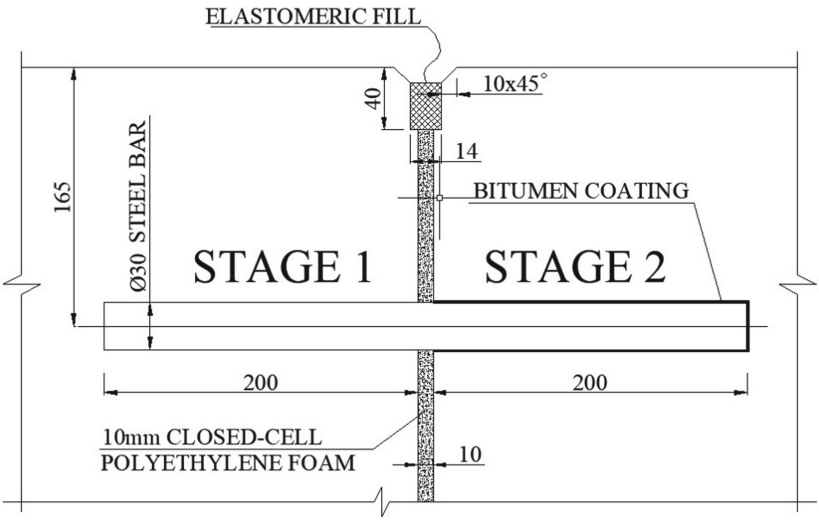

Fig. 4. The structural joint detail

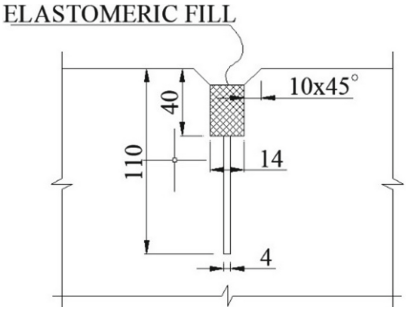

Fig. 5. Saw cut joint detail

Fig. 6. Cracks next to the saw cut joint

5 Conclusions

1. MSFRC pavements are more suitable for operation area of wharves for bulk and general cargo, than other known types of port pavements.
2. It is possible to add fibers both in concrete plant and on site.
3. The fill in the port MSFRC pavement joints should be deeper than in other types of floors.
4. According to the port's experience, though it occurred impossible to prevent a cracking in MSFRC pavements, it did not interfere with the operation of the pavement. After 12 years of intense cargo operations, the pavements does not require any repair.

References

1. ROM 4.1–94 Guidelines for the Design and Construction of Port Pavements. Puertos del Estado, Spain (1994)
2. Knapton, J., Meletiou, M.: The Structural Design of Heavy Duty Pavements for Ports and other Industries. British Ports Association, UK (1996)
3. Roesler, J., Bordelon, A.: Fiber Reinforced Concrete Pavements and Overlays. Nacional Concrete Consortium, Webinar 1 of 3, USA (2018)
4. Chernov, V., Zlotnikov, H., Shandalov, M.: Structural synthetic fiber-reinforced concrete – experience with marine applications. Concr. Int. **28**(8), 56–61 (2006)

Service Life Design for Inland Concrete Structures in Africa: Kampala Case Study

S. O. Ekolu(✉)

Department of Civil Engineering Science, University of Johannesburg, Auckland Park, South Africa
sekolu@uj.ac.za

Keywords: Service life · Natural carbonation prediction · Probabilistic modelling · Durability design

1 Introduction

Although concrete is a highly durable material, its design requires careful consideration of various design parameters, which have to be specified or selected in consideration of the environmental factors. The specification of environmental factors necessitates understanding of the geographical location under consideration during concrete design. This approach is the normal practice for development and use of building and construction codes worldwide such as the ACI 318 (USA) [1], EC 2 (Europe) [2], BS 8110 (Great Britain) [3], AS 3600 (Australia) [4] etc. Concrete construction is of particular interest to Africa and other developing countries, as it provides an effective solution to the much needed infrastructure requirements for the continent's economic development and improvement in the quality of life.

This paper evaluated the relationship between service life and the durability requirements specified in BS 8110 (1997) [3]. The British design code is widely used for design of reinforced concrete structures in several tropical African countries including Uganda. International structural design codes such as mentioned in the foregoing, utilize specified durability requirements for structures under different exposure environments. Generally, these guidelines are prescriptive and not determined through design calculations using engineering or scientific methods. In this study, a rational approach was employed by using a natural carbonation prediction model [5] to evaluate the durability specifications in BS 8110 [3] and to determine their implications on the service lifespan of concrete structures. Kampala city location of subSaharan Africa was selected as a case study, being representative of the prevailing tropical conditions in the region.

2 Environmental Factors

2.1 Climate Regions of Africa

Haque et al. [11] divided the African region into three climatic regions comprising the:

© RILEM 2020
K. Kovler et al. (Eds.): ConcreteLife 2020, RILEM Bookseries 26, pp. 132–136, 2020.
https://doi.org/10.1007/978-3-030-43332-1_26

- Temperate climate at the North-West of Sahara bordering the Atlantic Ocean
- Arid zones located North of the Sahara Desert and at the Kalahari Desert of Southern Africa
- Tropical climate of East and Central Africa
- Subtropical climate of Southern Africa and parts of Northern Africa

The most important environmental considerations in durability design are the weather conditions comprising ambient temperature, relative humidity and precipitation [12]. As expected, these weather factors considerably vary geographically even within the same climate region. For practical durability design, it is necessary to establish and consider the local macro-climate conditions at the location of the study.

2.2 Case Study for Kampala City

Kampala is also the largest city in the country. It is an inland city located at the shores of Lake Victoria, the source of the white Nile. The weather conditions in the city are shown in Fig. 2 (https://www.worldweatheronline.com). Typically, Kampala weather consists of annual precipitation of 787 mm, 73% RH and 23 °C annual average temperature. Precipitation in Kampala is almost all year round except for the two dry months of January and February. The heaviest rainfall occurs from October to December, while the months of March to September are moderately wet. Being a tropical inland location, carbonation is the main mechanism of steel corrosion in reinforced concrete structures. No chloride exposure environment exists.

2.3 Durability Specifications

Given the foregoing constraints in concrete technology and cement availability, it follows that concrete strengths that are most commonly used in structural design of local concrete structures are 20 to 40 MPa, with 25 MPa and 30 MPa being most predominant. Accordingly, the specifications selected for service life design in the present study were: (i) *mild* exposure with 30 MPa/20 mm cover, 35 MPa/20 mm, 40 MPa/20 mm cover. (ii) *moderate* exposure with 35 MPa/35 mm cover, 40 MPa/30 mm. (iii) *severe* exposure with 40 MPa/40 mm. In all cases, CEM II and a CO_2 concentration of 400 ppm were used in the design calculations.

Table 1. Durability specifications [3]

Exposure conditions	Nominal cover (mm)				
Mild	25	20	20	20	20
Moderate	–	35	30	25	20
Severe	–	–	40	30	25
Very severe	–	–	50	40	30
Most severe	–	–	–	–	50
Lowest concrete grade (MPa)	C30	C35	C40	C45	C50

3 Stochastic Service Life Design

The environmental factors given in Fig. 1 and the durability specifications presented in Table 1, were employed in the service life design. The design was conducted using the natural carbonation prediction model, already described in Ekolu and Ballim [5] but repeated here for convenience. Equations (1) to (7) provide the various parameters considered in the model's calculations.

Service life prediction for each exposure class was conducted based on the stochastic applicative approach of calculating failure probability. According to the method, carbonation progression is taken to be the loading (S) and the concrete cover (R) is the concrete's resistance to carbonation ingress. Failure occurs upon fulfilment of the condition R(t) < S(t). The reliability index given in Eq. (8) was used to calculate failure probability [14]. Table 1 gives the parameters employed in the design calculations.

$$\beta(t) = \frac{\mu[R,t] - \mu[S,t]}{\sqrt{\sigma^2[R,t] + \sigma^2[S,t]}} \tag{8}$$

where μ = indicates the mean of, σ = standard deviation, β = the value along x-axis of NORMDIST curve (0,1).

4 Results and Discussion

It can be seen in Table 1 that a cover depth of 20 mm is recommended for *mild* exposure conditions. Figures 1 and 2 give the predictions of carbonation ingress and service lifespans for the concrete structures exposed to the *mild* and *moderate* exposure conditions. The results given in Table 2 show that the time taken for carbonation progression to penetrate through the full cover depth (t_c) of 20 mm was 4 to 7 years, with the longer ages corresponding to the specified higher strengths. Such a short lifespan may only suite temporary structures. However, the most significant improvements arise from increase in cover depth as evident in the comparison of carbonation progression for the *moderate* and *severe* exposure conditions. It can be seen that for the 35 MPa concrete, a 10 mm increase in cover from 20 mm to 30 mm, increased the t_c from 4.8 to 22.5 years, a 4.7-fold increase. Similarly for 40 MPa concrete, increases in cover from 20 mm to 30 mm to 40 mm gave corresponding t_c values of 7.3, 25.7 and 60 years, which are increases of $\times$3.5 and $\times$2.3, respectively. Clearly, 10 mm increase in cover increased t_c by two to three-fold.

Similarly, there is a corresponding geometric increase in the service life of concrete structures as a direct result of increase in cover depth. For 35 MPa concrete, the increase in cover from 20 mm to 35 mm gave a five-fold increase in service life i.e., $\times$3.3 per 10 mm increase in cover. Also, increases in cover from 20 mm to 30 mm to 40 mm for the 40 MPa concrete, gave corresponding service lifespans of 1.3, 5.3 and 12 years, which represent $\times$4.1 and $\times$2.3 increases in service life per 10 mm increase in cover. Generally, it can be concluded that an increase of 10 mm in cover depth, gives about a 3-fold increase in service lifespan.

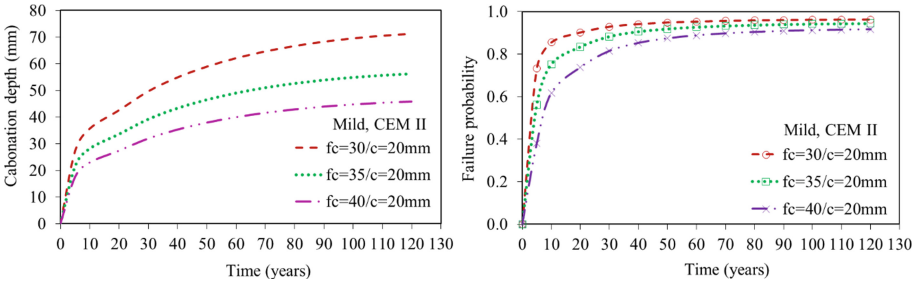

Fig. 1. Carbonation progression and failure probabilities for durability specifications under mild exposure

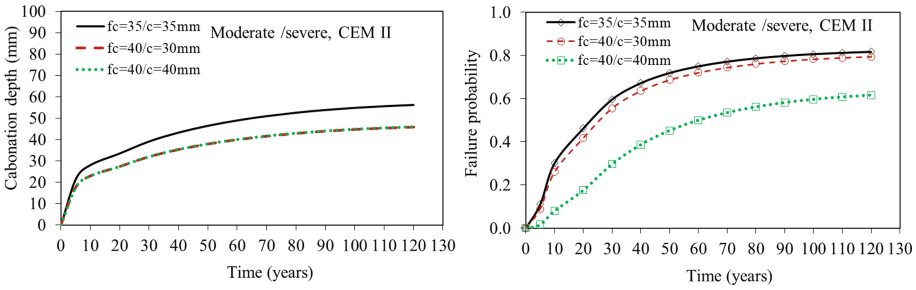

Fig. 2. Carbonation progression and failure probabilities for durability specifications under moderate or severe exposure

Table 2. Service lifespans for concrete structures under the various exposure classes

Exposure class	Specification	Carbonation depth after 50 years (mm)	Time taken for carbonation to reach steel, t_{cbn} (years)	Probabilistic Service life (years)
Mild	30 MPa/20 mm cover	58.8	3.7	0.7
	35 MPa/20 mm cover	46.5	4.8	1.0
	40 MPa/20 mm cover	37.9	7.3	1.3
Moderate	35 MPa/35 mm cover	46.5	22.5	5.0
	40 MPa/30 mm cover	37.9	25.7	5.3
Severe	40 MPa/40 mm cover	37.9	60	12

5 Conclusions

The present study has demonstrated the potential for rational service life design of concrete structures employing a practical prediction model for natural carbonation. A case study was conducted for the African topical climate focusing on Kampala city.

It was found that cover depth gives the most significant influence on service lifespan. A 10 mm increase in cover depth gives about a three-fold increase in the service life, being the time taken for carbonation to reach the level of steel reinforcement. Results showed that the specifications for *mild* conditions simply provide a meaningful service of only 4 to 7 years, which can only be appropriate for temporary structures. Economically feasible structures required to achieve 30 to 50 years of service life, have to be designed using the durability specifications for *moderate* and *severe* exposure classes.

References

1. ACI 318M, Building code requirements for structural concrete and commentary. American Concrete Institute, Farmington Hills, MI, USA (2002)
2. EC 2, CEN/TC 250 Structural Eurocodes: Eurocode 2: Design of concrete structures - Part 1–1: General rules and rules for buildings, pp. 47–52 (2004)
3. BS 8110, Structural use of concrete, Part 1, Code of practice for design and construction, London, British Standards Institution (BSI), 389 Chiswick High Road, London, W4 4AL, UK (1997)
4. AS 3600, Concrete Structures, Standards Australia, Sydney, Australia (1994)
5. Ekolu, S.O., Ballim, Y.: Technology transfer to minimize concrete construction failures. In: Proceedings 1st International Conference on Advances in Engineering and Technology, Entebbe, Uganda, pp. 91–98, July 2006

Effect of Alite Content in Sulphate-Resistant Cement on Heat Release in Massive Hydraulic Engineering Structures

V. R. Falikman[1(✉)], K. B. Safarov[2], and V. F. Stepanova[1]

[1] Scientific Research Institute for Concrete and Reinforced Concrete, Moscow, Russia
vfalikman@yahoo.com
[2] Rogun Hydropower Plant, Dushanbe, Tajikistan

Keywords: Sulphate-resistance cement · Alite · Heat release · Massive hydraulic engineering structures · Standardization

1 Introduction

The heat release of cement affects the quality and speed of concrete works, the implementation of the construction project management, and the durability of concrete structures, especially for massive hydraulic structures, in a construction of which sulfate-resistant cement is often used [1].

The greatest amount of heat is released during hydration of tricalcium aluminate C_3A and tricalcium silicate - alite C_3S. At the same time, the Interstate Standard GOST 22266-2013 on sulfate-resistant cement normalizes only the limit value of C_3A content (<3.5%) in mineralogical composition, when there are no special requirements to C_3S content.

Some thermo mechanical and thermo physical concrete properties depending on the ambient temperature, the amount of heat generated, and the mineralogical composition of sulfate-resistant cement coming from cement plants for the Rogun HPP construction are presented.

2 Results

Sulphate-resistant Portland cement of two different batches, with different mineralogical compositions, coming to the construction site of Rogun HPP from Dushanbe plant "Tajikcement" was investigated. According to GOST 22266-2013, mineralogical composition both of them (Table 1) corresponds to norms.

© RILEM 2020
K. Kovler et al. (Eds.): ConcreteLife 2020, RILEM Bookseries 26, pp. 137–140, 2020.
https://doi.org/10.1007/978-3-030-43332-1_27

Table 1. Cements: mineral composition by Bogue

	C_3S	C_2S	C_3 A	C_4AF
B1	52,7	18,3	2,76	16,10
B2	70,4	4,76	3,49	16,26

The heat release of the studied cement batches was determined, with a simultaneous assessment of their activity. The test results are shown in Table 2 and in Fig. 1.

The Building Code SP 41.13330.2010 [2] gives the norms for the allowable amount of cement heat hydration emitted in hardening time, according to which the studied cement from batch No. 2 does not meet the heat release criterion. An analysis of the results from Tables 1 and 2 allows to conclude that the reason for exceeding the allowable heat release of cement from batch No. 2 is the increased content of the tricalcium silicate C_3S (alite) in its composition.

Table 2. Cements: heat of hydration and strength

	C_3S content, %	Heat of hydration, kJ/kg (requirement according to SP 41)			Compressive strength, MPa (% grade strength)	
		3 days	7 days	28 days	2 days	28 days
B1	52,7	208,6 (< 250)	232,2 (< 295)	311,1 (< 345)	25,1 (63%)	42,1 (105%)
B2	70,4	290,1 (< 250)	358,1 (< 295)	409,6 (< 345)	26,6 (67%)	37,9 (94%)

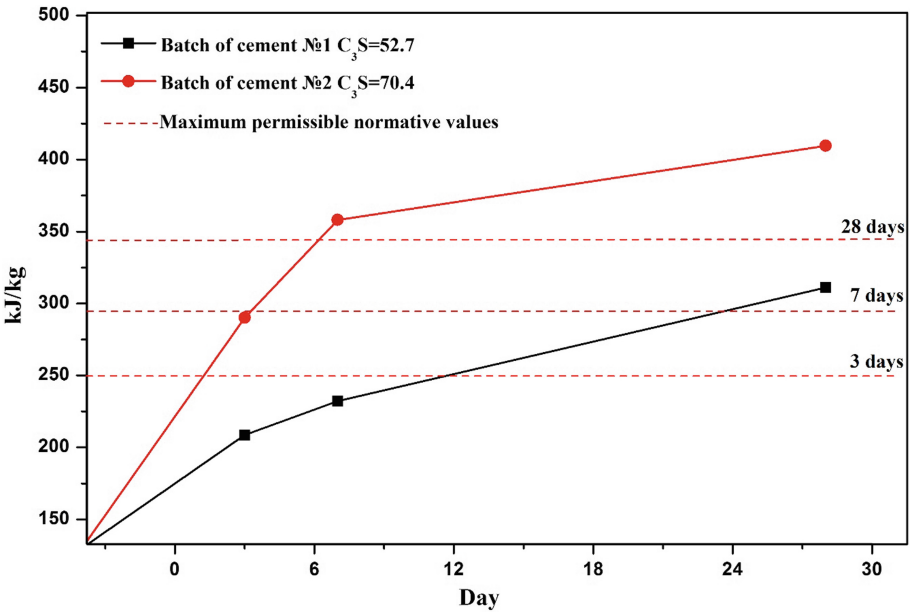

Fig. 1. Heat release of two cement batches

Consequently, in order to study a behavior of these batches of cement in massive reinforced concrete hydraulic structures, production (in-process) tests were carried out to determine the heat release, when industrial concrete mixes are used. Monitoring was carried out using thermocouple sensors installed in the epicenter of the concrete block (T1), on the surface of the reinforcement protective layer (T2) and outside the concrete space (T3). The test results are shown in Table 3.

Normative document VSN 31–83 [3] establishes that during concrete works the temperature difference between the core and the side surfaces of the array in hydraulic structures is allowed no more than 16–18 °C. When cement No. 1 (C_3S = 52.7%) used, the maximum temperature of the concrete structure core reached 63.1 °C, and the temperature of concrete surface at the same time was 46.2 °C. So, the temperature difference between the core and the surface was 16.9 °C, which meets the requirements of Building Codes SP 41.13330.2010 and VSN 31–83 according to the heat dissipation criterion (Fig. 2).

Table 3. Temperature difference between core and surface of structure.

	C_3S content, %	Temperature, °C				
		T_3 Outside	T_1 Core of structure	T_2 Concrete surface	$\Delta T = T_1 - T_2$	VSN 31–83 requirements ΔT
B1	52,7	20–30	63,1	46,2	16,9	Not more than 16–18 °C
B2	70,4	20–30	78,5	50,6	27,9	

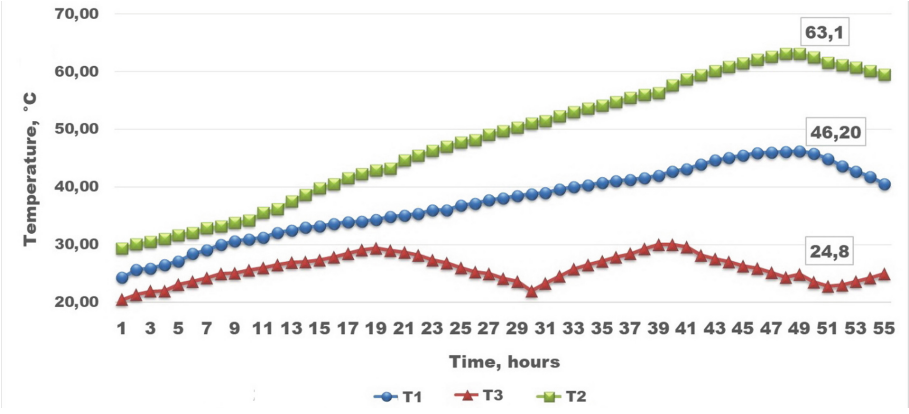

Fig. 2. Heat dissipation of concrete produced on cement B1

The maximum temperature of the core of concrete laid with cement No. 2 (C_3S = 70.4%) reached 78.5 °C, with a maximum concrete surface temperature of 50.6 °C. In this case, the temperature difference between the core and the concrete surface was 27.9 °C, which exceeds the permissible norm and does not meet the requirements of the standard (Fig. 3).

Sum Up: There seem to be necessary to determine the limit content of C_3S, in which the heat release of sulfate-resistant cements will develop within the permissible values of SP 41.13330.2010, and the thermal stress state of massive hydraulic concretes will meet the requirements of VSN 31–83.

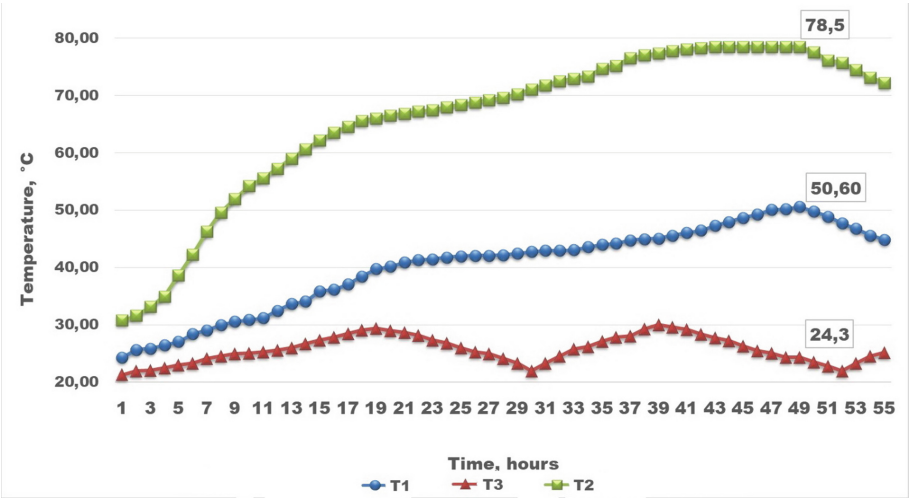

Fig. 3. Heat dissipation of concrete produced on cement B2

3 Conclusions

It is shown that the alite content in different batches of sulfate-resistant cement can significantly affect the thermo mechanical properties of hardened concrete, which ultimately could lead to cracking and reduce the durability of concrete structures. The experience at construction sites with unstable chemical and mineralogical composition of the delivered cement was considered. With regard to the concreting of massive structures, the norms for sulfate-resistant cement need to be clarified and revised (or updated) in terms of determining the requirements for its mineralogical composition.

References

1. Falikman, V.R., Safarov, K.B., Stepanova, V.F.: High performance concrete for hydraulic engineering projects with aggregates presenting an AAR Hazard. In: Santhanam, M., Gettu, R., Pillai, R.G., Nayar, S.K. (eds.) Advance in Construction Materials and Systems, Proceedings of International Conference (ICACMS). , RILEM PRO 118 (in 4 vol.), vol. 2, no. 662, pp. 233–242. RILEM Publishing S.A.R.L., Chennai, India (2017)
2. SP 41.13330.2010. Concrete and reinforced concrete structures of hydraulic facilities. Ministry of regional development of the Russian Federation, Moscow, p. 68 (2012)
3. VSN 31–83. Rules for the production of concrete works in the hydraulic structures construction. Ministry of energy of the USSR. Leningrad, p. 84 (1984)

Self-healing Stimulated by Crystalline Admixtures in Chloride Rich Environments: Is It Possible to Extend the Structure Service Life?

E. Cuenca[1], E. M. Gastaldo Brac[2], S. Rigamonti[1], V. Violante[2], and L. Ferrara[1(✉)]

[1] Department of Civil and Environmental Engineering, Politecnico di Milano, Milan, Italy
liberato.ferrara@polimi.it
[2] Penetron Italia, Collegno, Italy

Keywords: Self-healing concrete · Crystalline admixture · Chlorides · Service life

1 Introduction

Design code prescritpions on the service life of ordinary reinforced concrete structures may be difficult to be fulfilled in highly aggressive environments, in which premature degradation of the structural performance is most likely to occur. In these situations, in order to avoid expensive repair activities, advanced systems such as self-healing concrete could be adopted. In the last decade, researchers started to look at this functionality as a way to solve degradation problems in chloride-laden environments. If a significant degree of crack sealing is achieved, the mechanical and physical properties of a cracked element tend to those of an identical uncracked element, thus resulting into a slower penetration rate of aggressive substances.

In the broad literature on the stimulation/engineering and experimental assessment of self-healing functionalities in concrete [1, 2] and cement based materials, a relatively few number of studies has addressed the effectiveness of healing in reducing the chloride diffusion. As far as autogenous healing is concerned, several authors agreed that self-healing is able to induce a full recovery of the chloride diffusion resistance for crack widths below a certain threshold, in the range of few tens of microns [3–5]. Borg et al. [6] studied the crack sealing capacity of mortars containing supplementary cementitious materials (fuel ash and silica fume) or crystalline admixture in chloride-rich environments. They observed that sea-water may lead to an enhancement of the self-healing capacity of mortars with respect to distilled water, especially for higher chloride contents. They noticed that both the addition of fuel ash (with a replacement ratio lower than 20%) and silica fume (with a content of 15% by mass of cement) have a beneficial effect on the sealing capacity of cracks up to intermediate widths (0.15–0.3 mm). The mix containing the crystalline admixture, thanks to its hydrophilic behavior, guaranteed the highest crack sealing capacity in almost all the investigated conditions, especially for

© RILEM 2020
K. Kovler et al. (Eds.): ConcreteLife 2020, RILEM Bookseries 26, pp. 141–147, 2020.
https://doi.org/10.1007/978-3-030-43332-1_28

cracks up to 0.3 mm. Li et al. [7] tested high performance fiber reinforced concrete specimens pre-loaded up to 0.5%, 1.0%, and 1.5% tensile strain level and immersed in a 3% chloride solution for 30, 60 and 90 days. When they re-loaded the specimens after curing, they found that, due to self-healing, specimens partially recovered some of their mechanical features. Moreover, the results showed that under severe chloride exposure, the specimens remained durable with a good crack-controlling capability. Ling et al. [8] studied the effects of self-healing cracks in bacterial concrete on the penetration of chlorides. They considered ordinary Portland cement mortar specimens (control) and one mortar containing a microbial self-healing agent. It was observed that self-healing led to a reduction of chloride content for both mixes, but the chloride content in the specimens having the self-healing agent was lower. Van Belleghem et al. [9] used a concrete mixture containing fly ash and a polyurethane-based healing agent encapsulated into glass capsules. Some of the specimens were pre-cracked up to a crack width of 300 μm. The results showed that chloride ingress depends on the crack opening and increases almost exponentially along the depth of the crack. After the curing time, it was observed that the self-healing agent led to a reduction of the chloride ingress rate up to 75%. Maes et al. [10] also studied the improvement in service life of concrete specimens suffering chloride attack due to self-healing, introducing into their life prediction model a variable depending on the crack width.

The main problem in exploiting this phenomenon is its reliability. For this reason, an experimental campaign, was carried out which, besides aiming at assessing the influence of the environmental conditions on the strength development, focused on the recovery of chloride diffusion resistance in pre-cracked specimens. The investigation was also meant to obtain useful indications to design and build the "ordinary reinforced concrete" cell of a water basin in a geothermal power plant, to be compared on the one hand with the current construction practice, which requires wall as thick as 400 mm for mere durability issues, and, on the other with advanced solutions in which Ultra High Durability Concretes will be employed, in the framework of the H2020 project ReSHEALience [11].

2 Experimental Programme

Two mixes, differing because of the presence of a crystalline admixture, were considered, whose mix proportions are summarized in Table 1.

Table 1. Concrete compositions

Component	Without CA (kg/m^3)	With CA (kg/m^3)
Portland cement CEM II 42, 5 R	360	360
Water	180	180
Fine aggregate (sand 0–4 mm)	814	811
Coarse aggregate (gravel 4–16 mm)	1077	1077
Superplasticizer admixture	3.5	3.5
Crystalline admixture (Penetron Admix ®)	=	2.9

First, the average compressive strength of concrete after 7, 14, 28, 56 and 84 days curing in the above-listed environmental conditions was measured. For each curing time and type of concrete, at least 3 cylindrical specimens 200 mm high and with 100 mm diameter were tested.

For the measurement of the effects of healing on chloride diffusion resistance, 100 mm high cylinders with a 100 mm diameter were used. 7 or 28 days after casting, half of the specimens were pre-cracked by means of a splitting test. The two halves were then reunited, the crack width was visually analyzed by means of an image analysis software [12], and all the samples were cured for 1, 3 or 6 additional months, both permanently immersed in a 16.5% NaCl solution or subjected to wat/dry cycles in the same solutions. After curing, a visual inspection of the healed pre-cracked specimens was carriedout by means of an electronic microscope and an image-editing software, aimed at quantifying the extent of crack closure. Fourteen pictures of each crack were taken both immediately after pre-cracking and at the end of each curing time. These pictures were then processed by means of the image-editing software, thus allowing the identification of the surface crack width before and after the healing time and so the determination of the percentage of closure. Moreover, for each considered environmental condition, specimens were subjected to chemical titration (RILEM TC 178-TMC) to determine the chloride content.

3 Experimental Results

A limited influence of curing conditions on the strength development was observed (Fig. 1).

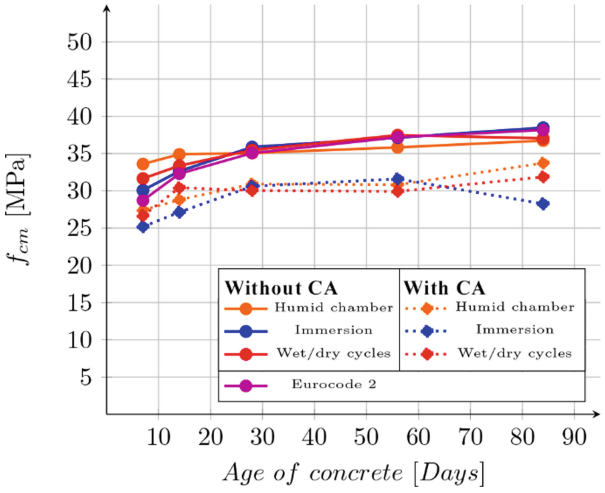

Fig. 1. Influence of curing conditions and crystalling admixture on strength development

In order to study the effect of crack self-sealing on the recovery of chloride diffusion resistance, first of all, from the microscope acquired images of the cracks, using an image-editing software, the average crack width w_{average} was measured and the percentage of crack closure *%sealing* was calculated according to Eq. 1

$$\%_{healing} = \frac{w_{initial} - w_{post-healing}}{w_{initial}} \cdot 100 \quad (1)$$

where: $w_{initial}$ is the crack width of the newly cracked specimen;
$w_{post\text{-}healing}$ is the crack width of the same specimen after curing;

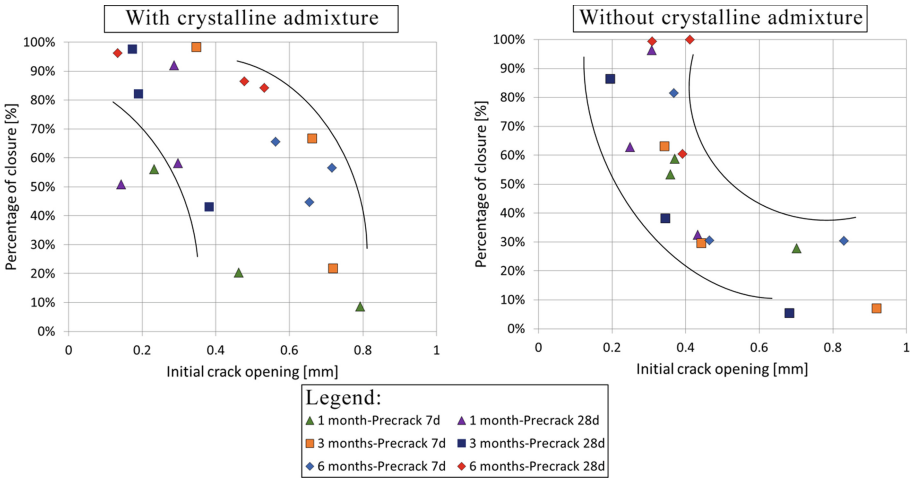

Fig. 2. Percentage of crack closure vs. initial crack opening for specimens immersed in a 16.5% NaCl aqueous solution.

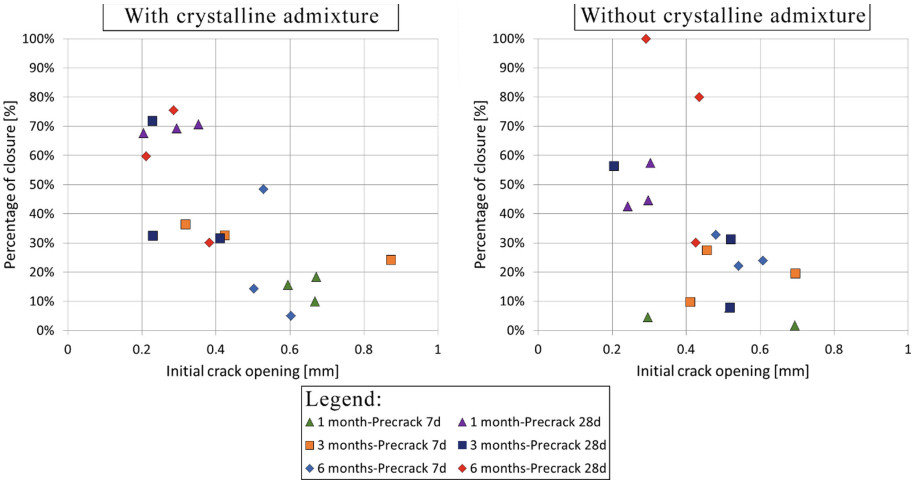

Fig. 3. Percentage of crack closure vs. initial crack opening for specimens subjected to wet and dry-cycles in a 16.5% NaCl aqueous solution.

Plotting the results obtained for immersed specimens (Fig. 2) it is possible to identify at first glance the abovementioned existing relationship between initial crack width and percentage of closure. It is also possible to observe the beneficial effects of the crystalline admixture for wider cracks (0.5–1 mm). Moreover, focusing on smaller cracks (<0.4 mm), it can be seen that the concrete samples with the healing agent have the potential to achieve a sealing capacity after 3 months of curing directly comparable to the one obtained after 6 months by the other mix. Considering then the samples subjected to wet/dry cycles (Fig. 3) a generally lower healing capacity with respect to submerged samples is observed. Also in this case a relation between initial crack width and crack closure exists and the use of crystalline admixture results on some benefits on the sealing capacity of cracks, even though its positive contribution seems not to be as important as for immersed specimens. Focusing on the pre-cracking age, it can be noted that the cracks obtained for specimens pre-cracked after 7 days are generally wider than those obtained by pre-cracking after 28 days. This outcome is probably due to the fact that when pre-cracking a younger concrete its tensile strength is not fully developed yet, thus making difficult to control the crack width generated through a splitting test.

Finally, chemical titration analyses were performed according to RILEM TC 178-TMC, which allowed the determination of the chloride content as a percentage by mass of concrete. Tests were performed on both uncracked and pre-cracked cylindrical concrete specimens and subjected to both exposure conditions up to 6 months. The experimental data obtained through the chemical tests were then fitted with Fick's second law and, in the case of specimens permanently immersed, the apparent diffusion coefficient D_{app} and the surface chloride content was determined. An example of results obtained for specimens both with and without the crystalline admixtures cured under water immersion or wet/dry cycles for one month is shown in Fig. 4a–b. Unfortunately, specimens cured for 3 and 6 months immersed in the aqueous solution have suffered from problems related to the formation of an undesired bi-directional diffusion phenomenon, due to the non-perfect waterproofness of the lateral surface sealing. The apparent diffusion coefficients obtained following this procedure are summarized in Table 2.

Besides highlighting the dramatic effect that a cracked state (which is the service state of a reinforced concrete structure) has on the chloride permeability, the results also highlight a general improvement for the specimens containing the crystalline admixture with respect to the reference mix ones, though this difference appears decreasing with continued curing and hence continuing healing. Moreover, the longer curing time under wet/dry cycles, and hence the higher sealing, also results in reduction of the chloride permeability coefficient, mainly in the case of concrete containing the crystalline admixture. The higher is the curing time of the pre-cracked sample, the closer the value of the apparent chloride diffusion coefficient D_app to that of an uncracked specimen, especially for specimens containing crystalline admixture.

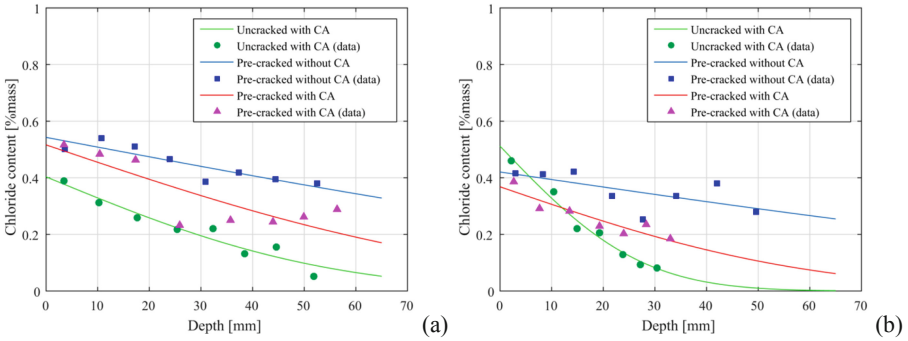

Fig. 4. Chloride profiles for specimens immersed continuously (a) and subjected to wet/dry cycles in the 16.5% NaCl aqueous solution for 1 month (CA:crystalline admixture).

Table 2. Apparent diffusion coefficients for specimens immersed in 16.5% NaCl solution.

Apparent diffusion coefficient D_{app} [m^2/s]		
	Without CA	With crystalline admixture
Uncracked, cured for 1 month	\	$3.80 \cdot 10^{-10}$
Pre-cracked at 28 days, cured for 1 month	$3.27 \cdot 10^{-9}$	$9.21 \cdot 10^{-10}$

4 Conclusions

In this paper an experimental study of autogenous and crystalline admixture stimulated crack self-sealing has been presented, in which the influence of crack sealing on the reduction of chloride diffusion was assessed. Different exposure conditions were investigated, including water immersion in a 16.5% NaCl aqueous solution and wet/dry cycles with the same aqueous solution, together with the influence of pre-cracking ages and healing time. Dependence on crack width and healing time was as expected, with a faster and more effective crack sealing generally achieved by the samples containing the healing agent. Moreover, significant differences could be identified between the values of apparent chloride diffusion coefficient, as affected by the crack sealing of concrete, with and without crystalline admixture. This result is a further proof of the importance of accounting for the presence of cracks when studying chloride diffusion. Such a result, besides confirming the importance of considering the cracked state service conditions in assessing the real durability of a structure in its service scenario, could be usefully accounted for when evaluating the effects of healing on the extension of service life in reinforced concrete structures exposed to aggressive environments.

Acknowledgements. The activity described in this paper has been performed in the framework of the project "Rethinking coastal defence and Green-energy Service infrastructures through enHancEd-durAbiLity high-performance cement-based materials-ReSHEALience", funded by the European Union Horizon 2020 research and innovation programme under GA No 760824.

References

1. de Belie, N., Gruyaert, E., Al-Tabbaa, A., Antonaci, P., Baera, C., Bajare, D., Darquennes, A., Davies, R., Ferrara, L., Jefferson, T., Litina, C., Miljevic, B., Otlewska, A., Ranogajec, J., Roig-Flores, M., Pain, K., Lukowski, P., Serna, P., Tulliani, J.M., Vucetic, S., Wang, J., Jonkers, H.M.: A review of self-healing concrete for damage management of structures. Adv. Mater. Interfaces **5**(17), 1–28 (2018)
2. Ferrara, L., Van Mullem, T., Alonso, M., Antonaci, P., Borg, R., Cuenca, E., Jefferson, A., Ng, P., Peled, A., Roig-Flores, M., Sánchez, M., Schroefl, C., Serna, P., Snoeck, D., Tulliani, J., De Belie, N.: Experimental characterization of the self-healing capacity of cement based materials and its effects on the material performance: a state of the art report by COST Action SARCOS WG2. Constr. Build. Mater. **167**(2018), 115–142 (2018)
3. Savija, B., Schalngen, E.: Autogeneous healing and chloride ingress in cracked concrete. Delft University of Technology (2016)
4. Sahmaran, M.: Effect of flexure induced transverse crack and self-healing on chloride diffusivity of reinforced mortar. J. Mater. Sci. **43**, 9131–9136 (2007)
5. Jacobsen, S., Sellevold, E.: Self-healing of high strength concrete after deterioration by freeze/thaw. Cem. Concr. Res. **26**, 55–62 (1995)
6. Borg, R., Cuenca, E., Gastaldo Brac, E., Ferrara, L.: Crack sealing capacity in chloride-rich environments of mortars containing different cement substitutes and crystalline admixtures. J. Sustain. Cem.-Based Mater. **7**(3), 141–159 (2018)
7. Li, M., Li, V.: Cracking and healing of engineered cementitious composites under chloride environment. ACI Mater. J. **108**(3), 333–340 (2011)
8. Ling, H., Chunxiang, Q.: Effects of self-healing cracks in bacterial concrete on the transmission of chloride during electromigration. Constr. Build. Mater. **144**, 406–411 (2017)
9. Van Belleghem, B., Van den Heede, P., Van Tittelboom, K., et al.: Quantification of the service life extension and environmental benefit of chloride exposed self-healing concrete. Materials **10**(5), 1–22 (2017)
10. Maes, M., De Belie, N.: Service life estimation of cracked and healed concrete in marine environment. In: International Conference on Concrete Repair, Thessaloniki, Greece (2016)
11. Ferrara, L., Bamonte, P., Suesta, C., Animato, F. et al.: An overview on H2020 project ReSHEALience. In: Proceeding IABSE Symposium, Guimaraes, 27–29 March 2019, pp. 184–191 (2019)
12. Cuenca, E., Tejedor, A., Ferrara, L.: A methodology to assess crack-sealing effectiveness of crystalline admixtures under repeated cracking-healing cycles in Fiber Reinforced Concrete. Constr. Build. Mater. **179**, 619–632 (2018)

Simulations of Electrical Conductivity of Composite Materials and Optimization of Artificial Neural Networks

S. Kekez(✉)

Silesian University of Technology, Gliwice, Poland
sofija.kekez@polsl.pl

Keywords: Structural health monitoring · Electrical conductivity · Cementitious composites · Carbon nanotubes · Artificial neural networks

1 Introduction

Structural health monitoring (SHM) has become an established field of engineering in the past few decades. SHM aims to give a diagnosis on the condition of materials, elements, and of the whole structure at every moment of the structure's lifespan. Design dictates the structure's nominal behavior and SHM allows keeping it in that nominal domain. Thanks to the time-dimension of monitoring, which builds a full historical database of the structure, it is possible to determine damage progression and residual life of the observed structure.

When it comes to concrete, i.e. cementitious materials, the lack of two main properties - electrical conductivity and piezoresistivity, hinders them from simultaneously becoming both structures and sensors. The application of nanotechnology can significantly improve the performance of traditional concrete, giving it novel abilities and improving overall mechanical properties [1]. Self-sensing materials used in SHM drastically change the maintenance planning process by minimizing human involvement and human errors and by aiming to replace scheduled and periodic maintenance inspections or at least to reduce the current maintenance labor, thus improving safety and reliability.

2 The Concept

Richard P. Feynman's idea (1959) of controlling matter at the nanoscale remained only a concept for several decades until the technology was developed enough and observations at a quantum level were possible. Since Iijima and Ichihashi published their discovery of "*single-shell tubules*" in 1993, there have been many discoveries regarding the properties and possible applications of single-walled carbon nanotubes (SWCNTs). Comparing to conventional materials, carbon nanomaterials possess some unusual size-/surface-dependent (e.g., morphological, electrical, optical, and mechanical) properties. They can exist in numerous forms, differing in structure, size,

© RILEM 2020
K. Kovler et al. (Eds.): ConcreteLife 2020, RILEM Bookseries 26, pp. 148–152, 2020.
https://doi.org/10.1007/978-3-030-43332-1_29

chemistry, and mechanical properties. The most represented and investigated materials are nanocarbons (C60, carbon black, carbon nanotubes (CNTs), graphene) because of their superior mechanical properties and conductive capabilities. Single-walled CNTs have been regarded as one of the most promising material, opening the door for multi-functional, cementitious composite applications. Concrete is an electrically non-conductive material, however, the addition of CNTs (Fig. 1) provides it with piezoresistivity which makes it an excellent choice for a sensor while preserving the role of a structure at the same time.

The most recent developments in SHM are connected to different types of nanosensors such as transducers, electrochemical and optical sensors, as well as techniques of environmental pollutants' detection via nanomaterials. While the development of nanoscale devices and nanoelectromechanical systems (NEMS) is an evolving area of nanotechnology, there is also considerable interest in making macroscopic engineered materials that can exploit these properties. Self-sensing CNT/concrete composites possess piezoresistivity, giving the ability to monitor strain by using the change in the electrical resistance i.e. self-sensing capability of large-scale structures [2]. CNT networks are highly valuable in SHM for strain mapping, damage detection, identification of crack initiation and propagation, and more.

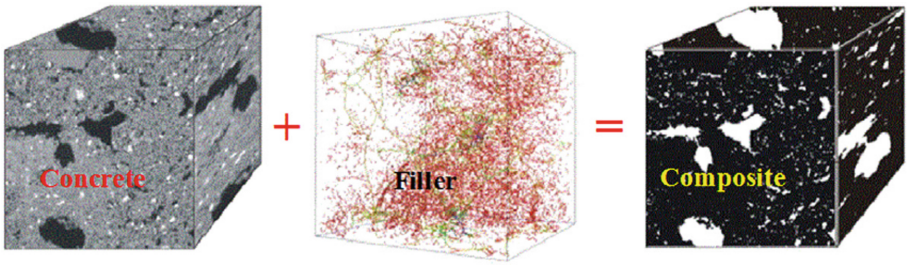

Fig. 1. Structure of self-sensing concrete [2]

The neural network approach is a way of modeling data based on computer learning in order to perform complex functions. The application of machine learning represents a new direction in the evolution of monitoring concrete structures. Artificial neural networks (ANNs) have been developed as an interconnected group of nodes inspired by a simplified representation of neurons in the brain. Although the original idea of ANN was to solve problems in the same way as a human brain would, over time it deviated from biology towards solving some specific tasks (pattern recognition, identification, classification, vision and control systems, cancer predictions, etc.). Recently, machine learning became an attractive tool to reduce model complexity and so ANNs have been successfully used for a variety of applications, some including structural analysis and material science, ranging from studies of atomic properties to the mechanical properties of concretes or an individual carbon nanotube [3]. The choice of ANNs to model so many different systems is, in part, due to their flexibility and adaptability as well as their easy application in software and hardware devices and materials [4].

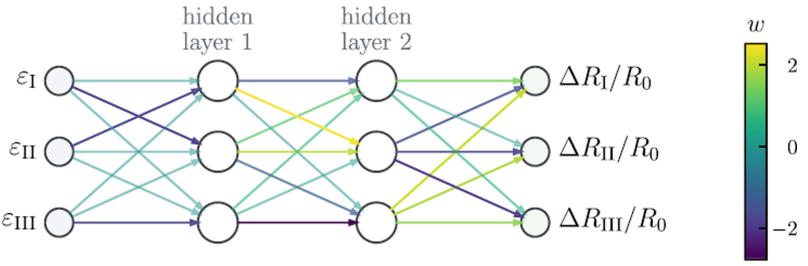

Fig. 2. Schematics of the optimized ANN and of respective weights [4]

3 The Methodology

Basic units of the neural network are artificial neurons, which represent the processing elements. Their connections typically have assumed weights that are adjusting as the learning proceeds based on the back-propagation rule. The architecture of the ANN is formed by the input and the output layer and a series of hidden layers, each of which is formed by a determined number of neurons (Fig. 2). Building of the artificial neural network starts with building its data library. Data library contains the data sets divided into 3 subsets: training, selecting and testing set. Data collection comprehends experimental data including laboratory investigations as well as numerical simulations of the mechanical properties of the composites. Data collected from Konsta-Gdoutos et al. [5], shown in Table 1, as an example of the information which may be used as training data and also as testing data, after supplementing it with the results of the measured sensitivity of the sensing ability (e.g. ΔR/R [%]).

Table 1. Mechanical properties of cement with 0.1% vol. and 0.5% vol. of CNT and 0.1% vol. of CNF, collected from [5]

Material	Fiber count	Age (days)	Compressive strength [MPa]	Young's modulus - bending test [GPa]	Young's modulus - compressive test [GPa]	Resistance [kΩ]	Resistivity [kΩ*cm]
Plain cement	\	3	19.8	9.2 ± 0.96	9.5 ± 0.97	12.6	8.4
		7	25.6	10.8 ± 0.87	11.5 ± 0.83		
		28	31.7	14.1 ± 0.71	13.9 ± 0.7		
0.1% CNT	3.61E+11	3	22.6	16 ± 0.44	15.4 ± 0.49	9.2	6.1
		7	26.5	18.1 ± 0.13	18.3 ± 0.15		
		28	33.8	27.4 ± 0.09	27.9 ± 0.12		
0.5% CNT	1.08E+12	3	22.7	9.9 ± 0.93	10.2 ± 0.94	10.6	7.1
		7	27.6	12.2 ± 0.74	12.3 ± 0.62		
		28	35.3	20.1 ± 0.67	20.9 ± 0.59		
0.1% CNF	1.69E+11	3	22.5	11.7 ± 0.78	12.0 ± 0.73	10.8	7.2
		7	25.2	16.9 ± 0.32	16.7 ± 0.46		
		28	33.7	27.6 ± 0.11	27.4 ± 0.14		

Among various modeling techniques, multiscale modeling (MM) showed to be the most efficient method that can model the mechanical behavior of the CNT and its composites accurately. The following scales are distinguished: quantum scale, nanoscale, microscale, macroscale, and continuum scale. The MM method entails solving physical problems that have important features at multiple scales. It is aimed at calculating material properties or system behavior at one scale using information from different scales, and at each scale, particular approaches describe each system. Garcıa-Macıas et al. [6] have presented a 3D generalization of the micromechanics models of the overall conductivity and uniaxial piezoresistivity of CNT-reinforced composite materials subjected to arbitrary strain states. The authors [6] have proposed an approach shown to be capable of determining the piezoresistivity coefficients. The presented technique showed to be able to reliably model the complex electromechanical behavior of the CNT/concrete composite materials.

This research work assumes testing of the mechanical properties and electrical conductivity of cementitious composite materials and further use of the results to train and test the ANN model. The numerical simulations include finite element models made using ANSYS software and the ANN model developed using MATLAB script. The training and selecting phase of the neural network will be conducted until the desired output and the network output don't relatively match, when the testing phase may be conducted. The architecture of the ANN model predicting the optimal mixture for self-sensing concrete is configured as follows. The input layer for the training of the ANN consists of 5 neurons: (1) water/cement ratio, (2) final weight of cement per 1 m^3 of concrete, (3) final weight of fine aggregate per 1 m^3 of concrete, (4) weight fraction of the functional filler, (5) conductivity of the functional filler. Output data include (i) electrical resistance of the composite material [Ω*cm], (ii) sensitivity of the sensing ability ($\Delta R/R_0$ [%]), (iii) compressive strength of the composite [MPa], (iv) flexural strength of the composite [MPa]. The output neurons can be represented by (v) stress sensitivity coefficient, (vi) gage factor and (vii) Young's modulus.

4 Conclusions

A novel approach to manufacturing self-sensing materials for SHM is now possible, implying concepts of determining mixtures and conductivity of specific self-sensing composites using artificial neural networks. The idea of a self-sensing structure is to mimic a biological system through sensing, actuation, adaptability, self-repair, etc. and the ultimate form of intelligent structures are the ones that have the additional ability to learn in contrast to the pre-programmed response. This learning feature is realized by employing ANNs. Real-time effective and cost-efficient monitoring of structures is possible to obtain by developing a conductive composite with a predetermined mixture predicted by a trained neural network. The application of machine learning implies a very low computational cost and can be immediately used by relatively inexperienced users [3].

References

1. Hanus, M.J., Harris, A.T.: Nanotechnology innovations for the construction industry. Progr. Mater. Sci. **58**, 1056–1102 (2013)
2. Han, B., Yu, X., Ou, J.: Self-Sensing Concrete in Smart Structures. Butterworth-Heineman, Oxford (2014)
3. Matos, M.A.S., Pinho, S.T., Tagarielli, V.L.: Application of machine learning to predict the multiaxial strain-sensing response of CNT-polymer composites. Carbon **146**, 265–275 (2019)
4. Matos, M.A.S., Pinho, S.T., Tagarielli, V.L.: Predictions of the electrical conductivity of composites of polymers and carbon nanotubes by an artificial neural network. Scripta Mater. **166**, 117–121 (2019)
5. Konsta-Gdoutos, M.S., Batis, G., Danoglidis, P.A., Zacharopoulou, A.K., Zacharopoulou, E.K., Falara, M.G., Shah, S.P.: Effect of CNT and CNF loading and count on the corrosion resistance, conductivity and mechanical properties of nanomodified OPC mortars. Constr. Build. Mater. **147**, 48–57 (2017)
6. Garcia-Macias, E., Castro-Triguero, R., Saez, A., Ubertini, F.: 3D mixed micromechanics-FEM modeling of piezoresistive carbon nanotube smart concrete. Comput. Methods Appl. Mech. Eng. **340**, 396–423 (2018)

A Rapid Method to Test the Effectiveness of Corrosion Inhibitors in Reinforced Concrete

I. Lapiro(✉), A. Mezhov, and K. Kovler

Faculty of Civil and Environmental Engineering,
National Building Research Institute, Technion – Israel Institute of Technology,
Haifa, Israel
igorlapiro@campus.technion.ac.il

Keywords: Steel corrosion · Reinforced concrete · Accelerated test · Inhibitor

1 Introduction

Corrosion of steel reinforced concrete (RC) is one of the major deterioration mechanisms causing economic and social losses [1]. The rate of corrosion depends strongly on the location of the structure. The major deterioration problems of RC structures are chloride-induced corrosion; sulfate-induced corrosion and carbonation. Another trigger of corrosion in RC is stray current [2].

For the last decades, the service life of RC structures is being considered in two phases: initiation and propagation of corrosion. The protection from the initiation phase is mainly achieved by designing of specific quality concrete. Various types of inhibitors are used for the mitigation of corrosion propagation. The high alkaline of pore solution passivates the steel embedded into the concrete. As long as the composition of the pore solution in concrete remains constant, the steel rebars are passivated. Whereas the passivated layer at the steel is destroyed, the propagation phase begins.

Currently, there are numerous strategies available for increasing the service life of reinforced structures exposed to severe environmental conditions, including the use of (a) low-permeability (high-performance) concrete, (b) chemical corrosion inhibitors, (c) protective coatings on steel reinforcement (e.g. epoxy-coated or galvanized steel), (d) corrosion-resistant steel (e.g. stainless steel), (e) non-ferrous reinforcement (e.g. fiber-reinforced plastics), (f) waterproofing membranes or sealants applied to the exposed surface of the concrete, (g) cathodic protection (applied at the time of construction), and (h) combinations of the above.

Corrosion inhibitors mostly act on the steel surface. The first mentioned of inhibitors in RC was examined in the late 1950s. Since then the most conventional inhibitor is calcium nitrite [3], but organic compounds are also known.

The standard methods for estimation of the efficiency of the chemical admixture against the corrosion in concrete are time-consuming (ASTM G109 - 07). However, industry and academia are always looking for a reliable accelerated test for this purpose. This paper is focused on the development of such an accelerated test providing the results within less than 10 days. The feasibility and efficiency of the proposed method are checked by testing two commercially available corrosion inhibitors.

© RILEM 2020
K. Kovler et al. (Eds.): ConcreteLife 2020, RILEM Bookseries 26, pp. 153–157, 2020.
https://doi.org/10.1007/978-3-030-43332-1_30

2 Materials and Methods

2.1 Materials

CEM I 52.5N supplied by Nesher Cement, Israel, is used for this study. Its mineral and chemical compositions are presented in Table 1.

Table 1. Mineral and chemical compositions of cement.

Mineral composition	wt.-%
Alite	61.02
Belite	12.95
C_3A cubic	5.86
C_4AF	12.42
Bassanite	1.87
Anhydrite	0.28
Portlandite	1.83
Calcite	2.25
Arcanite	0.97
Aphthitalite	0.55

Chemical composition	wt.-%
CaO	62.16
SiO_2	19.02
Al_2O_3	5.42
Fe_2O_3	3.82
MgO	1.31
TiO_2	0.53
K_2O	0.37
Na_2O	0.22
P_2O_5	0.4
Mn_2O_3	0.05
SO_3	2.48
IR	0.76
FL	2.8
LOI total	2.93

2.2 Inhibitors

Two commercially available inhibitors were taken. The first one was migrating corrosion inhibitor based on amine carboxylate (MCI-2005, Cortec Corporation); the second one was based on calcium nitrite (Sika CNI), which helps to anodic protection by creating a passivation layer (Fe_2O_3) by electrochemical reaction between NO_2^- and Fe_2^+. Sika CNI contains a minimum of 30% calcium nitrite by mass. Both meet all ASTM C1582 requirements.

2.3 Preparation of Mortar Samples

Cement was mixed with water, natural quartz sand (D_{max} = 2.36 mm) and admixtures in a pan mixer and then cast in molds 50 × 50 × 50 mm. Water/cement ratio was 0.55; mixture proportions and properties are shown in Table 2. After 24-h of hydration in sealed molds samples were immersed in water for 28 days (23 ± 2 °C). Compressive strength of the samples (with standard deviation) is shown in Table 3. Air contents and flow of hydraulic cement mortar of the samples was tested according to ASTM C109/C109 M, ASTM C185 - 15a and ASTM C1437 – 15.

Table 2. Mixture proportions and properties of mortar compositions

Material		Specific gravity	Relative mass	Unit weight [kg/m^3]	Air content [%]	Flow diameter [mm]
Reference	Sand	2.6	3.00	2,165	5.2	172
	Cement	3.1	1.00			
	Water	1.0	0.55			
MCI-2005 0.6/1000 liquids	Sand	2.6	3.00	2,261	1.9	172
	Cement	3.1	1.00			
	Water	1.0	0.55			
	Admixture	1.185	0.0015			
CNI 10/1000 liquids	Sand	2.6	2.97	2,146	7.1	166
	Cement	3.1	1.00			
	Water	1.0	0.525			
	Admixture	1.3	0.0283			

Table 3. Development of compressive strength of mortars in time

Compressive strength [MPa]					
Sample	1 day	3 days	7 days	28 days	90 days
Reference mortar	15.4 ± 0.72	31.3 ± 1.16	33.5 ± 2.41	44.1 ± 0.11	48.9 ± 1.20
Mortar with MCI-2005	13.4 ± 0.42	30.7 ± 1.80	33.9 ±1.38	42.1 ± 1.95	42.9 ± 2.60
Mortar with CNI	9.10 ± 0.07	24.5 ± 0.48	30.5 ± 1.00	38.8 ± 2.95	44.9 ± 1.05

2.4 Accelerated Test

To simulate the natural corrosion that occurs in RC structures, the specimens were exposed to the corrosive environment in the laboratory. The corrosion acceleration system is presented in Fig. 1(a) and consists of a plastic container filled with 5% NaCl solution (pH = 6.2…7.1). The specimens are 6 reinforced concrete cubes placed over wooden spacers and immersed in a solution, so that the top of the samples is higher than the surface of the solution by about 1 cm. The rebars protruding from the concrete samples are used as an anode, connected to a positive terminal, and the stainless-steel plates (cathode) are connected to the negative terminal of the direct current (DC) power supply. The process starts by applying a constant voltage to the system, which is set at 3.6 and 7.2 V. The electric current passing through the samples is measured every 1 min and the values are saved in the data logger. The experiment ended after crack width reached 0.10…0.15 mm; these values correspond to upper limits set by international standards in RC structures exposed to chloride attack. Figure 1 shows a schematic diagram of the system and a photo of the experimental system from one of the trials.

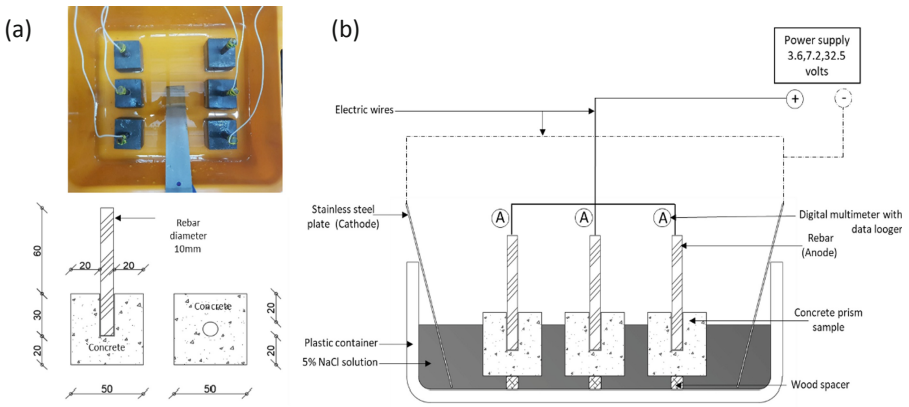

Fig. 1. Corrosion acceleration system (all dimensions are in mm)

3 Results

It was found that the introduction of a CNI inhibitor dramatically decreases the early-age strength (Table 3). However, after 90 days of hydration the strength is close to that of the reference. MCI-2005 admixture has also a negative influence on the early-age strength, but to lesser extent than CNI. Moreover, MCI-2005 notably reduces the air content, which is also directly related to the strength properties. In any case, all the samples exhibit similar 28-days strength, that allows comparing the influence of the inhibitors.

The samples are subjected to a constant electrical voltage, while electrical resistance (ER) develops over time (Fig. 1). The measurement proceeds until the drop of ER, which indicates the appearance of cracks along the rebar. As ER decreases, crack opening increases, until it reaches a steady state. Table 4 shows the times of crack formation in the samples tested with the electric voltage of 3.6 and 7.2 V, respectively. It can be seen, that CNI is not an effective inhibitor. This can be explained by the fact that the presence of chloride and sulftate ions can damage the passivation layer, so there is faster cracking development, than in the reference sample. Similar results have been already described elsewhere [4]. With the increase of electrical voltage, the effect of the inhibitors decreases. It is worth to note that the strength of the sample has a significant influence on the time of crack formation. A confirmation of these results is found in the work of Montes, Bremner and Lister [5]. The natural electrical voltage measured in our work was 0.17 ± 0.1 V, which corresponds to regular concrete. For such a small voltage both types of corrosion inhibitors are expected to serve better.

Table 4. Cracking time in mortar samples under 3.6 and 7.2 V

Sample	Reference		MCI-2005		CNI	
Voltage in the system [V]	3.6	7.2	3.6	7.2	3.6	7.2
Average time to crack [min]	6,534.5	3,961.5	8,812.5	4,234.5	4,936.5	3,861.0
Percentage [%]	100	100	135	106.8	75.5	97.5

4 Conclusions

The rapid laboratory method to test the effectiveness of corrosion inhibitors in reinforced concrete has been proposed. The observations from testing two types of corrosion inhibitors yielded the following conclusions:

- The proposed method is user-friendly and allows easy and quick estimation of the efficiency of corrosion inhibitors.
- The reliable results can be obtained within 10 days.
- At a voltage of 7.2 V, the effect of the inhibitor is negligible, and the strength of the concrete is act as the determining factor.
- It is shown that increasing the voltage reduces the duration of the experiment, while the reliability of the results decreased. The optimum voltage for the present seried of experiments is considered 3.6 V. This voltage might be reduced further to 1.2 V (the upper threshold in ordinary reinforced concrete) the future experiments, which in turn is going to increase the precision of the results.

References

1. Michel, A., Otieno, M., Stang, H., Geiker, M.R.: Propagation of steel corrosion in concrete: experimental and numerical investigations. Cem. Concr. Compos. **70**, 171–182 (2016)
2. Bertolini, L., Carsana, M., Pedeferri, P.: Corrosion behaviour of steel in concrete in the presence of stray current. Corros. Sci. **49**, 1056–1068 (2007)
3. Królikowski, A., Kuziak, J.: Impedance study on calcium nitrite as a penetrating corrosion inhibitor for steel in concrete. Electrochim. Acta **56**, 7845–7853 (2011)
4. Ahmad, Z.: Principles of Corrosion Engineering and Corrosion Control. Elsevier Publ., Amsterdam (2006)
5. Montes, P., Bremner, T.W., Lister, D.H.: Influence of calcium nitrite inhibitor and crack width on corrosion of steel in high performance concrete subjected to a simulated marine environment. Cem. Concr. Compos. **26**, 243–253 (2004)

External and Internal Aspects on the Durability of Concrete Structures

D. K. Panesar(✉), S. Narneni, and B. P. Gautam

Univeristy of Toronto, Toronto, ON, Canada
d.panesar@utoronto.ca

Keywords: Coupled degradation mechanisms · Stress application · Steel fibres · Confinement

1 Introduction

Although degradation due to freeze-thaw cycles, carbonation, corrosion, sulfate attack, etc. and the corresponding mechanisms have been studied for decades, we continue to be challenged by being able to translate the kinetics of degradation reactions, rates of damage, symptoms of damage on small-scale laboratory specimens that are unreinforced, unrestrained, mechanically unloaded specimens to large-scale, real life, reinforced structural elements, subjected to restraint, and mechanically loaded. There is a need for research to relate the performance of materials tested in the laboratory to the performance of structures in the field to improve the safety, sustainability, service life of existing and new concrete structures.

Although there are several aspects that warrant attention, this presentation will address two aspects, 'external' and 'internal', pertaining to understanding laboratory concrete durability testing to structural performance in the field. The scope of this paper specifically pertains to durability associated with internal swelling of concrete. The 'external' aspect deals with concrete behavior subjected to combined exposure conditions leading to degradation. The 'internal' aspects deals with the anisotropy behavior of concrete due to element geometry, effect of confinement due to steel reinforcing steel, steel fibres, and the role of multi-axial stresses and its implications on concrete's internal swelling response.

2 Discussion and Results

External Aspect: Combined Exposure Conditions

Several researchers [1, 2] have examined the influence of freeze-thaw damage in combination with chloride ingress, sulphate attack or carbonation processes. Although some coupled deterioration processes provoke and accelerate more serious damage than single loads, this is not necessarily always the case [3, 4]. One of the most common combination of concrete degradation mechanisms that has been published in the literature is: freeze thaw and chloride exposure studies. In contrast, markedly fewer

© RILEM 2020
K. Kovler et al. (Eds.): ConcreteLife 2020, RILEM Bookseries 26, pp. 158–161, 2020.
https://doi.org/10.1007/978-3-030-43332-1_31

studies have been conducted on the combined effect of alkali-silica reaction (ASR) and freeze-thaw or chloride exposure or carbonation or sulfate attack. In the Canadian context, this is of particular interest since ASR is infact prevalent in many structures that are in need of assessment and service life analysis. Canadian Standards Association (CSA) does allow the use of reactive aggregate in concrete with the requirement that specified supplementary cementious material (SCMs) are also used, since they are well reported to reduce ASR expansion (Fig. 1), however, SCMs can also increase vulnerability to carbonation reactions. Therefore, two research questions related to the competition of the chemical reactions are: What is the resistance of concrete (with and without SCMs) to combined ASR and carbonation? And, do the CSA requirements for SCMs help or harm concrete that is subjected to combined ASR and carbonation? This presentation will discuss these aspects.

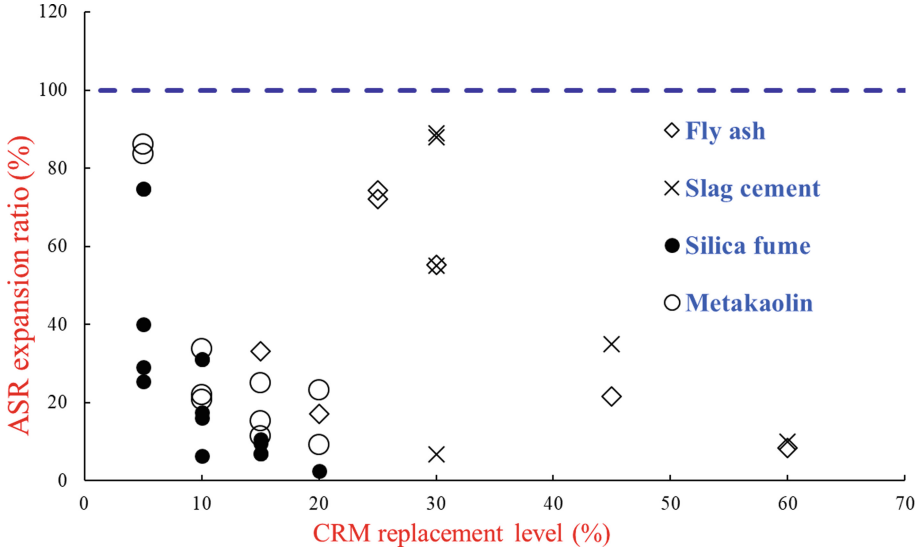

Fig. 1. Effect of cement replacement material (CRM) on ASR expansion

Internal Aspect: Anisotropic Behavior and Confinement of Concrete Due to Reinforcement

Although the direction of casting induces anisotropic behavior of concrete, the influence of this factor on the anisotropy of internal swelling behavior are inconclusive. This study has examined the multi-axial expansion and the damage rating index (DRI) of concrete that is: unreinforced; reinforced with one steel bar; steel fibre reinforcement; multi-axially loaded in compression. The concrete is designed in accordance with ASTM 1260 with reactive Spratt aggregate. For unreinforced concrete, the expansion in the transverse directions was markedly greater (3.72 times) than in the longitudinal direction. In the literature, relatively fewer studies have focused on the anistropic behavior of internal swelling of ASR-affected fibre-reinforced concrete. Although some studies indicate that fibers reduce ASR damage of concrete, other

sources indicate that longitudinal expansion was larger compared to the expansion of specimens without fibres [5].This behavior was attributed to the greater ductility of fibre-reinforced concrete, which allowed less cracking and more expansion [5]. Part of the conflicting observations may be associated with the fact that fibres are oriented in three-dimensional space, and their effect on the ASR performance of concrete cannot be understood by measuring axial expansion alone. Figure 2 highlights the differences in longitudinal, and transverse expansion of ASR-affected unreinforced concrete (M0.0-p), reinforced concrete with one bar (M0.0-r) as well as plain and reinforced concrete with 0.65% steel fibre (M0.65-p and M0.65-r) and plain concrete with 1.3% steel fibres (M1.3-p).

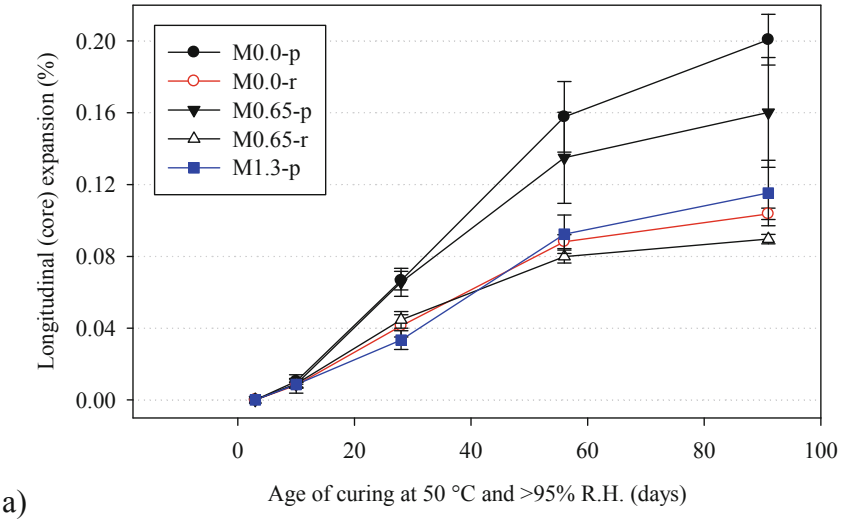

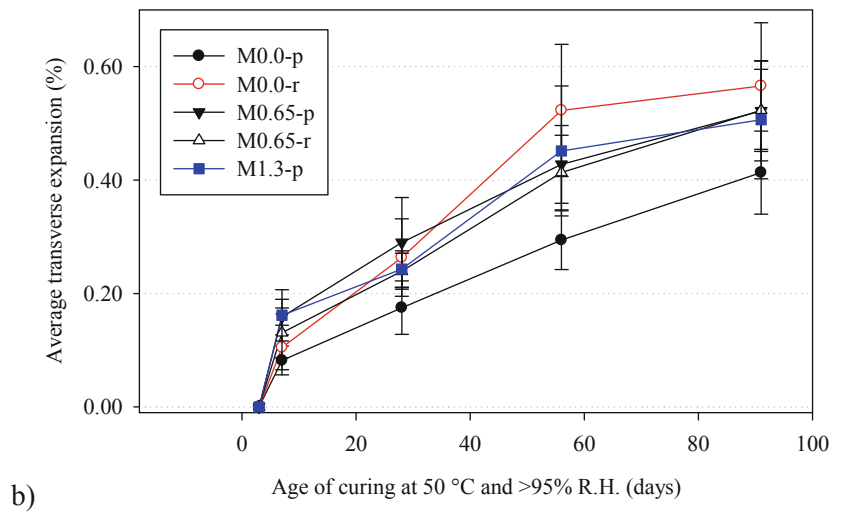

Fig. 2. Expansion of ASR affected specimens (a) longitudinal and (b) transverse

3 Conclusion

There is a need to translate results from laboratory studies of concrete durability to field durability of concrete structures which could lead to the development of: new protocols for the inspection, testing, and prognosis of existing structures that account for the anisotropic behavior; new laboratory test specifications to evaluate concrete exposed to coupled durability mechanisms; and more accurate service life predictions of concrete structures based the performance and properties of reinforced, mechanically loaded concrete specimens. With a strong effort by researchers from a collaborative materials and structural perspective, there is potential to bridge the disconnect between the interpretation of laboratory concrete durability tests and the field performance of structures.

References

1. Kessler, S., Thiel, C., Grosse, C.U., Gehlen, C.: Effect of freeze–thaw damage on chloride ingress into concrete. Mater. Struct. **50**, 121–134 (2017)
2. Jiang, L., Niu, D., Yuan, L., Fei, Q.: Durability of concrete under sulfate attack exposed to freeze–thaw cycles. Cold Reg. Sci. Technol. **112**, 112–117 (2015)
3. Maes, M., De Belie, N.: Resistance of concrete and mortar against combined attack of chloride and sodium sulphate. Cem. Concr. Compos. **53**, 59–72 (2014)
4. Ekolu, S.O., Thomas, M.D.A., Hooton, R.D.: Implications of pre-formed microcracking in relation to the theories of DEF mechanisms. Cem. Concr. Res. **37**, 161–165 (2007)
5. Haddad, R.H., Smadi, M.M.: Role of fibers in controlling unrestrained expansion and arresting cracking in Portland cement concrete undergoing alkali-silica reaction. Cem. Concr. Res. **34**, 103–108 (2004)

Performance of the Cement-Based Mortars for Repairing the Internal Lining of Steel Pipes for Drinking Water Supplying

R. Wasserman(✉)

Department of the Conservation and Restoration of the Monuments and Sites, Western Galilee Academic College (WGAC), Acre, Israel
wassermn@gmail.com

Keywords: Water-supplying steel pipes · Cement based internal lining · In-situ repair · Performance

1 Introduction

The common pathology oftenly observed in the water-supplying steel pipes is cracking and delaminating the cement based internal lining [1]. Thus, the quick in-situ repair of these defects is essential for preventing the possible steel corrosion in pipes [2–4]. The implemented repair mortar must meet the sanitary norms regarding the chemical composition of the materials allowed to be in contact with drinking water [5]. The criteria of the physical and mechanical properties of fresh and hardened lining mortar have been set based on the relevant international and national specifications.

2 Results

The current research was carried out in WGAC in collaboration with Mekorot – Israel National Water Co., during 2015–2017. The aim of the research was to reveal the most appropriate compositions of the cement-based mortars for the in-situ repair of internal lining of steel pipes.

The research program was based on:

- investigation of the physical and mechanical properties of 23 fresh and hardened "in-situ prepared" (18 mortars) and "ready-mix" (5 mortars) compositions (Figs. 1, 2);
- preparing the special models of the cement-based lining implemented on the steel plates (Fig. 3);
- study of the adhesion strength of cement-based lining implemented in the models, as a function of:
  - mortar composition (the type of chemical admixture and the granulometric composition of sands) and physical properties of the fresh mortars;
  - specific environmental exposure of lining mortars before their implementation on the steel plates;

© RILEM 2020
K. Kovler et al. (Eds.): ConcreteLife 2020, RILEM Bookseries 26, pp. 162–166, 2020.
https://doi.org/10.1007/978-3-030-43332-1_32

Fig. 1. Samples used in the tests of physical and mechanical properties of hardened mortars

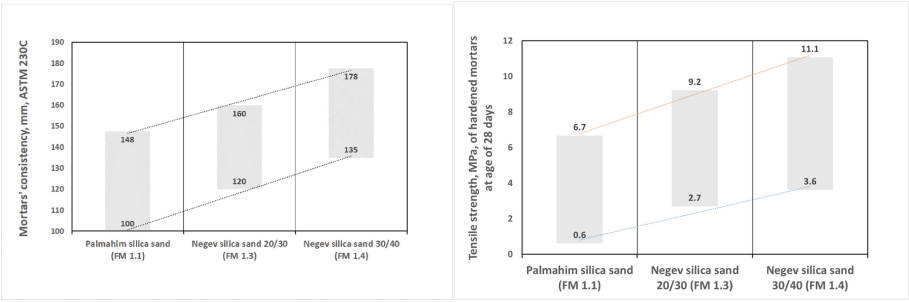

a) b)

Fig. 2. Effect of sand properties on the properties of in-situ prepared mortars; (a) consistency range of fresh mortar; (b) tensile strength of hardened mortar. FM – fineness modulus

Fig. 3. Special models of the cement-based lining implemented on the steel plates

Fig. 4. In-situ exposure of the cement based lining to the conditions inside the functioning water-supplying pipe line

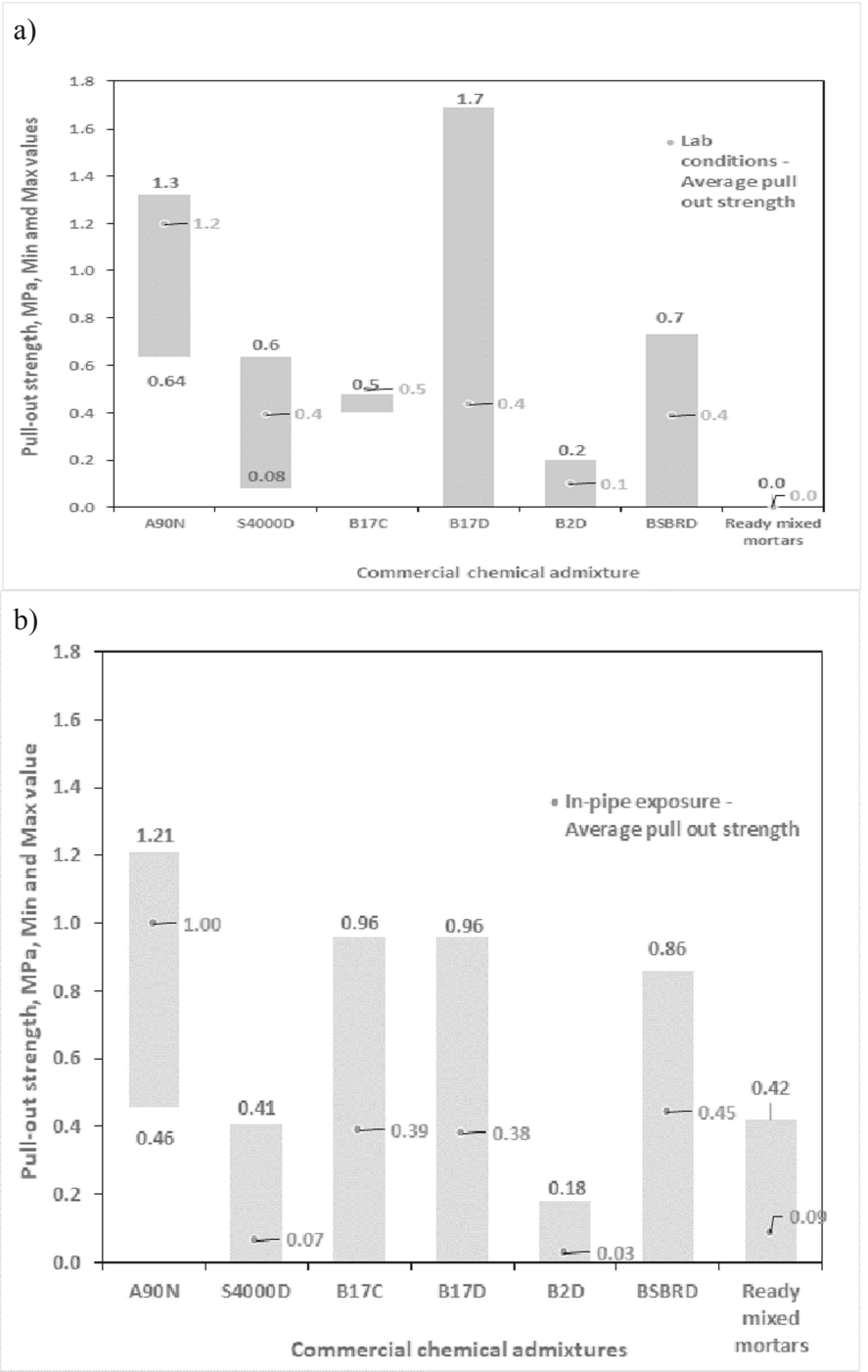

Fig. 5. Effect of commercial chemical admixture onpull out strength of ctmtnt-based lining: (a) exposure to lab conditions; (b) in-pipe exposure

- type of the surface preparation of steel plates before the implementation of cement-based lining;
- characteristics of the environmental exposure (different temperatures and relative humidity (ca. 55% RH & 100% RH) to which the lined steel plates were subjected for 3 to 9 months, in laboratory conditions, as well as in-situ, inside the functioning pipe line (Figs. 4 and 5).

The final criteria which were preliminary set basing on the relevant international and national specifications, were tested and reset. These criteria have been:

– the fresh mortar consistency measured at temperature 21 ± 3 °C and 55 ± 5% RH should be 160–180 mm;
– the mortars should keep almost the same consistency when exposed to the hot environment (34 ± 1 °C) for 60 min, at least. This criterion could be met by keeping the content of the solids in the commercial chemical admixture used in the mortar mix, as high as 45% (by mass), at least;
– it was revealed that only the mortars which were characterized in the hardened state (at age of 28 days) by the oven-dried bulk density of more than 1,970 kg/m^3 have the appropriate strength characteristics and the required performance in-situ;
– the strength characteristics of the hardened cement-based lining mortars at age of 28 days should be:
  - compressive strength – at least 30 MPa;
  - tensile strength – at least 5 MPa.
– the adhesive ability of lining made of the cement-based mortars to steel background should met the criteria of pull-out strength of 1.0 MPa, at least, whereas this value is mandatory after the exposure of cement-based lining to any service conditions occurred in water-supplying stainless-steel pipes.

3 Conclusions

The research resulted in checking the criteria set by the valid international specifications for cement-based internal lining used in the water supplying steel pipes, resetting the most important criteria in order to obtain the highly performing internal lining and finding out the ctmtnt-based mortar compositions meeting these criteria.

References

1. Water Agencies' Standards (WAS): Cement-mortar lined and coated steel pipe and specials. USA: Water Agencies' Standards, pp. 1–16 (2011)
2. ANSI/AWWA, ANSI/AWWA C205: Cement – Mortar Protective Lining and Coating for Steel Water Pipe—4 in. (100 mm) and Larger—Shop Applied, USA, vol. 07, p. 7 (2008)

3. Bärreis, J.: Cement Mortar Lining - A method of refurbishment for the long-lasting preservation of the piping infrastructure. Unitracc.com. http://www.unitracc.com/aktuelles/artikel/cement-mortar-lining–a-method-of-refurbishment-for-the-long-lasting-preservation-of-the-piping-infrastructure-en. Accessed 26 Feb 2020
4. Dransfield, J.: Admixtures for concrete, mortar and grout. In: Newman, J., Choo, B.S., (eds.) Advanced Concrete Technology. Constituent Materials, Oxford, UK, pp. 4/1–4/36. Elsevier (2003)
5. NSF International & ANSI, NSF/ANSI 61: Drinking Water System Components - Health Effects, USA, p. 196 (2013)

Prestressed Concrete Sleepers: Failure Investigation Case Study

D. Yurlov[1(✉)], A. Shishkin[2], and S. Zhutovsky[2]

[1] Israel Railways, Lod, Israel
denisy@rail.co.il
[2] Technion Israel Institute of Technology, Haifa, Israel

Keywords: Prestressed concrete · Railway sleepers · Failure analysis

1 Introduction

The efficiency of rail transport is crucial to compete with other transportation modes. Thus, over the years railway operators demand increasing rolling stock axle load and speeds. Hence, railway infrastructure improvements are crucial to withstand persistent increasing of bearing capacity expressed in significant dynamic load and cumulative traffic load.

Railway sleepers are key elements in track infrastructure that have been in ongoing development and enhancement. Since initially been introduced, the application of prestressed concrete sleepers steadily increases. Nowadays, concrete sleepers are the major type of sleepers used around the world. However, systematic failures of concrete sleepers are very common in the railway infrastructure. In this paper, a case of failure of prestressed monoblock concrete sleepers was investigated. The conducted investigation included field survey and laboratory analysis. The results of the study revealed problems in the durability design and curing process as the main cause of the failure.

2 Results

2.1 Field survey

The field survey included visual inspection and Non-Destructive Testing (NDT).

2.1.1 Visual Inspection

The visual inspection of the prestressed concrete sleepers revealed longitudinal cracks between 200 microns and several millimeters that in most cases passed through the prestressing cables. Cracks appeared in a variety of locations and diverse variations. An example of the characteristic longitudinal cracking of the sleepers is shown in Fig. 1. Nevertheless, the cracks passed around the prestressing cable zones, reflecting corrosion of the prestressing cables causing development, growth, and opening of these cracks. In addition, on the uninstalled concrete sleepers, cracking was observed as well, illustrating net cracking pattern on its surface as shown in Fig. 1 suggesting the failure cause could be either alkali-silica reaction of aggregates or ettringite formation caused by either internal or external sulfate attack.

© RILEM 2020
K. Kovler et al. (Eds.): ConcreteLife 2020, RILEM Bookseries 26, pp. 167–170, 2020.
https://doi.org/10.1007/978-3-030-43332-1_33

Fig. 1. Characteristic longitudinal cracking on top (left) and side surfaces (center). The net cracking pattern on the surface of a new concrete sleeper (right).

2.1.2 Non Destructive Testing

The NDT was done by Schmidt hammer and Ultrasonic Pulse Velocity (UPV) on several sleepers. These results are graphically summarized in Fig. 3 below. The error bars in these figures indicate the confidence interval of 95%, which corresponds to twice Standard Deviation (SD).

The field tests were conducted in different zones of the sleepers as indicated in Fig. 2 below, as well as, on different sleepers conditions such as new, partially cracked, and fully cracked sleepers. The results of field testing confirm that mechanical properties of concrete used for sleepers production are satisfactory and therefore the reason for failure most probably is not of mechanical origin.

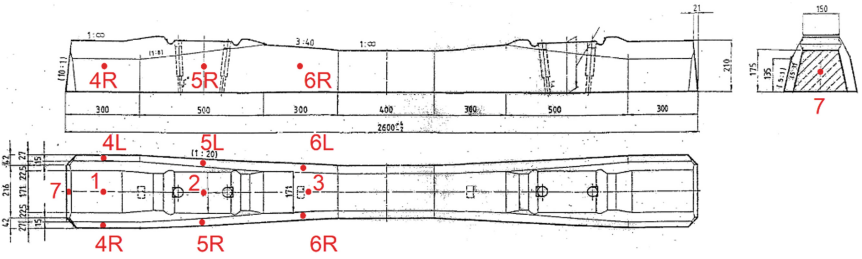

Fig. 2. NDT testing points layout

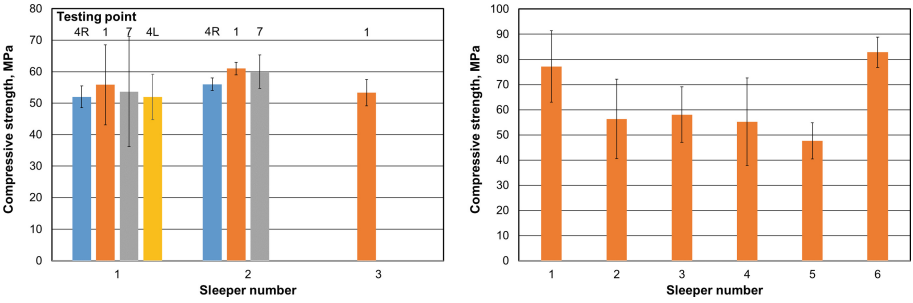

Fig. 3. Evaluation of compressive strength based on in situ Schmidt rebound hammer test (left) and UPV measurement (right)

2.2 Laboratory study

2.2.1 Compressive Strength

Compressive strength testing results of the drilled cores from failed sleeper demonstrate wide distribution but satisfying the manufacturing requirements. Furthermore, generally strength testing results on drilled cores are usually lower than specially casted and cured samples due to the damage introduced during drilling and during the service life of the element.

2.2.2 Mineralogical Composition

The mineralogical composition was determined on three different samples taken from three locations of the cracked concrete sleeper. The summary of the composition is given in Table 1 below and an example of the X-ray Diffractogram (XRD), including Rietveld fitting curves, and difference plot are shown in Fig. 4 below.

Table 1. Mineral composition by XRD, % wt.

	Dolomite	Calcite	Quartz	Portlandite	Ettringite	Brucite	Hydrocalumite	Gypsum	Other
Crack	56.4	16.9	23.6	0.6	1.5	0.0	1.0	0.0	0.0
Surface	30.5	37.7	28.3	0.3	0.0	0.0	0.0	0.0	3.2
Center	76.0	7.7	4.9	0.8	0.3	0.1	3.4	0.6	6.2

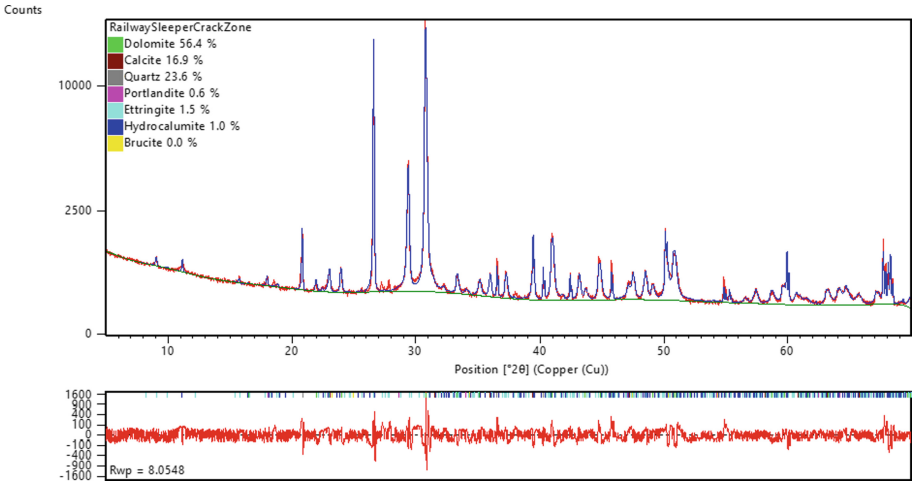

Fig. 4. XRD diffractogram of concrete from crack, edge and center zone of sleeper

This test reveals the concentration of Hydrocalumite and Ettringite. Hydrocalumite, also known as Friedel's salt, is chloride salt that is formed when chlorides come into contact with cement paste. According to the international standards [1–3], chlorides are thoroughly excluded from concrete composition.

The presence of ettringite in the concrete sleeper suggests delayed ettringite formation since it's likely to exist only either in fresh concrete, or at a very early age then ettringite quickly transformed to monosulfate. One of the explanations of presence of ettringite in the sleeper is high curing temperature [4], i.e. exceeding 80 °C. In this case ettringite crystals could form in the concrete at later ages after hardening while expanding. Since the concrete can not resist the expansive formation of ettringite the net cracking pattern is formed (Fig. 1, right above).

2.2.3 Chemical Composition

The chemical composition of the cracked concrete sleeper is summarized in Table 2 below. The XDR and the Inductively-Coupled Plasma (IPC) spectroscopy analysis were done from the same location in the sleeper. Note that with the ICP method chloride content cannot be determined. The chemical decomposition did not demonstrate any abnormality.

Table 2. Chemical composition by ICP, % wt.

	SiO_2	CaO	Al_2O_3	Fe_2O_3	MgO	SO_3	K_2O	Mn_2O_3	Na_2O	P_2O_5	TiO_2	V_2O_5	ZnO	LOI
Crack	37.7	19.7	1.1	0.6	6.7	1.9	0.1	0.0	0.1	0.2	0.8	0.0	0.0	31.1
Surface	45.0	19.5	1.6	1.1	3.4	1.9	0.4	0.0	0.1	0.4	1.2	0.0	0.0	25.3
Center	29.7	21.7	0.9	0.4	9.0	2.0	0.1	0.0	0.1	0.1	0.7	0.1	0.0	35.2

3 Conclusions

According to the results of the study, the failure of prestressed concrete sleepers was due to corrosion and expansion of prestressing cables. The determined reason for that was by chloride attack, which probably was accelerated by sulfate attack that resulted in delayed ettringite formation. Moreover, accumulated high dynamic traffic load accelerated sleepers' failure. Severe cracking of concrete sleepers was observed on the inspected sites. Although the strength of concrete material as high, the integrity and load-bearing capacity of concrete sleepers are significantly degraded by cracking. Currently, it is not clear how to determine the residual bearing capacity of cracked concrete sleepers and criteria for the proactive replacement are not well-defined. Further research and testing are needed to clarify these aspects that are of primary importance to the railway authority.

References

1. ASTM C617-15: Standard Practice for Capping Cylindrical Concrete Specimens, American Society for Testing and Materials (2015)
2. ASTM C39-17: Standard Test Method for Compressive Strength of Cylindrical Concrete Specimens, American Society for Testing and Materials (2017). https://doi.org/10.1520/c0039
3. BS EN 197-1:2011: Cement Part 1: Composition, specifications and. British Standard Institution (2011)
4. BS EN 13230-1:2016: Railway applications—Track—Concrete sleepers and bearers Part 1: General requirements. British Standard Institution (2016)

Author Index

© RILEM 2020
K. Kovler et al. (Eds.): ConcreteLife 2020, RILEM Bookseries 26, pp. 171–172, 2020.
https://doi.org/10.1007/978-3-030-43332-1